4-20-2018

Cationic Ruthenium Complexes in Catalysis: The Activation of Propargylic Alcohols Through Electronically Tuned Complexes

Matthew James Stark
University of Missouri - St. Louis, mjs2qc@mail.umsl.edu

Cationic Ruthenium Complexes in Catalysis:
The Activation of Propargylic Alcohols Through Electronically Tuned Complexes

Matthew J. Stark

B.S. Chemistry, Southern Illinois University Edwardsville, 2010
M.S. Chemistry, Saint Louis University, 2013

A Dissertation Submitted to The Graduate School at University of Missouri-St. Louis
in partial fulfillment of the requirements for the degree
Doctor of Philosophy in Chemistry

May
2018

Advisory Committee

Eike Bauer, Ph.D.
Chairperson

Alexei Demchenko, Ph.D.

Nigam Rath, Ph.D.

Janet Braddock-Wilking, Ph.D.

Acknowledgements

I would like to acknowledge the people in my life who made this thesis a reality. First of all, my mother Karen Stark, who has believed in my potential since I was a child. My family and friends, for understanding the struggles.

Dr. Cristina De Meo, for teaching me valuable laboratory experience through handling really small amounts of expensive and fragile carbohydrates. Dr. Brent Znosko, for teaching me to think more critically about literature and to question data. Dr. Alexei Demchenko, for giving me sage advice over the years. Dr. Mike Shaw, for believing in me as a scientist and giving me guidance on so many occasions. Dr. Nigam Rath, whose work on structures has been important to my research. Dr. Janet Braddock-Wilking, who has been a patiently dealt with all of my last-minute requests. Dr. Winters, Mr. Kramer, and Dr. Lou for all of the help with spectroscopy. The professors at UMSL, SLU, and SIUE for all of their education and assistance over the years.

Thank you to the University of Missouri – Saint Louis, the National Science Foundation for funding, and the Graduate School for a fellowship.

Last but not least, Dr. Eike Bauer, for his patience and guidance over the last few years. Without his support, I would have not become a better scientist. He has continually taught me things important for life… and the exam.

Without your help, this would have not been possible. Thank you.

Table of Contents

List of Figures

List of Schemes

List of Tables

Structural Listing of New Metal Complexes

Chapter 2:

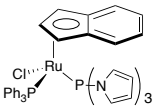

[RuCl(Ind)(PPh_3){P(pyrl)$_3$}]

13

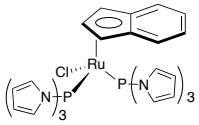

[RuCl(Ind){P(pyrl)$_3$}$_2$]

14

Chapter 3:

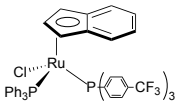

[RuCl(Ind)(PPh_3){P(*p*-$C_6H_4CF_3$)$_3$}]

26

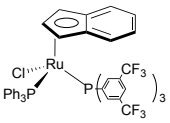

[RuCl(Ind)(PPh_3){P(*3,5*-$C_6H_3(CF_3)_2$)$_3$}]

27

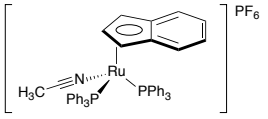

[Ru(MeCN)(Ind)(PPh_3)$_2$] PF_6

28

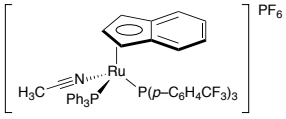

[Ru(MeCN)(Ind)(PPh_3){P(*p*-$C_6H_4CF_3$)$_3$}] PF_6

29

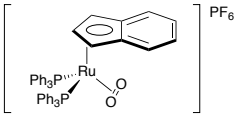

[Ru(η−2)(Ind)(PPh_3)$_2$] PF_6

30

Chapter 4:

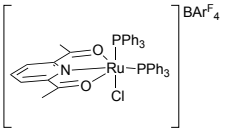

[RuCl(dap)(PPh_3)$_2$]$BAr^F{}_4$

35

Abstract

Synthesis of fine organic molecules often requires employing meticulously selected reagents and conditions to optimize yields. One such tool in organic synthesis is a transition metal complex that may act as a catalyst for a reaction. Catalysts accelerate chemical reactions and often lower the temperature required; therefore, effective catalysts have a major economic impact in chemical industry. Transition metals can be chemically modified by the addition of ligands to form metal complexes. Metal complexes can exhibit high levels of complexity and provide benefits to solubility, temperature tolerance, and catalytic activity compared to simple transition metal salts. With increasing complexity of these metal complexes, it is of worthwhile interest to pursue systematic examinations of ligand modifications to study their impact on the reactivity of the catalyst.

This research aims to examine the details of a few catalytic reactions involving propargylic alcohols and to a lesser extent terminal alkynes, which are important starting materials for a variety of organic products. We were interested to study how changing ligands on metal complexes can affect their catalytic efficiency in these transformations. A number half–sandwich ruthenium complexes of the general formula [RuCl(η^5–C_9H_7)(L^1)(L^2)] were synthesized and fully characterized, where ligand L was systematically changed to fine-tune the electronic properties of the complex. In this method, we can investigate structure-activity relationships of the metal complexes in catalytic application.

In the first part of the study, the known ruthenium indenyl "parent" complex [RuCl(η^5–C_9H_7)(PPh_3)$_2$] was electronically tuned by systematic replacement of the PPh_3 ligands by tris(pyrrolyl)phosphine ligands $PPyrl_3$ to obtain the two complexes [RuCl(η^5–

$C_9H_7)(L^1)(L^2)]$ with L^1=PPh_3, L^2= $PPyrl_3$ and L^1=L^2=$PPyrl_3$. The unique inductive properties of pyrrole attached to phosphorus allowed us to investigate any potential effects on catalysis when that phosphine is used as a ligand in this system. Both complexes were structurally characterized, revealing that the steric properties of the new complexes are similar to those of the parent complex. However, cyclic voltammetry (CV) measurements showed that the new complexes are more difficult to oxidize, which is in line with the increased electron-withdrawing properties of $PPyrl_3$ compared to PPh_3. The new complexes showed catalytic activity in the etherification of propargylic alcohols and in the formation of oxygen-containing heterocycles from propargylic alcohols and diketones.

To build upon the knowledge of the limits of fine–tuning catalysis, the same half–sandwich ruthenium complex $[RuCl(\eta^5–C_9H_7)(PPh_3)_2]$ was employed to study the effects of increasing electron–withdrawing fluorinated phosphine ligands on catalysis. By systematically exchanging PPh_3 in $[RuCl(\eta^5–C_9H_7)(PPh_3)_2]$ with aryl phosphines that contained one or two $–CF_3$ substituents, it was hypothesized that decreased electron density at the metal center of the complex could translate to an increase in catalytic activity. Two new complexes $[RuCl(\eta^5–C_9H_7)(PPh_3)(PAr_3)]$ were synthesized, and structurally characterized, where PAr_3 are phosphine ligands with an increasing number of CF_3 substituents. The new complexes were compared to the parent complex in terms of structural, electronic, and catalytic differences. Again, the structural differences, as judged from X-ray data, are marginal. However, the new complexes are, as expected, more difficult to oxidize, as shown by CV experiments. The new complexes were, together with the parent complex, applied in propargylic etherification reactions. While the new complexes showed catalytic activity, their reactivity did not differ significantly from the

parent complex. The results suggested that the electronic differences did not have a major impact on the activity of the metal complex.

Ruthenium complexes with a tridentate ligand were considered as avenues for catalytic activity changes, because polydentate ligands tend to form more stable metal complexes. A new complex, $[RuCl(dap)(PPh_3)_2]BAr^F_4$, was synthesized using 2,6-diacetylpyridine (dap) as a ligand and fully characterized. The reactivity of the complex was not on par with previously published data for the nucleophilic substitution of propargylic alcohols as mentioned above, but the complex was found to have excellent reactivity and selectivity in the Markovnikov addition of carboxylic acids to terminal alkynes to give enol esters. We synthesized a number of enol esters using this system, providing a new avenue for obtaining Markovnikov–substituted enol esters with excellent selectivity.

We were furthermore interested to determine whether iron complexes could also catalytically activate propargylic alcohols. Advantages of iron over ruthenium are its lower cost and toxicity, as iron is geologically prevalent and environmentally benign. It was hypothesized that substituted ferrocenium cations could act as Lewis acids with substituents that could be chiral, thus conferring chirality on the transition state and onto the product. Several examples of iron catalysts based on ferrocenes were synthesized and screened for reactivity after chemical oxidation. Results indicate that chirality of the substituent was unable to be confirmed after oxidation of the ferrocene. However, it was found that ferrocene boronic acid, when oxidized with $AgSbF_6$, showed catalytic activity in the etherification of propargylic alcohols.

Chapter 1. Introduction

1. Introduction

Complex organic synthesis has experienced a boon with an ever-expanding library of transition metal catalyzed reactions.[1-3] Interactions of metals and organic molecules with relevance in organic synthesis were noted quite some time ago; the discovery of alkylation of an aromatic ring utilizing aluminum chloride by Friedel and Craft is a notable example of such an interaction with wide applications in organic synthesis.[4] Exploration of the possibilities that metals brought to organic chemistry has since expanded. One particular advantage of metal-promoted reactions is that their use is not limited in stoichiometric amounts in reactions, but that they can be employed in sub–stoichiometric or catalytic amounts. Another advantage in the use of transition metals is that they facilitate transformations so that these transformations may be carried out at lower temperatures over shorter timeframes when compared to metal-free conditions.[5] Today, transition metal catalysis proves to be a powerful tool in bulk and fine chemical synthesis, as the demand for complex organic target molecules steadily increases.[6-8]

Common transition metal catalysts contain metal centers such as ruthenium, nickel, or copper.[3,9,10] Some rare metals such as molybdenum, rhenium, or cobalt are potentially cost prohibitive.[11] Palladium catalysts have become synthetic workhorses, with use in reduction and coupling reactions, but economic and ecological considerations have made finding cheaper alternatives an attractive goal.[12,13] While ruthenium exists in much lower abundance than its smaller "relative" iron does, it has found its place in synthetic chemistry as an efficient catalyst in olefin metathesis.[14-16]

1.1. Grubbs and the Olefin Metathesis Revolution

Progress in catalyst development has recently focused on creating ancillary ligands with increasingly elaborate functionalization. Efforts to fine-tune catalysts through ligands have resulted in a considerable progress, allowing for greater selectivity, reactivity, and tolerance of functional groups on the target molecule.[6] This trend is well exemplified by the work of Robert H. Grubbs.[17] Grubbs' work with olefinic systems showed the promise of using ruthenium complexes in catalytic amounts for ring opening and closing metathesis reactions and cross metathesis reactions.[18] Famous for the first generation catalyst bearing Grubbs' name (**1** in Figure 1.1.), it was discovered that the activity of a ruthenium system for a ring closing metathesis was greatly increased by the addition of a carbene ligand to the ruthenium.[19] The catalyst was further tuned by the inclusion of a dihydroimidazole ligand, which in turn was further tweaked by changing the substituents on the heterocyclic ring.[20] This so-called second generation of Grubbs' catalyst **2** has become a mainstay in olefin metathesis. The configuration of the ligands on the ruthenium center increased solubility and temperature tolerance, which increased the interest in developing catalysts that possessed these desirable traits.[21]

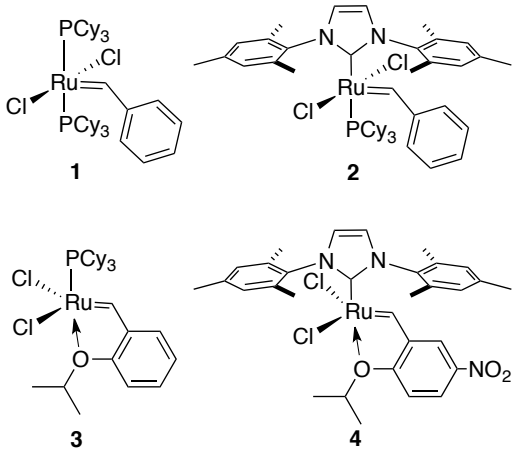

Figure 1.1. Grubbs's and Grubbs-Hoveyda catalysts.

1.2. Ligands Provide an Opportunity to Alter Reactivity

As interest in the use of ruthenium in metathesis reactions grew, others took up the effort. In the work of Hoveyda, modification of the first generation Grubbs catalyst **1** to include a chelating ether **3** showed excellent air stability while maintaining high reactivity (Figure 1.1.).[22] Further studies demonstrated an electronic effect on the chelating ligand by the addition of a nitro group **4** on the styrene carbene.[23] This allowed for easier dissociation of the chelating ether (shown in Scheme 1.1.), which is considered to be a necessary step in the catalytic cycle, thus translating to an increase in reactivity. This open position on the metal complex is often referred to as the 'active site', as it removes hindrances or vacates orbitals in which to facilitate catalytic activity.

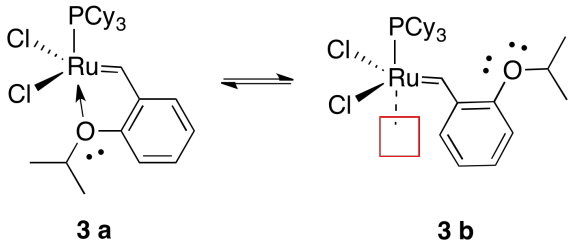

3 a **3 b**

Scheme 1.1. In Grubbs-Hoveyda catalysts, the ether chelate displaces and provides an 'active site' for catalytic activity.

Overall, various optimizations of the Grubbs-Hoveyda systems have resulted in a wide range of tailored catalysts.[6,24,25] As demonstrated in these systems, electronic modifications of the ligands do seem to impart reactivity changes at the metal center. Modifications by addition of chirality to the complexes have also been performed, with the hopes of imparting enantiomeric selectivity to the product.[26,27]

1.3. Activation of Catalysts

Metal complexes are sometimes too stable to perform catalytic functions, while their counterpart reactive too unstable to be isolated or stored. Therefore, an activation of

the molecule is sometimes required to generate a catalytically active species.[28] In a similar fashion as the Grubbs-Hoveyda catalyst ether chelate dissociating to create an active site (Scheme 1.1., **3a** → **3b**), the full dissociation of a ligand can also provide an open active site. For olefin cross metathesis reactions, the catalytically active species was determined to be the carbene species that formed *in situ* from the reactants.[18] For Grubbs's first generation of catalyst, the ruthenium complex $RuCl_2(PCy)_3$ was 'activated' by the loss of a phosphine and formation of a stable carbene complex for use in catalysis (forming **1**). This carbene loss also plays an important role in the olefin catalysis reactions, as postulated by Chauvin's mechanism, where the carbene reacts with substrate molecules and frees the coordination sphere for other molecules to take its place. Other stable metal complexes are sometimes isolated as dimers which can be activated by splitting the dimer into two molecules. Some examples of this include ruthenium and palladium complexes that dissociate *in situ* to form their catalytically active species.[29-31] In a variety of catalytic applications, ligand dissociation is often a necessary step in the catalytic pathway.[32]

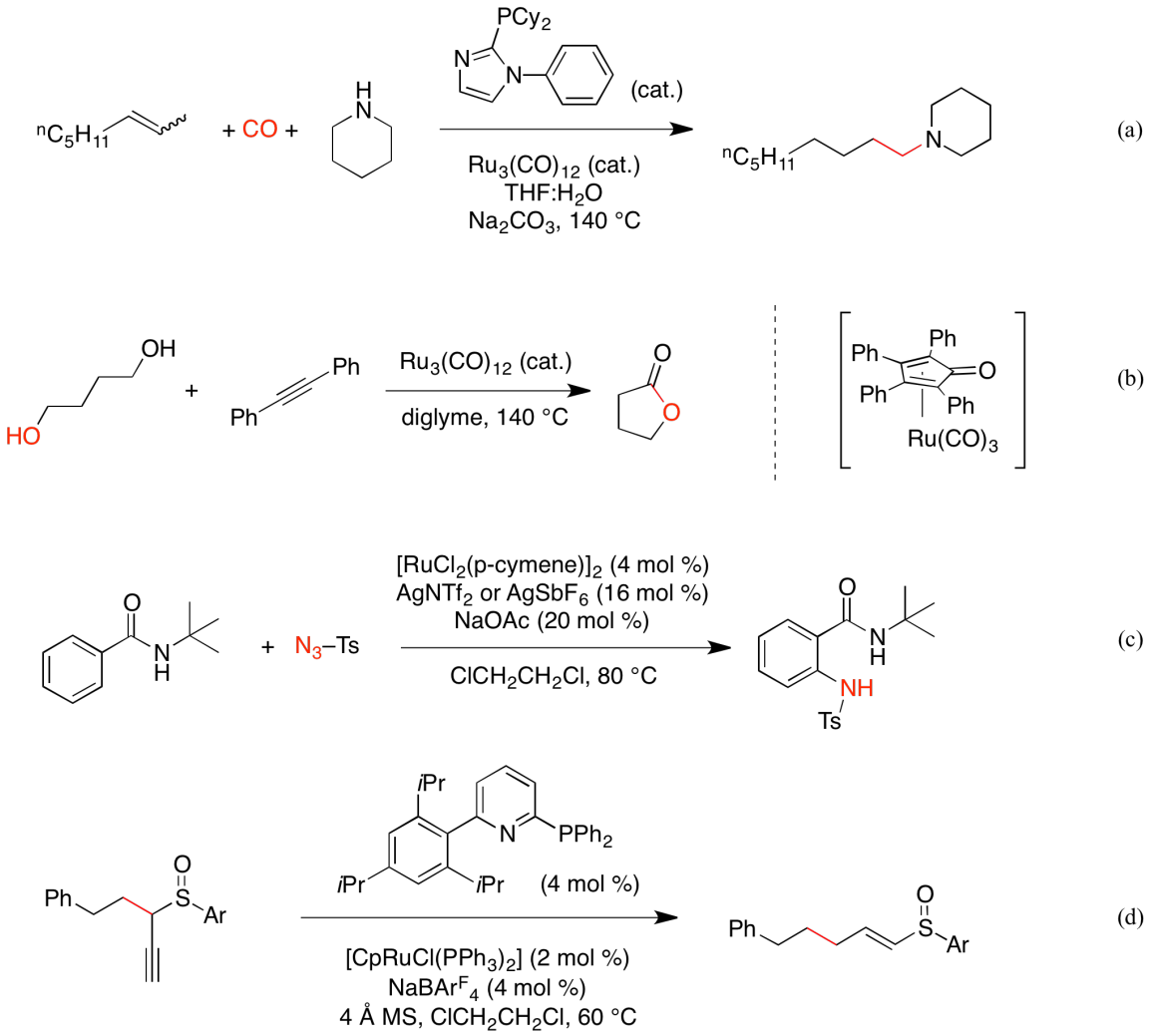

Scheme 1.2. Examples of *in situ* catalyst activation. References: (a)[33], (b)[34], (c)[35], (d)[36].

By far, the most common method of activating a catalyst is to add an additional reagent to the reaction mixture; activation *in situ* bypasses the need to isolate an unstable species and simplifies the reaction set up. Examples of catalytic studies using *in situ* activation are presented here in Scheme 1.2. Ligands, salts, and other additives have shown to be an effective means of stabilizing reactive intermediates that form through decomposition or generating the intermediates through the liberation of ligands from the stable complex.[32] When ligands on a metal complex dissociate, they leave behind a

coordinately unsaturated species. A salt or another ligand may be used to stabilize the new species formed from that decomposition product, which may be catalytically active. For example, $Ru_3(CO)_{12}$ in Scheme 1.2. is used in catalytic amounts in each reaction, but the active intermediate is a decomposition product stabilized by the catalytic amount of ligand that was placed into the reaction (a) or stoichiometric amounts of material used to create an active species with ligands that participate in the reaction (b). In the circumstance of activation by facilitating decomposition, Scheme 1.2. (c) and (d) offer examples of silver and sodium salts being used as chloride scavengers; the cation of the salt favors dissociation of the dative chloride on the metal complex, leaving behind a more reactive, coordinately unsaturated species.

1.4. Reactions of Alkynes and Propargylic Alcohols

Alkynes are an attractive functional group to be employed in the synthesis of complex organic molecules. They offer a readily reducible triple bond and are sufficiently electron-rich enough to react with electrophiles. Terminal alkynes offer an easy synthetic pathway to more complex subunits such as internal alkynes, alkenyl halides, carbonyls, and alkenes. The possibilities increase when functional groups adjacent to the triple bond are considered.

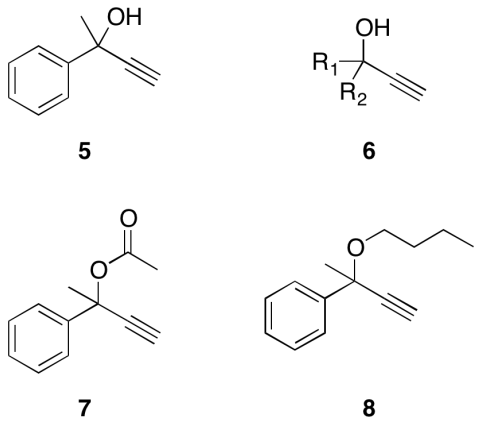

5 **6** **7** **8**

Figure 1.2. Propargylic alcohols, acetates, and ethers.

Propargylic groups have found use in synthesis; a functional group on the carbon vicinal to the alkyne can allow different pathways to be exploited. For instance, propargylic alcohols (Figure 1.2.) **5** and **6** and acetates **7** may be used to create vinyl aldehydes, allenes, or involved in intramolecular cyclizations.[15,37-39] Since propargylic alcohols are readily available starting materials, their widespread use in large synthetic schemes is desirable.[40-44] Propargyl etherification is particularly attractive because propargylic ethers **8** have been used to obtain vinyl ethers or employed in intramolecular cyclizations.[45-48]

1.5. Catalysis

Propargylic replacement reactions aim to change the functional group that lies adjacent to an alkyne. Some reactions employing propargylic alcohols are shown in Scheme 1.3. The etherification of propargylic alcohols through replacement offers synthetic pathways to more complex synthetic targets. This was first demonstrated by Nicholas with the use of $Co_2(CO)_8$ in stoichiometric amounts.[49] As cobalt carbonyl

complexes are highly toxic, a suitable less-toxic metal that could be used in catalytic quantities was highly desired. Other work has shown that iron, bismuth, copper, and ruthenium have all been used to catalyze replacement of a propargylic alcohol with a nucleophile.[50-54] The mechanism for this replacement reaction is not yet firmly established in literature. As many literature examples demonstrate, the reaction can proceed using a variety of metals. As such, the mechanism may be highly dependent on the metals used. The majority of literature believes this reaction to happen via either of two pathways: through a carbocation[50,55] or an allenylidene[56,57] intermediate.

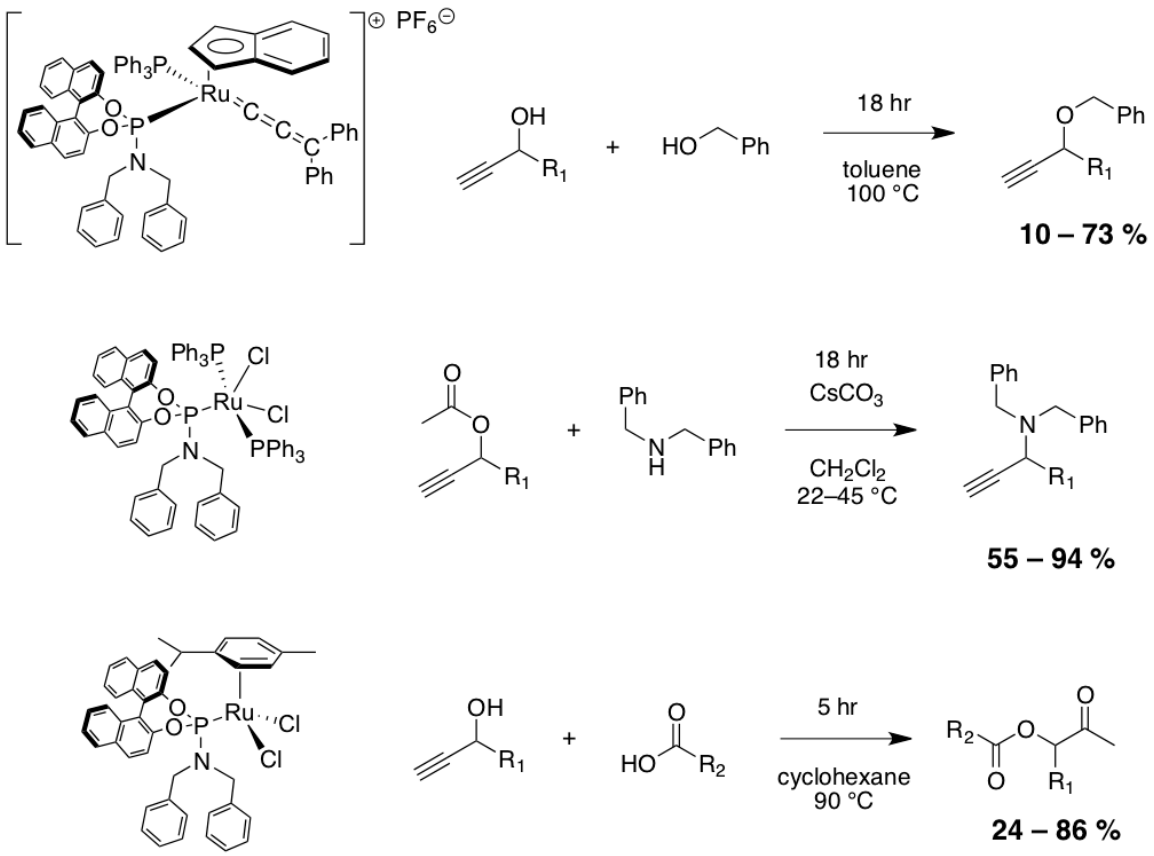

Scheme 1.3. Nucleophilic substitution reactions using ruthenium catalysts with propargylic alcohols and acetates. Etherification using an allenylidene complex.[58] Amination using a phosphoramidite complex.[59] Addition and transesterification into β–oxo esters using a cymene complex.[60]

Zhan and coworkers have demonstrated the use of iron and bismuth in propargylic replacement reactions, in which these metals are believed to behave as Lewis acids (Scheme 1.4.). The metal center coordinates to the oxygen of the alcohol, followed by dissociation of the hydroxide and nucleophilic attack of the carbocation.[50,51] This is the traditional S_N1 pathway to nucleophilic substitution where the leaving group is interacting with the catalyst.

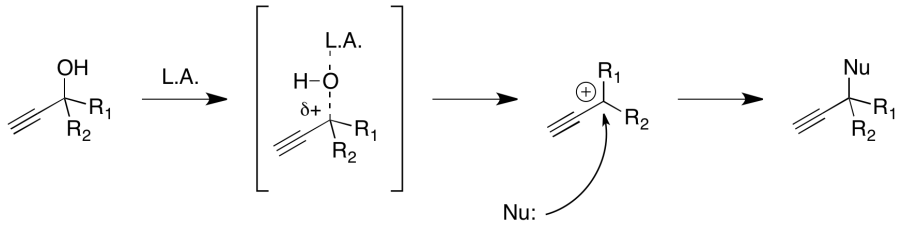

Scheme 1.4. Hypothesized mechanism for Lewis acid-catalyzed carbocation pathway.

Nakajima and coworkers have demonstrated that by using a copper complex, etherification can be performed through the supposed mechanistic route of copper coordination to the alkyne, indicating that non-Lewis acid catalysis is a viable pathway.[52] However, the use of ruthenium in propargylic etherification reactions may proceed through the allenylidene pathway. A potential catalytic mechanism is shown here in Scheme 1.5.

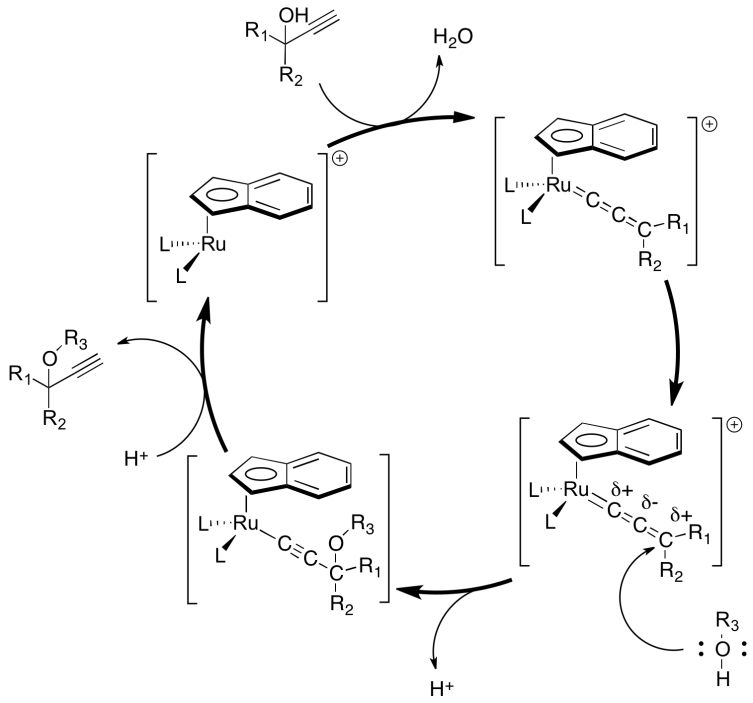

Scheme 1.5. Allenylidene pathway to ruthenium-catalyzed propargylic etherification reactions.

In this pathway, the metal center coordinates to the terminal alkyne, facilitating the loss of water to form an unsaturated allenylidene carbon chain. The ɣ carbon of the allenylidene chain is partially positively charged, offering an easy target for a weak nucleophile.[56] This mechanism has been regarded as established for several systems through experimental and computational investigations.[53,54,58,61,62] Numerous examples of ruthenium allenylidene complexes are known and characterized by common techniques.[56,62-65] A general structure of an allenylidene **11** is shown in Scheme 1.6.

Some X-ray structures of these unique metal complexes have been solved. It should be noted that these structures are often bulky, using phenyl groups as substituents on the allenylidene chain, large non-coordinating anions like aryl borates, or crystallized as bimetallic compounds.[53,66-68] To contrast these structures, several σ-alkynyl complexes

have also been published.[65,69-71] A generalized structure of a σ-alkynyl ruthenium complex **10** is shown in Scheme1.6. From the various reports, it is possible that the interaction between the alkyne and ruthenium center may interchange between the various transition states. Furthermore, it may be possible to influence any of the transition states by using ligands that withdrawal or donate electron density to the metal center.

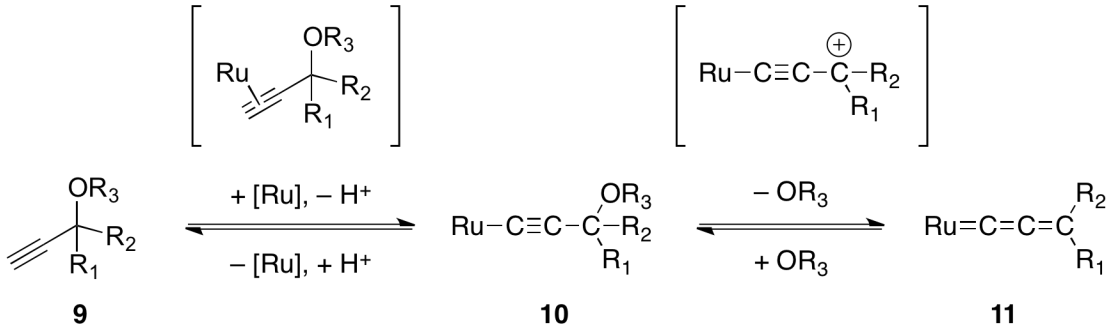

Scheme 1.5. Isomerization of the reactive metal σ-alkynyl complex and metal allenylidene.

1.6 Specific Aims

This research aims to examine the details of a few catalytic reactions involving propargylic alcohols and to a lesser extent terminal alkynes, which are important starting materials for a variety of organic products. We were interested to study how changing ligands on metal complexes can affect their catalytic efficiency in these transformations. A number half–sandwich ruthenium complexes of the general formula [RuCl(η^5–C_9H_7)(L^1)(L^2)] were synthesized and fully characterized, where ligand L was systematically changed to fine-tune the electronic properties of the complex. In this method, we can investigate structure-activity relationships of the metal complexes in catalytic application.

In the first part of the study, the known ruthenium indenyl "parent" complex [RuCl(η^5–C_9H_7)(PPh_3)$_2$] was electronically tuned by systematic replacement of the PPh_3 ligands by tris(pyrrolyl)phosphine ligands $PPyrl_3$ to obtain the two complexes [RuCl(η^5–C_9H_7)(L^1)(L^2)] with L^1=PPh_3, L^2= $PPyrl_3$ and L^1=L^2=$PPyrl_3$. The new complexes showed catalytic activity in the etherification of propargylic alcohols and in the formation of oxygen-containing heterocycles from propargylic alcohols and diketones.

To build upon the knowledge of the limits of fine–tuning catalysis, the same half–sandwich ruthenium complex [RuCl(η^5–C_9H_7)(PPh_3)$_2$] was employed to study the effects of increasing electron–withdrawing fluorinated phosphine ligands on catalysis. By systematically exchanging PPh_3 in [RuCl(η^5–C_9H_7)(PPh_3)$_2$] with aryl phosphines that contained one or two –CF_3 substituents, it was hypothesized that decreased electron density at the metal center of the complex could translate to an increase in catalytic activity. Two new complexes [RuCl(η^5–C_9H_7)(PPh_3)(PAr_3)] were synthesized with PAr_3 phosphine ligands that have an increasing number of CF_3 substituents. The new complexes were compared to the parent complex in terms of structural, electronic, and catalytic differences. While the new complexes showed catalytic activity, their reactivity did not differ significantly from the parent complex. The results of structural, electronic, and catalytic activity are compared.

In the third part of this study, ruthenium complexes with a tridentate ligand were considered as avenues for catalytic activity changes, because polydentate ligands tend to form more stable metal complexes. A new complex, [RuCl(dap)(PPh_3)$_2$]BAr^F_4, was synthesized using 2,6-diacetylpyridine (dap) as a ligand and fully characterized. The reactivity of the complex was not on par with previously published data for the nucleophilic

substitution of propargylic alcohols as mentioned above, but the complex was found to have excellent reactivity and selectivity in the Markovnikov addition of carboxylic acids to terminal alkynes to give enol esters. We synthesized a number of enol esters using this system, providing a new avenue for obtaining Markovnikov–substituted enol esters with excellent selectivity.

Lastly, we were interested to determine whether iron complexes could also catalytically activate propargylic alcohols. It was hypothesized that substituted ferrocenium cations could act as Lewis acids with substituents that could be chiral, thus conferring chirality on the transition state and onto the product. Several examples of iron catalysts based on ferrocenes were screened for reactivity after chemical oxidation. Results indicate that chirality of the substituent was unable to be confirmed after oxidation of the ferrocene. However, it was found that ferrocene boronic acid, when oxidized with $AgSbF_6$, showed catalytic activity in the etherification of propargylic alcohols.

Overall, the uniform strategy of this study was to examine how fine–tuning ligands can change electron density at the metal center and translate to catalytic performance. By systematically changing ligands attached to a ruthenium or iron complexes, we hope to provide examples of fine–tuning catalysts.

1.7. References:

(1) Touré, B. B.; Hall, D. G. *Chem. Rev.* **2009**, *109* (9), 4439–4486.
(2) Herndon, J. W. *Coord. Chem. Rev.* **2005**, *249* (9-10), 999–1083.
(3) Jana, R.; Pathak, T. P.; Sigman, M. S. *Chem. Rev.* **2011**, *111* (3), 1417–1492.
(4) Friedel, C.; Crafts, M. *J. Chem. Soc.* **1877**, *32* (0), 725–791.
(5) Crabtree, R. H. *The Organometallic Chemistry of the Transition Metals*, 5 ed.; John Wiley & Sons, Inc.: Hoboken, 2014; pp 1–522.
(6) Bieniek, M.; Bujok, R.; Cabaj, M.; Lugan, N.; Lavigne, G.; Arlt, D.; Grela, K. *J. Am. Chem. Soc.* **2006**, *128* (42), 13652–13653.
(7) Rueping, M.; Nachtsheim, B. J. *Beilstein J. Org. Chem.* **2010**, *6*, 1–24.
(8) Fürstner, A. *Angew. Chem. Int. Ed.* **2000**, *39*, 3012–3043.

(9) Guo, X.-X.; Gu, D.-W.; Wu, Z.; Zhang, W. *Chem. Rev.* **2015**, *115* (3), 1622–1651.
(10) Bauer, E. B. *Curr. Org. Chem.* **2008**, *12* (16), 1341–1369.
(11) Mao, J.; Yan, H.; Rong, G.; He, Y.; Zhang, G. *Chem. Rec.* **2016**, *16* (3), 1096–1105.
(12) Phan, N. T. S.; Van Der Sluys, M.; Jones, C. W. *Adv. Synth. Catal.* **2006**, *348* (6), 609–679.
(13) Egorova, K. S.; Ananikov, V. P. *Angew. Chem. Int. Ed.* **2016**, *55* (40), 12150–12162.
(14) Nolan, S. P.; Clavier, H. *Chem. Soc. Rev.* **2010**, *39* (8), 3305–3316.
(15) Alcaide, B.; Almendros, P.; Luna, A. *Chem. Rev.* **2009**, *109* (8), 3817–3858.
(16) Sanford, M. S.; Love, J. A.; Grubbs, R. H. *J. Am. Chem. Soc.* **2001**, *123* (27), 6543–6554.
(17) Trnka, T. M.; Grubbs, R. H. *Acc. Chem. Res.* **2001**, *34* (1), 18–29.
(18) Grubbs, R. H.; Burk, P. L.; Carr, D. D. *J. Am. Chem. Soc.* **1975**, *97* (11), 3265–3267.
(19) Schwab, P.; Grubbs, R. H.; Ziller, J. W. *J. Am. Chem. Soc.* **1996**, *118* (1), 100–110.
(20) Scholl, M.; Ding, S.; Lee, C. W.; Grubbs, R. H. *Org. Lett.* **1999**, *1* (6), 953–956.
(21) Vougioukalakis, G. C.; Grubbs, R. H. *Chem. Rev.* **2010**, *110* (3), 1746–1787.
(22) Kingsbury, J. S.; Harrity, J. P. A.; Bonitatebus, P. J.; Hoveyda, A. H. *J. Am. Chem. Soc.* **1999**, *121* (4), 791–799.
(23) Michrowska, A.; Bujok, R.; Harutyunyan, S.; Sashuk, V.; Dolgonos, G.; Grela, K. *J. Am. Chem. Soc.* **2004**, *126* (30), 9318–9325.
(24) Bieniek, M.; Samojłowicz, C.; Sashuk, V.; Bujok, R.; Śledź, P.; Lugan, N.; Lavigne, G.; Arlt, D.; Grela, K. *Organometallics* **2011**, *30* (15), 4144–4158.
(25) Olszewski, T.; Bieniek, M.; Skowerski, K.; Grela, K. *Synlett* **2013**, *24* (08), 903–919.
(26) Van Veldhuizen, J. J.; Gillingham, D. G.; Garber, S. B.; Kataoka, O.; Hoveyda, A. H. *J. Am. Chem. Soc.* **2003**, *125* (41), 12502–12508.
(27) Meek, S. J.; O'Brien, R. V.; Llaveria, J.; Schrock, R. R.; Hoveyda, A. H. *Nature* **2011**, *471* (7339), 461–466.
(28) Nuñez-Zarur, F.; Solans-Monfort, X.; Rodríguez-Santiago, L.; Sodupe, M. *Organometallics* **2012**, *31* (11), 4203–4215.
(29) Nishiyama, H.; Itoh, Y.; Matsumoto, H. *J. Am. Chem. Soc.* **1994**, *116* (5), 2223–2224.
(30) Na, Y.; Park, S.; Han, S. B.; Han, H.; Ko, S.; Chang, S. *J. Am. Chem. Soc.* **2004**, *126* (1), 250–258.
(31) Dong, X.-F.; Fan, J.; Shi, X.-Y.; Liu, K.-Y.; Wang, P.-M.; Wei, J.-F. *J. Organomet. Chem.* **2015**, *779*, 55–61.
(32) Naota, T.; Takaya, H.; Murahashi, S.-I. *Chem. Rev.* **1998**, *98* (7), 2599–2660.
(33) Liu, J.; Kubis, C.; Franke, R.; Jackstell, R.; Beller, M. *ACS Catal.* **2016**, 907–912.
(34) Blum, Y.; Shvo, Y. *J. Organomet. Chem.* **1985**, *282* (1), C7–C10.
(35) Shin, K.; Kim, H.; Chang, S. *Acc. Chem. Res.* **2015**, *48* (4), 1040–1052.
(36) Zheng, R.; Wang, Y.; Zhang, L. *Tetrahedron Letters* **2015**, *56* (23), 3144–3146.
(37) Cadierno, V.; Crochet, P.; García-Garrido, S. E.; Gimeno, J. *Dalton Trans.* **2010**, *39* (17), 4015–4031.
(38) Pirkle, W. H.; Boeder, C. W. *J. Org. Chem.* **1978**, *43* (10), 1950–1952.
(39) Tokimizu, Y.; Oishi, S.; Fujii, N.; Ohno, H. *Angew. Chem.* **2015**, *127* (27), 7973–7977.
(40) Willwacher, J.; Kausch-Busies, N.; Fürstner, A. *Angew. Chem. Int. Ed.* **2012**, *51* (48), 12041–12046.
(41) Trost, B. M.; Rudd, M. T. *Org. Lett.* **2003**, *5* (9), 1467–1470.
(42) Trost, B. M.; Doherty, G. A. *J. Am. Chem. Soc.* **2000**, *122* (16), 3801–3810.
(43) Bose, S.; Yang, J.; Yu, Z.-X. *J. Org. Chem.* **2016**, *81*, 6757–6765.
(44) Mori, M. *Adv. Synth. Catal.* **2007**, *349* (1-2), 121–135.
(45) Bruneau, C.; Dixneuf, P. H. *Adv. Synth. Catal.* **2002**, *344*, 585–595.
(46) Liang, T.; Zhang, W.; Chen, T.-Y.; Nguyen, K. D.; Krische, M. J. *J. Am. Chem. Soc.* **2015**, *137* (40), 13066–13071.
(47) Fukuda, Y.; Utimoto, K. *Bull. Chem. Soc. Jpn.* **1991**, *64* (6), 2013–2015.
(48) Bauer, E. B. *Synthesis* **2012**, *44* (8), 1131–1151.
(49) Nicholas, K. M. *Acc. Chem. Res.* **1987**, *20*, 214–221.
(50) Zhan, Z.-P.; Yu, J.-L.; Liu, H.-J.; Cui, Y.-Y.; Yang, R.-F.; Yang, W.-Z.; Li, J.-P. *J. Org. Chem.* **2006**, *71* (21), 8298–8301.
(51) Zhan, Z.-P.; Yang, W.-Z.; Yang, R.-F.; Yu, J.-L.; Li, J.-P.; Liu, H.-J. *Chem. Commun.* **2006**, No. 31, 3352.

(52) Nakajima, K.; Shibata, M.; Nishibayashi, Y. *J. Am. Chem. Soc.* **2015**, *137* (7), 2472–2475.
(53) Nishibayashi, Y.; Milton, M. D.; Inada, Y.; Yoshikawa, M.; Wakiji, I.; Hidai, M.; Uemura, S. *Chem. Eur. J.* **2005**, *11* (5), 1433–1451.
(54) Bustelo, E.; Dixneuf, P. H. *Adv. Synth. Catal.* **2007**, *349* (6), 933–942.
(55) Schreiber, S. L.; Sammakia, T.; Crowe, W. E. *J. Am. Chem. Soc.* **1986**, *108* (11), 3128–3130.
(56) Cadierno, V.; Gimeno, J. *Chem. Rev.* **2009**, *109* (8), 3512–3560.
(57) Werner, H. *Chem. Commun.* **1997**, No. 10, 903–904.
(58) Alkhaleeli, D. F.; Baum, K. J.; Rabus, J. M.; Bauer, E. B. *Catal. Commun.* **2014**, *47*, 45–48.
(59) Widaman, A. K.; Rath, N. P.; Bauer, E. B. *New. J. Chem.* **2011**, *35* (11), 2427–2434.
(60) Costin, S.; Rath, N. P.; Bauer, E. B. *Adv. Synth. Catal.* **2008**, *350* (14-15), 2414–2424.
(61) Trost, B. M.; Martinez, J. A.; Kulawiec, R. J. *J. Am. Chem. Soc.* **1993**, *115*, 10402–10403.
(62) Fürstner, A.; Liebl, M.; Lehmann, C. W.; Picquet, M.; Kunz, R.; Bruneau, C.; Touchard, D.; Dixneuf, P. H. *Chem. Eur. J.* **2000**, *6* (10), 1847–1857.
(63) Cadierno, V.; Gamasa, M. P.; Gimeno, J.; González-Cueva, M.; Lastra, E.; Borge, J.; García-Granda, S.; Pérez-Carreño, E. *Organometallics* **1996**, *15* (8), 2137–2147.
(64) Gamasa, M. P.; Gimeno, J.; Martin-Vaca, B. M.; Borge, J.; García-Granda, S.; Pérez-Carreño, E. *Organometallics* **1994**, *13* (10), 4045–4057.
(65) Cadierno, V.; Conejero, S.; Gamasa, M. P.; Gimeno, J.; Pérez-Carreño, E.; García-Granda, S. *Organometallics* **2001**, *20* (14), 3175–3189.
(66) Miyazaki, T.; Tanabe, Y.; Yuki, M.; Miyake, Y.; Nishibayashi, Y. *Organometallics* **2011**, *30* (11), 3194–3199.
(67) Smith, E. J.; Johnson, D. G.; Thatcher, R. J.; Whitwood, A. C.; Lynam, J. M. *Organometallics* **2013**, *32* (24), 7407–7417.
(68) Wong, C.-Y.; Lai, L.-M.; Lam, C.-Y.; Zhu, N. *Organometallics* **2008**, *27* (22), 5806–5814.
(69) Cadierno, V.; Conejero, S.; Gamasa, M. P.; Gimeno, J.; Falvello, L. R.; Llusar, R. M. *Organometallics* **2002**, *21* (18), 3716–3726.
(70) Cadierno, V.; Gamasa, M. P.; Gimeno, J. *Organometallics* **1997**, *16*, 4453–4463.
(71) Cadierno, V.; Conejero, S.; Gamasa, M. P.; Gimeno, J. *Dalton Trans.* **2003**, No. 15, 3060–3066.

Chapter 2. Pyrrole Phosphine Substitution and Ligand Effects on Catalysis

Chapter 2. Pyrrole Phosphine Substitution and Ligand Effects on Catalysis

2.1. Aim

In an effort to demonstrate the effect a ligand has on catalytic activity, we set out to compare yields of propargylic etherification reactions across several structurally similar catalysts with electronically modified ligands. A well-defined ruthenium catalyst, $[RuCl(\eta^5\text{-}C_9H_7)(PPh_3)_2]$, was subjected to ligand exchange by sequentially substituting a tris pyrrolyl phosphine, $\{P(pyrl)_3\}$, in place of a triphenylphoshine, PPh_3. As a ligand, $\{P(pyrl)_3\}$ is known to be electron–withdrawing and should give an electron–poor metal center on a ruthenium complex. Using these new metal complexes as catalysts, the improvements of the yields of propargylic etherification reactions could demonstrate a noticeable amount of change in reactivity, thus demonstrating that ligands can make a measurable impact on catalytic efficiency.

2.2. Introduction

To compare complexes by ligand substitution, we chose to work with the well–known η^5-coordinated indenyl (half-sandwich) ruthenium complexes. Indenyl (abbreviated Ind = C_9H_7) is a well characterized π-ligand, first reported by Pauson and colleagues in 1951 using iron and cobalt as the transition metal centers.[1] Ruthenium was later used to synthesize numerous stable indenyl complexes, of the general formula $[RuCl(Ind)(L)_2]$, that have been fully characterized.[2-4] Structurally analogous to cyclopentadienyl ligands ($Cp = C_5H_5$), indenyl ligands offer a well-defined platform for observing possible effects the ligands exert on the activity of the complex.

Literature provides many examples of transition metal complexes that have powerful catalytic applications for a variety of reactions; of those many metal complexes, some have the above mentioned aromatic η^5-coordinated ligands.[5,6] Ruthenium complexes containing Cp and phosphine ligands have demonstrated to be catalytically active for a variety of organic reactions involving our substrate of interest, e.g. propargylic moieties.[7-10] One such metal complex, $[RuCl(Ind)(PPh_3)_2]$ (Scheme 2.1., **12**), was chosen as our starting point for this study as its interaction with propargylic moieties is well studied.[4,11,12] Furthermore, it is also known that phosphine ligands can be substituted on the complex with little effort through a dissociation and association of ligands, known as ligand substitution or metathesis.[13,14] Serving as the reference material, different phosphine ligands could replace the PPh_3 ligands in complex **12** with increasing propensity for electronic effects on the metal center.

If the new ligands were to induce electron-withdrawing effects at the metal center, we hypothesized that each ligand substitution could make a consistent and measurable impact on catalytic activity. Through comparison of the original complex **12** and the new complexes, we could obtain direct evidence of ligand effects on catalytic efficiency for propargylic alcohol substitution reactions. The ligand we chose to work with for this study was the electron–withdrawing ligand tris(pyrrolyl)phosphine (abbreviated $\{P(pyrl)_3\}$; it offers unique electronic properties that may be ideal for studying electronic effects. Aromaticity in the pyrrole ring arises from the lone pair delocalization off of the nitrogen atom, which in turn acts upon the phosphorus–nitrogen bond in the molecule.[15] This conjugation offers a ligand that associates with a metal center in decreased σ-character and increased π-character; it is not as stable of a ligand as the PPh_3 it will be

compared to.[16-19] The π-acceptor characteristics of pyrrolyl phosphine ligands has been studied in similar metal complexes of rhodium and molybdenum with modified pyrrolyl groups, which revealed the electron-withdrawing character of the ligand through studying infrared CO stretching frequencies on metal complexes.[20] We anticipated this electron-withdrawing character could to translate to electronic deficiencies at the metal center, leading to more efficient catalysis by means of more reactive intermediates.

2.3. Results

2.3.1. Metal Complexes

The parent complex, [RuCl(Ind)(PPh_3)$_2$] (**12**), was subjected to iterative substitution of the {P(pyrl)$_3$}; this allowed for differences between the metal complexes efficiencies in catalysis to be attributable to the effects imparted by a single ligand exchange. The synthesis of the two new metal complexes is shown here in Scheme 2.1.

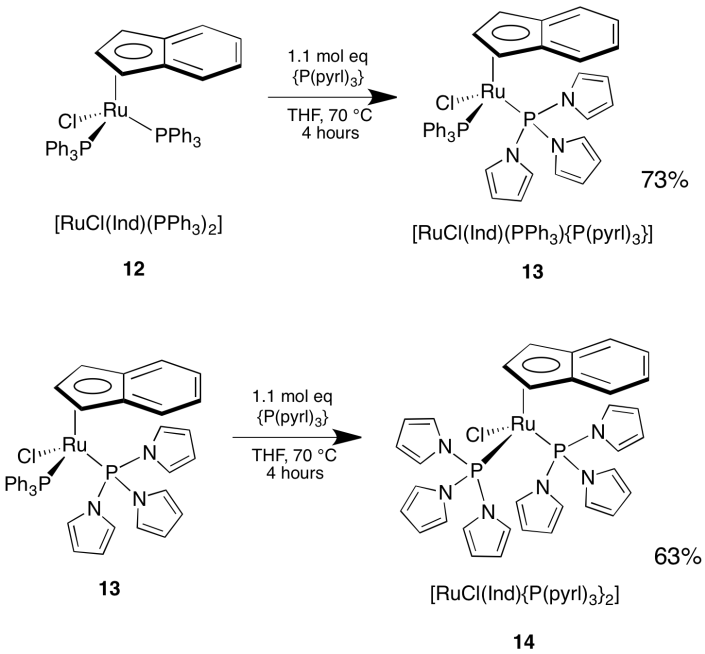

Scheme 2.1. Synthesis of the two new complexes [RuCl(Ind)(PPh_3){P(pyrl)$_3$}] (**13**) and [RuCl(Ind){P(pyrl)$_3$}$_2$] (**14**).

Two new metal complexes were synthesized and fully characterized for this study, [RuCl(Ind)(PPh_3){P(pyrl)$_3$}] (**13**) and [RuCl(Ind){P(pyrl)$_3$}$_2$] (**14**) (Scheme 2.1.). In both cases, the starting metal complex **12** was gently refluxed with the ligand {P(pyrl)$_3$} in freshly distilled THF under Schlenk conditions. The first substitution with the {P(pyrl)$_3$} ligand starting with the parent complex **12** gave a 73% isolated yield of the complex **13**. With complex **13**, the second substitution to give **14** was achieved in 63% isolated yield. Both metal complexes were recrystallized from dichloromethane layered with hexanes resting for several days at 0 °C to yield X-ray quality crystals. Both of these new metal complexes were fully characterized by standard methods of nuclear magnetic resonance (NMR), mass spectroscopy (MS), X-ray crystallography (X-ray), elemental analysis, and cyclic voltammetry (CV).

The ligand was only successfully substituted in diminishing yields through iteration. This is not necessarily surprising. The new complex should be less stable due to lower σ-donation of {P(pyrl)$_3$} when compared to how firmly PPh_3 coordinates to a metal center. Thus, the coordination of the new ligand to the metal association will be of lower quantity, and iterative substitution will return successively lower yields than the previous. This relationship has been demonstrated in a variety of metal complexes from the Nolan group, including similar ruthenium complexes that were used in this study.[18,21-23]

2.3.2. NMR Characterization

Each of the new complexes were characterized by NMR spectroscopy for three different nuclei, ^{1}H, $^{13}C\{^{1}H\}$, and $^{31}P\{^{1}H\}$. For reference, the free ligand {P(pyrl)$_3$} has a $^{31}P\{^{1}H\}$ NMR chemical shift of δ = 78.8 ppm in $CDCl_3$ solution, but shifts significantly

downfield when bound to the ruthenium indenyl metal complex. The complex [RuCl(Ind)(PPh_3){P(pyrl)$_3$}] (**13**) was found by X-ray to have a geometry with the two magnetically inequivalent phosphines in *cis* position to one another. This is corroborated by an expected set of two doublets in the $^{31}P\{^1H\}$ NMR spectrum, at 122.8 and 40.4 ppm with a $^2J_{P,P}$ coupling constant of 144 Hz. The doublets occur due to magnetically inequivalent phosphorus atoms; the two ligands PPh_3 and {P(pyrl)$_3$} have different electronic environments and thus relax within different timeframes. The twice-substituted complex [RuCl(Ind){P(pyrl)$_3$}$_2$] (**14**) has a singlet observed at δ = 122.2; both phosphines are identical in their magnetic environment and produce the same observable chemical shift in the $^{31}P\{^1H\}$ NMR spectrum, as expected. The ^1H NMR spectrum exhibited signals that were in accordance to literature for similar complexes: the aromatic region was heavy due to the PPh_3 ligands, there were three distinct signals for the three η^5–coordinated indenyl ring protons, and the pyrrole protons were observed as two distinct singlets in the olefinic region.[11,24] The $^{13}C\{^1H\}$ NMR spectrum did not indicate anything out of the ordinary, but some signals were difficult to assign in the aromatic region due to the large number of aromatic carbon atoms.

2.3.3. Cyclic Voltammetry

Using recrystallized samples, both of the new complexes were characterized by cyclic voltammetry (CV). This experimental method can give insight into the electronic properties of the new complexes, allowing for comparison of how the ligand substitution affects the oxidation potential to the parent complex. Voltammograms of the complexes are shown in Figure 2.1.; these scans were completed using conditions of 0.8 V/s in an

electrolyte solution of 0.1 M tetrabutyl ammonium chloride in CH_2Cl_2 at 298 K and referenced to decamethylferrocene in solution.

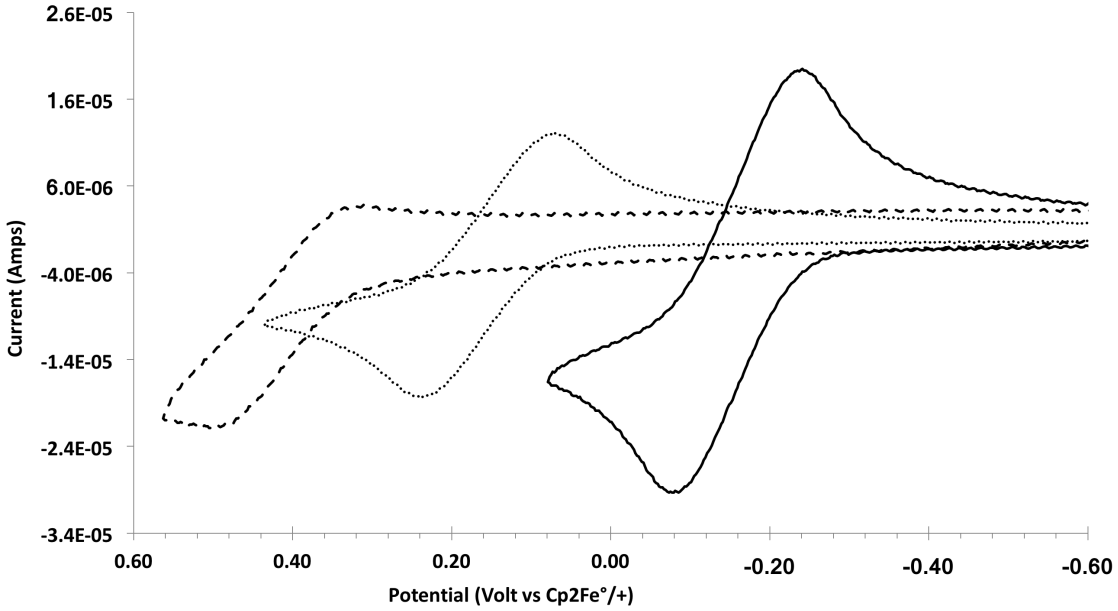

Figure 2.1. Cyclic voltammograms of [RuCl(Ind)(PPh_3)$_2$] (**12**, solid line), [RuCl(Ind)(PPh_3){P(pyrl)$_3$}] (**13**, dotted line), and [RuCl(Ind){P(pyrl)$_3$}$_2$] (**14**, dashed line).

Table 2.1. Oxidation potentials and reversibility for complexes **12**, **13**, and **14**.

Complex	E°' (Ru)	i_{pc}/i_{pa}
[RuCl(Ind)(PPh_3)$_2$] (**12**)	– 0.023	1.03
[RuCl(Ind)(PPh_3){P(pyrl)$_3$}] (**13**)	+ 0.345	1.02
[RuCl(Ind){P(pyrl)$_3$}$_2$] (**14**)	+ 0.706	0.73

Oxidation potentials are referenced to ferrocene. Ratio of reversibility obtained from scan rates of 0.8 mV/s.

The CV data collected for the parent complex **12** provides an ideal example in which to compare the electronic properties of the new complexes. The parent complex exhibited very nice redox reversibility as shown in the curve, indicating that oxidation and reduction of the metal complex happens smoothly over the range of voltage. The oxidation potential (*E*°' value, top peak of the curve) for the parent complex was measured to be –0.023 V (versus $Cp^*_2Fe^{0/+}$). Oxidation potentials are often used to compare metal complexes with varying substituents as the electronic properties within the molecule often manifest themselves in the ability to make the metal complex easier or more difficult to oxidize.[25] The complex [RuCl(Ind)(PPh_3){$P(pyrl)_3$}] (**13**) showed some degree of reversibility, while the complex [RuCl(Ind){$P(pyrl)_3$}$_2$] (**14**) generated an asymmetrical and poorly reversible curve. The oxidation potentials for the new complexes were higher than the parent complex and observed to be +0.34 and +0.71 V, respectively. The higher oxidation potentials for the two new complexes were expected; the π-acidity of the {$P(pyrl)_3$} ligand has been well-established and successive introduction of the electron–withdrawing ligand correlates to decreased electron density at the metal center caused by the ligands.[20]

2.3.4. X-ray Crystallography

The structure for each of the new complexes were determined by X-ray crystallography. A molecular structure representation is shown in Figure 2.2., while pertinent bond lengths and angles are given in Table 2.2. Corresponding values for the parent complex are available from literature and have been supplied for comparison.[26] All three of the complexes take on geometry typical of half-sandwich Ru complexes, often described as distorted octahedral as indicated by bond angles of 89.510(13)° to

99.008(14)° between the monodentate ligands.[24,27,28] The indenyl ligand appears to exhibit typical η^5–coordination with the π electrons in the smaller ring.[29] As well, those bond length and angles do not have any values that immediately appear to be out of the ordinary.

Table 2.2. Selected bond lengths (Å) and angles (°) from the X-ray structures.

	[RuCl(Ind)(PPh_3){$P(pyrl)_3$}] (**13**)	[RuCl(Ind){$P(pyrl)_3$}$_2$] (**14**)	[RuCl(Ind)(PPh_3)$_2$] (**12**)
Ru-P(1)	2.2323(15) *{P(Pyr)$_3$}*	2.2042(4)	2.3306(5)
Ru-P(2)	2.2760(14) *(PPh_3)*	2.2716(4)	2.2681(5)
Ru-Cl	2.4362(15)	2.4251(4)	2.4370(5)
P-N average [a]	1.712	1.716	–
P(1)-Ru-P(2)	97.89(5)	99.008(14)	99.205(18)
Cl-Ru-P(1)	93.51(5)	90.684(14)	92.423(17)
Cl-Ru-P(2)	91.79(5)	89.510(13)	92.187(18)
Ru-Cp [b]	1.902	1.928	1.918
Fold angle [c]	7.06°	7.33°	7.07°

[a] P–N average is the distance between P and N in {$P(pyrl)_3$}. [b] Distance between the Cp centroid of the indenyl ligand and the ruthenium center. [c] Fold angle refers to the pucker of the 5-membered ring of indene that binds to the ruthenium center.

Notably, the Ru–P bond lengths in all three complexes fall within the range from 2.2042(4) to 2.3306(5) Å. Neither of the new structures offer significant variation from the parent complex; in the parent complex, one Ru–P is longer than the other, and this trait exists in both new structures as well. The Ru–P bond lengths on the {$P(pyrl)_3$}–

containing complexes are slightly shorter than those in the parent complex. This may be the result of increased backbonding to the {P(pyrl)$_3$} ligand from the ruthenium center. Moloy et al have demonstrated this π–acceptor character of the {P(pyrl)$_3$}ligand in rhodium complexes.[15] No clear trend can be discerned from bond lengths from the metal center to the centroid of the Cp ring or the chloride atom as they are similar values for each complex.

One particular parameter of interest is the P(1)–Ru–P(2) bond angles. For both [RuCl(Ind)(PPh$_3$)$_2$] (**12**) and [RuCl(Ind){P(pyrl)$_3$}$_2$] (**14**), the angle between the phosphines is similar (99.205(18)° to 99.0008(14)° respectively). However, the [RuCl(Ind)(PPh$_3$){P(pyrl)$_3$}] (**13**) complex has a slightly smaller P(1)–Ru–P(2) bond angle of 97.89(5)°. One reason we offer for this difference is the possibility of steric repulsions between the PPh$_3$ and {P(pyrl)$_3$} ligands could be pushing them further apart. It should be noted that roughly 2° is far from a significant deviation and as a result this may not affect the overall stability of the complex. Again, these angles are different from what would be expected in an octahedral (90°) or tetrahedral (109.5°) geometry, which leads to the apt description of distorted octahedral.

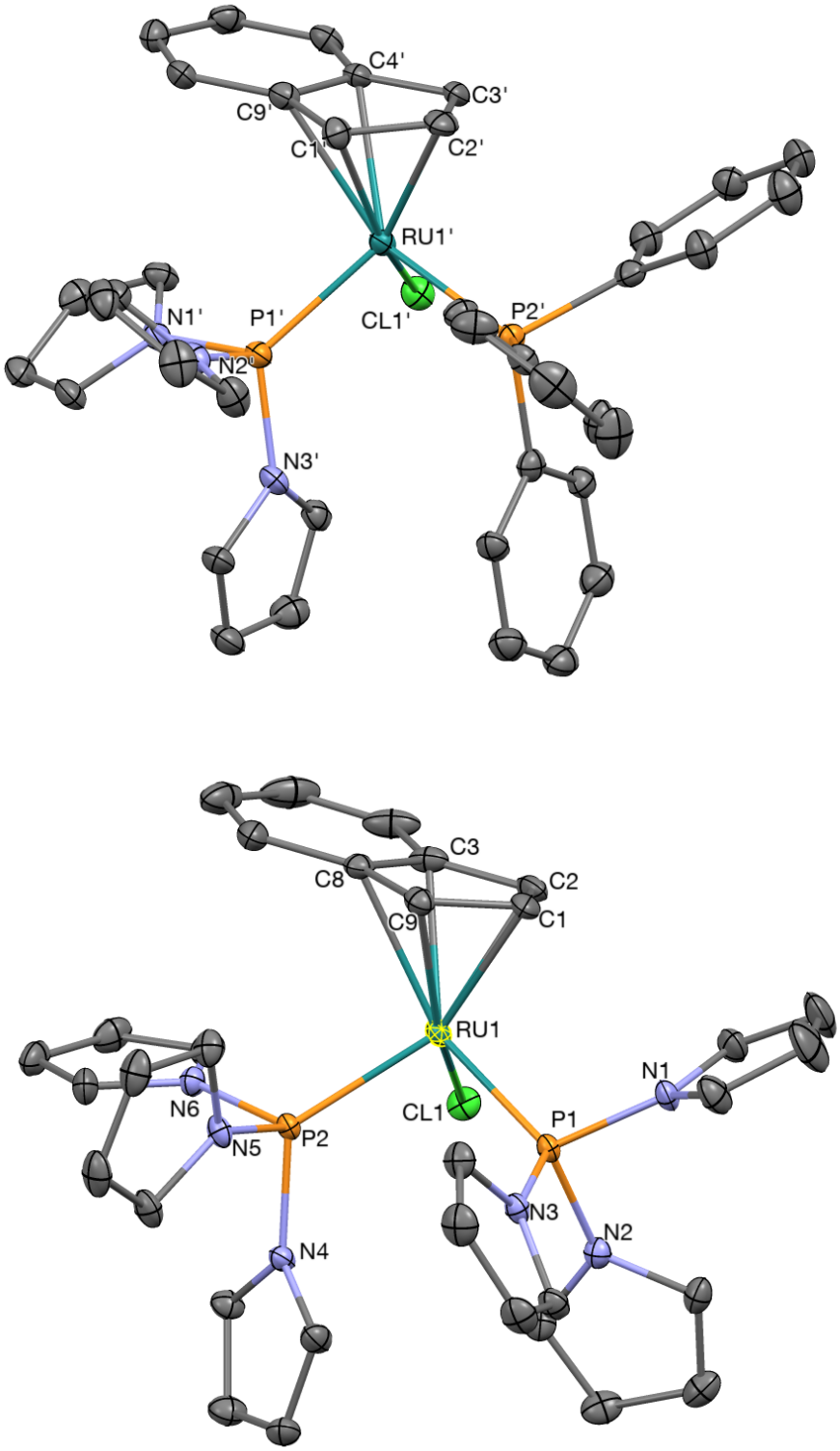

Figure 2.2. Molecular structures for [RuCl(Ind)(PPh_3){P(pyrl)$_3$}] (**13**, top) and [RuCl(Ind){P(pyrl)$_3$}$_2$] (**14**, bottom). Structures are depicted as 50 % probability ellipsoids, with hydrogen atoms and solvent molecules removed for clarity.

2.3.5 Catalyst Activation

Both of the new complexes were found to be catalytically inactive up to 100 °C in toluene for propargylic etherification reactions using a propargylic alcohol as a substrate and a benzyl alcohol as a nucleophile. These conditions were found to be effective in previous work from our laboratory and were chosen to test the complexes for any reactivity.[30] To make a complex more reactive, we chose to try to abstract the chloride from the metal complex, generating a catalytically active ruthenium complex with an open coordination site. The method of abstraction was treatment of the metal complex with triethyloxonium hexafluorophosphate ($Et_3O^+PF_6^-$). In this method (Scheme 2.2.), the partially negatively charged chloride on the ruthenium can attack a partially positive carbon atom on one of the ethyl substituents of the Et_3O^+ cation, yielding an 'open coordination site' on the metal complex. The resulting ruthenium complex was expected to then be catalytically active, as previous literature had used this same method for 'activating' a metal complex using silver salts.[31,32]

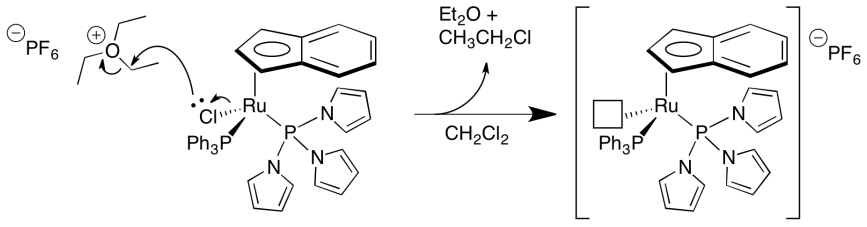

Scheme 2.2. Chloride abstraction with $Et_3O^+PF_6^-$.

Characterization of the active complex was attempted, but data was not conclusive. The NMR spectra were difficult to interpret; it appeared that after this 'activation' step,

the metal complexes produced a variety of possible decomposition products. Without reasonable data, precise mechanistic details of how the catalyst worked could not be provided alongside of the results for catalysis. An example of this NMR spectra is shown in Figure 2.3., before and after 'activation'. For reference, PPh_3 and other similar phosphines occur near $\delta = -5$ ppm and $O{=}PPh_3$ occurs at approximately $\delta = 26$ ppm in $^{31}P\{^1H\}$ NMR.[33-35] As seen in the spectra, a significant amount of phosphine decomposition products are created upon treatment of the once–clean metal complex.

While there is an amount of decomposition product present in the spectrum, it does appear that the starting material complex is completely absent and a new complex has taken its place. The original doublets of complex **13** have now shifted by a small amount after chloride abstraction, where the doublet at ~ δ = 122.8 ppm has shifted downfield to ~ δ = 125.8 ppm and the doublet at ~ δ = 40.4 ppm has shifted upfield to ~ δ = 38.2 ppm. This is significant, as it demonstrates that both the PPh_3 and $P(pyrl)_3$ are still coordinated to the metal complex. The peaks appearing around δ = 0 ppm are tentatively identified as free phosphines. The intensity of the peaks is not indicative of amounts of materials in the sample; as coordinated ligands are subjected to a higher degree of shielding, their signals appear weaker than that of free ligands.

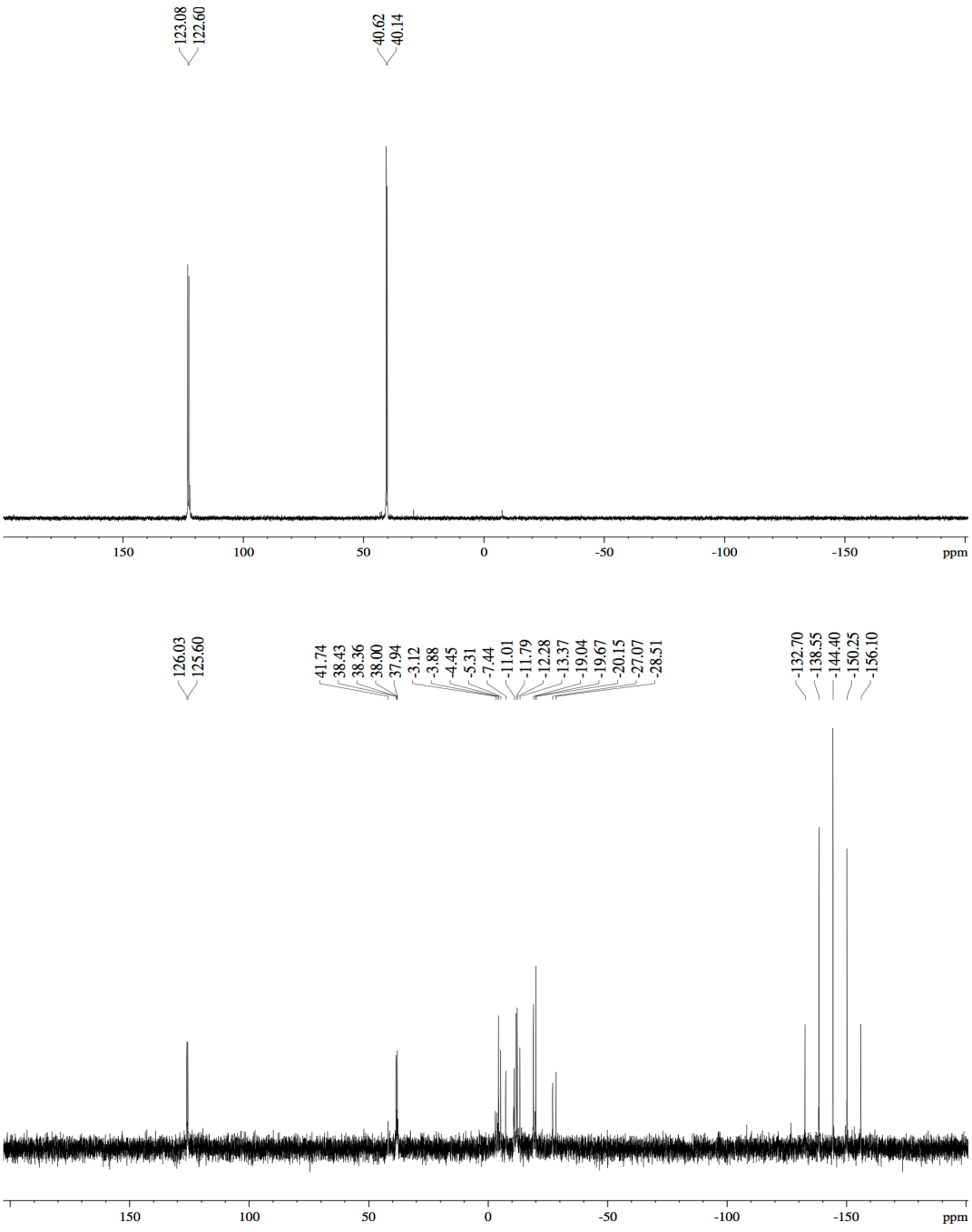

Figure 2.3. The complex [RuCl(Ind)(PPh_3){P(pyrl)$_3$}] (**13**, top) was treated with $Et_3O^+PF_6^-$ for 'activation' (bottom).

2.3.6. Catalytic Applications of the New Complexes

The two new complexes were tested in catalytic applications, starting with propargylic alcohols to give propargylic ethers. Yields varied for these etherification

reactions, where the propargylic alcohol was combined with a substrate alcohol to create an ether. The results are summarized here in Table 2.3. Yields ranged from 27 to 42 %. It can be noted that the yields did not exceed what has already been published in literature.[36,37] Screening reaction conditions lead to the finding that neither complex showed catalytic activity at temperatures lower than 70 °C. Best results were obtained when time and temperature conditions exceeded 16 hours and 90 °C. Previous literature demonstrated that toluene was a solvent of choice for similar reactions and that remained true for our catalyst system.[30]

Upon further investigation, we found that the complexes were catalytically active in condensation reactions involving diketones and propargylic alcohols. These results are presented in Table 2.4. The products obtained in this series of reactions was determined to be products of aldol condensation reactions that formed after a Meyer-Shuster rearrangement of the propargylic alcohol to the corresponding aldehyde, which were then followed by a cyclization.[38] The reaction is shown here in Scheme 2.3. Conditions were screened to optimize the yields obtained. Relatively non-polar solvents such as cyclohexane, toluene, and 1,2-dichloroethane proved to be useful in increasing yields, as the tautomerization equilibrium favors the ketone in non-polar solvents.[39] We believe product yields were lower in polar solvents as the keto-enol tautomerization equilibrium of the diketone resulted expedient polymerization of the diketone substrate, as observed by disappearance of that starting material in GC chromatographs.

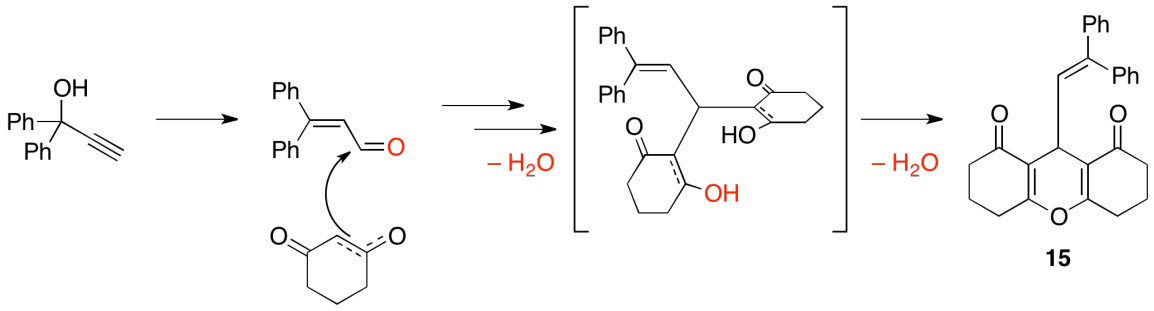

Scheme 2.3. Condensation of propargylic alcohols and diketones to form xanthenones.

Table 2.3. Isolated yields of etherification reactions.

Table y. Isolated Yields.

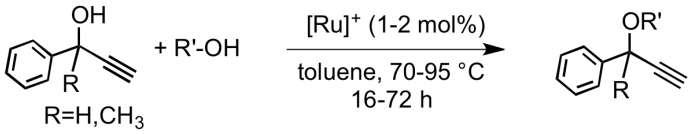

Entry [a]	Substrates	Product	Yield / %
1	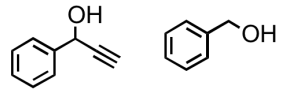	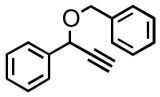	38 [b]
2	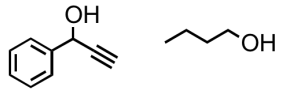	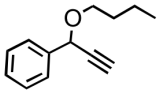	37 [b]
3	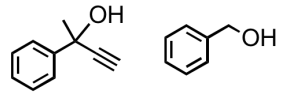	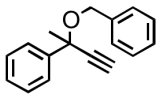	42 [c]
4	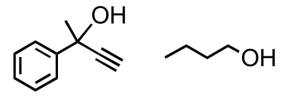	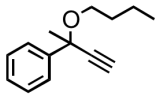	41 [d]
5	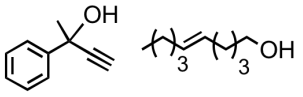	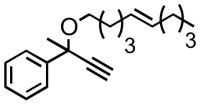	27 [c]

[a] General conditions: Propargylic alcohol (0.7 mmol) and alcohol R'-OH (1 mmol) in toluene (2 mL) catalyzed by $[Ru(Indenyl)(PPh_3)\{P(pyr)_3\}]^+$ (0.007 mmol). The products were isolated chromatographically.
[b] 70 °C for 16 h. [c] 85 °C for 18 h. [d] 95 °C for 72 h.

Table 2.4. Isolated yields of enol-addition-condensation reactions.

Entry	Substrates	Product	
1 [a]	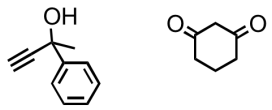	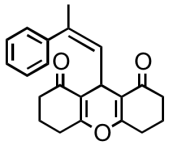	22% [b] 34% [c]
2 [a]	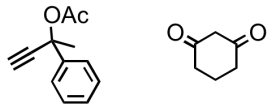	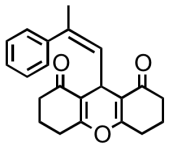	46% [b] 67% [c]
3 [a]	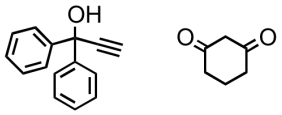	**15** 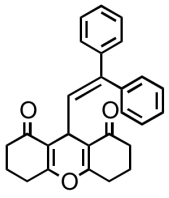	69% [c]
4 [d]	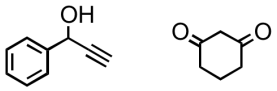	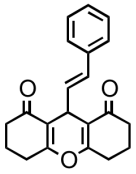	29% [c]
5 [e]	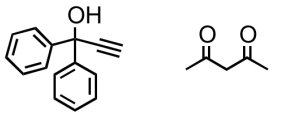	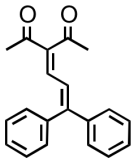	34% [b] 40% [c]
6 [f]	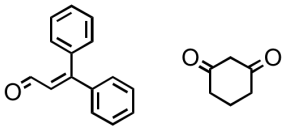	**15** 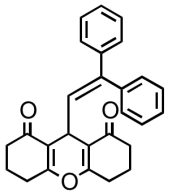	32% [c]

[a] Conditions: 2.5 mol equivalents dione, in 1,2-dichloroethane (2 mL) for 72 hours at 80-95 °C. The products were isolated chromatographically.
[b] Catalyst 1-2 mol% $[Ru(Indenyl)\{P(pyr)_3\}_2]^+$.
[c] Catalyst 1-2 mol% $[Ru(Indenyl)(PPh_3)\{P(pyr)_3\}]^+$.
[d] Conditions: 2.5 mol equivalents diketone, in cyclohexane (2 mL) for 16 hours at 90 °C. The products were isolated chromatographically.
[e] Conditions: 2.5 mol equivalents diketone, in 1,2-dichloroethane (2 mL) for 18-48 hours at 85-90 °C. The products were isolated chromatographically.
[f] Conditions: 2.5 mol equivalents diketone, in 1,2-dichloroethane (2 mL) for 18 hours at 85 °C. 4 mol% catalyst loading.The product was isolated chromatographically.

2.3.7. Reactivity Studies for Hammett Plot

In an effort to help determine the mechanism by which the reactions proceed, a series of etherification reactions were conducted with different substituents in the *para* position on the aryl rings adjacent to the reaction site on the propargylic alcohol substrate molecule. This type of study results in a Hammett plot (Figure 2.4) that demonstrates the extent of the linear relationship between kinetics of a reaction and its equilibrium constants specific for the reaction.[40] A series of experiments varying from electron-withdrawing and electron-donating para-substituents on the phenyl ring adjacent to the alcohol leaving group may help us determine if the reaction builds up a positive charge, negative charge, or no charge at that reaction site. The established reaction of a terminal propargylic alcohol, benzyl alcohol, in deuterated toluene with the catalyst synthesized from **13** after treatment with Et_3OPF_6 was used to determine product formation over time. Equilibrium values that were used in calculating reactions rates were determined by integration of peaks in the NMR spectra. Spectra were acquired at consistent intervals to minimize errors. The k/k_0 values were determined and plotted against the σ values for the substituents to give the graph in Figure 2.4.

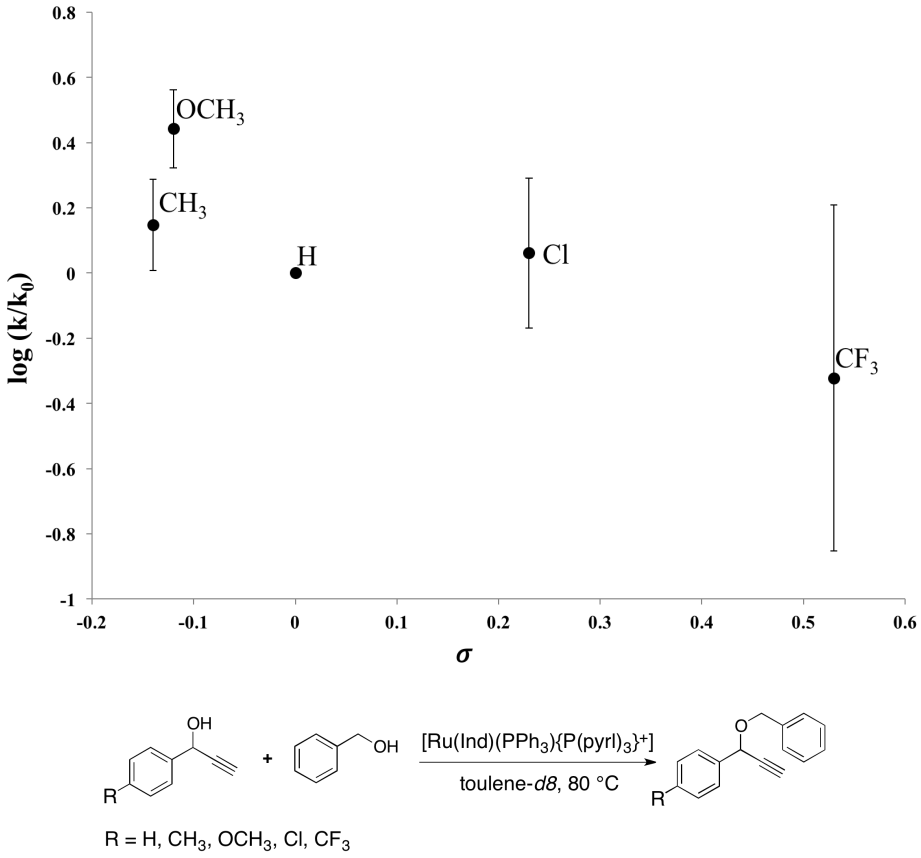

Figure 2.4. Hammett plot utilizing *p*-substituted propargylic alcohols.

2.4. Discussion

2.4.1. Catalyst Activation

Activation of a metal complex for catalysis is common in literature; it is often achieved by the addition of one or two additives to the reaction mixture. A frequently-used example of catalyst activation is the addition of NH_4PF_6 in equimolar amount to the ruthenium complex to generate a catalytically active species *in situ* through chloride abstraction.[41-43] While this practice is prevalent, the underlying examination of what is happening to the metal complex is often left undone. Good results are accepted at face value and understanding of the mechanism is little more than what can be concluded from

a table of different additives in the reaction mixture. This is acceptable for most applications. However, for a project that attempts systematic investigation of ligand modification in metal complexes to improve catalytic activity, the identification of the catalytically active species has significant importance.

We attempted to gain more understanding of the mechanism of the etherification reaction by looking at the metal complex before, during, and after the catalysis by NMR. Each catalyst was fully characterized prior to catalytic application, so any transformations of the catalyst during the reactions should have been easily discerned. However, examination of the catalyst in spectra during or after catalysis proved to be a difficult task; even the simple $^{31}P\{^{1}H\}$ spectra had changed to an extremely complex mixture of signals. Thus, the catalytically active species seems to be a stable form of the chloride abstracted species, but remains inconclusively identified.

2.4.2. Catalytic Results

Etherification of propargylic alcohols using ruthenium complexes has been well studied.[30,36,37] The etherification reactions presented in this study underperform when compared to previous literature. Yields ranging from 27 – 42 % fell short of expectations. For example, Zhan and coworkers published propargylic substitution reactions using common Lewis acids, $FeCl_3$ and $BiCl_3$, with ether yields for internal and terminal propargylic alcohols in upwards of 92 %.[44,45] Nishibayashi and coworkers obtained yields over 50 % using ruthenium complexes.[37]

The conditions required for these etherification reactions to take place are also more undesirable than what has been previously published. Of the studies previously mentioned above, room temperature to slightly elevated temperatures were required for

catalysis. In some of those cases, reaction time was as little as one hour to completion. In a previous study, our lab presented Ru-based catalytic etherification at 100 °C in toluene for 18 hours.[30] This study required similar conditions. These higher temperatures and longer timeframes are undesirable for the synthesis of more complex molecules at the industrial scale. Thus, using the ruthenium complexes presented in this study for etherification reactions does not seem to offer any advantages for this reaction.

We had intended to explore new opportunities for substrates and with this catalyst in hand we chose carbon-centered nucleophilic addition. Carbon-carbon bond formation was of interest and diketones seemed to be an attractive starting point of a molecule to be employed as a nucleophile. Using a variety of propargylic alcohols with either 1,3-cyclohexanedione or 2,4-pentanedione, we found that xanthenone derivatives (Table 2.3., entries 1–4) could be obtained in yields ranging from 22 – 69 %. Xanthenones are polyheterocyclic molecules that have been acknowledged for a range of therapeutic uses including receptor antagonists to inhibit HIV activity, obesity, or tumor growth.[31,46-49]

We suspected the products were due to an initial Meyer-Schuster rearrangement of the propargylic alcohol, followed by an aldol condensation (Scheme 2.3.). This particular series of transformations to propargylic alcohols had previously been published by Sanz and coworkers, using Brønsted acid conditions.[50] The original study of rearrangements by Meyer and Schuster subjected propargylic alcohols to acetic acid and heat to form vinyl aldehydes.[51] In retrospect, with the knowledge of that this series of products can be formed using Brønsted acids and of the rearrangement of the propargylic alcohol, we cannot rule out the possibility that a Brønsted acid formed during the reaction.

As stated previously, Scheme 2.3. lays out the probable mechanism of the rearrangement-condensation that leads to xanthenone **15**. To test this, we employed a vinyl aldehyde in place of the propargylic alcohol and obtained the same product, albeit in lower yield (Table 2.4., entry 5). The xanthenone products were characterized by NMR, mass spec, and X-ray for xanthenone **15**, which is shown here in Figure 2.5.

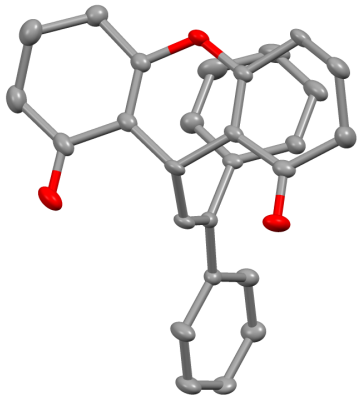

Figure 2.5. Molecular Structure of 9-(2,2-Diphenylvinyl)-3,4,5,6,7,9-hexahydro-1H-xanthene-1,8(2H)-dione (**15**), product of Table 2.3., entry 3. Hydrogen atoms and solvent molecules omitted for clarity.

2.4.3. Mechanism of Etherification Reactions

We attempted to gain further understanding of the mechanism by which the etherification reactions were proceeding by development of a Hammett plot. Using the Hammett equation, a series of reactions using modified substituents may elucidate the charge buildup occurring at the reaction site. In the current model of propargylic substitution reactions, we are in agreement with literature that suggests a positive or partial positive charge buildup occurs at the carbon atom bearing the leaving group in the transition state of the molecule (Scheme 2.4.).

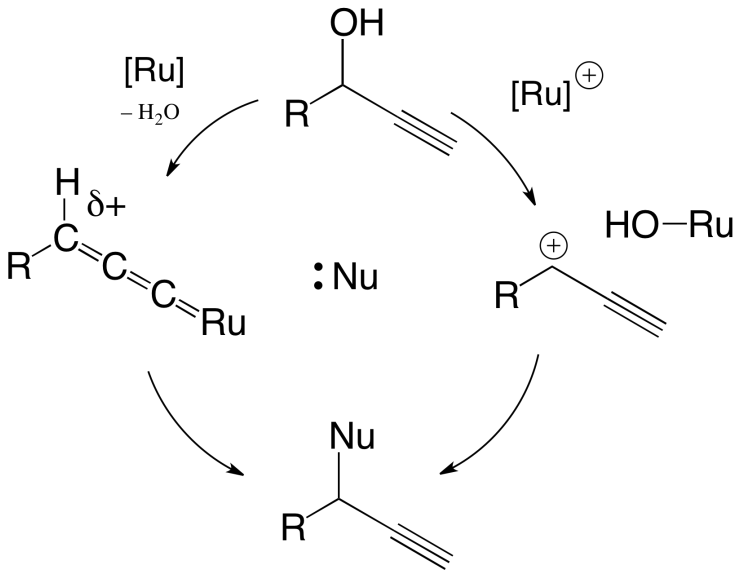

Scheme 2.4. Propargylic etherification mechanism taking either the allenylidene (left) pathway or the Lewis acid and carbocation (right) pathway.

To investigate a potentially charged intermediate, we used a series of *para*-substituted propargylic alcohols in etherification reactions and followed progress over time. In the resulting plot, the slope (ρ) indicates either a positive or negative charge buildup; a slope less than zero is associated with a positive charge buildup and a slope greater than zero is associated with a negative charge buildup. To illustrate how the Hammett plot can be helpful, the dichotomy that the relationship creates is presented in Figure 2.6.

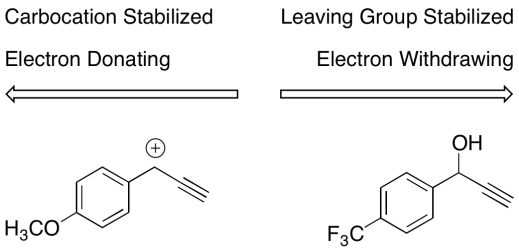

Figure 2.6. In the Hammett plot, electron donating substituents help stabilize a positive charge buildup at the center of the reaction, increasing the speed of the reaction. Electron withdrawing groups will slow down the reaction by stabilizing the leaving group.

The Hammett plot given in Figure 2.4., is constructed with error bars of the observed ρ-value by their standard deviation. Lack of a linear Hammett plot is quite common, especially in studies with complex reaction mechanisms.[52,53] Non-linear data from the Hammett plot is often ascribed to a change in the rate-determining step of the reaction.[54,55] In the plot in Figure 2.4., we observe a somewhat linear relationship; this study examined five substituents and the errors may be too high to firmly establish a complete picture of the mechanism. The plot exhibits a slight negative slope, which is indicative of a positive charge buildup in the rate–determining step. While the plot does not make an unequivocal case for a positively charged transition state, it provides no indication of negative charge buildup, nor is there an indication of a radically different rate-determining step.[55]

A more confident observation of this study is that the error of measurement seemed to grow disproportionately with the use of increasingly electron-withdrawing substituents. This suggests that the rate at which the OH^- group dissociates from the transition state is far more significant than the metal association step.[55,56] This error could also be an indication that the mechanism that actually facilitates the OH^- leaving the molecule is somewhat inconsistent, or that the mechanism differs depending on the substituent at the aromatic ring. This should eventually lead us to the hypothesis that perhaps both of the allenylidene and Lewis acid carbocation mechanisms (Scheme 2.4.) may operate in the reaction mixture concomitantly during the reaction, as the extent of the positive charge buildup is inconsistent with solely one or the other model. Therefore, while the evidence presented could not firmly establish a mechanism for propargylic etherification, we have a slightly better understanding of it.

2.5 Summary

This project attempted to compare ligand effects on catalysis by systematically modifying ligands attached to the metal center in [RuCl(Ind)(PPh_3)(L)] systems. Two new metal complexes were synthesized and characterized. Activation of the metal complexes into catalysts required the use of an additive, which generated the catalytically active species along with a mixed uncoordinated phosphine ligands in solution. A handful of catalysis examples with secondary and tertiary propargylic etherification reactions resulted in moderate isolated yields of 27 – 42 %. The two complexes were also observed to have reactivity in rearrangement–condensation reactions of diketones. In both cases, reaction conditions required higher temperatures of up to 95 °C. Under these circumstances, the use of tris(*N*-pyrrolyl) phosphine as a ligand for this systematic study did not grant isolated yields greater than previously published studies. By employing the metal complexes in catalytic applications outside of etherification, the new method of synthesis of xanthenones was demonstrated with isolated yields of 22 – 69 %. As well, Hammett plot reactivity studies offered insight into possible etherification reaction mechanisms.

2.6. Experimental

General.[57]

All reactions except for catalysis were carried out under an inert N_2 atmosphere using standard Schlenk techniques. All chemicals were used as supplied from Sigma-Aldrich unless otherwise noted. [RuCl(Ind)(PPh_3)$_2$] was synthesized according to literature

procedures.[4] THF was distilled from Na/benzophenone under N_2. Pentane, hexane, toluene, CH_2Cl_2, and diethyl ether were used as received. Pyrrole was vacuum distilled over $CaCl_2$. Triethylamine (Et_3N) was vacuum distilled over KOH. All propargylic alcohols, alcohols and ketones were obtained and used as provided from Sigma-Aldrich, unless otherwise specified. 1-phenyl-2- propyn-1-ol was synthesized according to literature procedures for a Grignard reaction of benzaldehyde and ethynylmagnesiumbromide.[58,59]

NMR spectra for characterization were collected at room temperature on a Varian Unity 300 MHz or Bruker Avance 300 MHz instrument; all chemical shifts (δ) are reported in ppm and are referenced to a residual solvent signal. IR spectra were collected on a Thermo Nicolet 360 FT-IR spectrometer. FAB and exact mass data were collected on a JEOL MStation [JMS-700] mass spectrometer. Melting points were determined on a Thomas Hoover uni-melt capillary melting point apparatus and are uncorrected. Elemental analyses were performed by Atlantic Microlab Inc., Norcross, GA, USA.

N-pyrrolyl phosphine, P(pyrl)$_3$.

N-pyrrolyl phosphine was synthesized via a modified literature procedure as described by Moloy.[15] Pyrrole (9.7 g, 144 mmol), Et_3N (14.6 g, 144 mmol), and freshly distilled THF (150 mL) were placed in a three-neck 250 mL round-bottom flask via syringe transfer. The solution was allowed to stir at −78 °C for 10 min prior to quick addition of phosphorus trichloride (PCl_3, 5.7 g, 42 mmol) via syringe. The pale-yellow solution was allowed to stir for an additional 30 minutes at −78 °C and then at room temperature overnight, affording a dark yellow solution and a white precipitate. The solids were removed by vacuum filtration and the THF volume was reduced via rotary

evaporation to a minimum of solvent. The product was obtained through recrystallization using cold pentane, isolated by vacuum filtration as an off-white solid, 37% yield (3.5 g, 15 mmol). Spectroscopic data matched what has previously been described.[2] ^{1}H NMR ($CDCl_3$): δ = 6.84 (m, 6H), 6.41 (t, 6H); $^{31}P\{^{1}H\}$ NMR ($CDCl_3$): δ = 78.8.

*[RuCl(ind)(PPh_3){P(pyrl)$_3$}] (**13**).*

A Schlenk flask containing [RuCl(ind)(PPh_3)$_2$] (0.658 g, 0.848 mmol), P(pyrl)$_3$ (0.214 g, 0.932 mmol), and THF (8 mL) was heated gently under reflux for 4 h under nitrogen. The solvent was removed in vacuo. The complex was isolated as a red solid (0.462 g, 0.622 mmol, 73 %) by column chromatography (silica gel 2 × 15 cm, CH_2Cl_2 as eluent); m.p. 120–122 °C (dec.).

^{1}H NMR (300 MHz, $CDCl_3$): δ = 7.51–7.45 (m, 6 H, arom.), 7.33–7.13 (m, 13 H, arom.), 6.14 (br s, 6 H), 6.03 (br s, 6 H), 4.86 (s, 1 H, ind), 4.75 (s, 1 H, ind), 4.54 (s, 1 H, ind) ppm. $^{13}C\{^{1}H\}$ NMR (75 MHz, $CDCl_3$) δ 136.9 (d, $J_{C,P}$ = 42.6 Hz), 133.5 (d, $J_{C,P}$ = 10 Hz), 129.8 (s), 129.6 (s), 129.5 (s), 128.2 (d, $J_{C,P}$ = 9.5 Hz), 124.9 (s), 124.4 (s), 124.2 (d, $J_{C,P}$ = 6 Hz), 114.8 (s), 114.7 (s), 111.2 (d, $J_{C,P}$ = 6.5 Hz), 93.9 (s), 70.5 (d, $J_{C,P}$ = 7.5 Hz), 68.3 (d, $J_{C,P}$ = 6.0 Hz) ppm. $^{31}P\{^{1}H\}$ NMR (121 MHz, $CDCl_3$): δ = 122.81 (d, $J_{P,P}$ = 144 Hz), 40.37 (d, $J_{P,P}$ = 144 Hz) ppm. IR (neat, solid): $\tilde{\nu}$ = 3133 (w), 3052 (w), 2962 (w), 2359 (w), 1454 (m), 1437 (m), 1287 (w), 1178 (s), 1056 (s), 1036 (s), 732 (s), 696 (m), 623 (m) cm^{-1}. HRMS: calcd. for $C_{39}H_{34}N_3P_{21}0_2Ru$ [Ru(ind){P(pyr)$_3$}$_2$]$^{+}$ 708.1249; found 708.1282. $C_{39}H_{34}ClN_3P_2Ru$ (743.09): calcd. C 63.03, H 4.61; found C 62.77, H 4.59.

*[RuCl(ind){P(pyrl)$_3$}$_2$] (**14**).*

A Schlenk flask containing [RuCl(ind)(PPh$_3$){P(pyrl)$_3$}] (0.140 g, 0.188 mmol), P(pyrl)$_3$ (0.086 g, 0.380 mmol), and THF (5 mL) was heated gently under reflux for 5 h under nitrogen. The solvent was removed in vacuo. The complex was isolated as an orange-yellow solid (0.083 g, 0.117 mmol, 62 %) by column chromatography (silica gel 2 × 15 cm, CH_2Cl_2 as eluent); m.p. 126–128 °C (dec.).

^{1}H NMR (300 MHz, $CDCl_3$): δ = 7.19–7.16 (m, 4 H, arom.), 6.40 (d, $J_{H,H}$ = 1.8Hz, 12H), 6.17 (d, $J_{H,H}$ = 1.8Hz, 12H), 5.21 (br s, 2H, ind), 4.75 (br s, 1H, ind) ppm. ^{13}C{^{1}H} NMR (75 MHz, $CDCl_3$): δ = 131.1 (s), 124.4 (s), 124.2 (s), 112.9 (s), 112.4 (s), 96.1 (s), 70.8 (s) ppm. ^{31}P{^{1}H} NMR (121 MHz, CDCl3): δ = 122.2 (s) ppm. IR (neat, solid): $\tilde{\nu}$ = 3127 (w), 3106 (w), 1453 (m), 1176 (s), 1083 (m), 1055 (s), 1033 (s), 736 (s), 712 (s), 703 (m), 614 (m) cm^{-1}. HRMS: calcd. for $C_{33}H_{31}N_6P_21_02Ru$ [Ru(ind)(PPh$_3$){P(pyr)3}]$^+$ 675.1138; found 675.1140. $C_{33}H_{31}ClN_6P_2Ru$ (710.08): calcd. C 55.82, H 4.40; found C 55.80, H 4.32.

Activation of Metal Complexes through Chloride Abstraction.

[RuCl(ind)(PPh$_3$){P(pyrl)$_3$}] was placed into a Schlenk tube, along with a molar equivalent of triethyloxonium hexafluorphosphate (Et_3OPF_6), and CH_2Cl_2. The mixture was stirred under N_2 for 2-4 hours, followed by removal of the solvent via vacuum to isolate the activated catalyst as a dark tan solid.

*Propargyl Ethers***.**

(1-(benzyloxy)prop-2-yn-1-yl)benzene.[30]

To a small screw-cap vial containing 1-phenylprop-2-yn-1-ol (0.100 g, 0.76 mmol), benzyl alcohol (0.102 g, 0.95 mmol) was added, along with toluene (2 mL). The activated

catalyst was added (0.010 g, 0.007 mmol, 0.9 mol-%) and mixture was heated at 70 °C for 48 hours. The product was isolated by column chromatography (silica gel, 1.5×15cm, 2:1 hexane/CH_2Cl_2) as a yellow-orange oil (0.065 g, 0.29 mmol, 38%). ^{1}H NMR (300 MHz, $CDCl_3$): δ = 7.61-7.60 (m, 2H, arom.), 7.46-7.39 (m, 8H, arom.), 5.30 (d, J_{HH}=2 Hz, 1H, C*H*), 4.78 (d, J_{HH}=11.7 Hz, C*H*2, 2H), 2.76 (d, J_{HH}=2 Hz, ≡C*H*, 1H). ^{13}C{^{1}H} NMR (75 MHz, $CDCl_3$): δ = 138.5 (s), 137.9 (s), 128.8 (s), 128.7 (s), 128.4 (s), 128.1 (s), 127.7 (s), 81.9 (s), 76.1 (s), 70.6 (s), 70.3 (s).

(1-butoxyprop-2-yn-1-yl)benzene.[30]

To a small screw-cap vial containing 1- phenylprop-2-yn-1-ol (0.103 g, 0.78 mmol), n-butanol (0.071 g, 0.96 mmol) was added, along with toluene (2 mL). The activated catalyst (0.010 g, 0.007 mmol, 0.9 mol-%) and the mixture was heated at 70 °C for 48 hours. The product was isolated by column chromatography (silica gel, 1.5×15 cm, 2:1 hexane/CH_2Cl_2) as a yellow oil (0.055 g, 0.29 mmol, 37%). ^{1}H NMR (300 MHz, $CDCl_3$) δ 7.60-7.57 (m, 2H, arom.), 7.46-7.37 (m, 3H, arom.), 5.21 (d, 3 J_{HH}=2 Hz, 1H, C*H*), 3.77-3.71 (m, 1H, C*H*H'), 3.60-3.53 (m, 1H, CH*H*'), 2.67 (d, J_{HH}=2 Hz, 1H, ≡C*H*), 1.71-1.64 (m, 2H, CH_2), 1.51-1.43 (m, 2H, CH_2), 0.98 (t, J_{HH}=7 Hz, 3H, C*H*3). ^{13}C{^{1}H} NMR (75 MHz, $CDCl_3$) δ 138.8 (s), 128.6 (s), 128.5 (s), 127.4 (s), 82.3 (s), 75.4 (s), 71.5 (s), 68.5 (s), 31.9 (s), 19.5 (s), 14.0 (s).

(2-(benzyloxy)but-3-yn-2-yl)benzene.[30]

To a small screw-cap vial containing 2-phenyl- 3-butyn-2-ol (0.105 g, 0.72 mmol), benzyl alcohol (0.154 g, 1.4 mmol) was added, along with toluene (2 mL). The activated catalyst was added (0.010 g, 0.007 mmol, 1 mol-%) and the mixture was heated at 100 °C for 72 hours. The product was isolated by column chromatography (silica gel, 1.5×15 cm,

2:1 hexane/CH_2Cl_2) as a dark yellow oil (0.071 g, 0.30 mmol, 44%). ^{1}H NMR (300 MHz, $CDCl_3$) δ 7.52-7.38 (m, 10H, arom.), 4.71 (s, 2H, C*H*), 2.91 (s, 1H, ≡C*H*), 1.96 (s, 3H, C*H*$_3$). ^{13}C{^{1}H} NMR (75 MHz, $CDCl_3$) δ 142.8 (s), 138.8 (s), 128.6 (s), 128.5 (s), 128.1 (s), 128.0 (s), 127.6 (s), 126.2 (s), 84.3 (s), 76.5 (s), 75.9 (s), 67.4 (s), 33.1 (s).

(1-butoxybut-3-yn-2-yl)benzene.[30]

To a small screw-cap vial containing 2-phenyl-3-butyn-2-ol (0.099 g, 0.68 mmol), n-butanol (0.194 g, 2.62 mmol) was added, along with toluene (2 mL). The activated catalyst (0.007 g, 0.008 mmol, 1.2 mol-%) was added and the mixture was heated at 95 °C for 72 hours. The product was isolated by column chromatography (silica gel, 1.5×15 cm, 2:1 hexane/CH_2Cl_2) as a yellow oil (0.063 g, 0.28 mmol, 42%). ^{1}H NMR (300 MHz, $CDCl_3$) δ 7.54-7.51 (m, 2H, arom.), 7.28-7.17 (m, 3H, arom.), 3.53-3.45 (dt, J_{HH}=7 Hz, J_{HH}=7 Hz, 1H), 3.07-2.99 (dt, J_{HH}=7 Hz, J_{HH}=7 Hz, 1H), 2.59 (s, 1H, ≡C*H*), 1.64 (s, 3H, C*H*3), 1.46 (quint, 2H, CH_2), 1.32-1.24 (m, 2H, CH_2), 0.80 (t, J_{HH}=7 Hz, 3H, C*H*3). ^{13}C{^{1}H} NMR (75 MHz, $CDCl_3$) δ 143.2 (s), 128.4 (s), 127.9 (s), 126.0 (s), 84.5 (s), 75.8 (s), 75.3 (s), 64.8 (s), 32.5 (s), 33.1 (s), 19.6 (s), 14.1 (s).

(E)-(2-(dec-5-en-1-yloxy)but-3-yn-2-yl)benzene.

To a small screw-cap vial containing 2-phenyl-3-butyn-2-ol (0.058 g, 0.389 mmol), *trans*-5-decen-1-ol (0.099 g, 0.634 mmol) was added, along with toluene (2 mL). The activated catalyst was added (0.006 g, 0.007 mmol, 1.8 mol-%) and the mixture was heated at 85 °C for 18 hours. The product was isolated by column chromatography (silica gel, 1.5×15 cm, 2:1 hexane/CH_2Cl_2) as a yellow oil (0.029 g, 0.103 mmol, 27%). ^{1}H NMR (300 MHz, $CDCl_3$) δ 7.53-7.50 (m, 2H, arom.), 7.29-7.19 (m, 3H, arom.), 5.29 (m, 2H, alkene), 3.49 (m, 1H), 3.03 (m, 1H), 2.60 (s, 1H, ≡C*H*), 1.88 (m, 4H), 1.64 (s, 3H,

C*H*$_3$), 1.49 (m, 2H), 1.32 (m, 2H), 1.21 (m, 4H), 0.80 (m, 3H). $^{13}C\{^1H\}$ NMR (75 MHz, $CDCl_3$) δ 143.3 (s), 130.9 (s), 130.2 (s), 128.4 (s), 127.9 (s), 126.1 (s), 84.7 (s), 75.9 (s), 75.2 (s), 65.0 (s), 33.1 (s), 32.6 (s), 32.5 (s), 32.1 (s), 29.7 (s), 26.4 (s), 22.4 (s), 14.2 (s). $C_{20}H_{28}O$ (284.21): calcd. C 84.45, H 9.92; found C 84.19, H 9.79.

Xanthones

(Z)-9-(2-phenylprop-1-en-1-yl)-3,4,5,6,7,9-hexahydro-1H-xanthene-1,8(2H)-dione.

From propargyl alcohol. To a small screw-cap vial containing 2-phenyl-3-butyn-2-ol (0.138 g, 0.943 mmol), 1,3-cyclohexanedione (2.5 eq./mol, 0.267 g, 2.381 mmol) was added, along with $ClCH_2CH_2Cl$ (2 mL). Catalyst was added (0.010 g, 0.012 mmol, 1.3%/mol) and mixture was heated at 80 °C for 72 hours. Product was isolated by column chromatography (silica gel, 1.5×15cm, 2:5 ethyl acetate/hexane). Product was off-white solid (0.066 g, 0.197 mmol, 21%). A 1:10 ratio of the other isomer was observed via NMR and gas chromatography.[60] $C_{22}H_{22}O_3$ (334.16): calcd. C 79.02, H 6.63; found C 79.27, H 6.64.

Major Z isomer: ^1H NMR (300 MHz, CDCl3): δ = 7.53–7.09 (m, 5 H, Ph), 5.17 (d, $J_{H,H}$ = 9.9 Hz, 1 H), 4.62 (d, JH,H = 9.9 Hz, 1 H), 2.45 (m, 11 H), 1.97 (m, 4 H) ppm. $^{13}C\{^1H\}$ NMR (75 MHz, CDCl3): δ = 196.7 (s), 164.5 (s), 144.1 (s), 136.3 (s), 128.7 (s), 128.1 (s), 126.7 (s), 126.1 (s), 116.1 (s), 37.2 (s), 27.4 (s), 26.2 (s), 20.6 (s), 16.3 (s) ppm.

Minor E Isomer: 1H NMR (300 MHz, CDCl3, partial): δ = 5.56 (d, $J_{H,H}$ = 8.7 Hz), 4.24 (d, JH,H = 8.7 Hz) ppm. $^{13}C\{^1H\}$ NMR (75 MHz, CDCl3): δ = 163.9 (s), 142.6 (s), 138.0 (s), 128.3 (s), 127.9 (s), 127.3 (s), 126.4 (s), 116.5 (s), 42.3 (s), 38.3 (s), 37.1 (s), 27.8 (s), 27.2 (s), 26.3 (s), 21.9 (s), 20.3 (s) ppm.

From propargyl acetate. To a small screw-cap vial containing 2-phenyl-3-butyn-2-acetate (0.175 g, 0.934 mmol), 1,3-cyclohexanedione (2.5 eq./mol, 0.265 g, 2.36 mmol) was added, along with 1,2-dichloroethane (2 mL). Catalyst was added (0.010 g, 0.012 mmol, 1.3%/mol) and mixture was heated at 80 °C for 72 hours. The product was isolated by column chromatography (silica gel, 1.5×15cm, 2:5 ethyl acetate/hexane) as an off-white solid (0.145 g, 0.435 mmol, 46%). ^{1}H and ^{13}C NMR matched what was described above for the product from propargylic alcohol.

9-styryl-3,4,5,6,7,9-hexahydro-1H-xanthene-1,8(2H)-dione.[61,62]

To a small screw-cap vial containing 1-phenylprop-2-yn-1-ol (0.133 g, 1.01 mol), 1,3-cyclohexanedione (2.6 mol-%, 0.292 g, 2.60 mmol) was added, along with cyclohexane (3 mL). Catalyst was added (0.016 g, 0.018 mmol, 1.8%/mol) and mixture was heated at 90 °C for 16 hours. Product was isolated by column chromatography (silica gel, 1.5×15cm, 2:5 ethyl acetate/hexane) as an off-white solid (0.095 g, 0.296 mmol, 29% crude). Matches spectra previously described in literature. ^{1}H NMR (300 MHz, $CDCl_3$) δ 7.43-7.18 (m, 5H, arom.), 6.27 (s, 2H), 4.72 (s, 1H), 2.52 (m, 8H), 2.12 (m, 4H). $^{13}C\{^{1}H\}$ NMR (75 MHz, $CDCl_3$) δ 196.7 (s), 164.8 (s), 137.5 (s), 131.4 (s), 130.2 (s), 128.5 (s), 127.3 (s), 126.6 (s), 115.7 (s), 37.2 (s), 28.2 (s), 27.4 (s), 20.6(s). $C_{21}H_{20}O_3$ (320.38): calcd. C 78.73, H 6.29; found C 78.03, H 6.45.

9-(2,2-diphenylvinyl)-3,4,5,6,7,9-hexahydro-1H-xanthene-1,8(2H)-dione.

To a small screw-cap vial containing 1,1-diphenylprop-2-yn-1-ol (0.110 g, 0.528 mmol), 1,3-cyclohexanedione (2.5 eq./mol, 0.212 g, 1.35 mmol) was added, along with $ClCH_2CH_2Cl$ (2 mL). Catalyst was added (0.010 g, 0.014 mmol, 2.2 mol-%) and mixture was heated at 85 °C for 72 hours. Product was isolated by column chromatography (silica

gel, 1.5×15cm, 2:5 ethyl acetate/hexane). Product was off-white solid (0.144 g, 0.363 mmol, 69%). ^{1}H NMR (300 MHz, $CDCl_3$) δ 7.32-7.21 (m, 3H, arom.), 7.06-7.04 (m, 2H, arom.), 6.08 (d, J_{HH}=9 Hz, 1H), 4.32 (d, J_{HH}=9 Hz, 1H), 2.23 (m, 8H), 1.82 (m, 4H). $^{13}C\{^{1}H\}$ NMR (75 MHz, $CDCl_3$) δ 196.6 (s), 164.3 (s), 143.4 (s), 142.1 (s), 139.9 (s), 130.4 (s), 130.3 (s), 127.9 (s), 127.7 (s), 127.4 (s), 127.0 (s), 126.9 (s), 116.1 (s), 36.9 (s), 27.2 (s), 26.7 (s), 20.6(s). $C_{27}H_{24}O_3$ (396.48): calcd. C 81.79, H 6.10; found C 81.63, H 6.12.

3-(3,3-diphenylallylidene)pentane-2,4-dione.

To a small screw-cap vial containing 1,1-diphenylprop-2-yn-1-ol (0.111 g, 0.532 mmol), 2,4-pentanedione (2.7 eq./mol, 0.146 g, 1.45 mmol) was added, along with 1,2-dichloroethane (2 mL). The catalyst was added (0.010 g, 0.012 mmol, 2.4 mol-%) and mixture was heated at 85 °C for 16 hours. The product was isolated as tan oil by column chromatography (silica gel, 1.5×12cm, 2:5 ethyl acetate/hexane). Tan oil was dried via vacuum and dissolved into warm hexanes. Upon cooling, the product formed as an orange-white solid (0.054 g, 0.186 mmol, 34%). ^{1}H NMR (300 MHz, $CDCl_3$) δ 7.53-7.46 (m, 4H, arom.), 7.41-7.32 (m, 4H, arom.), 7.32-7.25 (m, 2H, arom.), 7.19 (d, J_{HH}=11.8 Hz, 1H), 7.07 (d, J_{HH}=11.8 Hz, 1H), 2.46 (s, 3H, CH_3), 2.20 (s, 3H, CH_3'). $^{13}C\{^{1}H\}$ NMR (75 MHz, $CDCl_3$) δ 203.6 (s), 197.5 (s), 155.5 (s), 141.9 (s), 140.8 (s), 140.3 (s), 138.2 (s), 130.6 (s),129.6 (s), 129.0 (s), 128.7 (s), 128.5 (s), 128.5 (s), 122.2 (s), 31.9 (s), 26.3 (s). $C_{20}H_{18}O_2$ (290.26): calcd. C 82.73, H 6.25; found C 82.28, H 6.24.

Cyclic Voltammetry.

The voltammograms were recorded with a three-electrode BAS electrochemical cell in a Vacuum Atmospheres HE-493 drybox under an atmosphere of argon with samples in

0.1 M NBu_4PF_6/CH_2Cl_2 at 298 K. A 1.6 mm Pt disk electrode was used as the working electrode, a platinum wire was used as the auxiliary electrode, and a silver wire was used a pseudoreference electrode. The potentials were calibrated against the $Cp^*_2Fe^{0/+}$ couple (Cp* = pentamethyl-cyclopentadienyl), which occurs at –0.548 V versus the $Cp_2Fe^{0/+}$ couple for this solvent.[63] The potentials in this paper can be changed to saturated calomel electrode (SCE) reference values by the addition of 0.56 V. The voltammograms were collected at scan rates of 0.05–1.6 V/s with an EG&G PAR 263A potentiostat interfaced to a computer operated with the EG&G PAR Model 270 software.

X-ray Structure Determination for [RuCl(ind)(PPh3){P(pyr)3}], [RuCl(ind){P(pyr)3}2], and 9-(2,2-Diphenylvinyl)-3,4,5,6,7,9-hexahydro-1H-xanthene-1,8(2H)-dione.

Crystals of the metal complexes were obtained by the slow diffusion of hexanes into a CH_2Cl_2 solution of the compounds, and crystals of the organic dione were obtained by layering an ethyl acetate solution of the compound with hexanes. The crystals of appropriate dimension were mounted on MiTeGen cryoloops in random orientations. Preliminary examination and data col- lection were performed with a Bruker X8 Kappa Apex II charge- coupled device (CCD) detector system single-crystal X-ray diffractometer equipped with an Oxford Cryostream LT device. All data were collected with graphite-monochromated Mo-*K*α radiation (λ = 0.71073 Å) from a fine-focus sealed-tube X-ray source. The preliminary unit-cell constants were determined with a set of 36 narrow-frame scans. Typical data sets consisted of combinations of ω and Φ scan frames with a typical scan width of 0.5° and a counting time of 15 s per frame at a crystal-to-detector distance of 4.0 cm. The collected frames were integrated by using an orientation matrix determined from the narrow-frame scans. The Apex II and SAINT

software packages were used for data collection and data integration.[64] The analysis of the integrated data did not show any decay. The final cell constants were determined by global refinement of reflections harvested from the complete data set. The collected data were corrected for systematic errors by SADABS on the basis of the Laue symmetry by using equivalent reflections.[64]

Structure solutions and refinements were performed with the SHELXTL-PLUS software package.[65] The structures were solved by direct methods and refined successfully in the space groups, *Pbca*, $P2_1/c$, and *P*-1 for [RuCl(ind)(PPh_3){$P(pyr)_3$}], [RuCl(ind){$P(pyr)_3$}$_2$], and 9-(2,2-Diphenylvinyl)-3,4,5,6,7,9-hexahydro-1H-xanthene-1,8(2H)-dione, respectively. Full-matrix least-squares refinements were performed by minimizing $\Sigma w(F_o^2 - F_c^2)^2$. The non-hydrogen atoms were refined anisotropically to convergence. All hydrogen atoms were treated with an appropriate riding model (AFIX m3). The crystal data and intensity data collection parameters are published.[57]

CCDC 1053440 (for 9-(2,2-Diphenylvinyl)-3,4,5,6,7,9-hexahydro-1H-xanthene-1,8(2H)-dione), 1053441 (for [RuCl(ind){$P(pyr)_3$}$_2$]), and 1053442 (for [RuCl(ind)(PPh_3){$P(pyr)_3$}]) contain the supplementary crystallographic data.

2.7. References

(1) Pauson, P. L.; Wilkinson, G. *J. Am. Chem. Soc.* **1954**, *76* (7), 2024–2026.
(2) Boeda, F.; Clavier, H.; Nolan, S. P. *Chem. Commun.* **2008**, No. 24, 2726–2740.
(3) Fürstner, A.; Guth, O.; Düffels, A.; Seidel, G.; Liebl, M.; Gabor, B.; Mynott, R. *Chemistry* **2001**, *7* (22), 4811–4820.
(4) Oro, L. A.; Ciriano, M. A.; Campo, M.; Foces-Foces, C. *J. Organomet. Chem.* **1985**, *289* (1), 117–131.
(5) Trost, B. M.; Toste, F. D.; Pinkerton, A. B. *Chem. Rev.* **2001**, *101* (7), 2067–2096.
(6) Kumar, P.; Gupta, R. K.; Pandey, D. S. *Chem. Soc. Rev.* **2014**, *43* (2), 707–733.
(7) Trost, B. M.; Flygare, J. A. *J. Am. Chem. Soc.* **1992,** 114, 5476–5477.
(8) Senda, Y.; Nakajima, K.; Nishibayashi, Y. *Angew. Chem.* **2015**, *127* (13), 4132–4136.
(9) Zheng, R.; Wang, Y.; Zhang, L. *Tetrahedron Letters* **2015**, *56* (23), 3144–3146.
(10) Murugesan, S.; Jiang, F.; Achard, M.; Bruneau, C.; Dérien, S. *Chem. Commun.* **2012**, *48* (52), 6589.
(11) Cadierno, V.; Gamasa, M. P.; Gimeno, J.; González-Cueva, M.; Lastra, E.; Borge, J.; García-

Granda, S.; Pérez-Carreño, E. *Organometallics* **1996**, *15* (8), 2137–2147.
(12) Gamasa, M. P.; Gimeno, J.; González-Bernardo, C.; Martín-Vaca, B. M.; Borge, J.; García-Granda, S. *Inorganica Chimica Acta* **2003**, *347*, 181–188.
(13) Gamasa, M. P.; Gimeno, J.; González-Bernardo, C.; Martin-Vaca, B. M.; Monti, D.; Bassetti, M. *Organometallics* **1996**, *15* (1), 302–308.
(14) Verschoor-Kirss, M. J.; Hendricks, O.; Renna, L.; Hill, D.; Kirss, R. U. *Dalton Trans.* **2014**, *43* (40), 15221–15227.
(15) Moloy, K. G.; Petersen, J. L. *J. Am. Chem. Soc.* **1995**, *117* (29), 7696–7710.
(16) Burrows, A. D. *CrystEngComm* **2001**, *3* (46), 217.
(17) Haar, C. M.; Nolan, S. P.; Marshall, W. J.; Moloy, K. G.; Prock, A.; Giering, W. P. *Organometallics* **1999**, *18* (4), 474–479.
(18) Fernandez, A.; Reyes, C.; Ying Lee, T.; Prock, A.; Giering, W. P.; Haar, C. M.; Nolan, S. P. *J. Chem. Soc., Perkin Trans. 2* **2000**, No. 7, 1349–1357.
(19) Rodriguez, V.; Donnadieu, B.; Sabo-Etienne, S.; Chaudret, B. *Organometallics* **1998**, *17* (17), 3809–3814.
(20) Huang, A.; Marcone, J. E.; Mason, K. L.; Marshall, W. J.; Moloy, K. G.; Serron, S.; Nolan, S. P. *Organometallics* **1997**, *16* (15), 3377–3380.
(21) Nolan, S. P.; Clavier, H. *Chem. Soc. Rev.* **2010**, *39* (8), 3305–3316.
(22) Li, C.; Nolan, S. P.; Horváth, I. T. *Organometallics* **1998**, *17* (3), 452–456.
(23) Serron, S.; Nolan, S. P.; Moloy, K. G. *Organometallics* **1996**, *15* (20), 4301–4306.
(24) Costin, S.; Rath, N. P.; Bauer, E. B. *Inorganic Chemistry Communications* **2011**, *14* (3), 478–480.
(25) Batterjee, S. M.; Marzouk, M. I.; Aazab, M. E.; El-Hashash, M. A. *Appl. Organometal. Chem.* **2003**, *17* (5), 291–297.
(26) Kamigaito, M.; Watanabe, Y.; Ando, T.; Sawamoto, M. *J. Am. Chem. Soc.* **2002**, *124* (34), 9994–9995.
(27) Costin, S.; Rath, N. P.; Bauer, E. B. *Inorganica Chimica Acta* **2009**, *362* (6), 1935–1942.
(28) Cadierno, V.; Conejero, S.; Gamasa, M. P.; Gimeno, J. *Dalton Trans.* **2003**, No. 15, 3060–3066.
(29) Belli, R. G.; Burton, K. M. E.; Rufh, S. A.; McDonald, R.; Rosenberg, L. *Organometallics* **2015**, *34* (23), 5637–5646.
(30) Alkhaleeli, D. F.; Baum, K. J.; Rabus, J. M.; Bauer, E. B. *Catal. Commun.* **2014**, *47*, 45–48.
(31) Shin, Y.; Han, S.; De, U.; Park, J.; Sharma, S.; Mishra, N. K.; Lee, E.-K.; Lee, Y.; Kim, H. S.; Kim, I. S. *J. Org. Chem.* **2014**, *79* (19), 9262–9271.
(32) Liang, L.; Fu, S.; Lin, D.; Zhang, X.-Q.; Deng, Y.; Jiang, H.; Zeng, W. *J. Org. Chem.* **2014**, *79* (20), 9472–9480.
(33) Vedejs, E.; Snoble, K. A. J. *J. Am. Chem. Soc.* **1973**, *95* (17), 5778–5780.
(34) Lui, M.-C.; Chung, C.-P.; Chang, W.-C.; Lin, Y.-C.; Wang, Y.; Liu, Y.-H. *Organometallics* **2009**, *28* (17), 5204–5211.
(35) Reitz, A. B.; Mutter, M. S.; American, B. M. J. O. T.; 1984. *J. Am. Chem. Soc.* **1984**, *106* (6), 1875–1876.
(36) Nakajima, K.; Shibata, M.; Nishibayashi, Y. *J. Am. Chem. Soc.* **2015**, *137* (7), 2472–2475.
(37) Nishibayashi, Y.; Milton, M. D.; Inada, Y.; Yoshikawa, M.; Wakiji, I.; Hidai, M.; Uemura, S. *Chem. Eur. J.* **2005**, *11* (5), 1433–1451.
(38) Swaminathan, S.; Narayanan, K. V. *Chem. Rev.* **1971**, *71* (5), 429–438.
(39) Manbeck, K. A.; Boaz, N. C.; Bair, N. C.; Sanders, A. M. S.; Marsh, A. L. *J. Chem. Educ.* **2011**, *88* (10), 1444–1445.
(40) Hansch, C.; Leo, A.; Taft, R. W. *Chem. Rev.* **1991**, *91* (2), 165–195.
(41) Morandini, F.; Consiglio, G.; Lucchini, V. *Organometallics* **1985**, *4* (7), 1202–1208.
(42) Trost, B. M.; Martinez, J. A.; Kulawiec, R. J. *J. Am. Chem. Soc.* **1993**, *115*, 10402–10403.
(43) Rigaut, S.; Touchard, D.; Dixneuf, P. H. *Coord. Chem. Rev.* **2004**, *248* (15-16), 1585–1601.
(44) Zhan, Z.-P.; Yang, W.-Z.; Yang, R.-F.; Yu, J.-L.; Li, J.-P.; Liu, H.-J. *Chem. Commun.* **2006**, No. 31, 3352.
(45) Zhan, Z.-P.; Yu, J.-L.; Liu, H.-J.; Cui, Y.-Y.; Yang, R.-F.; Yang, W.-Z.; Li, J.-P. *J. Org. Chem.* **2006**, *71* (21), 8298–8301.
(46) Kasralikar, H. M.; Jadhavar, S. C.; Bhusare, S. R. *Bioorg. Med. Chem. Lett.* **2015**, *25* (18), 3882–3886.

(47) Sato, N.; Jitsuoka, M.; Shibata, T.; Hirohashi, T.; Nonoshita, K.; Moriya, M.; Haga, Y.; Sakuraba, A.; Ando, M.; Ohe, T.; Iwaasa, H.; Gomori, A.; Ishihara, A.; Kanatani, A.; Fukami, T. *J. Med. Chem.* **2008**, *51* (15), 4765–4770.
(48) Kostakis, I.; Konstantinos, G.; Pouli, N.; Marakos, P.; Skaltsounis, A.-L.; Leonce, S.; Caignard, D. H.; Atassi, G. *Il Farmaco* **2000**, *55* (6-7), 455–460.
(49) Barbera, M.; Kettunen, M. I.; Caputo, A.; Hu, D.-E.; Gobbi, S.; Brindle, K. M.; Carrara, M. *International Journal of Oncology* **2009**, *34* (1), 273–279.
(50) Sanz, R.; Miguel, D.; Martínez, A.; Álvarez-Gutiérrez, J. M.; Rodríguez, F. *Org. Lett.* **2007**, *9* (4), 727–730.
(51) Meyer, K. H.; Schuster, K. *Eur. J. Inorg. Chem.* **1922**, *55* (4), 815–819.
(52) Um, I.-H.; Kim, E.-H.; Lee, J.-Y. *J. Org. Chem.* **2009**, *74* (3), 1212–1217.
(53) Leventis, N.; Meador, M. A. B.; Zhang, G.; Dass, A.; Sotiriou-Leventis, C. *J. Phys. Chem. B* **2004**, *108* (30), 11228–11235.
(54) Rana, A.; Cinar, M. E.; Samanta, D.; Schmittel, M. *Org. Lett.* **2016**, *18* (1), 84–87.
(55) Um, I.-H.; Han, H.-J.; Ahn, J.-A.; Kang, S.; Buncel, E. *J. Org. Chem.* **2002**, *67* (24), 8475–8480.
(56) Pregel, M. J.; Dunn, E. J.; Buncel, E. *J. Am. Chem. Soc.* **1991**, *113* (9), 3545–3550.
(57) Stark, M. J.; Shaw, M. J.; Rath, N. P.; Bauer, E. B. *Eur. J. Inorg. Chem.* **2016**, No. 7, 1093–1102.
(58) Pünner, F.; Hilt, G. *Chem. Commun.* **2012**, *48* (30), 3617–3619.
(59) Sathyamoorthy, B.; Axelrod, A.; Farwell, V. *Organometallics* **2010**, 3431–3441.
(60) Krasovskiy, A. L.; Haley, S.; Voigtritter, K.; Lipshutz, B. H. *Org. Lett.* **2014**, *16* (16), 4066–4069.
(61) Narayana, V. R.; Pudukulathan, Z.; Varala, R. *Organic Communications* **2013**, *6* (3), 110–119.
(62) Singh, K.; Staig, S. J.; Weaver, J. D. *J. Am. Chem. Soc.* **2014**, *136* (14), 5275–5278.
(63) Barrière, F.; Geiger, W. E. *J. Am. Chem. Soc.* **2006**, *128* (12), 3980–3989.
(64) *Bruker Analytical X–ray*; Madison, WI, 2012.
(65) Sheldrick, G. M. *Acta Cryst.* **2008**, *A64*, 112–122.

Chapter 3. Trifluoromethyl-Substituted Phosphines and Extent of Ligand Effects

Chapter 3. Trifluoromethyl-Substituted Phosphines and Extent of Ligand Effects

3.1. Aim

In continuance of the pursuit to systematically study how electronic properties of a ligand affect catalytic activity, we employed a well-defined complex and two derivatives of it containing ligands of increasing electron-withdrawing character in propargylic etherification reactions. By substituting CF_3-containing phosphines for PPh_3, any electronic changes in the characteristics of the complex or its catalytically efficiency could point to direct influence of a ligand on the electronics of the transition state of catalysis. This could then help in understanding ways to better tune similar metal complexes that are to be employed in catalysis. Catalytic results are presented and compared for propargylic etherification reactions.

3.2. Introduction

Transition metal catalysis has dramatically increased synthetic opportunities in organic chemistry over the last few decades. Ligand choice for use in these metal complexes is a topic of specialized research. Selection of ligands allows for the fine-tuning of catalysts, so that they may provide better results in the particular application they are being used for.[1] Ligands provide a range of steric and electronic effects that have shown to increase yields and enantioselectivity.[2-5]

In asymmetrical catalysis, the use of chiral catalysts can direct substrate reactivity to favor one stereoisomer product over another.[6,7] Often, the choice of ligands has followed efforts to tune the spatial demands of a catalyst. By using the steric interferences of the ligands, catalysts can achieve higher levels of regio- and stereoselectivity.[8] This may be the most powerful synthetic tool a chemist can use in natural product synthesis, as

stereoselectivity proves challenging even on the simplest of molecules. Furthermore, the need for such selectivity is driven by a large number of therapeutic molecules requiring specific stereochemistry to provide activity.[9,10] Catalytic access to chiral pharmaceuticals is in high demand, as gaining control over stereoselectivity in catalysis means less waste and greater efficiency.

While the aspect of steric influence on catalysis has been frequently reviewed in literature, the impact of ligands' electronics effect on catalysis has only more recently become more frequently systematically studied. Primary focus on electronic effects in ruthenium-based catalysis has been directed towards olefin metathesis reactions, as this particular carbon-carbon bond formation reaction has been regarded as one of the most powerful tools at a chemist's disposal.[11] Early work by Chauvin, Schrock, and Grubbs escalated olefin metathesis from using simple metal halides to employing complex metal-carbene complexes that provided superior results.[12] Although olefin metathesis using $RuCl_3$ was discovered in the mid-1950s, development of well-defined catalysts and fine-tuning of ligands did not commence until several decades later.[13] A simple diagram of the evolution of olefin metathesis catalysts is presented in Scheme 3.1.

3.2.1. The Evolution of Electronic Tuning

Grubbs and coworkers sought to enhance understanding of olefin metathesis reactions by employing $[RuCl_2(PPh_3)_3]$ (**16**) to generate vinylalkylidene and later alkylidene complexes like **18** for use in olefin metathesis reactions.[14-16] This was inspired by the early work by Chauvin and Hérisson, who proposed a four-membered ring transition state like what is shown in **17** during their work on olefin reactions using tungsten metal

complexes.[17] Over time, further studies created even more ornate metal complexes for olefin metathesis reactions.

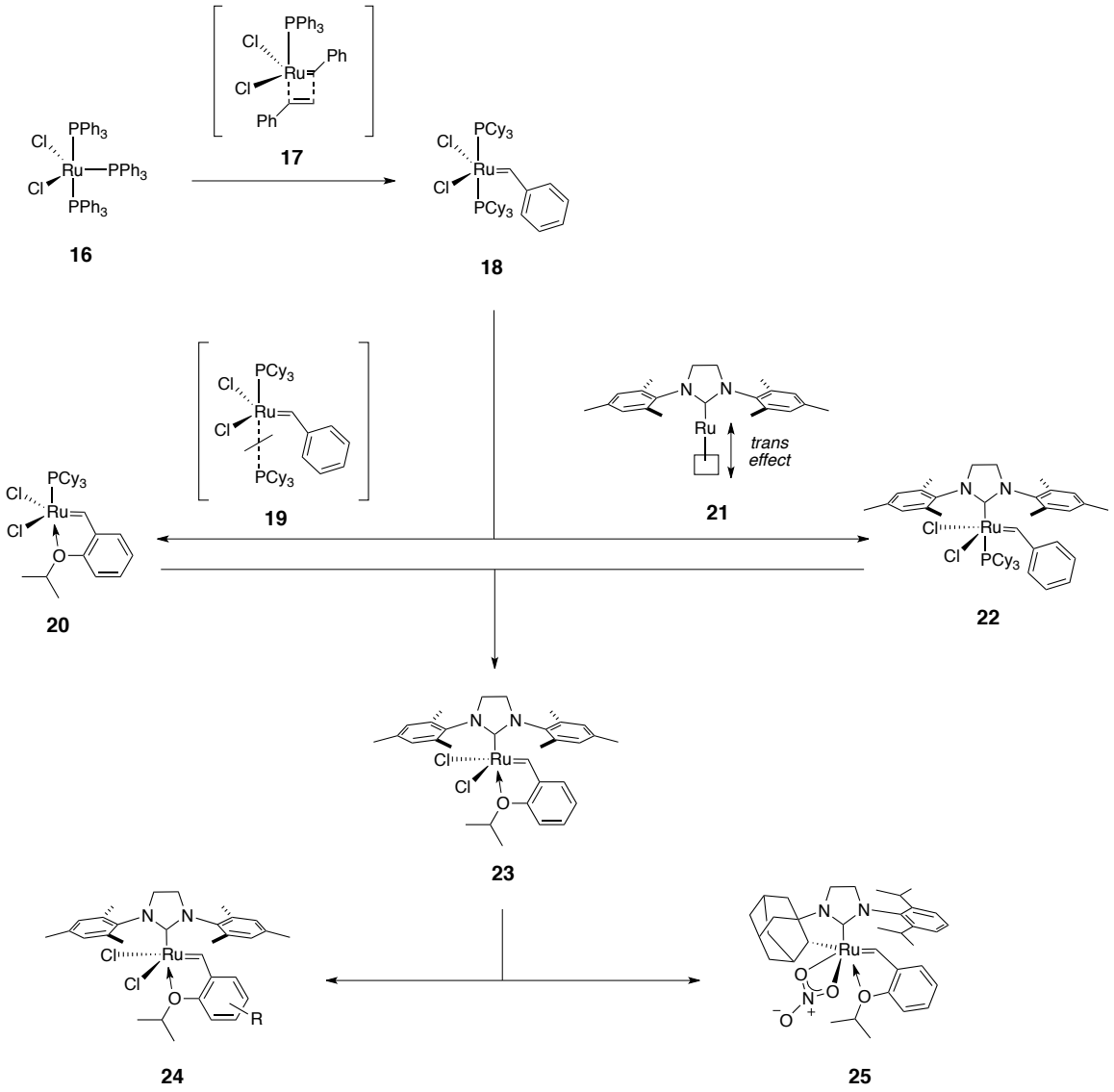

Scheme 3.1. A brief diagram of the evolution of olefin metathesis catalysts.

The desire to improve metathesis increased after Grubb's first-generation catalyst **18**, leading to a myriad of literature using ligands to fine-tune the different aspects of the metal complexes' activity. The square planar four-member intermediate **17** for the cross

metathesis of styrene, became more widely accepted as the mechanism for these reactions. One school of thought turned towards improving the necessary first step of phosphine dissociation. Hoveyda and coworkers explored the idea of aryl ethers as bidentate chelating ligands; mechanistic investigations into their previous work using ruthenium for olefin metathesis reactions in the presence of styryl ethers lead to the discovery of a recyclable metathesis catalyst **20**.[18,19] The chelating ether on the styryl ligand replaces the need for phosphine dissociation shown in intermediate **19**, improving recyclability of the catalyst, which then improved the complexes' turnover numbers and economy in catalysis reactions.[19-21]

In a different methodology, Grubbs continued to work on catalysts by focusing on the substrate interaction step by tuning ligands that would be in *trans* position to the alkene reactants. The *trans* influence is observed as the influence a ligand has on another ligand opposite to it on a metal complex; where a ligand may have the ability to lengthen or weaken a bond between the metal and ligand in the *trans* position to it.[22-24] As shown in structure **21**, Grubbs and coworkers intended to manipulate the reactivity through the use of *N*-heterocyclic carbenes (NHC) in *trans* position to where the reactants would react with the metal center. Grubbs's second generation of catalyst **22** proved to be effective at a variety of catalytic olefin metathesis reactions and efforts to further tune the use of NHCs continued.[12,25,26]

Metal complex **23** is often referred to as Grubbs–Hoveyda catalyst, as the different methods of tuning were combined to produce a class of catalysts like it that gave impressive performances.[20] In the late 1990s, electronic tuning of ligands began to accelerate, with focus again diverging into different aspects of improving the catalytic

efficiency. Grela and coworkers produced a variety of metal complexes with modified chelating ethers **24** (Scheme 3.1.), aimed at improving the kinetics of the rate–limiting ether dissociation and initiation reaction.[27] Modest gains in performance were made when an electron–withdrawing group was placed on the aromatic ring of the ether and, conversely, a performance decrease was observed when an electron–donating group was added.[11,20,28,29] More recently, modifications of the NHC ligand in complexes like **25** (Scheme 3.1.) have provided even more fine–tuning results to a robust catalytic system.[30-32]

As evidenced above, ruthenium olefin metathesis catalysts have largely forged the path for fine–tuning of ligands for asymmetric catalysis. For example, modification of NHC ligands has proven as valuable as it is complex. Systematically changing the groups attached to the heterocyclic nitrogen atoms and whether or not those groups interact with the ruthenium metal center have been a more recent area of study. Studies by the Grubbs lab demonstrate that modifications of the *N*–mesitylene and *N*–adamantane groups provided excellent increasing in Z–selectivity of olefin products.[33-35] With further examination, both experimental and calculations–based studies seem to suggest that the electronic effects of such modifications can be observed at the metal center, propagated through inductive effects from groups on the aromatic *N*–substituents on the heterocyclic carbene ligand.[31,36,37] Additional literature focused on electronic tuning in olefin catalysis provides some examples of electronic effects generated by catecholates, κ–coordinated ligands, and other various ligands with possible inductive properties.[11,38-41]

3.2.2. Electronic Tuning of Catalysts by Employing Phosphines

While the NHC system has been more recently studied, the electronic effects of other ligand types have been the subject of more systematic approaches. Furthermore, the findings of NHC seem to correlate to electronic effects observed in other ligand categories.[42] Of those other ligands, none have been as utilitarian as phosphines. Wilkinson and coworkers' seminal work with rhodium hydrogenation catalysis established a clear difference in the rate of reaction between rhodium halides and their PPh_3–containing analogues in the hydrogenation of olefins.[43,44] During their earlier studies, they discovered pyridine–containing rhodium complexes that formed during the hydrogenation, which then led to the use of more π–acidic phosphines as a more stable ligand for what would become known as Wilkinson's catalyst.

In 1970, Tolman provided a solid foundation of work that systematically compared infrared frequencies of carbonyl stretching in nickel complexes bearing different phosphine ligands.[45] The publication provided a comparison of the electronic properties of different triply–substituted phosphines to offer an expedient method of ranking substituent effects of the ligands. The findings demonstrated a correlation between the CO stretching frequencies and the substituents on the phosphines; when more electron–withdrawing substituents were used on phosphines, the higher observed CO stretching. A visual representation of this is shown in Figure 3.1. This data suggested that electronic effects of substituents on phosphine ligands were additive and may influence the electron density at the metal center. In later work, Tolman suggests that electronic effects and steric effects are intimately intertwined; one may affect the other and in some cases steric

effects dominated.[46] Tolman's work is still considered essential for understanding the electronic and steric properties of phosphine ligands.[47]

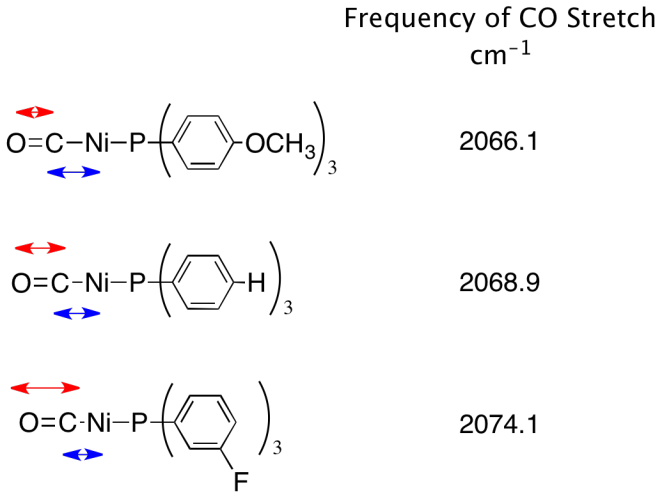

Figure 3.1. Visual representation of selected findings by Tolman and contemporaries. As more electron–withdrawing substituents are employed on aromatic rings of tri-substituted phosphines, π–backbonding increases (blue arrow) and C–O stretching relaxes (red arrow).[45]

With the knowledge that the electronic properties of the ligands may instill electronic changes at the metal, our goal of this project was to synthesize new metal complexes with electronically different phosphines and investigate any changes in catalytic reactivity that may be imparted on the complex by those ligands. The three phosphines compared in this study had an increasing number of $–CF_3$ groups on the aryl rings attached to the phosphorus, shown in Figure 3.2. It was our hypothesis that if we employed the phosphines on ruthenium in catalysis, the electronic differences in the ligands would translate to differences at the metal center, thus affecting the catalytic activity.

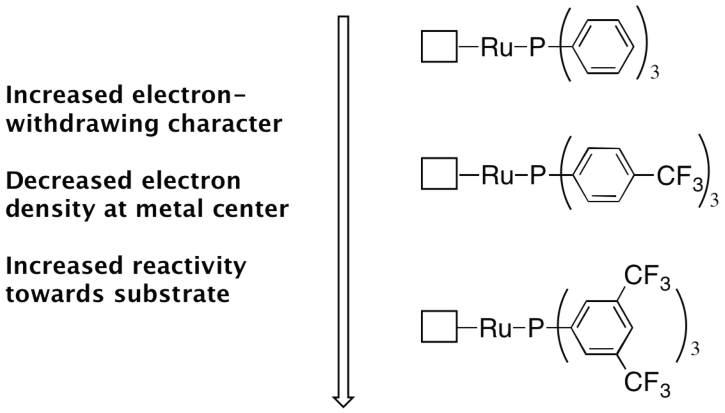

Figure 3.2. Phosphine ligands of increasing electron-withdrawing character were used to test our hypothesis of possible influence on metal–substrate affinity. Ligands used are PPh_3 (top), {P(*p*–$C_6H_4CF_3)_3$} (middle), or {P(3,5–$C_6H_3(CF_3)_2)_3$} (bottom).

3.3. Results

3.3.1. Metal Complexes

Using the well-established metal complex [RuCl(ind)$(PPh_3)_2$] (**12**), we exchanged one of the phosphine ligands for either {P(*p*–$C_6H_4CF_3)_3$} or {P(3,5–$C_6H_3(CF_3)_2)_3$} ligands through thermal exchange in refluxing THF under Schlenk conditions for approximately 4 hours. The synthesis of these two new metal complexes is shown here in Scheme 3.2.

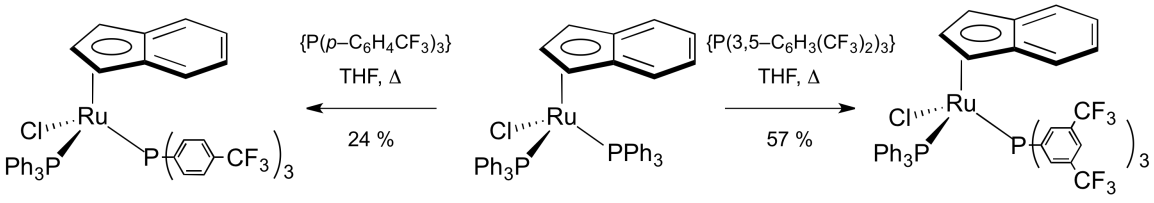

Scheme 3.2. Synthesis of two new metal complexes [RuCl(Ind)(PPh_3){P(*p*–$C_6H_4CF_3)_3$}] (**26**) and [RuCl(Ind)(PPh_3){P(3,5–$C_6H_3(CF_3)_2)_3$}] (**27**).

The substitution of the {P(*p*–$C_6H_4CF_3)_3$} ligand starting with the parent complex **12** gave a 24 % yield of the complex **26** after purification by flash chromatography. Similarly, with the same parent material **12**, the phosphine {P(3,5–$C_6H_3(CF_3)_2)_3$} was

substituted to give new complex **27** in 57 % yield after purification. Both metal complexes were recrystallized from CH_2Cl_2 layered with hexanes resting for several days at 0 °C to yield X-ray quality crystals. These new metal complexes were fully characterized by standard methods of nuclear magnetic resonance (NMR), mass spectroscopy (MS), X-ray crystallography (X-ray), elemental analysis, and cyclic voltammetry (CV).

3.3.2. NMR Characterization

Each of the new complexes were characterized by NMR spectroscopy for three different nuclei, ^{1}H, $^{13}C\{^{1}H\}$, and $^{31}P\{^{1}H\}$. The complexes were expected to follow similar complexes, having a geometry with the two phosphines in cis position.[48] This would present a set of two doublets in each $^{31}P\{^{1}H\}$ NMR spectrum. The complex $[RuCl(Ind)(PPh_3)\{P(p\text{–}C_6H_4CF_3)_3\}]$ (**26**) exhibited a set of doublets at δ = 50.1 and 44.2 ppm, with a $^{2}J_{P,P}$ coupling constant of 42 Hz. The other complex $[RuCl(Ind)(PPh_3)\{P(3,5\text{–}C_6H_3(CF_3)_2)_3\}]$ (**27**) exhibited a set of doublets at δ = 50.1 and 47.8 ppm, with a $^{2}J_{P,P}$ coupling constant of 42 Hz. The doublets occur due to magnetically inequivalent phosphorus atoms; each of the phosphine ligands have different electronic environments and thus relax within different timeframes. The ^{1}H NMR spectrum exhibited signals that were in accordance to literature for similar complexes: the aromatic region was heavy due to aromatic protons on the phosphine ligands, there were three distinct aromatic signals for the three η–coordinated indenyl ring protons, δ = 4.7, 4.5, and 3.8 ppm.[48-50] The $^{13}C\{^{1}H\}$ NMR spectrum did not indicate anything out of the ordinary, but some signals were difficult to assign in the aromatic region due to the quantity of aromatic atoms.

3.3.3 Cyclic Voltammetry

Using recrystallized samples, both of the new complexes were characterized by Cyclic Voltammetry (CV). This experimental method can shed insight into the electronic properties of the new complexes, allowing for comparison of how the ligand substitution affects the oxidation potential to the parent complex. Voltammograms of the complexes are shown here in Figure 3.3.; these scans were completed using conditions of 0.2 V/s in an electrolyte solution of 0.1 M tetrabutyl ammonium in CH_2Cl_2 at 298 K and referenced to decamethylferrocene in solution.

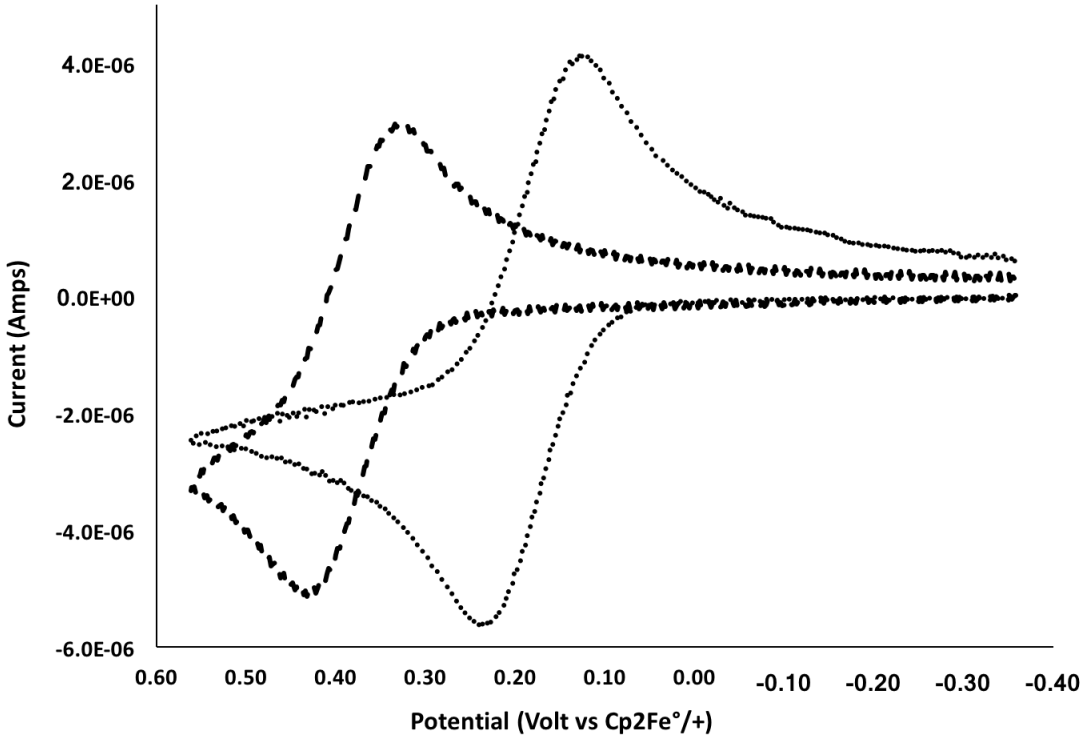

Figure 3.3. Cyclic voltammograms of [RuCl(Ind)(PPh_3){P(*p*–$C_6H_4CF_3$)$_3$}] (**26**, dotted line), and [RuCl(Ind){P(3,5–$C_6H_3(CF_3)_2$)$_3$}] (**27**, dashed line).

Table 3.1. Oxidation potentials and reversibility for complexes **12**, **26**, and **27**.

Complex	E°' (Ru)	i_{pc}/i_{pa}
[RuCl(Ind)(PPh_3)$_2$] (**12**)	– 0.023	1.0
[RuCl(Ind)(PPh_3){P(*p*–$C_6H_4CF_3$)$_3$}] (**26**)	+ 0.173	1.0
[RuCl(Ind)(PPh_3){P(3,5–$C_6H_3(CF_3)_2$)$_3$}] (**27**)	+ 0.370	0.98

Oxidation potentials are referenced to ferrocene. Ratio of reversibility obtained from scan rates of 0.2 mV/s.

The CV data collected for the parent complex **12** provides an ideal example in which to compare the electronic properties of the new complexes. All three complexes exhibited very nice reversibility as observed in the i_{pc}/i_{pa} ratio near 1, indicating that oxidation and reduction of the metal complex happens smoothly over the range of volts. The oxidation potential (*E*°' value) for the parent complex was measured to be –0.023 V (versus $Cp_2Fe^{0/+}$). Oxidation potentials are often used to compare metal complexes with varying substituents, as the electronic properties within the molecule often manifest themselves in the ability to make the metal complex easier or more difficult to oxidize.[51] The oxidation potentials for the new complexes were higher than the parent complex and observed to be +0.173 and +0.370 V, respectively. The higher oxidation potentials for the two new complexes follow an expected trend. The addition of CF_3–groups to the aromatic rings create inductive effects that change the electron–donating capacity of the phosphine ligand. This change in π–acidity then manifests as a change in electron density within both the phosphorus and the metal center, similar to what has been observed in other transition metal complexes.[52-55] This is further supported by the small downfield shift of

the $^{31}P\{^{1}H\}$ signals for the coordinated phosphines, where the ligand {P(3,5–$C_6H_3(CF_3)_2)_3$} (δ = 47.8 ppm) appears slightly more downfield than {P(*p*–$C_6H_4CF_3)_3$} (δ = 44.2 ppm) due to a decrease in shielding of the phosphorus.[45,56] The cyclic voltammetry data suggests that the –CF_3 groups have an observable effect on the electronics of the complex that they are coordinated to. In comparison to the P(pyrl)$_3$ complexes **13** and **14** from the previous study, these new complexes indicate they possess significantly more stability.

3.3.4 X-ray Crystallography

The structure for each of the new complexes were determined by X-ray crystallography. A structure representation is shown in Figure 3.4., while pertinent bond lengths and angles are given in Table 3.2. Corresponding values for the parent complex [RuCl(Ind)($PPh_3)_2$] (**12**) are available from literature and have been supplied for comparison.[57] All three of the complexes take on a geometry typical of half-sandwich Ru complexes, as their bond angles of monodentate ligands range from 91.612(17)° to 99.585(19)°, which fit the description of distorted octahedral.[50,58,59] The indenyl ligand appears to follow with typical η^5–coordination with the π electrons of the smaller ring.[60] As well, those bond length and angles do not have any values that immediately appear to be out of the ordinary.

Table 3.2. Selected bond lengths (Å) and angles (°) from the X-ray structures.

	[RuCl(Ind)(PPh_3){P(*p*–$C_6H_4CF_3$)$_3$}] (**26**)	[RuCl(Ind)(PPh_3){P(3,5–$C_6H_3(CF_3)_2$)$_3$}] (**27**)	[RuCl(Ind)(PPh_3)$_2$] (**12**)
Ru-P(1)	2.2696(5) *(PPh_3)*	2.2707(9) *(PPh_3)*	2.3306(5)
Ru-P(2)	2.3203(5)	2.2929(9)	2.2681(5)
Ru-Cl	2.4422(5)	2.4372(8)	2.4370(5)
P(1)-Ru-P(2)	99.585(19)	95.59(3)	99.205(18)
Cl-Ru-P(1)	92.389(18)	93.03(3)	92.423(17)
Cl-Ru-P(2)	91.612(17)	95.50(3)	92.187(18)
Ru-Cp [a]	1.904	1.903	1.918
Fold angle [b]	9.57°	7.45°	7.07°

[a] Distance between the Cp centroid of the indenyl ligand and the ruthenium center. [b] Fold angle refers to the pucker of the 5-membered ring of indene that binds to the ruthenium center.

The Ru–P bond lengths in both of the new complexes fall within the range from 2.2696(5) to 2.3203(5) Å. Neither of the new structures offer significant variation from the parent complex **12**; one Ru–P bond is longer than the other and this trait exists in both new structures. While complex **26** may be similar to **12** in terms of Ru–P bond length, complex **27** appears to have slightly shorter bond lengths for both ligands. This may be the result of increased back bonding to the more electron–withdrawing ligands from the ruthenium center. Computational studies have observed that the π–acidity of an aryl phosphine correlates with the number of attached fluorines atoms on the ligand.[61,62] Unlike the data obtained for NMR and CV, the solved structure data firmly demonstrates the structural similarity of the complexes. No clear trend can be discerned from bond

lengths from the metal center to the centroid of the Cp ring or the chloride atom as they are similar values for each complex.

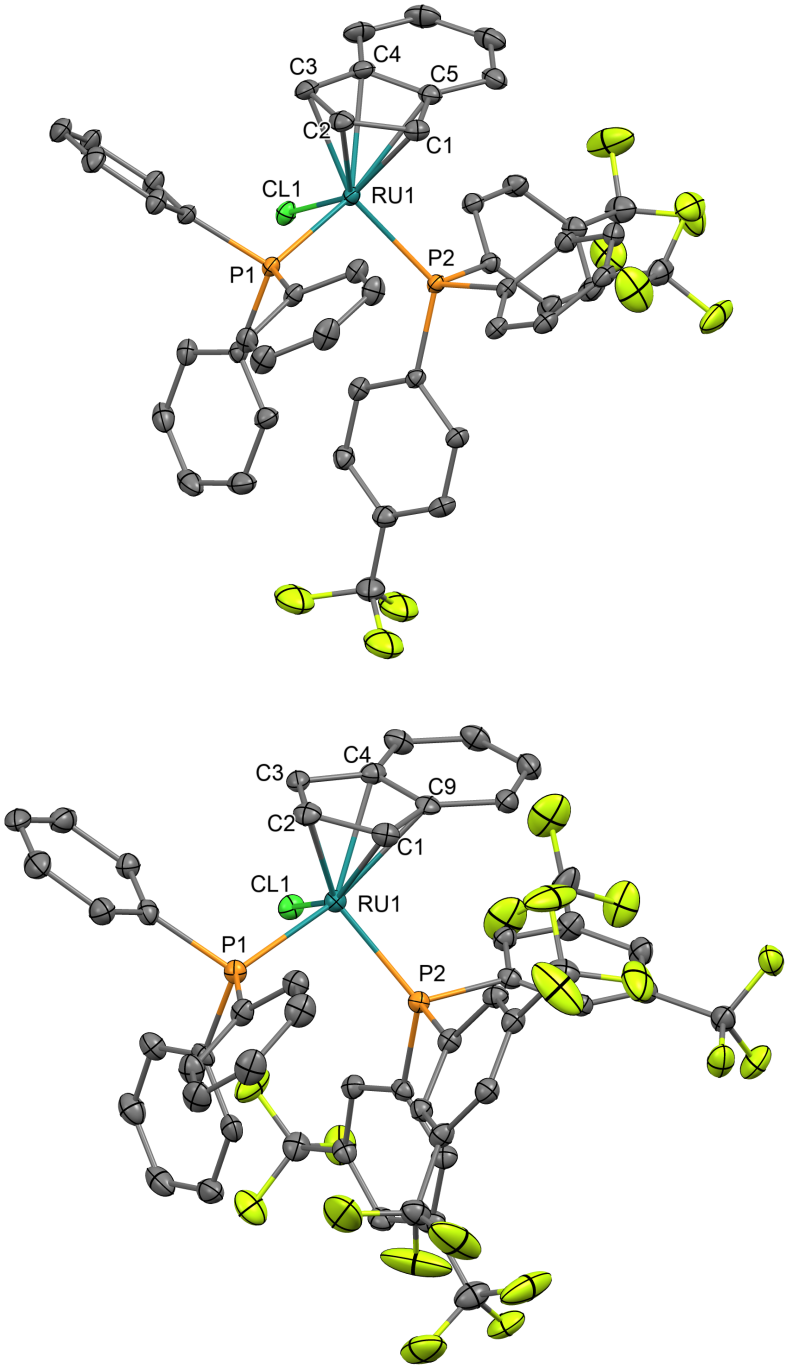

Figure 3.4. Molecular structures for [RuCl(Ind)(PPh_3){P(*p*–$C_6H_4CF_3$)$_3$}] (**26**, top) and [RuCl(Ind)(PPh_3){P(3,5–$C_6H_3(CF_3)_2$)$_3$}] (**27**, bottom). Structures are depicted as 50 % probability ellipsoids, with hydrogen atoms and solvent molecules removed for clarity.

3.3.5 Catalyst Activation and Screening

Both of the new complexes were found to be catalytically inactive up to 100 °C in toluene for propargylic etherification reactions using a propargylic alcohol as a substrate and a benzyl alcohol as a nucleophile. These conditions were found to be effective in previous work from our laboratory and were chosen to test the complexes for any reactivity.[63] To make a complex more reactive, we chose to try to abstract the chloride from the metal complex, generating a catalytically active ruthenium complex. Previous experiments with [RuCl(Ind)(PPh_3){P(pyrl)$_3$}] demonstrated chloride abstraction with $Et_3O^+PF_6^-$ to be an effective, although inconsistent reagent for activating ruthenium chloride complexes.[48] We chose to use *in situ* activation of these complexes for this project as the results should be more reproducible; metal complexes without stabilizing ligands could decompose into catalytically inactive complexes. The reagent to perform the chloride abstraction was chosen to be $NaPF_6$ as it has is well-known to be useful in the formation of ruthenium allenylidene complexes.[49,64-66] Scheme 3.3. offers an example of *in situ* generation of an acetonitrile intermediate following chloride abstraction that should form during the activation step.

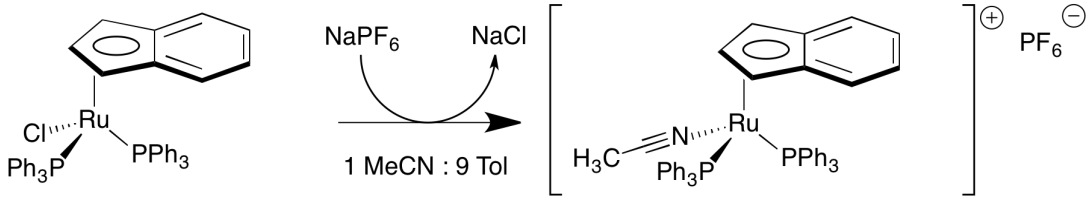

28

Scheme 3.3. Chloride abstraction of (**26**) *in situ* to form a catalytically active intermediate complex (**28**) before a catalytic reaction takes place.

A narrow variety of salt additives ($NaPF_6$, KPF_6, and $NaClO_4$) were employed to screen the for catalytic activity after chloride abstraction. A catalytic screening table is

provided in Table 3.3. to summarize the findings. Silver salts were avoided due to the propensity of silver to interact with alkynes, which could result in unwanted side products. Organic bases were added to encourage deprotonation of the nucleophilic alcohol or mitigate accumulation of free protons. When $NaPF_6$ was found to be an effective additive, we set out to determine the catalytic intermediate in the reactions.

Table 3.3. Catalytic screening for catalytic activity.

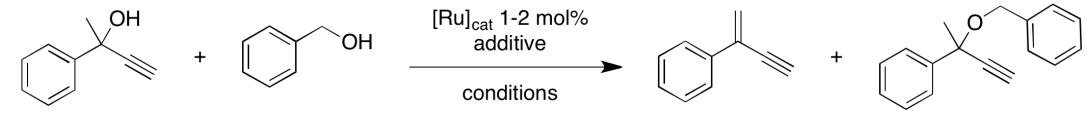

propargylic alcohol — elimination — ether

	Conditions [a]	Metal Complex [b]	Additive [c]	Ratio of Products [d]
1	MeCN:Tol, 8 hr	$[RuCl(Ind)(PPh_3)_2]$ (**12**)	$NaPF_6$ (1 eq)	No Reaction
2	MeCN:Tol, 8 hr	$[RuCl(Ind)(PPh_3)_2]$ (**12**)	$NaPF_6$ (5 eq)	3.9 propargylOH : 1 elimination : 3.8 ether
3	MeCN:Tol, 8 hr	$[RuCl(Ind)(PPh_3)_2]$ (**12**)	$NaPF_6$ (10 eq)	0 propargylOH : 1 elimination : 1 ether
4	Tol, 4 hr	$[Ru(MeCN)(Ind)(PPh_3)_2]PF_6$ (**28**)	None	3.5 propargylOH : 1 elimination : 5.4 ether
5	MeCN:Tol, 4 hr	$[RuCl(Ind)(PPh_3)_2]$ (**12**)	$NaPF_6$ (6 eq)	0 propargylOH : 1 elimination : 4.1 ether
6	MeCN:Tol, 4 hr	$[RuCl(Ind)(PPh_3)_2]$ (**12**)	KPF_6	No Reaction
7	MeCN:Tol, 16 hr	$[RuCl(Ind)(PPh_3)_2]$ (**12**)	$NaClO_4$ (10 eq)	No Reaction
8	Tol, 45 °C, 72 hr	$[Ru(MeCN)(Ind)(PPh_3)_2]PF_6$ (**28**)	None	No Reaction
9	Tol, 16 hr	$[Ru(MeCN)(Ind)(PPh_3)_2]PF_6$ (**28**)	None	44 % ether (isolated yield)
10	Tol, 16 hr	$[Ru(MeCN)(Ind)(PPh_3)_2]PF_6$ (**28**)	DBU	No Reaction
11	Tol, 16 hr	$[Ru(MeCN)(Ind)(PPh_3)_2]PF_6$ (**28**)	DIPEA	No Reaction
12	Tol, 4 hr	$[Ru(MeCN)(Ind)(PPh_3)_2]BAr_4^F$	None	Trace ether
13	Tol, 4 hr	$[Ru(MeCN)(Ind)(PPh_3)_2]PF_6$ (**28**)	None	1 propargylOH : 1 elimination : 1 ether
14	Tol, 4 hr	No Ru	$NaPF_6$	Only elimination detected
15	Tol, 4 hr	$[RuH(Ind)(PPh_3)_2]$ (**31**)	none	No Reaction
16	Tol, 4 hr	$[RuH(Ind)(PPh_3)_2]$ (**31**)	KPF_6	No Reaction
17	Tol, 4 hr	$[RuH(Ind)(PPh_3)_2]$ (**31**)	DBU	No Reaction

[a] Temperatures ranged from 80–85 °C. Solvent mixture of 1 MeCN : 9 Tol. [b] Metal complex used in quantities of 1–2 mol %. [c] Additives are in molar equivalence to ruthenium. [d] Ratios of molecules detected were determined by GC integration.

3.3.6 Metal Complex Derivatives

We were determined to investigate whether or not a stable acetonitrile complex is part of the catalytically active species. We attempted to isolate each of the acetonitrile–containing ruthenium complexes from activation of **12**, **26**, and **27,** adapted from literature procedures for the acetonitrile derivative of **12** with BF_4 anion.[67] Scheme 3.4 depicts the formation of acetonitrile and other chloride–abstracted species. The new complex $[Ru(MeCN)(Ind)(PPh_3)_2]PF_6$ (**28**) was isolated in 62 % yield from treatment of **12** with $NaPF_6$ in a 1:10 (vol/vol) mixture MeCN and MeOH. This complex was able to be fully characterized by NMR, mass spectroscopy, and X-ray. The solved structure obtained is presented in Figure 3.5. Pertinent X-ray parameters for **28** are listed in Table 3.4. In a similar fashion, the new complex $[Ru(MeCN)(Ind)(PPh_3)\{P(p\text{–}C_6H_4CF_3)_3\}]$ (**29**) was also isolated from **26** in 70 % isolated yield. This complex was unable to be successfully recrystallized, so full characterization was incomplete. Unfortunately, our attempt to isolate the acetonitrile derivative **27** was unsuccessful using the same methodology.

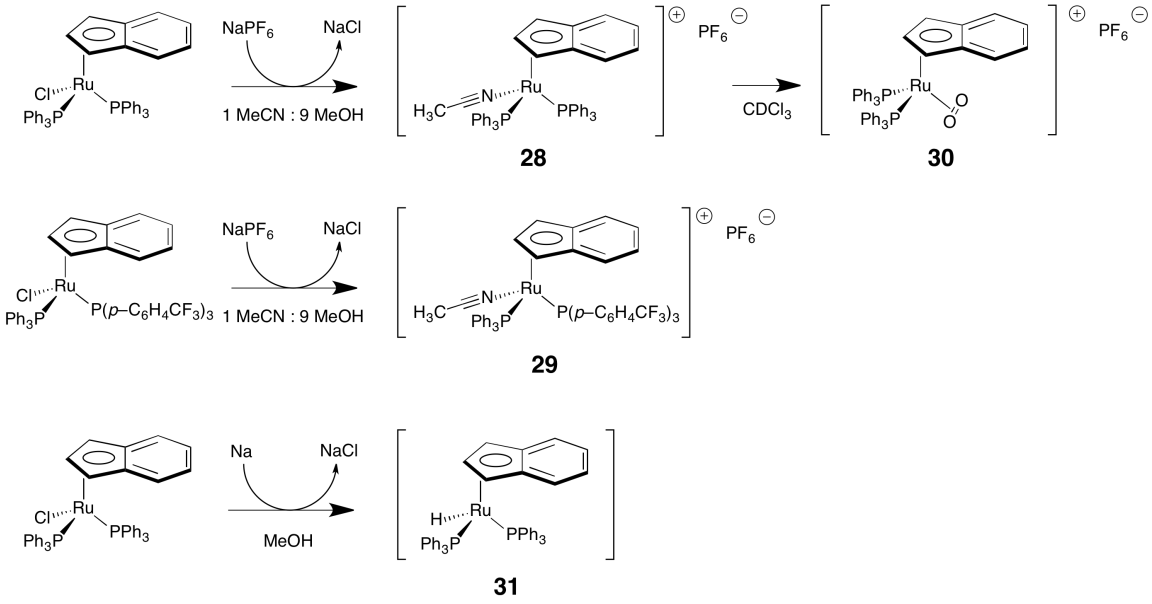

Scheme 3.4. Derivatization of metal complexes.

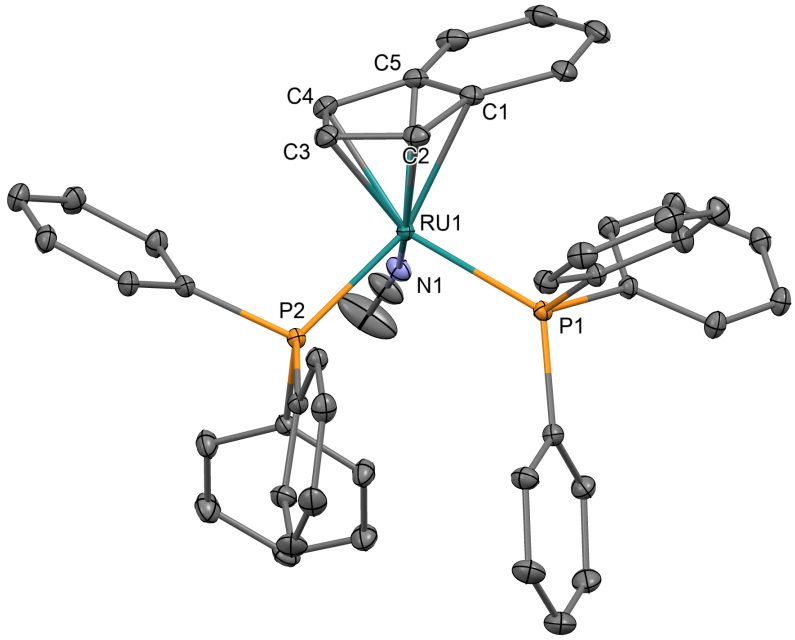

Figure 3.5. X–ray structure of $[Ru(MeCN)(Ind)(PPh_3)_2]PF_6$ (**28**). Structure is depicted as 50 % probability ellipsoids, with hydrogen atoms, solvent molecules, and coordinating anion removed for clarity.

The new orange–colored complex **28** exhibited a singlet at δ = 47.7 ppm in the $^{31}P\{^{1}H\}$ NMR spectrum, a slight shift from the red–colored precursor **12** at 46.5 ppm.[68] The $^{31}P\{^{1}H\}$ spectrum for the acetonitrile derivative **29** indicated a slight shift as well; accompanying a color change, a set of doublets at δ = 50.1 and 44.2 ppm shifted to δ = 49.5 and 47.4 ppm with a decrease in coupling from 42 Hz to 35 Hz, respectively. For **28**, the ESI-MS produced an ion peak of 782 *m/z*, indicative of the coordinated acetonitrile. Further fragmentation found ions without the acetonitrile, as expected. ESI-MS for the derivative **29** produced an acetonitrile–containing peak at 986 *m/z* with further fragmentation.

While characterizing **28**, an NMR tube with the complex in $CDCl_3$ was left on the lab bench overnight. The following morning dark crystals had precipitated from the solution. Some of these crystals were separated for X-ray characterization, leading to the solved structure of **30** presented in Figure 3.6. An η^2–O_2 complex was identified, corroborated by a strong IR stretch associated with Ru–O_2 species, 828 cm^{-1}.[69,70] The identity of the ligand as η^2–O_2 is also supported by an O–O bond length of 1.409(6) Å, falling within error of a similar complex from literature with an η^2–O_2 O–O length of 1.405(5) Å.[69] Attempts to independently synthesize the peroxo complex **30** were unsuccessful. Only limited in repeated similar conditions to which the first crystals were obtained by resting an NMR sample on the bench top, there may be better ways to synthesize such a complex that were not attempted. Pertinent X-ray parameters of **30** are listed in Table 3.4.

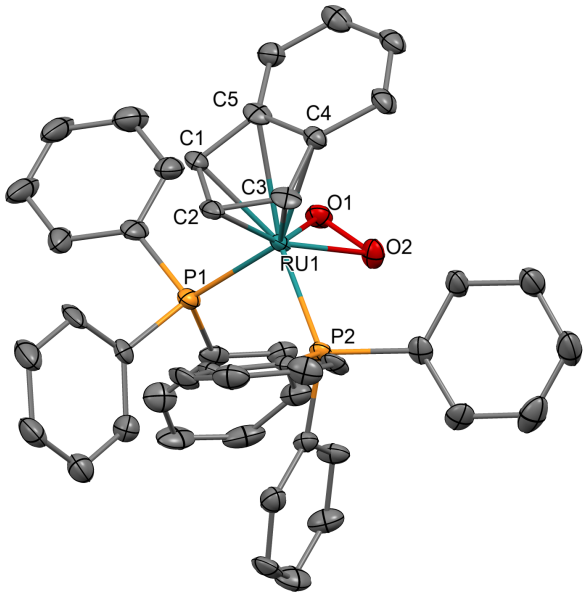

Figure 3.6. X–ray structure of $[Ru(\eta^2–O_2)(Ind)(PPh_3)_2]PF_6$ (**30**). Structure is depicted as 50 % probability ellipsoids, with hydrogen atoms, solvent molecules, and coordinating anion removed for clarity.

Table 3.4. Selected bond lengths (Å) and angles (°) from the X-ray structures of **28** and **30**.

	$[Ru(MeCN)(Ind)(PPh_3)_2]PF_6$ (**28**)	$[Ru(\eta^2–O_2)(Ind)(PPh_3)PF_6$ (**30**)	$[RuCl(Ind)(PPh_3)_2]$ (**12**)
Ru–P(1)	2.3913(4)	2.3415(16)	2.3306(5)
Ru–P(2)	2.2958(4)	2.3782(17)	2.2681(5)
Ru–L	2.0436(12) (CH_3CN)	2.003(5) (O1) 2.008(5) (O2)	2.4370(5) (Cl)
O1–O2	–	1.409(6)	–
P(1)–Ru–P(2)	103.540(12)	96.30(6)	99.205(18)
L–Ru–P(1)	93.56(4) (CH_3CN)	81.78(13) (O1) 105.38(14) (O2)	92.423(17) (Cl)
L–Ru–P(2)	84.87(2) (CH_3CN)	83.86(14) (O1) 119.85(14) (O2)	92.187(18) (Cl)
O1–Ru–O2	–	41.13(18)	–
Ru-Cp [a]	1.889	1.952	1.918
Fold angle [b]	6.34°	5.70°	7.07°

[a] Distance between the Cp centroid of the indenyl ligand and the ruthenium center.
[b] Fold angle refers to the pucker of the 5-membered ring of indene that binds to the ruthenium center.

3.3.7. Catalytic Applications of the New Complexes

We employed the complexes **12**, **26**, and **27** in propargylic etherification reactions and compared the yields. We believe this is a practical measure of how slight modifications in ligands can affect the usefulness of a complex in catalysis. By comparing isolated yields, we can observe the effects of electron–withdrawing groups on the phosphines in this catalyst system. Previous efforts in our laboratory have attempted to make improvements in this field with different ruthenium and iron complexes.[48,63,71-73] The results of these efforts are summarized in Scheme 3.5.

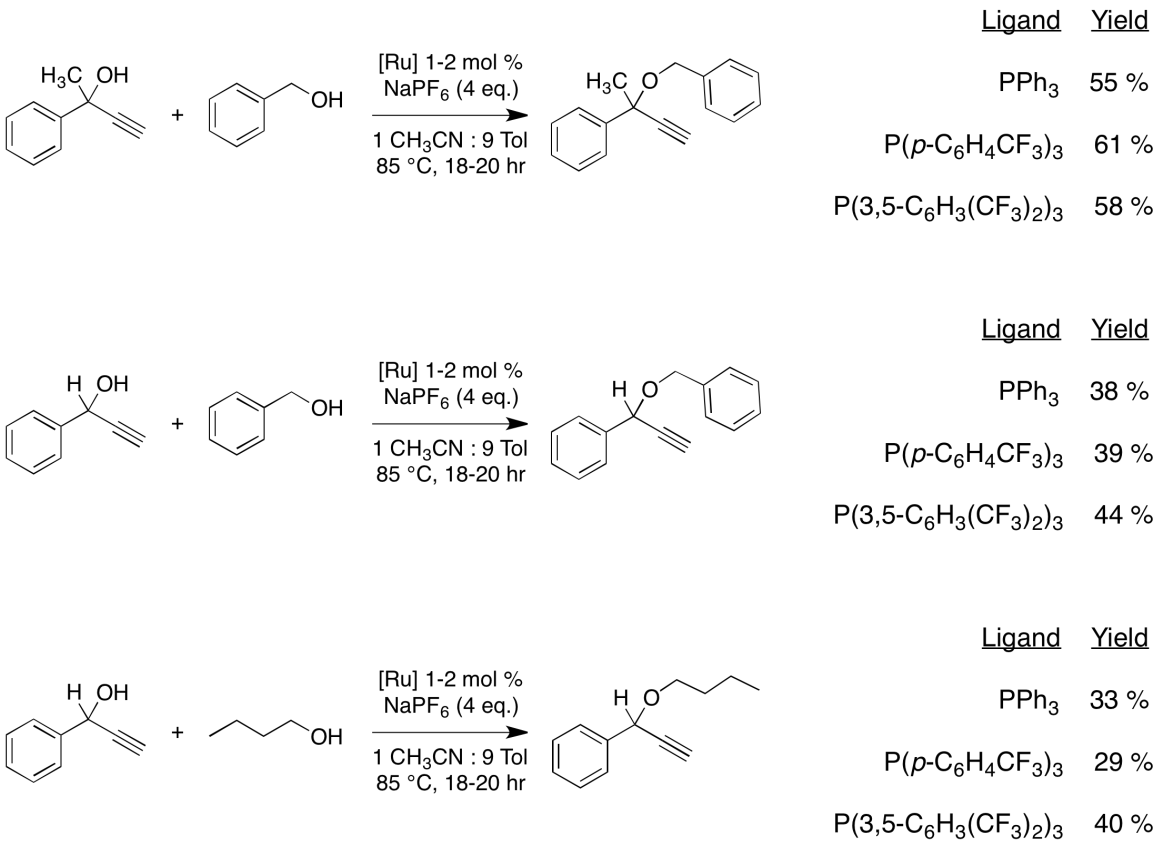

Scheme 3.5. Results of propargylic etherification reactions.
[Ru] = [RuCl(Ind)(PPh_3){Ligand}]

For the parent complex **12** and each of the new complexes **26** and **27**, the metal complex was mixed with $NaPF_6$ in a 1 : 9 mixture of MeCN and toluene and heated at 85 °C for 20 minutes. The propargylic alcohol and nucleophilic alcohol were then added to the reaction mixture and allowed to heat at 85 °C overnight for 18–20 hours. Three different propargylic ethers were synthesized in yields ranging from 29 – 61 %. Tertiary alcohols gave higher yields than the secondary alcohols for all catalysts. Generally, all metal complexes appeared to perform roughly the same for each reaction tested, with the complex **27** performing slightly better than the others for the reactions with secondary alcohols. Propargylic alcohols with internal alkynes or primary propargyli alcohols were not tested.

3.3.8. Kinetic Comparison of the New Complexes

In an effort to better understand the behavior of the catalytic reaction, we studied the kinetics by monitoring the reaction by NMR over specific time intervals. A minimum of three reactions for each metal complex using the standard screening reaction (shown in Figure 3.7) were conducted. Each metal complex used was added to the NMR tube for the activation similar to what is outlined in the catalytic applications section, with a consistent 0.1 mL of MeCN, 2 mol % [Ru], and 1-2 mol % of $NaPF_6$. ^1H NMR spectra were obtained with an internal standard of *p*–methoxybenzene using Toluene-d_8 (0.6 mL) as the solvent. The integration of the singlet from the secondary propargylic alcohol and the diastereotopic benzyl ether peaks allowed for accurate quantification of product formation. The results were averaged for each time interval and error was recorded as standard deviation. A plot of this activity is shown in Figure 3.7.

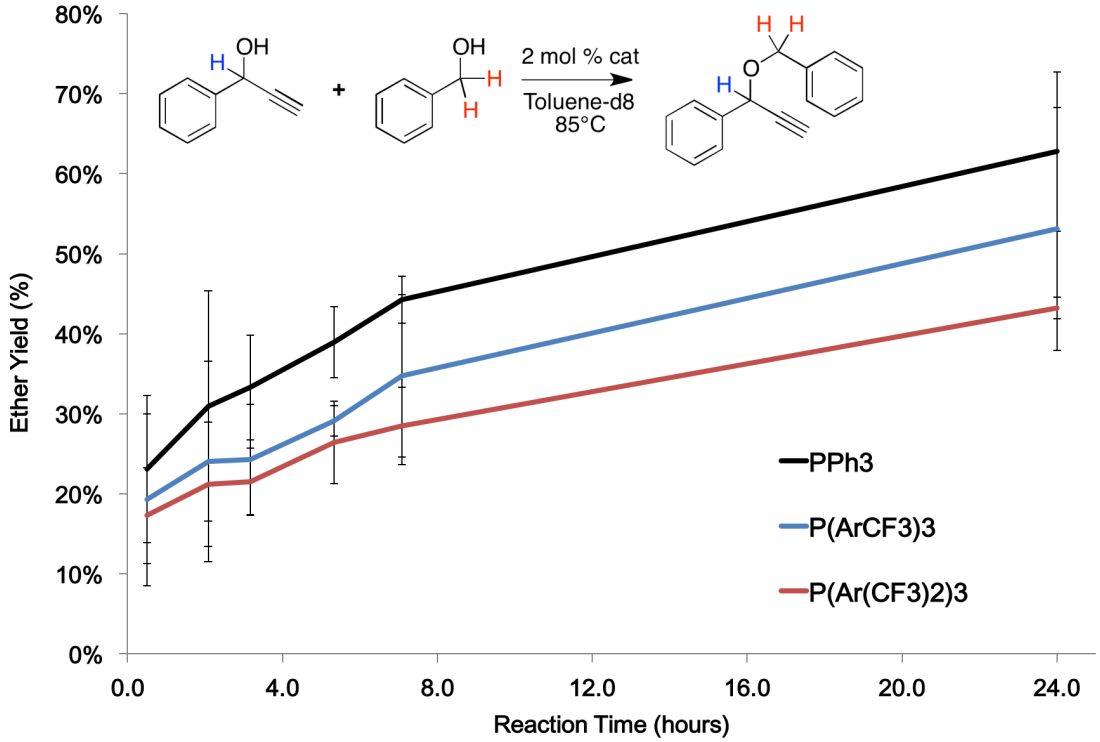

Figure 3.7. Rate of reaction comparison for all three metal complexes.

The kinetics of the reaction using each complex progressed in a similar manner, as the rate of appearance of the ether product stayed relatively consistent through the course of the reaction. While the averages of the plot appear to show some differentiation of the rate induced by the catalysts, the errors of each experiment often closely overlap. The existence of this error comes from at least two factors. The first is the variance of the number of catalytically active metal complexes in solution, as the activation was performed *in situ*. The activation method was consistent throughout all trials in the experiment, yet small variations in amount of complex or salt sticking to the sides of the NMR tube or slight differences in the concentration of solvent measured out may have played a role. The second significant source of error comes from the NMR spectrum

integration. Small changes in where the integration was selected on the spectrum may have translated to larger variability in the measurements, which translated to changes in the percent of product molecule in solution. Due to the error, the data suggests that we cannot definitively conclude that the ligand exchanges result in slower catalysis, even though it appears to be a correct assumption by means of the averaged plot.

3.4. Discussion

3.4.1. Catalytic Active Species and Decomposition Pathways

During screening, the catalytic results of the new characterized acetonitrile complex **28** was compared to the results of the *in situ* activated **12**. Although both complexes were catalytically active, the *in situ* activation appeared to be more effective in the timeframe of 4 hours (Table 3.3., entry 4 and 5). An uncharacterized BAr_4^F salt of the acetonitrile complex, $[Ru(MeCN)(Ind)(PPh_3)_2]BAr^F_4$ was also synthesized using previously mentioned procedures.[68] Catalytic results were compared, but this complex produced only trace amounts of the ether product within the 4-hour timeframe (entry 12). The active catalysis seems to be somewhat dependent on the amount of $NaPF_6$ used as an additive (entries 1–3). Adding KPF_6 or $NaClO_4$ to the catalytic mixture proved ineffective, in which the potassium may not be strong enough to abstract the chloride from this complex while also suffering from poor solubility.

Upon investigating catalytic activity of the complexes using NMR, several peculiarities were observed. First, the ^1H NMR provided evidence of a small triplet at approximately $\delta = -12$ ppm in the spectrum, which is typical for ruthenium hydride species.[74-76] The $^{31}P\{^1H\}$ spectrum supports this hypothesis and helped identify a known

species of ruthenium hydride that formed during catalysis, [RuH(Ind)(PPh_3)$_2$] (**31**).[68] It was hypothesized that this could be an active intermediate in the test reaction between the propargylic alcohol and benzyl alcohol. The hydride complex **31** was synthesized according to literature procedures using sodium dissolved into methanol (Scheme 3.4.).[68] This complex was then employed in catalytic screening, providing no reaction at all (Table 3.3., entries 15–17). It may be that the hydride is simply a decomposition pathway of the metal complex during catalysis, which limits the turnover of the catalytically active species.

Another significant finding in the NMR observations was pointing towards decomposition of the metal complexes. Over the course of the catalytic reactions, it was noticed that multiple species had formed in the $^{31}P\{^1H\}$ spectrum. A spectrum for the complex **26** is shown in Figure 3.8. We were able to identify several species based upon literature values. The aforementioned hydride species was found at δ = 62.3 ppm with another unknown species (possibly hydride) resonating at δ = 64.9 ppm. A set of doublets indicative of the desired acetonitrile species, [Ru(MeCN)(Ind)(PPh_3){P(*p*–$C_6H_4CF_3$)$_3$}]PF_6 (**29**), was located at δ = 49.5 and 47.4 ppm. An unknown complex was located at δ = 48 ppm. A metathesis product, the formation of the bis–PPh_3 acetonitrile species **28** was located in the spectrum. This could be indicative of the thermodynamic stability of the bis–PPh_3 species [Ru(Ind)(PPh_3)$_2$]$^+$; decomposition of the complexes with CF_3–containing phosphines lose their CF_3–containing phosphines and associate with free PPh_3 to yield a more stable complex in solution. This metathesis is a valid assumption, as the means to synthesize the new complexes required ligand exchange in refluxing THF. To corroborate this, a significant peak at δ = 25.7 ppm was identified as the oxidized

ligand, O=P(p–$C_6H_4CF_3$)$_3$. To discern this, we took the phosphine ligand and oxidized it with a small amount of H_2O_2 in $CDCl_3$ and recorded the $^{31}P\{^1H\}$ spectrum. Furthermore, a mixture of a number of oxidized phosphine species was observed in the range of δ = 30–28 ppm, which includes O=PPh_3 and other unknown phosphines. The complex **27** behaved in a similar fashion, yielding dissociated oxidized phosphines, metal hydrides, and a bis–PPh_3 species.

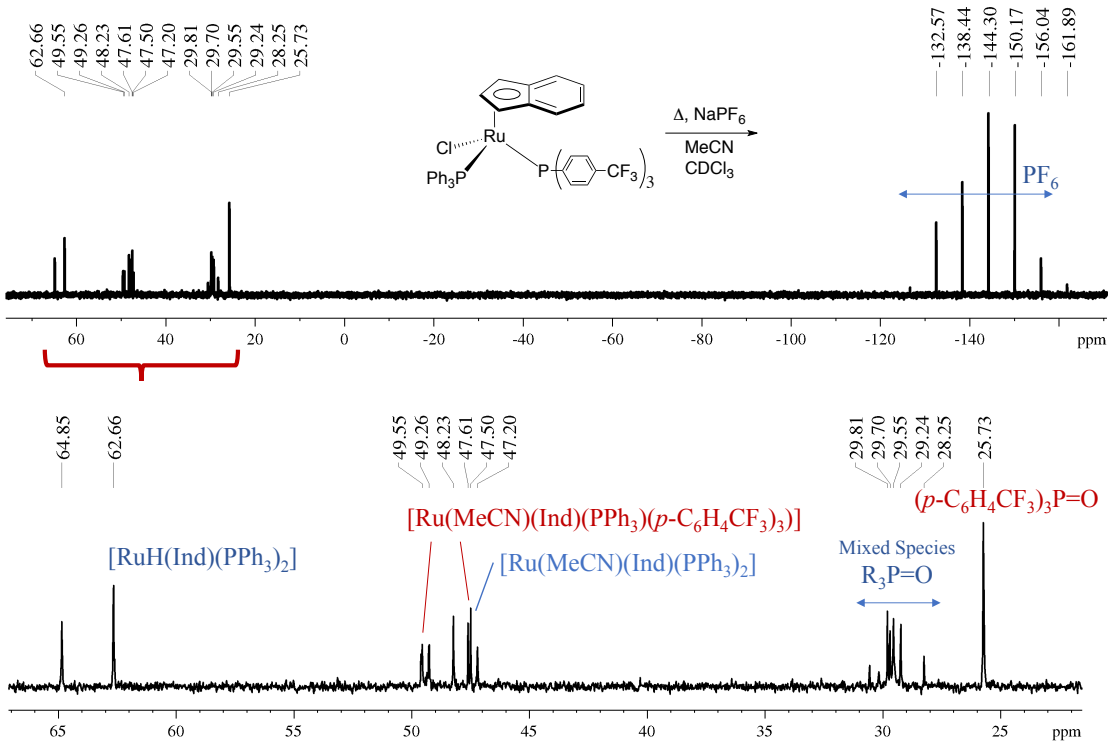

Figure 3.8. $^{31}P\{^1H\}$ NMR spectrum of the chloride abstraction and decomposition products of **26**.

Out of some curiosity, we chose to observe the ^{19}F NMR spectrum of the complexes before and after catalysis. A significant finding of possible decomposition of the PF_6 anion was detected. We attempted to identify these species from literature data, as this hydrolysis has been previously documented.[77-80] After complex **12** was activated using in

situ catalytic conditions, the mixture was vacuum dried to remove acetonitrile and dissolved in $CDCl_3$ for NMR spectroscopy (Figure 3.9.). To our surprise, the ^{19}F spectrum not only had the doublet indicative of PF_6 (δ = –72.4 ppm), but also other fluorine atom–containing species. An example spectrum is shown at the top of Figure 3.9. We were able to identify PO_3F^{2-}, $PO_2F_2^-$, and HF in the spectrum at δ = –76.7, ~ –80, and +151.9 ppm, respectively, based upon literature findings.[81]

^{19}F NMR spectrum – $[RuCl(Ind)(PPh_3)_2]$ heated with $NaPF_6$ in 1 CH_3CN : 9 Toluene
Vacuum dried, Redissolved in $CDCl_3$

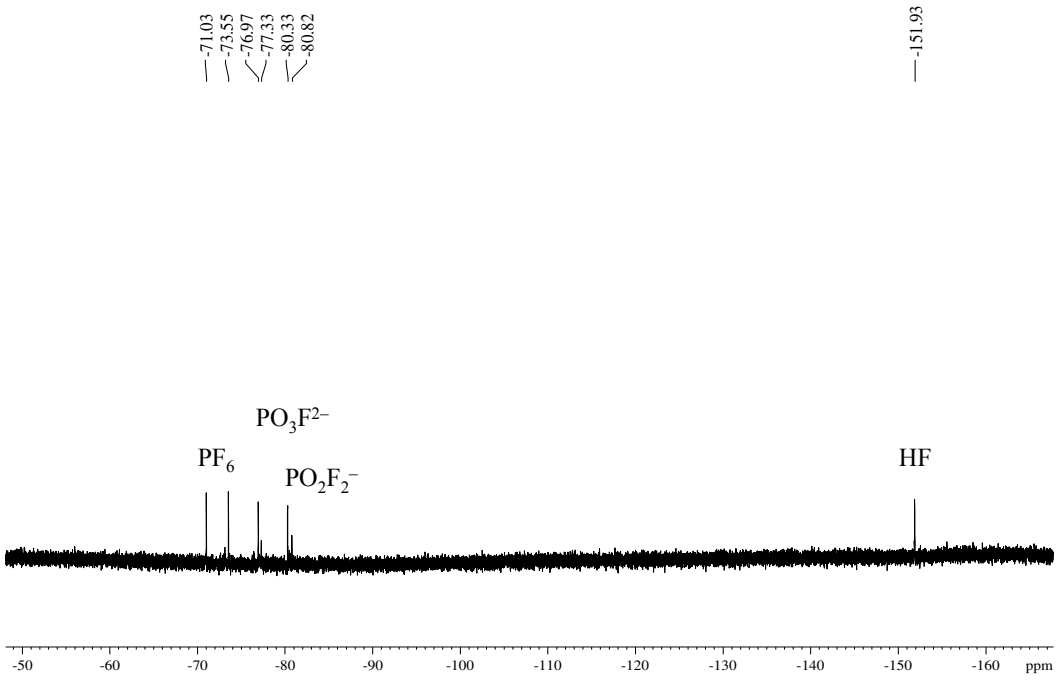

^{19}F NMR spectrum – $[Ru(MeCN)(Ind)(PPh_3)_2]PF_6$ after a catalytic reaction in $CDCl_3$

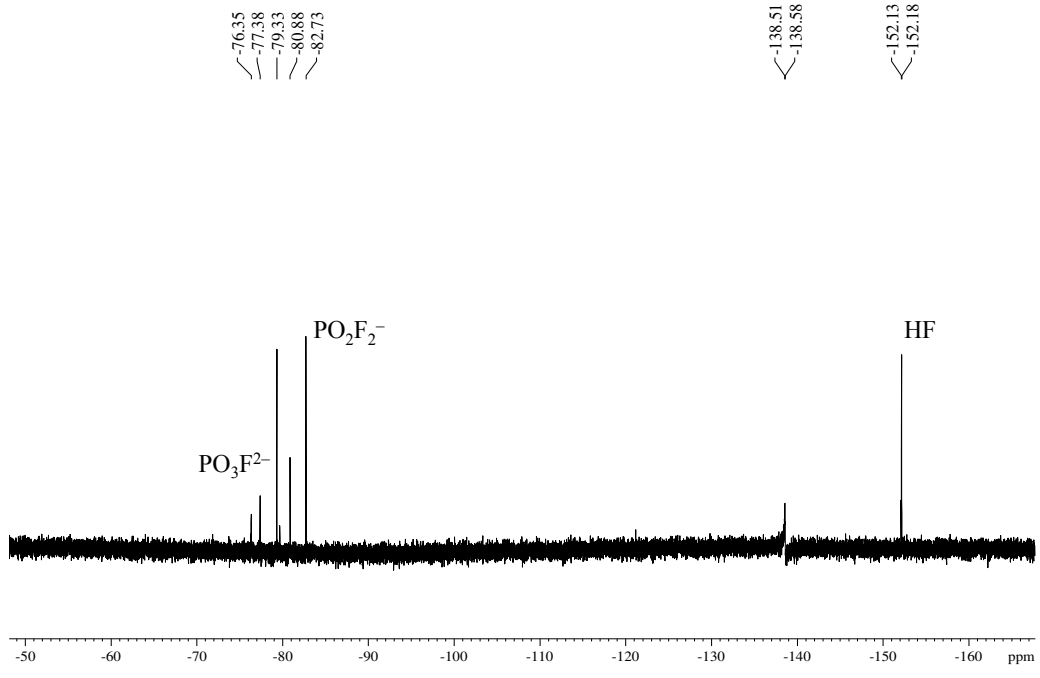

Figure 3.9. ^{19}F NMR spectra identifying some of the decomposition products of PF_6.

We continued to explore this, by observing the ^{19}F spectrum after a catalytic reaction. Using the typical screening reaction, we observed the complete disappearance of the doublet for PF_6 in the reaction mixture (Figure 3.9., bottom). We found an increased signal for the fluorinated phosphonates mentioned above, an unknown at approximately δ = +138 ppm, and again HF at approximately δ = +152 ppm. From this, we can assert that the PF_6 anion is being hydrolyzed during the course of the reaction, possibly due to dissolved oxygen or water and the further release of water during catalysis from the propargylic alcohol. It is somewhat speculation, however, to make any judgements on whether or not the PF_6 hydrolysis products play any amount of participation in the catalysis of the etherification of propargylic alcohols.

3.4.2. The Effect of Electron–Withdrawing Ligands

The substitution of fluorinated ligands did not seem to provide evidence of a significant change in the rate of reaction or any evidence of increased stability of the metal complexes *in situ*. More so, the observed degradation of catalytic complexes in the $^{31}P\{^1H\}$ spectra suggest that the substitution of the CF_3–containing ligands may not provide a measurable benefit to catalysis in this metal complex system for this series of reactions. The metathesis of the phosphine ligands to the bis–PPh_3 complex and evidence of oxidation of the CF_3–containing ligands further supports the hypothesis of a common catalytically active [Ru(MeCN)(Ind)$(PPh_3)_2$] (**28**) intermediate. The gradual evolution of a metal complex towards a thermodynamically stable complex is inevitable and beneficial, as the stable complex is capable of higher turnover numbers and catalytic efficiency.

3.4.3. Insights Towards the Reaction Mechanism

The well-accepted mechanism for propargylic etherification reactions seems to be the allenylidene pathway, illustrated on the left side of Scheme 3.6.[82] Contrary to this, an alternative pathway is the formation of a carbocation using a Lewis acid.[83] In the current model of propargylic substitution reactions, we are in agreement with literature that suggests a positive or partial positive charge buildup occurs at the carbon atom bearing the leaving group in the transition state of the molecule.[84]

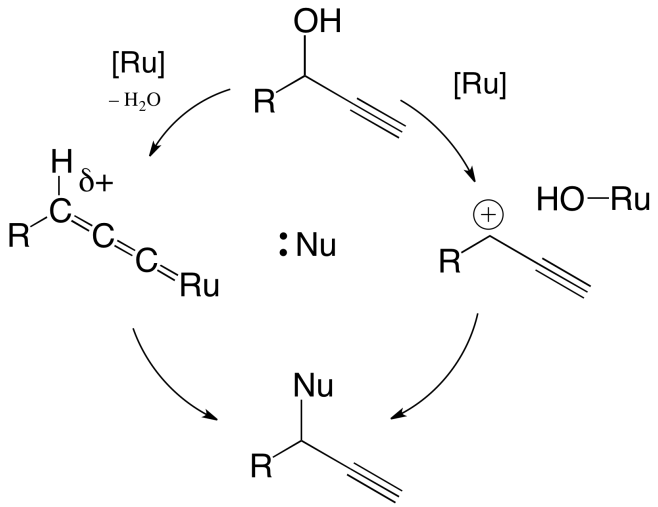

Scheme 3.6. Allenylidene catalytic pathway (left) and Lewis acid – carbocation catalytic pathway (right).

Based upon the findings of our catalytic applications in this study, there is a strong case that favors the Lewis acid – carbocation mechanism. From the kinetics experiments and observation of decomposition pathways, we have hypothesized that the catalytic reactions used in this study seem to have a common catalytically active intermediate, which would translate into the observed marginal differences in catalytic productivity.

This could mean that any coordinately–unsaturated ruthenium complex could be participating as a Lewis acid. The evidence of proton accumulation as HF in the ^{19}F spectra also supports the case for a carbocation intermediate; protonation of the hydroxyl makes it a better leaving group. Lastly, the finding of reactions using tertiary alcohols producing higher yields than those of the secondary alcohols is indicative of a carbocation as tertiary carbocations are more stable than secondary ones.

To test one more aspect of this hypothesis, we chose to react a propargylic alcohol with an alcohol for etherification using a catalyst that fulfills the requirements listed above – a Brønsted acid and a Lewis acid. We chose to employ HBF_4•Et_2O as a catalyst and observe if any of the desired propargylic ether was formed. Work up was performed by aqueous wash with bicarbonate, followed by solvent removal, and filtration through a small pipette of silica. The unpublished ^1H NMR spectrum of the crude product is shown here in Figure 3.10. The product matches literature for the propargylic ether of (2-butoxybut-3-yn-2-yl)benzene.[63] This demonstrates as evidence that a Brønsted acid can catalyze this reaction, but it defines neither the optimized conditions, nor the scope of substrates this would be possible with.

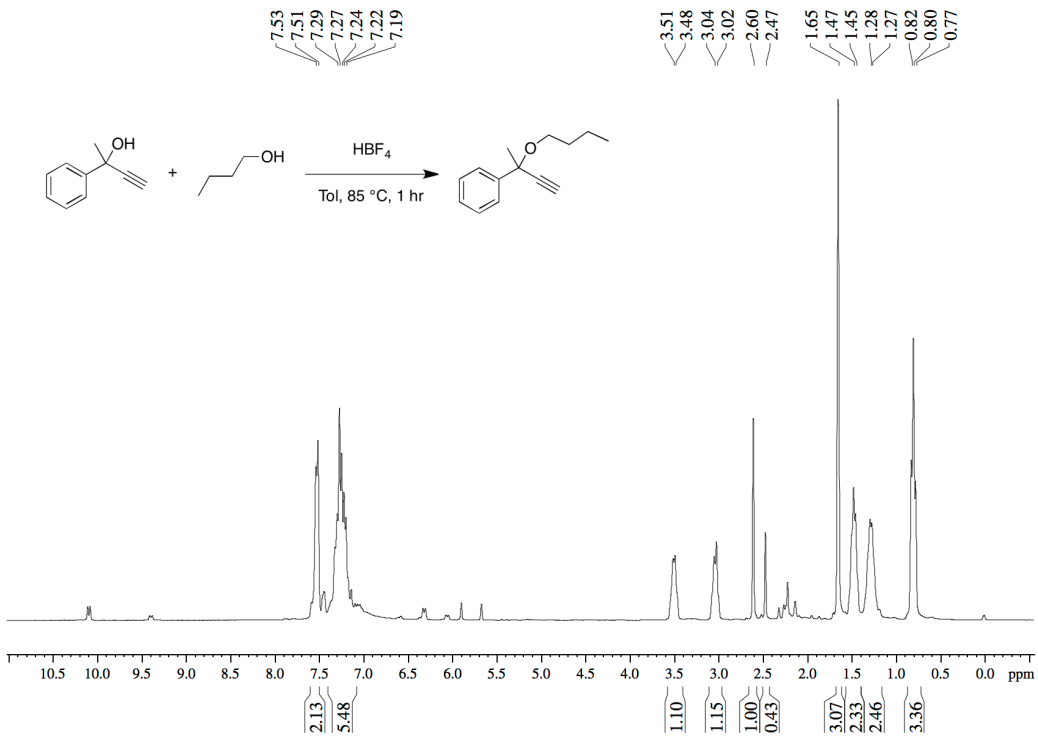

Figure 3.10. ^{1}H NMR of (1-butoxybut-3-yn-2-yl)benzene.

3.5. Summary and Perspective

This study set out to test some limits of fine–tuning of catalysis through the use of electron–withdrawing ligands. We synthesized and characterized two new electronically tuned metal complexes starting from a well–studied ruthenium complex. By comparing minute differences in product yield and kinetic observations among the complexes, we hypothesized we could infer the extent at which measurable electronic differences of the metal complexes could translate to gains in catalytic efficiency. We chose to continue work on trying to improve propargylic etherification reactions. Employing the parent complex and the two new derivatives, we observed marginal changes in yields for three different reactions ranging from 29 – 61 %. While the substitution of CF_3–containing phosphine ligands did not translate into substantial improvements of this catalytic system,

this study offers significant insight into possible mechanism of propargylic etherification. As the ruthenium complexes break down, coordinately–unsaturated ruthenium may act as a Lewis acid. As well, hydrolysis of the PF_6 anion may provide a strong Brønsted acid that may participate in this catalytic system. Together, this contributes to the knowledge that may direct further study in this catalytic system. Employing expertly–tuned Lewis acids may improve results and expand the scope. Expanded scope of this organic transformation could be employing a range of Lewis acids with or without Brønsted acids and comparing catalytic results.

3.6. Experimental

General.[85]

All propargylic alcohols, alcohols, and $NaPF_6$ for catalysis were obtained from Sigma-Aldrich and used as is. $[RuCl(Ind)(PPh_3)_2]$ was synthesized according to literature procedures.[68] NMR spectra were obtained at 300 K on a Bruker Avance 300 MHz or a Varian Unity Plus 300 MHz instrument and referenced to a residual solvent signal; all assignments are tentative and the coupling constants *J* are given in Hz. Exact masses were obtained on JEOL MStation (JMS-700) Mass spectrometer. Melting points are uncorrected and were taken on an Electrothermal 9100 instrument. Elemental analyses were performed by Atlantic Microlab Inc., Norcross, GA, USA.

Catalysis.

Unless otherwise indicated, metal complexes were placed into a screw-capped vial containing 1 mL of acetonitrile in toluene (1 CH_3CN : 9 Toluene), and $NaPF_6$ (4 molar equivalents with respect to ruthenium), and heated for approximately 20 minutes. To this

solution, the propargyl alcohol and substituent nucleophile were added and allowed to heat for the remainder of the reaction time.

[RuCl(ind)(PPh$_3$){P(p-C$_6$H$_4$CF$_3$)$_3$}] (**26**)

A Schlenk flask containing [RuCl(ind)(PPh$_3$)$_2$] (0.260 g, 0.335 mmol), P(p-C$_6$H$_4$CF$_3$) (0.158 g, 0.339 mmol), and THF (5 mL) was refluxed gently for 4 h under nitrogen. The solvent was removed via vacuum. The complex was isolated as a red solid (0.148 g, 0.125 mmol, 57 %) by column chromatography, silica gel (2 × 10 cm) using CH_2Cl_2 and petroleum ether (1:3/v:v) as eluent. The product was recrystallized from CH_2Cl_2 layered with hexanes. m. p. 122–124 °C (dec., capillary). ^{1}H NMR (300 MHz, $CDCl_3$) δ 7.40–7.29 (m, 24H, arom.), 7.20–7.11 (m, 6H, arom.), 6.92–6.81 (m, 2H, arom.), 4.73–4.70 (m, 1H, indenyl), 4.43 (br s, 1H, indenyl), 3.74 (s, 1H, indenyl); ^{13}C{^{1}H} NMR (75 MHz, $CDCl_3$) δ 140.7 (s), 140.2 (s), 136.6 (s), 136.0 (s), 134.2 (s), 134.1 (s), 133.8 (s), 133.6 (s), 131.6 (s), 131.2 (s), 130.8 (s), 130.3 (s), 129.7 (s), 129.4 (s), 129.0 (s), 128.6 (s), 127.8 (s), 127.7 (s), 125.8 (s), 125.5 (s), 124.7 (m), 123.4 (s), 122.2 (s), 118.6 (s), 112.8 (s), 112.7 (s), 110.6 (br s), 89.6 (s), 70.9 (s), 70.8 (s), 64.8 (s), 53.7 (s, CH_2Cl_2), 31.8 (s, hexanes), 22.9 (s, hexanes), 14.4 (s, hexanes); ^{31}P{^{1}H} NMR (121 MHz, $CDCl_3$) δ 50.1 (d, J_{PP}= 42 Hz), 44.2 (d, J_{PP}= 42 Hz); ^{19}F{^{1}H} NMR (282 MHz, $CDCl_3$) δ 62.9. IR (neat, solid): $\tilde{\nu}$ = 3041 (w), 2956 (w), 2923 (w), 1604 (w), 1479 (w), 1395 (w), 1317 (w), 1162 (w), 1113 (w), 1085 (s), 1055 (s), 1012 (s), 842 (m), 823 (m), 778 (m), 746 (m) cm^{-1}. FAB-MS m/z (%) 718 (20) [RuCl(ind){P(p-C$_6$H$_4$CF$_3$)$_3$}]$^+$, 683 (22) [Ru(ind){P(p-C$_6$H$_4$CF$_3$)$_3$}]$^+$, 483 (32) [O=P(p-C$_6$H$_4$CF$_3$)$_3$]$^+$, 466 (100) [P(p-C$_6$H$_4$CF$_3$)$_3$]$^+$, 321 (15) [P(p-C$_6$H$_4$CF$_3$)$_2$]$^+$, 262 (43) [PPh$_3$]$^+$. C$_{48}$H$_{34}$ClF$_9$P$_2$Ru (980.24): calcd. C 58.81, H 3.50; found C 59.19, H 3.89.

[RuCl(ind)(PPh$_3$){P(3,5-C$_6$H$_3$(CF$_3$)$_2$)$_3$}] (**27**)

A Schlenk flask containing [RuCl(ind)(PPh$_3$)$_2$] (0.171 g, 0.219 mmol), P(3,5-C$_6$H$_3$(CF$_3$)$_2$)$_3$ (0.165 g, 0.242 mmol), and THF (5 mL) was refluxed gently for 4 h under nitrogen. The solvent was removed via vacuum. The complex was isolated as a red solid (0.077 g, 0.079 mmol, 24%) by column chromatography, silica gel (2 × 10 cm) using CH_2Cl_2 and petroleum ether (1:3/v:v) as eluent. The complex was recrystallized from CH_2Cl_2 layered with hexanes, mp 141–143 °C (dec., capillary). ^{1}H NMR (300 MHz, $CDCl_3$) δ 7.89–7.85 (m, 9H, arom.), 7.39–7.27 (m, 10H, arom.), 7.19–7.14 (m, 6H, arom.), 6.95–6.92 (m, 1H, arom.), 6.59–6.55 (m, 2H, arom.), 5.15 (br s, 1H, indenyl), 4.84 (m, 1H, indenyl), 3.82 (s, 1H, indenyl); ^{13}C{^{1}H} NMR (75 MHz, $CDCl_3$) δ 138.3 (s), 137.8 (s), 136.5 (s), 135.9 (s), 133.5 (d, J_{CP}= 9.7 Hz), 133.3 (m), 131.8 (d, J_{CP}= 9.1 Hz), 131.4 (d, J_{CP}= 9.1 Hz), 129.9 (s), 129.3 (s), 128.0 (d, J_{CP}= 9.7 Hz), 126.7 (s), 124.8 (s), 123.9 (s), 121.1 (s), 111.0 (s), 109.4 (s), 91.9 (s), 75.9 (s), 75.8 (s), 63.3 (s), 53.7 (s, CH_2Cl_2); ^{31}P{^{1}H} NMR (121 MHz, $CDCl_3$) δ 50.1 (d, J_{PP}= 42 Hz), 47.8 (d, J_{PP}= 42 Hz); ^{19}F{^{1}H} NMR (282 MHz, $CDCl_3$) δ 62.8. IR (neat, solid): $\tilde{\nu}$ = 3053 (w), 3022 (w), 2308 (w), 2117 (w), 1888 (w), 1821 (w), 1614 (w), 1478 (w), 1432 (w), 1351 (s), 1275 (s), 1176 (m), 1117 (s), 1088 (s), 893 (m), 843 (m), 816 (m), 748 (m) cm^{-1}. HRMS: calcd. for $C_{51}H_{31}F_{18}P_2Ru$ 1149.0657; found 1149.047. $C_{51}H_{31}ClF_{18}P_2Ru$ (1184.23): calcd. C 51.73, H 2.64; found C 50.72, H 2.70.

[Ru(ind)(CH$_3$CN)(PPh$_3$)$_2$]PF$_6$ (**28**)

A Schlenk flask containing [RuCl(ind)(PPh$_3$)$_2$] (0.311 g, 0.401 mmol), $NaPF_6$ (0.070 g, 0.417 mmol), CH_3CN (0.200 mL, 3.829 mmol), and MeOH (15 mL) was refluxed gently for 4 h under nitrogen. An orange precipitate formed. The precipitate was isolated

by vacuum filtration and dried under high vacuum to give the product as an orange solid (0.230 g, 0.248 mmol, 62%). ^{1}H NMR (300 MHz, $CDCl_3$) δ 7.29–7.21 (m, 20H, arom.), 7.18–7.12 (m, 14H, arom.), 6.88–6.80 (m, 14H, arom.), 4.66 (br s, 1H, indenyl), 4.42 (s, 2H, indenyl), 2.12 (s, 3H, CH_3CN); $^{31}P\{^{1}H\}$ NMR (121 MHz, $CDCl_3$) δ 47.7 (s), 146.0 (septet, J_{FP}= 712 Hz, PF_6). IR (neat, solid): ṽ = 3637 (w), 3322 (w), 3049 (w), 2278 (w), 1626 (w), 1582 (w), 1531 (w), 1478 (m), 1431 (m), 1329 (w), 1187 (w), 1156 (w), 1088 (w), 1026 (w), 996 (w), 829 (s), 755 (s), 746 (s) cm^{-1}. FAB-MS m/z (%) 741 (80) [Ru(ind)(PPh3)2] $^{+}$, 479 (100) $[Ru(ind)(PPh_3)]^{+}$. ESI-MS m/z (%) 782 (20) $[Ru(ind)(CH_3CN)(PPh_3)_2]^{+}$, 741 (100) $[Ru(ind)(PPh_3)_2]^{+}$.

$[Ru(ind)(CH_3CN)(PPh_3)\{P(p\text{-}C_6H_4CF_3)_3\}]PF_6$ (**29**)

A Schlenk flask containing $[RuCl(ind)(PPh_3)\{P(p\text{-}C_6H_4CF_3)_3\}]$ (0.042 g, 0.043 mmol), $NaPF_6$ (0.008 g, 0.050 mmol), CH_3CN (0.200 mL, 3.829 mmol), and MeOH (10 mL) was stirred at room temperature for 1.5 h under nitrogen. The solvent was removed and solids were washed with diethyl ether and dried. The residue was passed through a cotton-filled pipette using chloroform. The residue was dried and the product was isolated as a yellow-orange solid (0.034 g, 0.030 mmol, 69.9%). ^{1}H NMR (300 MHz, $CDCl_3$) δ 7.29–7.21 (m, 20H, arom.), 7.18–7.12 (m, 14H, arom.), 6.88–6.80 (m, 14H, arom.), 4.66 (br s, 1H, indenyl), 4.42 (s, 2H, indenyl), 2.12 (s, 3H, CH_3CN); $^{31}P\{^{1}H\}$ NMR (121 MHz, $CDCl_3$) δ 49.5 (d, J_{PP}= 35 Hz), 47.4 (d, J_{PP}= 35 Hz), 141.0 (septet, JFP = 712 Hz, PF 6). IR (neat, solid): ṽ = 3069 (w), 2930 (w), 2864 (w), 2320 (w), 1604 (w), 1478 (w), 1433 (w), 1394 (w), 1318 (s), 1165 (m), 1120 (s), 1088 (m), 1056 (s), 1012 (m), 824 (s), 745 (m). FAB-MS m/z (%) 945 (70) $[Ru(ind)\{P(p\text{-}C_6H_4CF_3)_3\}(PPh_3)]^{+}$, 683 (40) $[Ru(ind)\{P(p\text{-}C_6H_4CF_3)_3\}]^{+}$, 479 (100) $[Ru(ind)(PPh_3)]^{+}$. ESI-MS m/z (%) 986 (25)

$[Ru(ind)(CH_3CN)(PPh_3)\{P(p\text{-}C_6H_4CF_3)_3\}]^+$, 945 (100) $[Ru(ind)(PPh_3)(P(p\text{-}C_6H_4CF_3)_3)]^+$.

$[Ru(ind)(\eta^2\text{-}O_2)(PPh_3)2]PF_6$ (**30**)

A NMR tube containing $[Ru(ind)(CH_3CN)(PPh_3)_2]PF_6$ in $CDCl_3$ was allowed to rest on the bench top for 72 h, over which dark solid crystals deposited. IR (neat, solid): $\tilde{\nu}$ = 3056 (w), 2920 (m), 2850 (w), 2283 (w), 1479 (m), 1432 (m), 1186 (w), 1087 (m), 996 (w), 909 (m), 828 (s, η^2-O_2), 723 (s) cm^{-1}. From X-ray sample (in Nujol): FAB-MS m/z (%) 741 (52) $[Ru(ind)(PPh_3)_2]$, 625 (10) $[Ru(PPh_3)_2]^+$, 479 (100) $[Ru(ind)(PPh_3)]^+$, 363 (16) $[Ru(PPh_3)]$, 279 (64) $[O{=}PPh_3]$. From separate crystal: ESI-MS m/z (%) 782 $[Ru(ind)(CH_3CN)(PPh_3)2]^+$, 741 $[Ru(ind)(PPh_3)_2)]^+$.

Activity Determinations

The respective precursor complex (0.0061 mmol, 2 mol %) was placed into an NMR tube along with $NaPF_6$ (0.006 g, 0.036 mmol) and CH_3CN (0.02 mL). The mixture was heated for 5 min at 85 C. A solution containing 1-phenyl-2-propyn-1-ol (1a, 0.041 g, 0.31 mmol), benzyl alcohol (2b, 42 mg, 0.39 mmol) and p-dimethoxybenzene (internal standard, 0.002 g) in toluene-d_8 (0.6 mL) was added to each NMR tube. The mixture was heated at 85 °C for 24 h, where ^1H NMR spectra were recorded for each reaction mixture over a consistent time period. Integration of the diastereotopic doublets at δ 4.78 (d, JHH = 11.7 Hz, CH_2, 2H) for the product in the spectrum were referenced to the aromatic protons of p-dimethoxybenzene at δ 6.71 (4H).

(1-butoxybut-3-yn-2-yl)benzene.

A small screw-cap vial containing $[RuCl(ind)(PPh_3)_2]$ (0.008 g, 0.010 mmol, 1.5%/mol), $NaPF_6$ (0.008 g, 0.047 mmol) and 1 mL of toluene / CH_3CN (9:1) was heated at 85 °C for 0.5 hours, over which the solution shifted to a lighter yellow-orange. After

removing from heat, 2- phenyl-3-butyn-2-ol (0.103 g, 0.706 mmol), *n*-butyl alcohol (0.084 g, 1.137 mmol) was added. The mixture was heated at 85 °C for 18 hours. The product was isolated by column chromatography (silica gel, 1.5 × 15 cm, 2:1 hexane/CH_2Cl_2) as an orange oil (0.048 g, 0.235 mmol, 33%). ^{1}H NMR (300 MHz, $CDCl_3$) δ 7.54–7.51 (m, 2H, arom.), 7.28–7.20 (m, 3H, arom.), 3.49 (dt, J_{HH}=9 Hz, J_{HH}=7 Hz, 1H), 3.03 (dt, J_{HH}=9 Hz, J_{HH}=7 Hz, 1H), 2.60 (s, 1H, ≡C*H*), 1.64 (s, 3H, CH_3), 1.48 (quint, J_{HH}=14 Hz, 2H, CH_2), 1.32-1.24 (m, 2H, CH_2), 0.80 (t, J_{HH}=7Hz, 3H, CH_3). ^{13}C{^{1}H} NMR (75 MHz, $CDCl_3$) δ 143.1 (s), 128.4 (s), 127.9 (s), 126.0 (s), 84.5 (s), 75.8 (s), 75.3 (s), 64.8 (s), 33.1 (s), 32.2 (s), 19.6 (s), 14.1 (s).

Catalyzed by [RuCl(ind)(PPh_3){P(*p*-$CF_3C_6H_4)_3$}]. A small screw-cap vial containing [RuCl(ind)(PPh_3){P(*p*-$CF_3C_6H_4)_3$}] (0.010 g, 0.010 mmol, 1.5 mol%), $NaPF_6$ (0.008 g, 0.047 mmol) and 1 mL of toluene / CH_3CN (9:1) was heated at 85 °C for 0.5 hours, over which the solution shifted to a lighter yellow-orange. After removing from heat, 2-phenyl-3-butyn-2-ol (0.104 g, 0.712 mmol), *n*-butyl alcohol (0.088 g, 1.189 mmol) was added. The mixture was heated at 85 °C for 18 hours. The product was isolated by column chromatography (silica gel, 1.5 × 15 cm, 2:1 hexane/CH_2Cl_2) as an orange oil (0.042 g, 0.209 mmol, 29%).

Catalyzed by [RuCl(ind)(PPh_3){P(3,5-$(CF_3)_2C_6H_3)_3$}]. A small screw-cap vial containing [RuCl(ind)(PPh_3){P(3,5-$(CF_3)_2C_6H_3)_3$}] (0.012 g, 0.010 mmol, 1.5%/mol), $NaPF_6$ (0.008 g, 0.047 mmol) and 1 mL of toluene / CH_3CN (9:1) was heated at 85 °C for 0.5 hours, over which the solution shifted to a lighter yellow-orange. After removing from heat, 2-phenyl-3-butyn-2-ol (0.102 g, 0.697 mmol), *n*-butyl alcohol (0.088 g, 1.189 mmol) was added. Mixture was heated at 85 °C for 18 hours. The product was isolated by

column chromatography (silica gel, 1.5 × 15cm, 2:1 hexane/CH_2Cl_2) as an orange oil (0.057 g, 0.283 mmol, 40%).

(1-(Benzyloxy)prop-2-yn-1-yl)benzene

A small screw-cap vial containing [RuCl(ind)(PPh_3)$_2$] (0.008 g, 0.010 mmol, 1.5%/mol), $NaPF_6$ (0.008 g, 0.047 mmol) and 1 mL of toluene / CH_3CN (9:1) was heated at 85 °C for 0.5 hours, over which the solution shifted to a lighter yellow-orange. After removing from heat, 1- phenylprop-2-yn-1-ol (0.101 g, 0.768 mmol), benzyl alcohol (0.117 g, 1.09 mmol) was added. Mixture was heated at 85 °C for 20 hours. The product was filtered through a small amount of alumina and isolated by column chromatography (silica gel, 1.5×15cm, 4:1 hexane/CH_2Cl_2) as a yellow-orange oil (0.065 g, 0.293 mmol, 38%). ^{1}H NMR (300 MHz, $CDCl_3$) δ 7.61–7.60 (m, 2H, arom.), 7.64–7.60 (m, 2H, arom.), 7.50–7.42 (m, 8H, arom.), 5.30 (s, 1H, C*H*), 4.78 (q, J_{HH}=12 Hz, CH_2, 2H), 2.77 (s, ≡C*H*, 1H). ^{13}C{^{1}H} NMR (75 MHz, $CDCl_3$) δ 138.1 (s), 137.6 (s), 128.6 (s), 128.5 (s), 128.2 (s), 128.2 (s), 127.9 (s), 127.5 (s), 100.4 (s), 81.6 (s), 76.0 (s), 70.2 (s), 70.0 (s).

Catalyzed by [RuCl(ind)(PPh_3){P(*p*-$CF_3C_6H_4$)$_3$}]. A small screw-cap vial containing [RuCl(ind)(PPh_3){P(*p*-$CF_3C_6H_4$)$_3$}] (0.010 g, 0.010 mmol, 1.5 mol%), $NaPF_6$ (0.008 g, 0.047 mmol) and 1 mL of toluene / CH_3CN (9:1) was heated at 85 °C for 0.5 hours, over which the solution shifted to a lighter yellow-orange. After removing from heat, 1-phenylprop-2-yn-1-ol (0.101 g, 0.763 mmol), benzyl alcohol (0.119 g, 1.100 mmol) was added. Mixture was heated at 85 °C for 20 hours. The product was filtered through a small amount of alumina and isolated by column chromatography (silica gel, 1.5×15cm, 4:1 hexane/CH_2Cl_2) as a yellow-orange oil (0.066 g, 0.298 mmol, 39%).

Catalyzed by [RuCl(ind)(PPh_3){P(3,5-$(CF_3)_2C_6H_3$)$_3$}]. A small screw-cap vial

containing [RuCl(ind)(PPh_3){P(3,5-$(CF_3)_2C_6H_3)_3$}] (0.012 g, 0.010 mmol, 1.5%/mol), $NaPF_6$ (0.009 g, 0.053 mmol) and 1 mL of toluene / CH_3CN (9:1) was heated at 85 °C for 0.5 hours, over which the solution shifted to a lighter yellow-orange. After removing from heat, 1-phenylprop-2-yn-1-ol (0.099 g, 0.756 mmol), benzyl alcohol (0.114 g, 1.05 mmol) was added. The mixture was heated at 85 °C for 20 hours. The product was filtered through a small amount of alumina and isolated by column chromatography (silica gel, 1.5×15cm, 4:1 hexane/CH_2Cl_2) as a yellow-orange oil (0.074 g, 0.333 mmol, 44%).

(2-(Benzyloxy)but-3-yn-2-yl)benzene

A small screw-cap vial containing [RuCl(ind)(PPh_3)$_2$] (0.008 g, 0.010 mmol, 1.5%/mol), $NaPF_6$ (0.007 g, 0.042 mmol) and 1 mL of toluene / CH_3CN (9:1) was heated at 85 °C for 0.5 hours, over which the solution shifted to a lighter yellow-orange. After removing from heat, 2-phenyl-3-butyn-2-ol (0.103 g, 0.705 mmol), benzyl alcohol (0.114 g, 1.05 mmol) was added. Mixture was heated at 85 °C for 18 hours. The product was filtered through a small amount of alumina and isolated by column chromatography (silica gel, 1.5×15cm, 4:1 hexane/CH_2Cl_2) as a yellow-orange oil (0.091 g, 0.384 mmol, 55%). ^{1}H NMR (300 MHz, $CDCl_3$) δ 7.75–7.72 (m, 2H, arom.), 7.43–7.36 (m, 8H, arom), 4.70 (d, J_{HH}=9 Hz, 1H, C*H*2), 4.21 (d, J_{HH}=9 Hz, 1H, CH_2), 2.81 (s, 1H, ≡CH), 1.86 (s, 3H, CH_3). ^{13}C{^{1}H} NMR (75 MHz, $CDCl_3$) δ 142.6 (s), 138.7 (s), 128.7 (s), 128.6 (s), 128.5 (s), 128.1 (s), 128.0 (s), 127.6 (s), 127.1 (s), 126.2 (s), 84.3 (s), 76.4 (s), 76.0 (s), 67.4 (s), 33.2 (s).

Catalyzed by [RuCl(ind)(PPh_3){P(*p*-$CF_3C_6H_4)_3$}]. A small screw-cap vial containing [RuCl(ind)(PPh_3){P(*p*-$CF_3C_6H_4)_3$}] (0.010 g, 0.010 mmol, 1.5 mol%), $NaPF_6$ (0.007 g,

0.042 mmol) and 1 mL of toluene / CH_3CN (9:1) was heated at 85 °C for 0.5 hours, over which the solution shifted to a lighter yellow-orange. After removing from heat, 2-phenyl-3-butyn-2-ol (0.102 g, 0.705 mmol), benzyl alcohol (0.113 g, 1.05 mmol) was added. Mixture was heated at 85 °C for 18 hours. The product was filtered through a small amount of alumina and isolated by column chromatography (silica gel, 1.5 × 15cm, 4:1 hexane/CH_2Cl_2) as a yellow-orange oil (0.101 g, 0.431 mmol, 61%).

Catalyzed by [RuCl(ind)(PPh_3){P(3,5-$(CF_3)_2C_6H_3)_3$}]. A small screw-cap vial containing [RuCl(ind)(PPh_3){P(3,5-$(CF_3)_2C_6H_3)_3$}] (0.012 g, 0.010 mmol, 1.5 mol%), $NaPF_6$ (0.008 g, 0.047 mmol) and 1 mL of toluene / CH_3CN (9:1) was heated at 85 °C for 0.5 hours, over which the solution shifted to a lighter yellow-orange. After removing from heat, 2-phenyl-3-butyn-2-ol (0.102 g, 0.705 mmol), benzyl alcohol (0.114 g, 1.05 mmol) was added. The mixture was heated at 85 °C for 18 hours. The product was filtered through a small amount of alumina and isolated by column chromatography (silica gel, 1.5 × 15cm, 4:1 hexane/CH_2Cl_2) as a yellow-orange oil (0.097 g, 0.410 mmol, 58%).

Cyclic Voltammetry

Voltammograms were recorded in a three-electrode BAS electrochemical cell in a Vacuum Atmospheres HE-493 drybox under an atmosphere of argon in 0.1M NBu_4PF_6/CH_2Cl_2 at 298 K. A 1.6 mm Pt disk electrode was used as the working electrode, a platinum wire was used as the auxiliary electrode, and a silver wire was used a pseudo-reference electrode. Potentials were calibrated against the $Cp^*_2Fe^{0/+}$ couple, which is known to occur at 0.548 V vs the $Cp_2Fe^{0/+}$ couple for this solvent medium.[86] The potentials in this paper can be changed to SCE reference values by addition of 0.56

V. Voltammograms were collected at 0.05–1.6 V/s with an EG&G PAR 263A potentiostat interfaced to a computer operated with EG&G PAR Model 270 software.

X-ray structure determination for [RuCl(ind)(PPh$_3$){P(p-C$_6$H$_4$CF$_3$)$_3$}], [RuCl(ind)(PPh$_3$){P(3,5-C$_6$H$_3$(CF$_3$)$_2$)$_3$}], [Ru(ind)(CH$_3$CN)(PPh$_3$)$_2$)]PF$_6$ and [Ru(ind)(η^2–O$_2$)(PPh$_3$)$_2$]PF$_6$.

Crystals of [RuCl(ind)(PPh$_3$){P(p-C$_6$H$_4$CF$_3$)$_3$}], [RuCl(ind)(PPh$_3$){P(3,5-C$_6$H$_3$(CF$_3$)$_2$)$_3$}] and [Ru(ind)(CH$_3$CN)(PPh$_3$)$_2$)]PF$_6$ were obtained by diffusion of hexane into CH$_2$Cl$_2$ solutions of the complexes. Crystals of [Ru(ind)(η^2-O$_2$)(PPh$_3$)$_2$]PF$_6$ were obtained by storage of a CDCl$_3$ solution of [Ru(ind)(CH$_3$CN)(PPh$_3$)$_2$)]PF$_6$ under aerobic conditions and directly taken from the reaction mixture. Crystals of approximate dimensions were mounted on MiTeGen cryoloops in random orientations. Preliminary examination and data collection were performed using a Bruker X8 Kappa Apex II Charge Coupled Device (CCD) Detector system single crystal X-ray diffractometer equipped with an Oxford Cryostream LT device. All data were collected using graphite monochromated Mo Kα radiation (λ = 0.71073 Å) from a fine focus sealed tube X-ray source. Preliminary unit cell constants were determined with a set of 36 narrow frame scans. Typical data sets consist of combinations of ω and Φ scan frames with typical scan width of 0.5° and counting time of 15 s/frame at a crystal to detector distance of 4.0 cm. The collected frames were integrated using an orientation matrix determined from the narrow frame scans. Apex II and SAINT software packages were used for data collection and data integration.[87] Analysis of the integrated data did not show any decay. Final cell constants were determined by global refinement of reflections harvested from the

complete data set. Collected data were corrected for systematic errors using SADABS based on the Laue symmetry using equivalent reflections.[87]

Crystal data and intensity data collection parameters are listed in Table 4.Structure solution and refinement were carried out using the SHELXTL-PLUS software package.[88] The structures were solved and refined successfully in the space groups $P2_1$ for $[Ru(ind)(CH_3CN)(PPh_3)_2)]PF_6$ and P–1 for all other complexes. Full matrix least-squares refinements were carried out by minimizing $\Sigma w(F_o^2-F_c^2)^2$. The non-hydrogen atoms were refined anisotropically to convergence. All hydrogen atoms were treated using appropriate riding model (AFIX m3).

Absolute structure determination was carried out using Parson's method for $[Ru(ind)(CH_3CN)(PPh_3)_2)]PF_6$ with Flack x = –0.021(4) from 10263 selected quotients.[89]

For the compound $[Ru(ind)(\eta^2\text{-}O^2)(PPh_3)_2]PF_6$ Platon-Squeeze was used to remove badly disordered solvent molecules ($3 \times CHCl_3$).[90] The counter ion PF_6 is also disordered and the disorder was resolved with partial occupancy F atoms with geometrical restraints.

For the complex $[RuCl(ind)(PPh_3)\{P(p\text{-}C_6H_4CF_3)_3\}]$, half a molecule of ethyl acetate was found in the lattice. Two CF_3 groups and the CH_3 of the solvent were disordered. The disorder was modeled with partial occupancy atoms and geometrical restraints.

The data for $[RuCl(ind)(PPh_3)\{P(3,5\text{-}C_6H_3(CF_3)_2)_3\}]$ was twinned. A two-component twin model was used for refinement with BASF = 0.49.1.5 molecules of $CHCl_3$/Ru were found in the lattice. Disordered CF_3 group was refined with partial occupancy F atoms with geometrical restraints.

3.7. References

(1) Flanagan, S. P.; Guiry, P. J. *J. Organomet. Chem.* **2006**, *691* (10), 2125–2154.
(2) Casalnuovo, A. L.; RajanBabu, T. V.; Ayers, T. A.; Warren, T. H. *J. Am. Chem. Soc.* **1994**, *116* (22), 9869–9882.
(3) Shaw, S.; White, J. D. *J. Am. Chem. Soc.* **2014**, *136* (39), 13578–13581.
(4) Voituriez, A.; Panossian, A.; Fleury-Brégeot, N.; Retailleau, P.; Marinetti, A. *J. Am. Chem. Soc.* **2008**, *130* (43), 14030–14031.
(5) Hoveyda, A. H.; Schrock, R. R. *Chem. Eur. J.* **2001**, *7* (5), 945–950.
(6) Dai, L.-X.; Tu, T.; You, S.-L.; Deng, W.-P.; Hou, X.-L. *Acc. Chem. Res.* **2003**, *36* (9), 659–667.
(7) Cao, Z. Y.; Brittain, W.; Fossey, J. S.; Zhou, F. *Catalysis Science & Technology* **2015**, *5*, 3427–3830.
(8) Jana, R.; Pathak, T. P.; Sigman, M. S. *Chem. Rev.* **2011**, *111* (3), 1417–1492.
(9) Halpern, J.; Trost, B. M. *Proc. Natl. Acad. Sci. U.S.A.* **2004**, *101* (15), 5347–5347.
(10) Wang, Y.; Lu, H.; Xu, P.-F. *Acc. Chem. Res.* **2015**, (48), 1832–1844.
(11) Deshmukh, P. H.; Blechert, S. *Dalton Trans.* **2007**, *60* (24), 2479–13.
(12) Straub, B. F. *Angew. Chem. Int. Ed.* **2005**, *44* (37), 5974–5978.
(13) Trnka, T. M.; Grubbs, R. H. *Acc. Chem. Res.* **2001**, *34* (1), 18–29.
(14) Grubbs, R. H.; Burk, P. L.; Carr, D. D. *J. Am. Chem. Soc.* **1975**, *97* (11), 3265–3267.
(15) Schwab, P.; Grubbs, R. H.; Ziller, J. W. *J. Am. Chem. Soc.* **1996**, *118* (1), 100–110.
(16) Dias, E. L.; Nguyen, S. T.; Grubbs, R. H. *J. Am. Chem. Soc.* **1997**, *119* (17), 3887–3897.
(17) Jean Louis Hérisson, P.; Chauvin, Y. *Macromolecular Chemistry and Physics* **1971**, *141* (1), 161–176.
(18) Joseph P A Harrity; Michael S Visser; John D Gleason, A.; Hoveyda, A. H. *J. Am. Chem. Soc.* **1997**, *119* (6), 1488–1489.
(19) Kingsbury, J. S.; Harrity, J. P. A.; Bonitatebus, P. J.; Hoveyda, A. H. *J. Am. Chem. Soc.* **1999**, *121* (4), 791–799.
(20) Bieniek, M.; Bujok, R.; Cabaj, M.; Lugan, N.; Lavigne, G.; Arlt, D.; Grela, K. *J. Am. Chem. Soc.* **2006**, *128* (42), 13652–13653.
(21) Bieniek, M.; Samojłowicz, C.; Sashuk, V.; Bujok, R.; Śledź, P.; Lugan, N.; Lavigne, G.; Arlt, D.; Grela, K. *Organometallics* **2011**, *30* (15), 4144–4158.
(22) Crabtree, R. H. *The Organometallic Chemistry of the Transition Metals*, 5 ed.; John Wiley & Sons, Inc.: Hoboken, 2014; pp 1–522.
(23) Anderson, K. M.; Orpen, A. G. *Chem. Commun.* **2001**, No. 24, 2682–2683.
(24) Coe, B. J.; Glenwright, S. J. *Coord. Chem. Rev.* **2000**, *203* (1), 5–80.
(25) Scholl, M.; Ding, S.; Lee, C. W.; Grubbs, R. H. *Org. Lett.* **1999**, *1* (6), 953–956.
(26) Sanford, M. S.; Love, J. A.; Grubbs, R. H. *J. Am. Chem. Soc.* **2001**, *123* (27), 6543–6554.
(27) Olszewski, T.; Bieniek, M.; Skowerski, K.; Grela, K. *Synlett* **2013**, *24* (08), 903–919.
(28) Michrowska, A.; Bujok, R.; Harutyunyan, S.; Sashuk, V.; Dolgonos, G.; Grela, K. *J. Am. Chem. Soc.* **2004**, *126* (30), 9318–9325.
(29) Bujok, R.; Bieniek, M.; Masnyk, M.; Michrowska, A.; Sarosiek, A.; Stępowska, H.; Arlt, D.; Grela, K. *J. Org. Chem.* **2004**, *69* (20), 6894–6896.
(30) Keitz, B. K.; Endo, K.; Patel, P. R.; Herbert, M. B.; Grubbs, R. H. *J. Am. Chem. Soc.* **2011**, *134* (1), 693–699.
(31) Paradiso, V.; Bertolasi, V.; Costabile, C.; Caruso, T.; Dąbrowski, M.; Grela, K.; Grisi, F. *Organometallics* **2017**, *36* (19), 3692–3708.
(32) Endo, K.; Herbert, M. B.; Grubbs, R. H. *Organometallics* **2013**, *32* (18), 5128–5135.
(33) Rosebrugh, L. E.; Herbert, M. B.; Marx, V. M.; Keitz, B. K.; Grubbs, R. H. *J. Am. Chem. Soc.* **2013**, *135* (4), 1276–1279.
(34) Denk, K.; Fridgen, J.; Herrmann, W. A. *Adv. Synth. Catal.* **2002**.
(35) Herbert, M. B.; Suslick, B. A.; Liu, P.; Zou, L.; Dornan, P. K.; Houk, K. N.; Grubbs, R. H. *Organometallics* **2015**, *34* (12), 2858–2869.
(36) Credendino, R.; Falivene, L.; Cavallo, L. *J. Am. Chem. Soc.* **2012**, *134* (19), 8127–8135.
(37) Jung, H.; Jung, K.; Hong, M.; Kwon, S.; Kim, K.; Hong, S. H.; Choi, T.-L.; Baik, M.-H. *J. Am. Chem. Soc.* **2018**, *140* (2), 834–841.

(38) Ahmed, T. S.; Grubbs, R. H. *J. Am. Chem. Soc.* **2017**, *139* (4), 1532–1537.
(39) Ahmed, M.; Barrett, A. G. M.; Braddock, D. C.; Cramp, S. M.; Procopiou, P. A. *Tetrahedron Letters* **1999**, *40* (49), 8657–8662.
(40) Monfette, S.; Camm, K. D.; Gorelsky, S. I.; Fogg, D. E. *Organometallics* **2009**, *28* (4), 944–946.
(41) Love, J. A.; Morgan, J. P.; Trnka, T. M.; Grubbs, R. H. *Angew. Chem. Int. Ed.* **2002**, *41* (21), 4035–4037.
(42) Crabtree, R. H. *J. Organomet. Chem.* **2005**, *690* (24-25), 5451–5457.
(43) Osborn, J. A.; Wilkinson, G.; Young, J. F. *Chem. Commun. (London)* **1965**, (2), 17–1.
(44) Osborn, J. A.; Jardine, F. H.; Young, J. F.; Wilkinson, G. *J. Chem. Soc., A* **1966**, *0* (0), 1711–1732.
(45) Tolman, C. A. *J. Am. Chem. Soc.* **1970**, *92* (10), 2953–2956.
(46) Tolman, C. A. *Chem. Rev.* **1977**, *77* (3), 313–348.
(47) Fey, N.; Orpen, A. G.; Harvey, J. N. *Coord. Chem. Rev.* **2009**, *253* (5-6), 704–722.
(48) Stark, M. J.; Shaw, M. J.; Rath, N. P.; Bauer, E. B. *Eur. J. Inorg. Chem.* **2016**, No. 7, 1093–1102.
(49) Cadierno, V.; Gamasa, M. P.; Gimeno, J.; González-Cueva, M.; Lastra, E.; Borge, J.; García-Granda, S.; Pérez-Carreño, E. *Organometallics* **1996**, *15* (8), 2137–2147.
(50) Costin, S.; Rath, N. P.; Bauer, E. B. *Inorganic Chemistry Communications* **2011**, *14* (3), 478–480.
(51) Batterjee, S. M.; Marzouk, M. I.; Aazab, M. E.; El-Hashash, M. A. *Appl. Organometal. Chem.* **2003**, *17* (5), 291–297.
(52) Kieltsch, I.; Dubinina, G. G.; Hamacher, C.; Kaiser, A.; Torres-Nieto, J.; Hutchison, J. M.; Klein, A.; Budnikova, Y.; Vicic, D. A. *Organometallics* **2010**, *29* (6), 1451–1456.
(53) Popeney, C.; Guan, Z. *Organometallics* **2005**, *24* (6), 1145–1155.
(54) Gonsalvi, L.; Adams, H.; Sunley, G. J.; Ditzel, E.; Haynes, A. *J. Am. Chem. Soc.* **2002**, *124* (45), 13597–13612.
(55) RajanBabu, T. V.; Radetich, B.; You, K. K.; Ayers, T. A.; Casalnuovo, A. L.; Calabrese, J. C. *J. Org. Chem.* **1999**, *64* (10), 3429–3447.
(56) Hunter, A. D.; Williams, T. R.; Zarzyczny, B. M.; Bottesch, H. W., II; Dolan, S. A.; McDowell, K. A.; Thomas, D. N.; Mahler, C. H. *Organometallics* **2016**, *35* (16), 2701–2706.
(57) Kamigaito, M.; Watanabe, Y.; Ando, T.; Sawamoto, M. *J. Am. Chem. Soc.* **2002**, *124* (34), 9994–9995.
(58) Costin, S.; Rath, N. P.; Bauer, E. B. *Inorganica Chimica Acta* **2009**, *362* (6), 1935–1942.
(59) Cadierno, V.; Conejero, S.; Gamasa, M. P.; Gimeno, J. *Dalton Trans.* **2003**, No. 15, 3060–3066.
(60) Belli, R. G.; Burton, K. M. E.; Rufh, S. A.; McDonald, R.; Rosenberg, L. *Organometallics* **2015**, *34* (23), 5637–5646.
(61) Lee, J. P.; Hankins, M. J.; Riner, A. D.; Albu, T. V. *Journal of Coordination Chemistry* **2016**, *69* (1), 21–39.
(62) Nuñez-Zarur, F.; Solans-Monfort, X.; Rodríguez-Santiago, L.; Sodupe, M. *Organometallics* **2012**, *31* (11), 4203–4215.
(63) Alkhaleeli, D. F.; Baum, K. J.; Rabus, J. M.; Bauer, E. B. *Catal. Commun.* **2014**, *47*, 45–48.
(64) Bruce, M. I. *Chem. Rev.* **1998**, *98* (8), 2797–2858.
(65) Fürstner, A.; Liebl, M.; Lehmann, C. W.; Picquet, M.; Kunz, R.; Bruneau, C.; Touchard, D.; Dixneuf, P. H. *Chem. Eur. J.* **2000**, *6* (10), 1847–1857.
(66) Costin, S.; Widaman, A. K.; Rath, N. P.; Bauer, E. B. *Eur. J. Inorg. Chem.* **2011**, *2011* (8), 1269–1282.
(67) Keisham, S. S.; Mozharivskyj, Y. A.; Carroll, P. J.; Kollipara, M. R. *J. Organomet. Chem.* **2004**, *689* (7), 1249–1256.
(68) Oro, L. A.; Ciriano, M. A.; Campo, M.; Foces-Foces, C. *J. Organomet. Chem.* **1985**, *289* (1), 117–131.
(69) Kuan, S. L.; Leong, W. K.; Webster, R. D.; Goh, L. Y. *Organometallics* **2012**, *31* (14), 5159–5168.
(70) Yu, H.; Fu, Y.; Guo, Q.; Lin, Z. *Organometallics* **2009**, *28* (15), 4443–4451.
(71) Costin, S.; Sedinkin, S. L.; Bauer, E. B. *Tetrahedron Letters* **2009**, *50* (8), 922–925.
(72) Queensen, M. J.; Rabus, J. M.; Bauer, E. B. *J Mol Catal A-Chem* **2015**, *407*, 221–229.
(73) Jourabchian, N.; Jurkowski, K.; Bauer, E. B. *Catal. Commun.* **2018**, *106*, 92–95.
(74) Wilson, R. J.; Kaminsky, L.; Ahmed, I.; Clark, D. A. *J. Org. Chem.* **2015**, *80* (16), 8290–8299.

(75) Gilbert-Wilson, R.; Field, L. D.; Bhadbhade, M. *Inorg. Chem.* **2014**, *53* (23), 12469–12479.
(76) Montserrat Oliván; Eric Clot; Odile Eisenstein, A.; Kenneth G Caulton. *Organometallics* **1998**, *17* (14), 3091–3100.
(77) Brooks, N. R.; Blake, A. J.; Champness, N. R.; Cunningham, J. W.; Hubberstey, P.; Schröder, M. *Crystal Growth & Design* **2001**, *1* (5), 395–399.
(78) Di Vaira, M.; Peruzzini, M.; Seniori Costantini, S.; Stoppioni, P. *J. Organomet. Chem.* **2006**, *691* (18), 3931–3937.
(79) Terborg, L.; Nowak, S.; Passerini, S.; Winter, M.; Karst, U.; Haddad, P. R.; Nesterenko, P. N. *Analytica Chimica Acta* **2012**, *714*, 121–126.
(80) da Cunha, T. T.; Pointillart, F.; Le Guennic, B.; Pereira, C. L. M.; Golhen, S.; Cador, O.; Ouahab, L. *Inorg. Chem.* **2013**, *52* (17), 9711–9713.
(81) Plakhotnyk, A. V.; Ernst, L.; Schmutzler, R. *J. Fluorine Chem.* **2005**, *126* (1), 27–31.
(82) Cadierno, V.; Gimeno, J. *Chem. Rev.* **2009**, *109* (8), 3512–3560.
(83) Zhan, Z.-P.; Yu, J.-L.; Liu, H.-J.; Cui, Y.-Y.; Yang, R.-F.; Yang, W.-Z.; Li, J.-P. *J. Org. Chem.* **2006**, *71* (21), 8298–8301.
(84) Bauer, E. B. *Synthesis* **2012**, *44* (8), 1131–1151.
(85) Stark, M. J.; Shaw, M. J.; Fadamin, A.; Rath, N. P.; Bauer, E. B. *J. Organomet. Chem.* **2017**, *847*, 41–53.
(86) Barrière, F.; Geiger, W. E. *J. Am. Chem. Soc.* **2006**, *128* (12), 3980–3989.
(87) *Bruker Analytical X–ray*; Madison, WI, 2012.
(88) Sheldrick, G. M. *Acta Cryst.* **2008**, *A64*, 112–122.
(89) Parsons, S.; Flack, H.; IUCr. *Acta Cryst.* **2004**, *A60*, S61.
(90) Spek, A. L. *Acta Cryst.* **1990**, *A46*, C34.

Chapter 4. Ruthenium-Catalyzed Enol Esters

Chapter 4. Ruthenium-Catalyzed Enol Esters

4.1. Aim

Ruthenium complexes with polydentate ligands were explored as an avenue of catalytic activation of terminal alkynes. We intended to employ a series of substituted Schiff bases as tridentate ligands for ruthenium complexes. We hypothesize that substituted pyridines could offer a reasonable scaffold for further electronic tuning studies. Furthermore, we hypothesized a tridentate ligand could make the ruthenium complex more thermally stable. Our catalytic systems with monodentate ligands frequently required high reaction temperatures, potentially leading to decomposition of the complexes. During our investigation, a new complex using a chelating 2,6–diacetylpyridine ligand was synthesized and characterized. This new complex was tested for catalytic activity and selectivity of isomers in reactions forming enol esters by addition of carboxylic acids to terminal alkynes.

4.2. Introduction

4.2.1. Polydentate Pyridine–Based Ligand Systems

Ruthenium complexes have been employed in a variety of catalytic applications with a wide variety of ligands attached to them. Some of these ligands offer steric and electronic properties that affect catalytic rates or selectivity. For example, the complex $[Ru(bpy)_3]^{2+}$ (Figure 4.1.) is well known to have extensive photophysical and photochemical properties.[1] Systematic studies of pyridine–based ligands over several decades has provided numerous examples of derivatives of pyridine ligands used in metal complexes with unique physical and electronic properties.[2-6] Often, these pyridine–based

ligands are applied in the form of polydentate ligands; a pyridine is substituted on the aromatic ring with imines (Schiff bases), amides pyrrazoles, pyrroles, pyridines, phosphines, or other chelating functional groups that wrap around the metal center and bind to it in two or more places in the coordination sphere.[7] These groups are further modified with electron–withdrawing or –donating side groups, with the hopes of fine–tuning the charge transfer reactions this series of complexes is well–known for.[8-11] A few pyridine–based ligands are shown below in Figure 4.1.

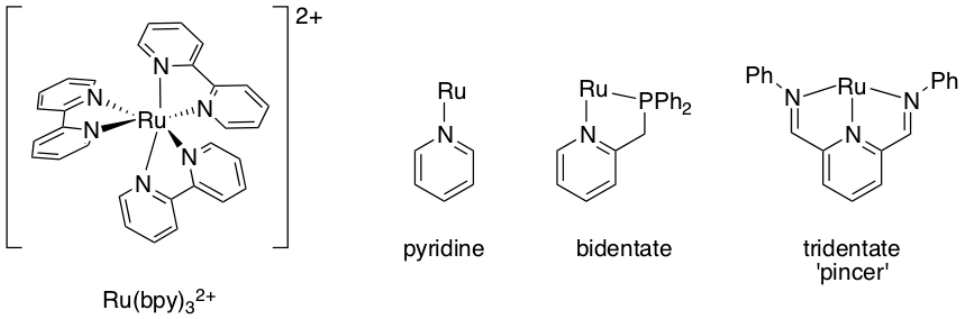

Figure 4.1. Example pyridine–based ligands.

Pyridine–based polydentate ligands, sometimes referred to as 'pincer ligands' when tridentate, have been extended into the realm of catalytic application applications due to being highly tunable in nature.[12,13] While there are numerous studies of using pyridine–based pincer ligands in transfer hydrogenation reactions, they have also been employed in catalytic oxidation, and coupling reactions.[14-27]

4.2.2. Enol Esters

Enol esters (**32**, **33**, and **34** in Scheme 4.1.) are simple molecules, where an ester functionality is attached to an alkene. These functional groups are a versatile class of precursors that can be synthetically important building blocks. Organic transformations

can employ enol esters in the synthesis of larger and more complex molecules by methods such as the synthesis of α–acetoxy ketones, Mannich–type condensations, olefin metathesis, Barbier–type reactions, and as a novel route to form aldehydes from alkynes.[28-38] Some of these transformations are shown below in Scheme 4.1.

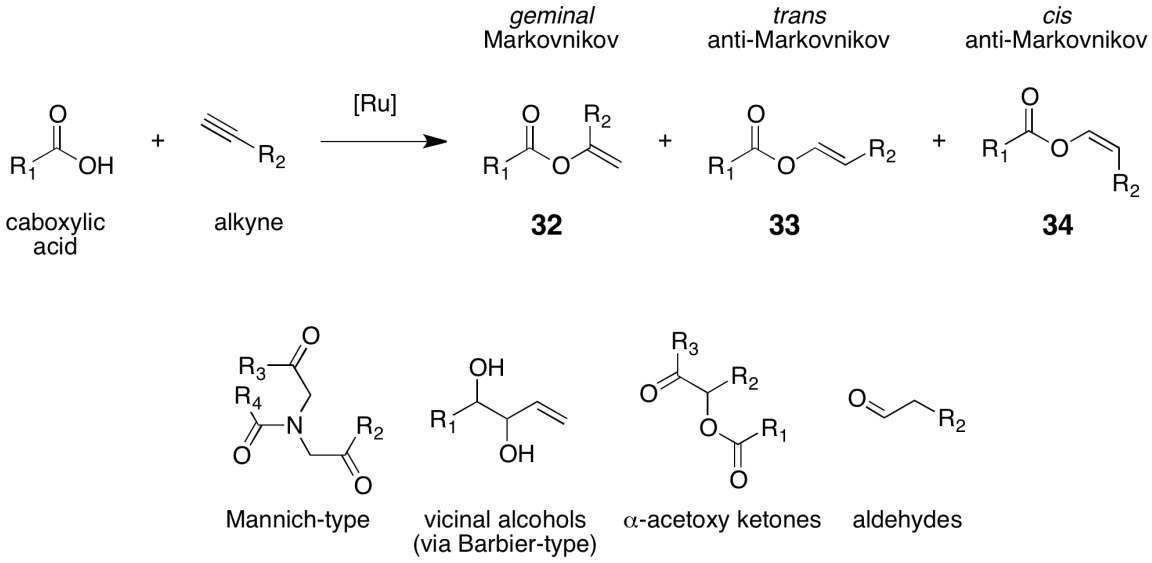

Scheme 4.1. Formation of enol esters and some products of their synthetic applications.

Current methods to synthesize enol esters employ readily available starting materials: a carboxylic acid and an alkyne. Most synthetic methods utilize a transition metal complex as a catalyst to achieve the addition of carboxylic acids to alkynes to afford enol esters. Some methods have successfully employed copper, rhodium, selenium, or potassium monopersulfate triple salt oxone to synthesize enol esters through addition reactions or through rearrangement reactions.[39-42] By far, the best catalytic systems for this reaction seem to be based on ruthenium.[43-47] A number of ruthenium complexes have been synthesized and used in this context to supply enol esters, predominantly generating

the Markovnikov addition product **32**. Regioselectivity of ruthenium complexes in these catalytic reactions frequently provides moderate to excellent selectivity of the geminal product for terminal alkynes. The isomers that can result from this reaction are shown above in a generalized form in Scheme 4.1.

4.3. Results

4.3.1. Synthesis of [RuCl(dap)(PPh$_3$)$_2$]BAr$^F_4$ (**35**)

We had originally intended to use 2,6-diacetylpyridine as the starting material for the synthesis of a Schiff base ligand. To our surprise, early exploratory experiments demonstrated that the diacetylpyridine was able to form a complex with ruthenium, qualitatively observed by a color change. The synthesis of the new complex, [RuCl(dap)(PPh$_3$)$_2$]BAr$^F_4$ (**35**), was carried out by ligand exchange under Schlenk conditions. The known starting complex [RuCl$_2$(PPh$_3$)$_3$], 2,6-diacetylpyridine (dap), and sodium tetrakis[3,5-bis(trifluoromethyl)phenyl]borate (NaBAr$^F_4$) were placed into a Schlenk tube with CH_2Cl_2 , and stirred for one hour at room temperature. The deep purple complex was isolated in 92 % after recrystallization from CH_2Cl_2 and hexanes.

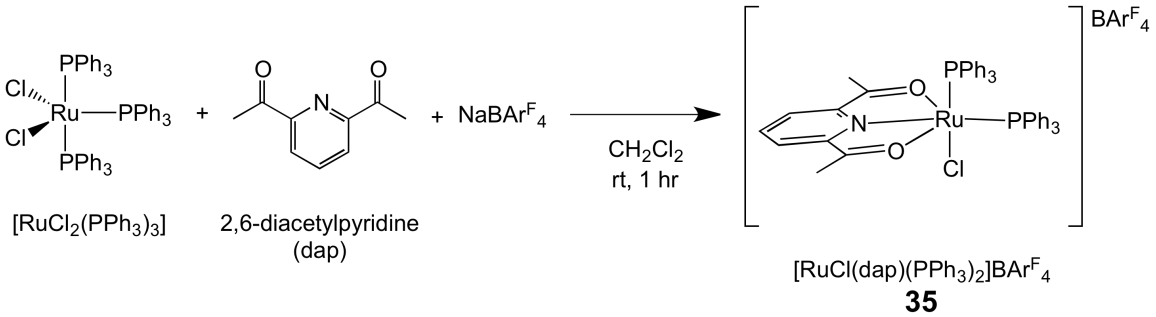

Scheme 4.2. The synthesis of [RuCl(dap)(PPh$_3$)$_2$]BAr$^F_4$ (**35**).

Complex **35** was characterized by NMR, IR, and MS methods. The $^{31}P\{^{1}H\}$ NMR presented two doublets, indicative of coupling by magnetically inequivalent phosphines ligands coordinated to the metal center. Although the ^{1}H NMR spectrum behaved as expected, not all peaks in the $^{13}C\{^{1}H\}$ NMR spectrum could be fully assigned; the resolution of the aromatic peaks was not sufficient enough to differentiate all signals from one another, even at maximum concentrations of the NMR sample in $CDCl_3$ for 12 hours. The mass spectrum (FAB) presented ions with and without a loss of the chloride at 789 and 824 *m/z*, respectively, confirming the formula of the complex and corroborating the elemental analysis.

4.3.2. X-ray Crystallography

To the best of our knowledge, this is the first ruthenium complex published with a 2,6-diacetylpyridine ligand. For the new complex **35**, the solved X-ray structure is provided in Figure 4.2. A search through literature provided only one similar structure, with one of the acetyl ketones replaced with a hydroxylamine **36** and a different anion, presented in Figure 4.3.[48] Another structure **37** with two alanine ligands and two PPh_3 ligands is provided for some relative comparison.[49] The structures of these complexes offer some comparison of the atomic distances and angles within the new complex, as values of atomic distances and angles appear to be in agreement with literature of similar distorted octahedral complexes.[12,27,48,49] Table 4.1. provides pertinent atomic distances and angles of complex **35** alongside values for **36** and **37** for comparison.

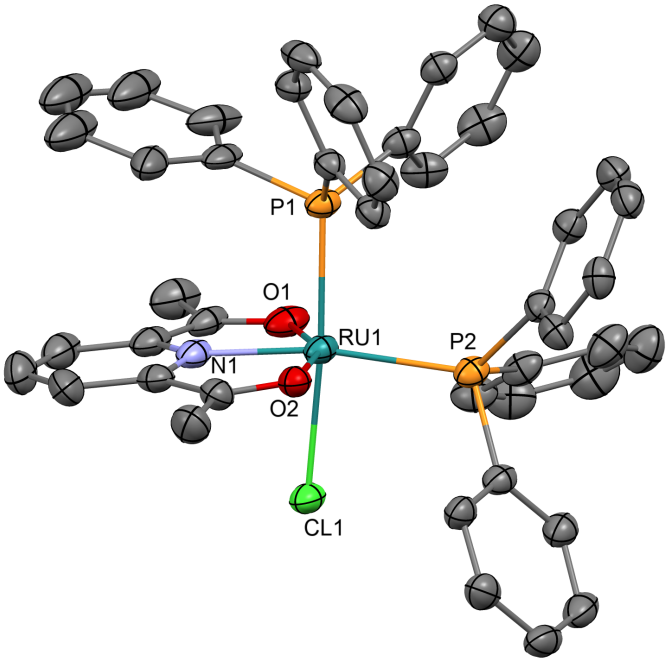

Figure 4.2. X-ray structure of $[RuCl(dap)(PPh_3)_2]BAr^F{}_4$ (**35**). Structure is depicted as 50 % probability ellipsoids, with hydrogen atoms, solvent molecules, and coordinating anion removed for clarity.

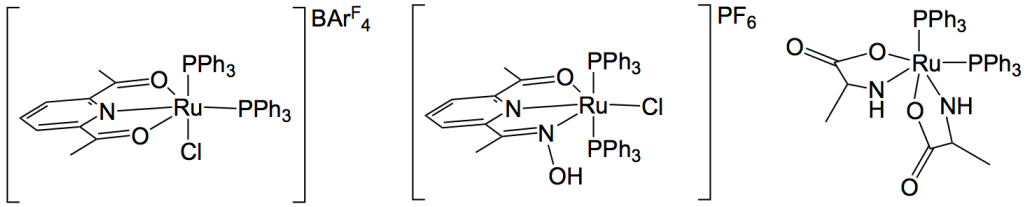

Figure 4.3. Structures of the new complex **35** and similar literature–known complexes for comparison of ligand distances and angles.

Table 4.1. Selected bond lengths (Å) and angles (°) from the X-ray structures of [RuCl(dap)$(PPh_3)_2$]$BAr^F{}_4$ (**35**) and literature complexes.

	[[RuCl(dap) $(PPh_3)_2$]$BAr^F{}_4$ (**35**)	[Ru(κ^3-dapmoH)Cl $(PPh_3)_2$]PF_6•H_2O (**36**)[a]	[Ru(L-ala)$_2$ $(PPh_3)_2$] (**37**)[b]
Ru–P(1)	2.3220(13)	2.3402(12)	2.298(4)
Ru–P(2)	2.3855(13)	2.3711(12)	2.318(4)
Ru–Cl	2.4210(12)	2.4920(14)	–
Ru–N(1)	1.990(4)	1.970(4)	2.135(10)
Ru–N(2)	–	2.025(3)	2.160(12)
Ru–O(1)	2.141(3)	2.104(3)	2.132(10)
Ru–O(2)	2.082(3)	–	2.108(10)
P(1)–Ru–P(2)	97.54(5)	175.05(4)	98.3(2)
Cl–Ru–P(1)	173.19(4)	83.07(5)	–
Cl–Ru–P(2)	86.84(4)	92.48(5)	–
O(1)–Ru–O(2)	154.01(14)	–	88.2(4)
O(1)–Ru–N(1)	76.64(16)	75.92(14)	77.2(4)
O(2)–Ru–N(1)	77.41(15)	–	164.3(5)
O(1)–Ru–Cl	86.43(9)	112.61(11)	–
P(1)–Ru–O(1)	87.32(9)	–	168.7(3)
P(2)–Ru–O(1)	106.51(11)	–	91.4(3)
P(1)–Ru–O(2)	95.08(9)	–	–
P(2)–Ru–O(2)	98.83(9)	–	–
N(1)–Ru–P(1)	92.54(12)	–	96.0(4)
N(1)–Ru–P(2)	169.54(12)	–	95.5(3)
N(1)–Ru–Cl	83.38(11)	–	–

Relevant bond lengths and angles are shaded for comparison. Blank spaces are unpublished or not applicable. [a][48] [b][49]

4.3.3. Catalytic Optimization

Starting from conditions listed in literature, we performed some optimization experiments of the catalytic title reaction (Table 4.2.).[43,44,47,50] Toluene was found to be the ideal solvent, providing good yields in reasonable timeframes (85 % in 16 hr at 85 °C). More polar solvents provided lower yields, with the exception of ethyl acetate. Nonpolar solvents like cyclohexane provided no reaction at all, possibly due to poor solubility of the carboxylic acids. The minimum temperature required for any reaction seemed to be at least 60 °C on the overnight timescale. As well, addition of a base

(organic or inorganic) seemed to prevent the reaction from proceeding. The alkyne was supplied in twice the molar quantity of the carboxylic acid, as it seemed the title reaction was competing with a slower polymerization reaction of the acetylenes. A summary of these experiments is provided in Table 4.2.

Table 4.2. Optimization experiments.

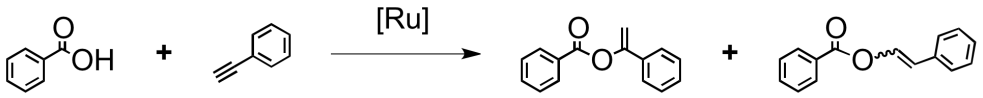

Solvent	Temperature (°C)	Time (hr)	Catalyst	Additive	Yield
Toluene	85	16	1 mol%	–	85 %
Toluene	80	12	5 mol%	–	61 %
Toluene	65	18	5 mol%	–	65 %
Toluene	45	18	5 mol%	–	0 %
Toluene	85	16	–	–	0 %
Toluene	85	16	1 mol%	DBU	0 %
Toluene	85	16	1 mol%	Et_3N	0 %
Toluene	85	16	1 mol%	Na_2CO_3	0 %
Ethyl Acetate	85	16	1 mol%	$NaHCO_3$	0 %
Ethyl Acetate	85	16	1 mol%	–	57 %
Ethanol	70	18	5 mol%	–	11 %
1,2-Dichloroethane	70	18	5 mol%	–	9 %
Tetrahydrofuran	70	18	5 mol%	–	4 %
Nitromethane	70	18	5 mol%	–	11 %

General conditions: Carboxylic acid (0.57 mmol), alkyne (1.14 mmol), and Ru (1-5 mol%) for specified time and temperature. All yields are of a mixture of isomers isolated by silica gel chromatography.

4.3.4. Catalytic Formation of Enol Esters

Using the optimized conditions, the catalyst **35** was employed to synthesize enol esters in good yields, ranging from 24 – 93 %. Results are summarized below in Table 4.3. We tested a variety of carboxylic acids, both aromatic and aliphatic, with phenylacetylene or 1-hexyne as the coupling partner. Most yields were obtained with toluene as the reaction solvent. In some cases, ethyl acetate provided higher yields than toluene. For entries 7 and 8, the use of ethyl acetate was mandatory as there was no observable amount of product when the reaction was performed in toluene. This may be due to a better solubility in ethyl acetate for those carboxylic acids with more polar functional groups attached to them. Compared to other catalyst systems known from literature, this atom–economical system only required the ruthenium catalyst in amounts of 1 mol % and did not need any additives in the reaction mixture for the reaction to proceed.[39,43,51,52]

Several further experiments screened methyl benzoate for addition of the carboxylate to the alkyne under similar conditions, which did not show any signs of any reactivity. As well, phenylsilane was employed as a reactant in a few screening reactions, with no product found in gas chromatography observation.

Table 4.3. Isolated yields of enol esters.

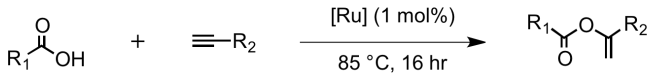

Entry	Alkyne / Acid	Product	Yield (%)	Entry	Alkyne / Acid	Product	Yield (%)
1	phenylacetylene / benzoic acid	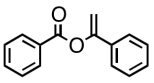	85[a] 57[b]	7	1-hexyne / 2-hydroxyisobutyric acid	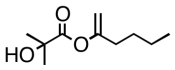	74[b]
2	phenylacetylene / 3-chlorobenzoic acid	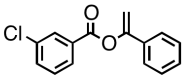	83[a]	8	phenylacetylene / 2-chloroacetic acid	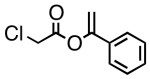	93[b]
3	phenylacetylene / 2-bromobenzoic acid	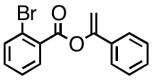	91[a]	9	phenylacetylene / glacial acetic acid	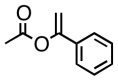	52[a] 24[b]
4	phenylacetylene / 4-methyl-3-nitro-benzoic acid	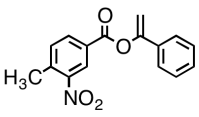	70[a] 79[b]	10	phenylacetylene / 2,2-diphenyl acetic acid	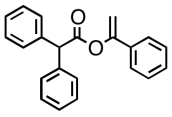	81[a]
5	1-hexyne / benzoic acid	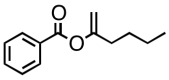	70[a]	11	1-hexyne / 2,2-diphenyl acetic acid	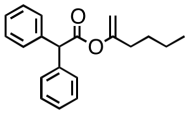	74[a]
6	1-hexyne / salicylic acid	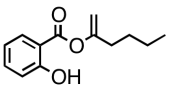	89[a]	12	3,3-dimethyl-1-butyne / 3-chlorobenzoic acid	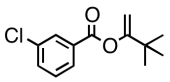	72[a]

General conditions: Carboxylic acid (0.57 mmol), alkyne (1.14 mmol), and Ru (1 mol%) for 16 hours at 85 °C. All product yields were were isolated by silica gel chromatography. [a] Toluene [b] Ethyl acetate

We chose to further examine the products of these reactions by isolating the entirety of the product mixture and quantifying the isomers present by ^{1}H NMR. Table 4.4. provides a summary of the regioselectivity of a selection of reactions from Table 4.3. Those reactions were performed separately; all products from the mixture were filtered through a short pipette of silica and the solvent was removed. The ratio of the isomers in the resulting mixture of products was calculated by integration of ^{1}H NMR peaks. Unlike

the results in Table 4.3., where the product was chromatographically isolated as a single isomer, the reactions for Table 4.4. was meant help us understand if the yields were truly maximized or if any amount of product was being lost due to small amounts of regioselectivity for minor isomers. The relative ratios of the three potential isomers could be assessed through these experiments.

Table 4.4. Regioselectivity of Product Formation as Determined by ^{1}H NMR.

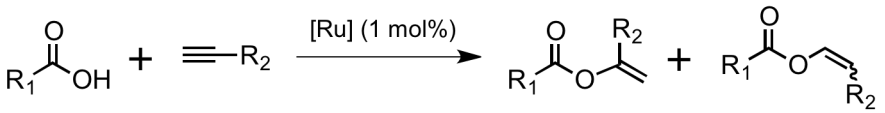

Entry		Isolated Yield	*gem : cis : trans* % selectivity
1	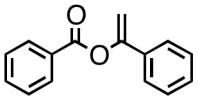	88 %	96 : 2 : 2
2	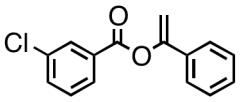	87 %	94 : 4 : 2
5	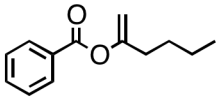	74 %	95 : 3 : 2
9	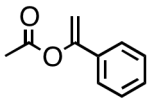	70 %	74 : 14 : 12
12	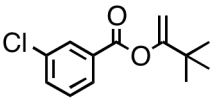	79 %	75 : 15 :10

General conditions: Carboxylic acid (0.57 mmol), alkyne (1.14 mmol), and Ru (1 mol%) for 16 hours at 85 °C in toluene. All product yields were were isolated by filtering through silica gel and isolating the mixture of isomers. [a] Ratio of constitutional isomers was determined by ratio of discrete peaks in ^{1}H NMR.

Internal alkynes were also explored as potential substrates, in a catalytic reaction of 3-hexyne and benzoic acid. The reaction was exothermic and allowed to stand for several hours, filtered, and examined by gas chromatography. There was no sign of a higher molecular weight compound in the mixture. It may be possible that the alkyne was simply too reactive for this transformation, generating alkyl benzene side–products due to polymerization. The chromatogram may have had this product peak hidden in the solvent peak, thus being missed during screening. This avenue was set aside as our attentions turned towards regioselectivity experiments.

4.4. Discussion

As can be inferred from Tables 4.3. and 4.4., the amount of *anti*–Markovnikov isomers was found to be marginal for most reactions. It appears that complex **35** offers excellent regioselectivity for most acids and alkynes. In the instance of acetic acid (entry 9 in Tables 4.3. and 4.4.), the regioselectivity is much lower. We hypothesize that this may be due to the smaller size of acetic acid, as it can avoid steric clashing that the larger acids may be subject to. Entry 12 from Table 4.4. may also be subject the opposite effect. The *tert*–butylacetylene may hinder nucleophilic Markovnikov addition, decreasing selectivity by slowing kinetics of the addition. Scheme 4.3. offers some insight to the selectivity of this addition.

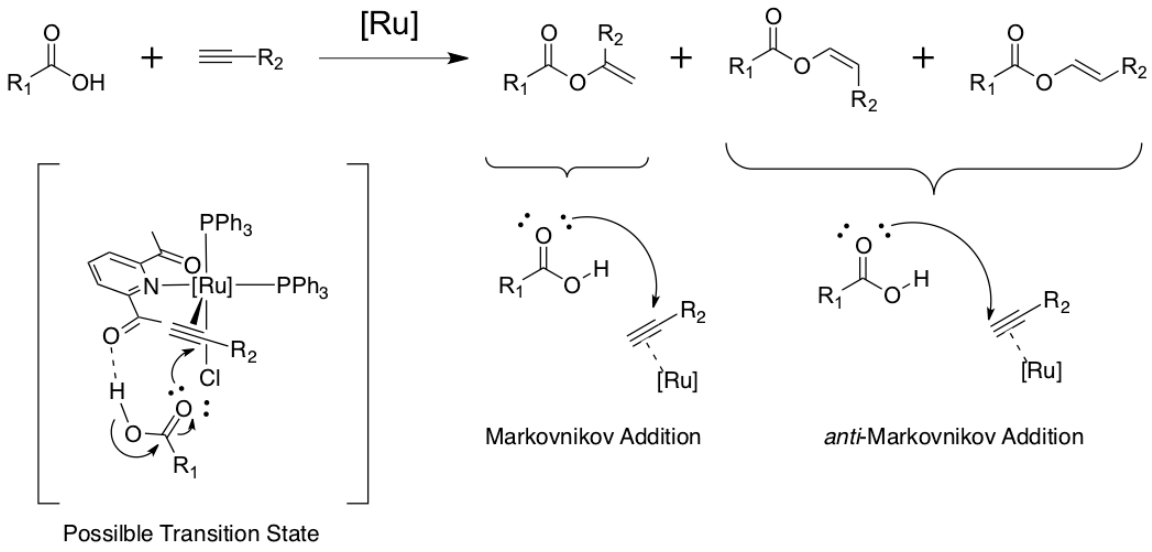

Scheme 4.3. Hypothesized kinetic selectivity of products.

Shown here in Scheme 4.3., Markovnikov selectivity comes from the addition of the carboxylate group to the innermost carbon of the terminal alkyne (the carbon attached to the R_2 group). A possible catalytic transition state is given in Scheme 4.3. Ruthenium is well–known to form σ–alkynyl or vinylidene complexes with terminal alkynes.[53-56] The exact binding (η^2 or σ) of the alkyne to the ruthenium is unknown for our reaction. Based on the regioselectivity of the addition reactions, it may be possible that the ruthenium coordinates to the alkyne in the way that offers the least accessibility of the carboxylate to attack the terminal carbon, which could be σ–coordinated to a deprotonated terminal alkyne. In addition, the phosphine ligands on the complex occupy significant space which could steer selectivity solely by steric interference. The influence of kinetic selectivity through sterics has been more recently explored in the field of olefin metathesis.[57,58]

Furthermore, the system presented herein proceeds without the addition of a base to the reaction mixture, unlike some of the other published studies.[50,59-61] It may be possible that the diacetylpyridine ligand acts as a built–in base, or may function as a hydrogen–

bonding director on the complex. This non–innocence has been hypothesized about amide– or imine–containing ligands used in hydrogen transfer reactions, where the nitrogen atom can act as hydrogen bond acceptor and directs the accompanying alcohol to position for hydrogen transfer.[13,62-65] In our complex, this process could work nearly the same way, where the carboxylic acid hydrogen bonds with the ketone closest to the alkynyl group, positioning it for attack in the Markovnikov position. The dissociation of the diacetylpyridine ligand is not anticipated. An experiment of the metal complex heated at 85 °C overnight in an NMR tube with $CDCl_3$ offered no change in the ^{1}H or $^{31}P\{^{1}H\}$ spectrum, indicating that the tridentate ligand is considerably stable. The kinetic selectivity of the Markovnikov product offers a reasonable explanation for the observations in this study. While this is all speculative, more experiments should be performed to elucidate an accurate mechanism of the reaction.

4.5 Summary and Perspective

A complex of the formula $[RuCl(dap)(PPh_3)_2]BAr^F_4$ was synthesized and characterized. We believe that the complex offers a platform for further exploring the fine–tuning of catalysis involving ruthenium complexes. The ruthenium complex was found to be catalytically active for the addition of carboxylic acids to terminal alkynes, in yields ranging from of 52 to 93 %. The complex also exhibited excellent selectivity for the geminal isomer, which is the Markovnikov product. This selectivity for the addition may be driven primarily by the sterics of the metal complex while interacting with the terminal alkyne.

The substrate scope seemed to be limited to terminal alkynes. Tuning the reactivity of the complex through the diacetylpyridine ligand may open the way to applications of internal alkynes using the ruthenium architecture described in this chapter. Mechanistic studies could further determine which ligands should be selected for further modification to investigate if sterics or electronics factors play a greater role in catalytic efficiency or selectivity. The complex $[RuCl(dap)(PPh_3)_2]BAr^F{}_4$ may be a promising candidate for the ruthenium–catalyzed addition of carboxylic acids to nitriles or isonitriles in the synthesis of vicinal acetoxyamides.[66,67] Another avenue could be exploring the use of peroxy acids to immediately generate vicinal diols from alkynes.[35]

4.6 Experimental

General.[68]

All chemicals were used as supplied from Sigma-Aldrich unless otherwise noted. Toluene, CH_2Cl_2, and Et_2O were freshly distilled. Starting carboxylic acid materials were used as received and acetylenes were distilled. $NaBAr^F{}_4$ and $[RuCl_2(PPh_3)_3]$ were synthesized following literature procedures.[69-71] NMR spectra for characterization were collected at room temperature on a Varian Unity 300 MHz or Bruker Avance 300 MHz instrument; all chemical shifts (δ) are reported in ppm and are referenced to a residual solvent signal. IR spectra were collected on a Thermo Nicolet 360 FT-IR spectrometer. FAB and exact mass data were collected on a JEOL MStation [JMS-700] Mass Spectrometer. Melting points were determined on a Thomas Hoover uni-melt capillary melting point apparatus and are uncorrected. Elemental analyses were performed by Atlantic Microlab Inc., Norcross, GA, USA.

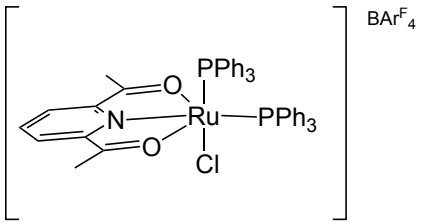

*[RuCl(PPh$_3$)$_2$(dap)][BAr$^F_4$] (**35**).*

A Schlenk flask containing $RuCl_2(PPh_3)_3$ (0.501 g, 0.52 mmol), 2,6-diacetylpyridine (dap) (0.090 g, 0.55 mmol), and sodium tetrakis[3,5-bis(trifluoromethyl)phenyl]borate (0.486 g, 0.55 mmol) was purged and filled with N_2. Distilled CH_2Cl_2 was added and the mixture was allowed to stir at room temperature for 1 hour, during which the wine-red solution transitioned to a deep purple color. The CH_2Cl_2 solution was filtered through a cotton-filled pipette to remove sodium chloride and then vacuum dried to obtain a dark residue. The residue was then dissolved in a minimal amount of distilled methanol (3 mL) and washed three times with hexanes (3 mL). The red alcohol solution was dried to yield a dark purple solid (0.810 g, 0.48 mmol, 92 %). The solid product is readily recrystallized from CH_2Cl_2 layered with hexanes to yield dark purple crystals suitable for X-ray crystallography. ^{1}H NMR (300 MHz, $CDCl_3$) δ 7.93 (d, 2H, dap, J_{HH}=3.9 Hz), 7.83 (dd, 1H, dap, J_{HH}=5.3 Hz), 7.69 (s, 8H, BAr$^F_4$), 7.49 (s, 4H, BAr$^F_4$), 7.38-7.17 (m, 21H, arom., PPh_3), 6.99-6.91 (m, 6H, arom., PPh_3), 6.71-6.55 (m, 5H, arom., PPh_3), 2.77 (s, 6H, CH_3). ^{13}C{^{1}H} NMR (75 MHz, $CDCl_3$) δ 135.0 (s), 134.5 (s), 134.3 (s), 133.7 (s), 133.2 (s), 131.2 (s), 130.5 (s), 130.4 (s), 129.3 (s),128.8 (s), 128.7 (s), 128.6 (s), 128.4 (s), 126.5 (s), 122.9 (s), 117.7 (s), 26.3 (s). ^{31}P{^{1}H} NMR (121 MHz, $CDCl_3$) δ 45.3 (d, J_{PP}=33.6 Hz), 32.2 (d, J_{PP}=33.5 Hz). ^{19}F{^{1}H} NMR (282 MHz, $CDCl_3$) δ -62.3 (s). IR (neat, solid): $\tilde{\nu}$ = 3059 (w), 2922 (w), 1610 (w), 1572 (w), 1482 (w), 1352 (m), 1275 (s),

1114 (s), 998 (w), 925 (w), 882 (m), 837 (m), 743 (m) cm^{-1}. m.p. 179-181 °C decomp. MS (FAB) *m/z* 1652 $[M + BAr^F_4 - Cl]^+$, 824 $[M + Cl - BAr^F_4]^+$, 789 $[M - Cl - BAr^F_4]^{++}$. $C_{77}H_{51}BClF_{24}NO_2P_2Ru$ (1687.18): calcd. C 54.81, H 3.05; found C 54.83, H 3.17.

General Catalytic Experiments.

The carboxylic acid (0.57 mmol) was placed into a screw-top scintillation vial along with 2 equivalents of the alkyne (1.14 mmol), the catalyst (0.010 g, 0.006 mmol, 1 mol %), and 1 mL solvent. A cap was tightened on the vial and the mixture was heated in a heating block for the specified time frame. The mixture was then filtered through a pipette with a small amount of silica gel and the solvent was removed. Purification was achieved via column chromatography using 1.5 cm x 10 cm silica with 9:1 v/v hexanes/ethyl acetate as eluent, unless otherwise specified.

Catalysis Products

1-phenylvinyl benzoate[43]

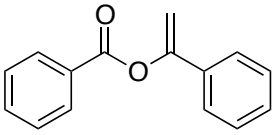

Benzoic acid (0.070 g, 0.57 mmol), phenylacetylene (0.118 g, 1.16 mmol), and catalyst (0.010 g, 1 mol%) were placed into a vial with toluene and heated for 16 hours at 80 °C. Yield: 0.114 g of an off-white solid, 0.51 mmol, 88.2 %, ratio = *geminal* 58.8 : *cis* 1.3 : *trans* 1 as determined by alkene proton ratio. ^{1}H NMR (300 MHz, $CDCl_3$) δ 8.27-8.16 (2H, m, arom.), 7.74-7.46 (5H, m, arom.), 7.43-7.28 (m, 3H, arom.), 6.62 (d, 1H, *E / cis*, CH, J_{HH}=12.8 Hz), 5.88 (d, 1H, *Z / cis*, CH, J_{HH}=7.1 Hz), 5.62 (d, 1H, *gem*, CH_2,

J_{HH}=2.2 Hz), 5.18 (d, 1H, *gem*, CH_2, J_{HH}=2.2 Hz). $^{13}C\{^1H\}$ NMR (75 MHz, $CDCl_3$) δ 164.9 (s), 153.3 (s), 134.4 (s), 133.7 (s), 130.3 (s), 129.5 (s), 129.1 (s), 128.8 (s), 128.7 (s), 125.0 (s), 102.5 (s). IR (neat, liquid): ṽ = 3068(m), 2942 (m), 2824(m), 2664 (m), 2546 (m), 2089 (w), 1681 (s), 1596 (m), 1579 (m), 1448 (m), 1416 (m), 1320 (m), 1276 (s), 1227 (m), 928 (m).

1-phenylvinyl 3-chlorobenzoate

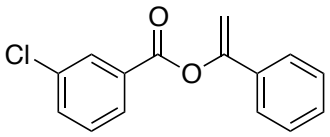

3-chlorobenzoic acid (0.090 g, 0.57 mmol), phenylacetylene (0.114 g, 1.12 mmol), and catalyst (0.010 g, 1 mol%) were placed into a vial with toluene and heated for 16 hours at 80 °C. Yield: 0.130 g of yellow solid, 0.50 mmol, 87.2 %, ratio = *geminal* 50 : *cis* 1.5 : *trans* 1 as determined by alkene proton ratio. ^1H NMR (300 MHz, $CDCl_3$) δ 8.18 (t, 1H, J_{HH}= 1.7 Hz), 8.10 (dt, 1H, J_{HH}=10.5, 1.5 Hz), 7.60 (d. quart., 1H, J_{HH}=8.2, 1.1 Hz), 7.54-7.49 (m, 2H, arom.), 7.44 (t, 1H, J_{HH}=7.9 Hz), 7.34 (dd, 3H, J_{HH}=5.4, 1.9 Hz), 6.61 (d, 1H, *E / cis*, CH, J_{HH}=12.6 Hz), 5.89 (d, 1H, *Z / cis*, CH, J_{HH}=7.2 Hz), 5.60 (d, 1H, *gem*, CH_2, J_{HH}=2.3 Hz), 5.17 (d, 1H, *gem*, CH_2, J_{HH}=2.3 Hz). $^{13}C\{^1H\}$ NMR (75 MHz, $CDCl_3$) δ 163.8 (s), 153.2 (s), 134.9 (s), 134.1 (s), 133.8 (s), 131.3 (s), 130.3 (s), 130.2 (s), 129.3 (s), 128.8 (s), 128.4 (s), 125.1 (s), 102.7 (s). IR (neat, solid): ṽ = 2987 (m), 2864 (m), 2826 (m), 2653 (m), 2541 (m), 2088 (w), 1747 (m), 1679 (s), 1601 (m), 1415 (m), 1288 (s), 1217 (s), 1181 (s), 913 (m).

1-phenylvinyl 2-bromobenzoate

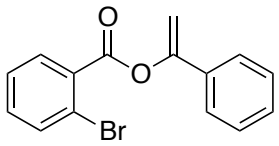

2-bromobenzoic acid (0.201 g, 0.56 mmol), phenylacetylene (0.116 g, 1.14 mmol), and catalyst (0.010 g, 1 mol%) were placed into a vial with toluene and heated for 16 hours at 80 °C. Yield: 0.155 g of dark yellow solid, 0.51 mmol, 87.2 %. ^{1}H NMR (300 MHz, $CDCl_3$) δ 8.04 (dd, 1H, arom., J_{HH}= 7.4, 2.2 Hz), 7.72 (dd, 1H, arom., J_{HH}= 7.5, 1.7 Hz), 7.59-7.53 (m, 2H, arom.), 7.46-7.32 (m, 5H, arom.), 5.59 (d, 1H, CH_2, J_{HH}= 2.3 Hz), 5.22 (d, 1H, CH_2, J_{HH}= 2.3 Hz). ^{13}C{^{1}H} NMR (75 MHz, $CDCl_3$) δ 164.2 (s), 153.3 (s), 134.9 (s), 134.2 (s), 133.4 (s), 132.1 (s), 131.3 (s), 129.3 (s), 129.3 (s), 127.6 (s), 125.3 (s), 122.6 (s), 102.8 (s). IR (neat, solid): ṽ = 2968 (m), 2869 (m), 2819 (m), 2648 (m), 2541 (m), 2088 (w), 1747 (m), 1676 (s), 1602 (m), 1415 (m), 1290 (m), 1216 (m), 1179 (m), 1132 (m), 911 (m).

1-phenylvinyl 4-methyl-3-nitrobenzoate

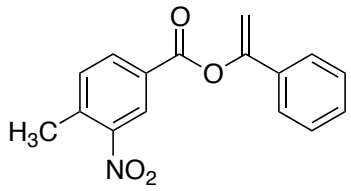

4-methyl-3-nitrobenzoic acid (0.109 g, 0.60 mmol), phenylacetylene (0.104 g, 1.14 mmol), and catalyst (0.010 g, 1 mol%) were placed into a vial with toluene and heated for 16 hours at 80 °C. Yield: 0.120 g of yellow oil, 0.50 mmol, 83.5 %. ^{1}H NMR (300 MHz, $CDCl_3$) δ 8.74 (d, 1H, arom, J_{HH}=1.7 Hz), 8.26 (dd, 1H, arom, J_{HH}=8.0, 1.8 Hz), 7.53-7.46 (m, 3H, arom), 7.36-7.30 (m, 3H, arom), 5.60 (d, 1H, CH_2, J_{HH}=2.4 Hz), 5.17 (d,

1H, CH_2, J= 2.4 Hz), 2.67 (s, 3H, CH_3). $^{13}C\{^1H\}$ NMR (75 MHz, $CDCl_3$) δ 162.9 (s), 153.1 (s), 149.5 (s), 139.9 (s), 134.0 (s), 133.9 (s), 133.5 (s), 129.3 (s), 128.8 (s), 128.7 (s), 126.3 (s), 124.9 (s), 102.8 (s), 20.8 (s). IR (neat, solid): $\tilde{\nu}$ = 3438 (w), 3098 (w), 2863 (w), 2321 (w), 1722 (s), 1638 (m), 1615 (m), 1526 (m), 1490 (m), 1338 (m), 1307 (m), 1234 (s), 1103 (s), 1068 (m).

hex-1-en-2-yl benzoate[43]

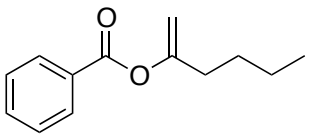

Benzoic acid (0.070 g, 0.57 mmol), 1-hexyne (0.097 g, 1.13 mmol), and catalyst (0.010 g, 1 mol%) were placed into a vial with toluene (1 mL) and heated for 16 hours at 80 °C. Yield: 0.009 g of yellow oil, 0.43 mmol, 73.9 %, ratio = *geminal* 37.6 : *cis* 1 : *trans* 1 as determined by alkene proton ratio. ^1H NMR (300 MHz, $CDCl_3$) δ 8.09-8.04 (m, 2H, arom), 7.60-7.53 (m, 1H, arom), 7.48-7.40 (m, 2H, arom), 5.58 (m, 2H, *E / trans*, CH_2), 4.99 (m, 2H, *Z / cis*, CH_2), 4.85-4.83 (m, 1H, *gem*, CH_2), 4.83-4.81 (m, 1H, CH_2), 2.32 (t, 2H, J_{HH}=7.5 Hz), 1.49 (m, 2H, J_{HH}=7.1 Hz), 1.36 (m, 2H, J_{HH}=5.6 Hz), 0.89 (t, 3H, CH_3, J= 7.2 Hz). $^{13}C\{^1H\}$ NMR (75 MHz, $CDCl_3$) δ 164.9 (s), 156.9 (s), 133.5 (s), 130.1 (s), 130.0 (s), 128.6 (s), 101.5 (s), 33.3 (s), 28.8 (s), 22.3 (s), 14.1 (s). IR (neat, liquid): $\tilde{\nu}$ = 3453 (w), 2955 (w), 2928 (w), 2616 (w), 1727 (s), 1267 (m), 1222 (s), 1167 (m), 1088 (m), 1064 (m), 1023 (m), 861 (m).

hex-1-en-2-yl 2-hydroxybenzoate

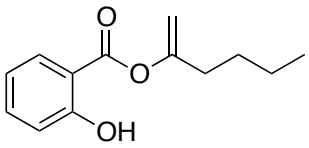

Salicylic acid (0.078 g, 0.57 mmol), 1-hexyne (0.100 g, 1.22 mmol), and catalyst (0.011 g, 1 mol%) were placed into a vial with toluene (1 mL) and heated for 16 hours at 80 °C. Yield: 0.111 g of yellow oil, 0.50 mmol, 88.7 %. ^{1}H NMR (300 MHz, $CDCl_3$) δ 10.60 (s, 1H), 7.88 (dd, 1H, arom., J_{HH}=7.9, 1.6 Hz), 7.46 (ddd, 1H, arom., J_{HH}=8.5, 7.1, 1.5 Hz), 6.98 (dd, 1H, arom., J_{HH}= 8.4, 0.8 Hz), 6.89 (ddd, 1H, arom., J_{HH}= 8.1, 7.2, 1.0 Hz), 4.86 (s, 2H, CH_2), 2.32 (t, 2H, CH_2, J_{HH}= 7.8 Hz), 1.56-1.44 (m, 2H, CH_2), 1.44-1.29 (m, 2H, CH_2), 0.90 (t, CH_3, J_{HH}= 7.2 Hz). ^{13}C{^{1}H} NMR (75 MHz, $CDCl_3$) δ 168.7 (s), 162.2 (s), 156.4 (s), 136.3 (s), 130.3 (s), 119.4 (s), 117.9 (s), 112.2 (s), 102.1 (s), 33.2 (s), 29.7 (s), 22.2 (s), 13.9 (s). IR (neat, liquid): $\tilde{\nu}$ = 3240 (w), 2956 (w), 2929 (w), 2862 (w), 1680 (s), 1612 (m), 1482 (m), 1332 (m), 1299 (m), 1203 (m), 1151 (s), 1130 (s), 1076 (m).

hex-1-en-2-yl 2-hydroxy-2-methylpropanoate

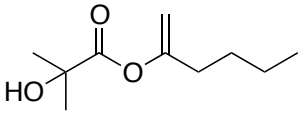

2-hydroxylisobutyric acid (0.061 g, 0.58 mmol), 1-hexyne (0.094 g, 1.14 mmol), and catalyst (0.010 g, 1 mol%) were placed into a vial with ethyl acetate (1 mL) and heated for 16 hours at 80 °C. Yield: 0.080 g of colorless oil, 0.43 mmol, 74 %. ^{1}H NMR (300 MHz, $CDCl_3$) δ 4.70 (d, 2H, CH_2, J_{HH}=8.4 Hz), 2.18 (t, 2H, CH_2, J_{HH}=7.7 Hz), 1.44 (s, 6H, CH_3), 1.43-1.19 (m, 4H, CH_2), 0.85 (t, 3H, CH_3, J_{HH}=6.9 Hz). ^{13}C{^{1}H} NMR (75

MHz, $CDCl_3$) δ 175.9 (s), 156.6 (s), 101.6 (s), 72.2 (s), 32.8 (s), 28.6 (s), 27.3 (s), 22.2 (s), 13.9 (s). IR (neat, liquid): $\tilde{\nu}$ = 3489 (w, br), 2957 (m), 2931 (m), 2871 (m), 1740 (s), 1664 (m), 1464 (m), 1254 (w), 1227 (w), 1121 (s), 975 (m), 866 (m).

1-phenylvinyl 2-chloroacetate

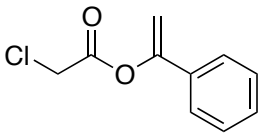

2-chloroacetic acid (0.062 g, 0.66 mmol), phenylacetylene (0.117 g, 1.15 mmol), and catalyst (0.012 g, 1 mol%) were placed into a vial with ethyl acetate (1 mL) and heated for 16 hours at 80 °C. Yield: 0.120 g of colorless oil, 0.61 mmol, 92.4 %. ^{1}H NMR (300 MHz, $CDCl_3$) δ 7.49-7.46 (m, 2H, arom.), 7.37-7.34 (m, 3H, arom.), 5.52 (d, 1H, CH_2, J_{HH}= 2.6 Hz), 5.10 (d, 1H, CH_2, J_{HH}= 2.6 Hz), 4.26 (s, 2H, CH_2). $^{13}C\{^1H\}$ NMR (75 MHz, $CDCl_3$) δ 165.6 (s), 152.8 (s), 133.6 (s), 129.4 (s), 128.8 (s), 124.9 (s), 102.7 (s), 40.9 (s). IR (neat, liquid): $\tilde{\nu}$ = 3056 (w), 2952 (w), 1756 (s), 1641 (m), 1492 (m), 1445 (m), 1406 (m), 1261 (m), 1228 (s), 1136 (s), 1090 (m), 960 (m).

1-phenylvinyl acetate[42,44]

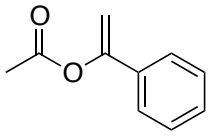

Glacial acetic acid (0.068 g, 1.13 mmol), phenylacetylene (0.243 g, 2.38 mmol), and catalyst (0.015 g, 0.8 mol%) were placed into a vial with toluene (1 mL) and heated for 16 hours at 80 °C. Products were isolated by silica column with 1 diethyl ether : 9

petroleum ether as eluent. Yield: 0.130 g of colorless oil, 0.80 mmol, 70.6 %, ratio = *geminal* 6.6 : *cis* 1.3 : *trans* 1 as determined by CH_3 ratio. ^{1}H NMR (300 MHz, $CDCl_3$) δ 8.03 (d, 1H, *Z* / *cis*, CH, J_{HH}=12.8 Hz), 7.75 (d, 1H, *E* / *trans*, CH, J_{HH}=7.2 Hz), 7.64-7.61 (m, 2H, arom.), 7.55-7.36 (m, 3H, arom.), 6.55 (d, 1H, *Z* / *cis*, CH, J_{HH}=12.8 Hz), 5.85 (d, 1H, *E* / *trans*, CH, J_{HH}=7.2 Hz), 5.64 (d, 1H, gem, CH, J_{HH}=2.12 Hz, major), 5.19 (d, 1H, gem, CH, J_{HH}=2.2 Hz, major), 2.41(s, 3H, CH_3, major), 2.38 (s, 3H, *Z* / *cis*, CH_3), 2.31 (s, 3H, *E* / *trans*, CH_3). ^{13}C{^{1}H} NMR (75 MHz, $CDCl_3$) δ 162.2 (s), 168.0 (s, minor), 167.5 (s, minor), 152.9 (s), 136.2 (s), 134.3 (s), 134.1 (s, minor), 134.0 (s, minor), 133.9 (s), 129.2 (s, minor), 129.0 (s), 128.8 (s, minor), 128.6 (s), 128.4 (s, minor), 127.5 (s, minor), 127.4 (s, minor), 126.2 (s, minor), 124.9 (s), 115.2 (s, minor), 111.8 (s, minor), 102.2 (s), 21.0 (s), 20.9 (s, minor), 20.7 (s, minor). IR (neat, liquid): $\tilde{\nu}$ = 2935 (w), 2730 (w), 1757 (s), 1643 (m), 1492 (m), 1367 (m), 1197 (s), 1094 (m), 1016 (m).

1-phenylvinyl 2,2-diphenylacetate[43]

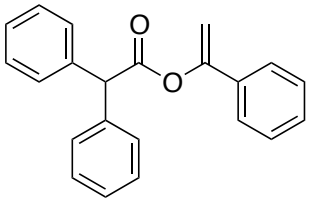

Diphenylacetic acid (0.123 g, 0.58 mmol), phenylacetylene (0.117 g, 1.14 mmol), and catalyst (0.010 g, 1 mol%) were placed into a vial with toluene (1 mL) and heated for 16 hours at 80 °C. Yield: 0.148 g of off-white solid, 0.47 mmol, 81.1 %. ^{1}H NMR (300 MHz, $CDCl_3$) δ 7.59-7.36 (m, 10H, arom.), 7.36-7.29 (m, 5H, arom.), 5.57 (d, 1H, CH_2, J_{HH}=2.3 Hz), 5.36 (s, 1H, CH), 5.14 (d, 1H, CH_2, J_{HH}=2.3 Hz). ^{13}C{^{1}H} NMR (75 MHz,

$CDCl_3$) δ 170.6 (s), 153.1 (s), 138.1 (s), 134.2 (s), 129.0 (s), 128.9 (s), 128.5 (s), 127.6 (s), 124.9 (s), 102.3 (s), 57.2 (s). IR (neat, solid): $\tilde{\nu}$ = 3472 (w), 3057 (w), 3024 (w), 2317 (w), 2107 (w), 1957 (w), 1889 (w), 1743 (s), 1634 (m), 1490 (m), 1448 (m), 1259 (m), 1178 (m), 1118 (s), 1076 (m), 1029 (m), 867 (m).

hex-1-en-2-yl 2,2-diphenylacetate

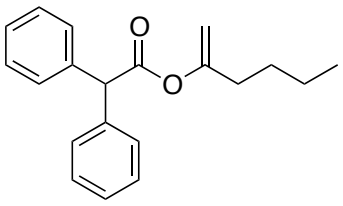

Diphenylacetic acid (0.123 g, 0.58 mmol), 1-hexyne (0.092 g, 1.10 mmol), and catalyst (0.011 g, 1 mol%) were placed into a vial with toluene (1 mL) and heated for 16 hours at 80 °C. Yield: 0.125 g of colorless oil, 0.43 mmol, 73.5 %. ^{1}H NMR (300 MHz, $CDCl_3$) δ 7.44-7.29 (m, 10H, arom.), 5.15 (s, 1H, CH), 4.78 (d, 2H, CH_2), 2.24 (t, 2H, CH_2, J_{HH}=7.1 Hz), 1.41-1.24 (m, 4H, CH_2), 0.89 (t, 3H, CH_3, J_{HH}=7.1 Hz). $^{13}C\{^1H\}$ NMR (75 MHz, $CDCl_3$) δ 170.8 (s), 156.7 (s), 138.4 (s), 128.8 (s), 128.7 (s), 127.5 (s), 101.3 (s), 57.2 (s), 32.9 (s), 28.5 (s), 22.1 (s), 13.9 (s). IR (neat, liquid): $\tilde{\nu}$ = 3061 (w), 3027 (w), 2954 (w), 2928 (w), 2861 (w), 1745 (s), 1663 (m), 1493 (m), 1451 (m), 1179 (m), 1121 (s), 868 (m).

3,3-dimethylbut-1-en-2-yl 3-chlorobenzoate

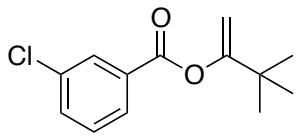

3-chlorobenzoic acid (0.093 g, 1.13 mmol), phenylacetylene (0.108 g, 1.31 mmol), and catalyst (0.010 g, 1 mol%) were placed into a vial with toluene (1 mL) and heated for 16 hours at 80 °C. Yield: 0.122 g of colorless oil, 0.51 mmol, 86 %, ratio = *geminal* 12 : *cis* 1.3 : *trans* 1 as determined by CH_3 ratio. ^{1}H NMR (300 MHz, $CDCl_3$) δ 7.98-7.94 (m, 1H, ar), 7.91-7.84 (m, 1H, arom.), 7.49-7.42 (m ,1H, arom.), 7.32 (t, 1H, arom., J_{HH}=7.1 Hz), 7.25 (d, 1H, *Z / cis*, CH, J_{HH}=12.6 Hz), 7.05 (d, 1H, *E* / *trans*, CH, J_{HH}=7.1 Hz), 5.67 (d, 1H, *Z* / *cis*, CH, J_{HH}=12.8 Hz), 4.97 (d, 1H, gem, CH, J= 2.12 Hz, major), 4.88 (d, 1H, *E* / *trans*, CH, J_{HH}=7.2 Hz), 4.76 (d, 1H, *gem*, CH, J_{HH}=2.2 Hz, major), 1.21 (s, 9H, *Z / cis*, CH_3), 1.15 (s, 9H, *gem*, CH_3, major), 1.08 (s, 9H, *E* / *trans*, CH_3). ^{13}C{^{1}H} NMR (75 MHz, $CDCl_3$) δ 163.8 (s), 162.8 (s), 134.8 (s), 133.7 (s, minor), 133.5 (s), 132.1 (s, minor), 131.9 (s), 130.1 (s), 130.0 (s), 128.2 (s), 128.1 (s), 128.0 (s, minor), 127.5 (s, minor), 124.6 (s, minor), 99.7 (s), 124.9 (s), 36.6 (s), 30.8 (s, minor), 29.9 (s, minor), 28.0 (s). IR (neat, liquid): $\tilde{\nu}$ = 2961 (m), 2906 (w), 2869 (w), 1733 (s), 1654 (m), 1573 (m), 1476 (m), 1422 (m), 1360 (m), 1281 (m), 1241 (s), 1137 (s), 1067 (s), 737 (s).

X-ray Crystallography Data for [RuCl(dap)(PPh$_3$)$_2$]BAr$^F{}_4$

Crystals of the complex were obtained by layering a CH_2Cl_2 solution of the complex with hexanes. A crystal of approximate dimensions 0.496 × 0.207 × 0.168 mm^3 was mounted on a MiTeGen cryoloop in a random orientation. Preliminary examination and data collection were performed using a Bruker X8 Kappa Apex II Charge Coupled Device

(CCD) Detector system single crystal X-Ray diffractometer equipped with an Oxford Cryostream LT device. All data were collected using graphite monochromated Mo Kα radiation (λ= 0.71073 Å) from a fine focus sealed tube X-Ray source. Preliminary unit cell constants were determined with a set of 36 narrow frame scans. Typical data sets consist of combinations of ω and Φ scan frames with scan width of 0.5° and counting time of 20 seconds/frame at a crystal to detector distance of 4.0 cm. The collected frames were integrated using an orientation matrix determined from the narrow frame scans. Apex II and SAINT software packages were used for data collection and data integration.[72] Analysis of the integrated data did not show any decay. Final cell constants were determined by global refinement of 9899 reflections harvested from the complete data set. Collected data were corrected for systematic errors using SADABS based on the Laue symmetry using equivalent reflections.[72]

Structure solution and refinement were carried out using the SHELXTL- PLUS software package.[73] The structure was solved and refined successfully in the monoclinic space group $P2_1/n$. Full matrix least-squares refinements were carried out by minimizing $\Sigma w(F_o^2-F_c^2)^2$. The non-hydrogen atoms were refined anisotropically to convergence. The CF3 groups were refined with geometrical restraints (SADI). Lattice includes the following solvents: one molecule of ethyl acetate and half molecule of diethyl ether and hexanes. The solvent molecules were refined with geometrical restraints (SADI). All hydrogen atoms were treated using appropriate riding model (AFIX m3). Crystal data and intensity data collection parameters, the final residual values and structure refinement parameters, and calculated and observed structure factors are available in electronic format.[68]

4.7 References

(1) Meyer, T. J. *Pure and Applied Chemistry* **1986**, *58* (9), 1193–1206.
(2) Mutai, T.; Cheon, J.-D.; Arita, S.; Araki, K. *J. Chem. Soc., Perkin Trans. 2* **2001**, No. 7, 1045–1050.
(3) Nazeeruddin, M. K.; Kay, A.; Rodicio, I.; Humphry-Baker, R.; Mueller, E.; Liska, P.; Vlachopoulos, N.; Graetzel, M. *J. Am. Chem. Soc.* **1993**, *115* (14), 6382–6390.
(4) Sinn, S.; Schulze, B.; Friebe, C.; Brown, D. G.; Jäger, M.; Kübel, J.; Dietzek, B.; Berlinguette, C. P.; Schubert, U. S. *Inorg. Chem.* **2014**, 140121111448001.
(5) Curtis, J. C.; Sullivan, B. P.; Meyer, T. J. *Inorg. Chem.* **1983**, *22* (2), 224–236.
(6) Batista, A. A.; Santiago, M. O.; Donnici, C. L.; Moreira, I. S.; Healy, P. C.; Berners-Price, S. J.; Queiroz, S. L. *Polyhedron* **2001**, *20* (17), 2123–2128.
(7) Younus, H. A.; Ahmad, N.; Su, W.; Verpoort, F. *Coord. Chem. Rev.* **2014**, *276*, 112–152.
(8) Malouf, G.; Ford, P. C. *J. Am. Chem. Soc.* **1974**, *96* (2), 601–603.
(9) Thummel, R. P.; Jahng, Y. *Inorg. Chem.* **1986**, *25* (15), 2527–2534.
(10) Nazeeruddin, M. K.; De Angelis, F.; Fantacci, S.; Selloni, A.; Viscardi, G.; Liska, P.; Ito, S.; Takeru, B.; Grätzel, M. *J. Am. Chem. Soc.* **2005**, *127* (48), 16835–16847.
(11) Gao, F.; Wang, Y.; Shi, D.; Zhang, J.; Wang, M.; Jing, X.; Humphry-Baker, R.; Wang, P.; Zakeeruddin, S. M.; Grätzel, M. *J. Am. Chem. Soc.* **2008**, *130* (32), 10720–10728.
(12) Pugh, D.; Danopoulos, A. A. *Coord. Chem. Rev.* **2007**, *251* (5-6), 610–641.
(13) Gunanathan, C.; Milstein, D. *Chem. Rev.* **2014**, *114* (24), 12024–12087.
(14) Tanaka, R.; Yamashita, M.; Nozaki, K. *J. Am. Chem. Soc.* **2009**, *131* (40), 14168–14169.
(15) Yamakawa, M.; Yamada, I.; Noyori, R. *Angew. Chem.* **2001**, *113* (15), 2900–2903.
(16) Haack, K.-J.; Hashiguchi, S.; Fujii, A.; Ikariya, T.; Noyori, R. *Angew. Chem. Int. Ed.* **1997**, *36* (3), 285–288.
(17) Kumar, P.; Singh, A. K.; Sharma, S.; Pandey, D. S. *J. Organomet. Chem.* **2009**, *694* (22), 3643–3652.
(18) Ye, W.; Zhao, M.; Yu, Z. *Chem. Eur. J.* **2012**, *18* (35), 10843–10846.
(19) Zerla, D. S.; Rimoldi, I.; Cesarotti, E.; Facchetti, G.; Pellizzoni, M.; Fusè, M. *J. Organomet. Chem.* **2007**, *771*, 2–8.
(20) Huff, C. A.; Sanford, M. S. *ACS Catal.* **2013**, No. 3, 2412–2416.
(21) Du, W.; Wang, L.; Wu, P.; Yu, Z. *Chem. Eur. J.* **2012**, *18* (37), 11550–11554.
(22) Wang, Q.; Du, W.; Liu, T.; Chai, H.; Yu, Z. *Tetrahedron Letters* **2014**, *55* (9), 1585–1588.
(23) Tseng, K.-N. T.; Kampf, J. W.; Szymczak, N. K. *Organometallics* **2013**, *32* (7), 2046–2049.
(24) Li, J.; Lutz, M.; Spek, A. L.; van Klink, G. P. M.; van Koten, G.; Gebbink, R. J. M. K. *Organometallics* **2010**, *29* (6) 1379–1387.
(25) Srimani, D.; Balaraman, E.; Gnanaprakasam, B.; Ben-David, Y.; Milstein, D. *Adv. Synth. Catal.* **2012**, *354* (13), 2403–2406.
(26) Srimani, D.; Ben-David, Y.; Milstein, D. *Angew. Chem. Int. Ed.* **2013**, *52* (14), 4012–4015.
(27) He, L.-P.; Chen, T.; Gong, D.; Lai, Z.; Huang, K.-W. *Organometallics* **2012**, *31* (14), 5208–5211.
(28) Zhu, Y.; Manske, K. J.; Shi, Y. *J. Am. Chem. Soc.* **1999**, *121* (16), 4080–4081.
(29) Zhu, Y.; Shu, L.; Tu, Y.; Shi, Y. *J. Org. Chem.* **2001**, *66* (5), 1818–1826.
(30) Isambert, N.; Cruz, M.; Arévalo, M. J.; Gómez, E.; Lavilla, R. *Org. Lett.* **2007**, *9* (21), 4199–4202.
(31) Kobayashi, S.; Matsubara, R.; Nakamura, Y.; Kitagawa, H.; Sugiura, M. *J. Am. Chem. Soc.* **2003**, *125* (9), 2507–2515.
(32) Crimmins, M. T. *Chem. Rev.* **1988**, *88* (8), 1453–1473.
(33) Fustero, S.; Simón-Fuentes, A.; Barrio, P.; Haufe, G. *Chem. Rev.* **2015**, *115* (2), 871–930.
(34) Barbier, P.; Mohr, P.; Muller, M.; Masciadri, R. *J. Org. Chem.* **1998**, *63* (20), 6984–6989.
(35) Keinicke, L.; Fristrup, P.; Norrby, P.-O.; Madsen, R. *J. Am. Chem. Soc.* **2005**, *127* (45), 15756–15761.
(36) Fedoryński, M.; Kubicka-Prusik, M.; Kursa, M.; Jończyk, A. *Tetrahedron* **1997**, *53* (3), 1053–1060.
(37) Landgrebe, J. A. *J. Org. Chem.* **1965**, *30* (9), 2997–3000.
(38) Lo, J. C.; Kim, D.; Pan, C.-M.; Edwards, J. T.; Yabe, Y.; Gui, J.; Qin, T.; Gutiérrez, S.;

Giacoboni, J.; Smith, M. W.; Holland, P. L.; Baran, P. S. *J. Am. Chem. Soc.* **2017**, *139* (6), 2484–2503.
(39) Huang, F.; Quach, T. D.; Batey, R. A. *Org. Lett.* **2013**, *15* (12), 3150–3153.
(40) Morales-Cerón, J. P.; Lara, P.; López-Serrano, J.; Santos, L. L.; Salazar, V.; Álvarez, E.; Suárez, A. *Organometallics* **2017**, *36* (13), 2460–2469.
(41) Zhang, S.-Y.; Zhang, X.; Li, H.; Niu, Z.; Shi, W.; Cheng, P. *Inorg. Chem.* **2015**, 54, 2310–2314.
(42) Poladura, B.; Martínez-Castañeda, Á.; Rodríguez-Solla, H.; Llavona, R.; Concellón, C.; del Amo, V. *Org. Lett.* **2013**, *15* (11), 2810–2813.
(43) Jeschke, J.; Gäbler, C.; Lang, H. *J. Org. Chem.* **2016**, *81* (2), 476–484.
(44) Mitsudo, T.; Hori, Y.; Yamakawa, Y. *J. Org. Chem.* **1987**, *52* (11), 2230–2239.
(45) Yi, C. S.; Gao, R. *Organometallics* **2009**, *28* (22), 6585–6592.
(46) Tan, S. T.; Fan, W. Y. *Eur. J. Inorg. Chem.* **2010**, *2010* (29), 4631–4635.
(47) Doucet, H.; Martin-Vaca, B.; Bruneau, C.; Dixneuf, P. H. *J. Org. Chem.* **1995**, *60* (22), 7247–7255.
(48) Trivedi, M.; Singh, S. K.; Pandey, D. S.; Zou, R.-Q.; Chandra, M.; Xu, Q. *J. Mol. Struct.* **2008**, *886* (1-3), 136–143.
(49) Sheldrick, W. S.; Exner, R. *Inorganica Chimica Acta* **1990**, *175* (2), 261–268.
(50) Goossen, L. J.; Paetzold, J.; Koley, D. *Chem. Commun.* **2003**, *0* (6), 706–707.
(51) Pham, M. V.; Cramer, N. *Angew. Chem. Int. Ed.* **2014**, *53* (52), 14575–14579.
(52) Rotem, M.; Shvo, Y. *J. Organomet. Chem.* **1993**, 448, 189–204.
(53) Lynam, J. M.; Welby, C. E.; Whitwood, A. C. *Organometallics* **2009**, *28* (5), 1320–1328.
(54) Cadierno, V.; Pilar Gamasa, M.; Gimeno, J.; Pérez-Carreño, E.; García-Granda, S. *J. Organomet. Chem.* **2003**, *670* (1-2), 75–83.
(55) Bustelo, E.; Jiménez-Tenorio, M.; Puerta, M. C.; Valerga, P. *Organometallics* **2007**, *26* (17), 4300–4309.
(56) Gamasa, M. P.; Gimeno, J.; Martin-Vaca, B. M.; Borge, J.; García-Granda, S.; Pérez-Carreño, E. *Organometallics* **1994**, *13* (10), 4045–4057.
(57) Ashworth, I. W.; Hillier, I. H.; Nelson, D. J.; Percy, J. M.; Vincent, M. A. *ACS Catal.* **2013**, *3* (9), 1929–1939.
(58) Montgomery, T. P.; Ahmed, T. S.; Grubbs, R. H. *Angew. Chem. Int. Ed.* **2017**, *39*, 11024–11036.
(59) Musengimana, E.; Fatakanwa, C. *J IRAN CHEM SOC* **2015**, *13* (2), 253–259.
(60) Cadierno, V.; Francos, J.; Gimeno, J. *Organometallics* **2011**, *30* (4), 852–862.
(61) Nicks, F.; Libert, L.; Delaude, L.; Demonceau, A. *Aust. J. Chem.* **2009**, *62* (3), 227–5.
(62) He, L.-P.; Chen, T.; Xue, D.-X.; Eddaoudi, M.; Huang, K.-W. *J. Organomet. Chem.* **2012**, *700*, 202–206.
(63) Gorgas, N.; Stöger, B.; Veiros, L. F.; Pittenauer, E.; Allmaier, G.; Kirchner, K. *Organometallics* **2014**, *33* (23), 6905–6914.
(64) Gunanathan, C.; Hölscher, M.; Pan, F.; Leitner, W. *J. Am. Chem. Soc.* **2012**, *134* (35), 14349–14352.
(65) Alonso, D. A.; Brandt, P.; Nordin, S. J. M.; Andersson, P. G. *J. Am. Chem. Soc.* **1999**, *121* (41), 9580–9588.
(66) Majireck, M. M.; Weinreb, S. M. *J. Org. Chem.* **2006**, *71* (22), 8680–8683.
(67) Li, X.; Danishefsky, S. J. *J. Am. Chem. Soc.* **2008**, *130* (16), 5446–5448.
(68) Stark, M. J.; Tang, D. T.; Rath, N. P.; Bauer, E. B. *Tetrahedron Letters* **2018**, *59* (10), 873–877.
(69) Reger, D. L.; Little, C. A.; Lamba, J.; Brown, K. J. *Inorganic Syntheses* **2004**, *34*, 5–8.
(70) Brookhart, M.; Grant, B.; Volpe, A. F., Jr. *Organometallics* **1992**, *11* (11), 3920–3922.
(71) Fox, M. A.; Harris, J. E.; Heider, S.; Pérez-Gregorio, V.; Zakrzewska, M. E.; Farmer, J. D.; Yufit, D. S.; Howard, J. A. K.; Low, P. J. *J. Organomet. Chem.* **2009**, *694* (15), 2350–2358.
(72) *Bruker Analytical X–ray*; Madison, WI, 2012.
(73) Sheldrick, G. M. *Acta Cryst.* **2008**, *A64*, 112–122.

Chapter 5. Ferrocenium-Catalyzed Propargylic Etherification

Chapter 5. Ferrocenium–Catalyzed Propargylic Etherification Reactions

5.1. Aim

Thus far, we considered ruthenium complexes as catalysts for the transformation of propargylic alcohols. Iron is located in the same row in the periodic table as ruthenium and offers some advantages compared to ruthenium. It is less expensive and virtually non-toxic. We were interested to determine whether iron complexes can catalytically activate propargylic alcohols. It was hypothesized that ferrocenium cations with substituted cyclopentadienyl ligands could act as Lewis acids to catalytically activate propargylic alcohols. The substituents on the cyclopentadienyl rings can be chiral, thus conferring chirality on the transition state and onto the product, finally inducing stereoinduction. Several examples of iron catalysts based on ferrocenes were screened for reactivity after chemical oxidation to their respective ferrocenium cations. The results indicated that the chirality of the ferrocenium cations could not be confirmed after oxidation of the ferrocene. However, it was found that ferrocene boronic acid, when oxidized with $AgSbF_6$, showed catalytic activity in the etherification of propargylic alcohols at a temperature lower than what other catalytic systems require.

5.2. Introduction

Transition metal catalysts are employed as an effective and atom economical means of organic transformations. Typically, transition metals such as ruthenium, iridium, rhodium or platinum are employed in transition metal catalysis, which are fairly toxic and only trace amounts of them can be present in pharmaceutical products to meet health standards. Iron, in turn, has the advantages of its lower cost and toxicity as iron is

geologically prevalent and environmentally friendly. The development of iron complexes as catalysts is an emerging field, broadening the use of iron in synthetic chemistry from simple salts as like $FeCl_3$ into employing intricate molecules for strategic and chiral transformations.[1] While the use of iron as a Lewis acid is not a recent finding, iron complexes are increasingly being employed for chemoselectivity, regioselectivity, and stereoselectivity.[2] Numerous publications are available, detailing applications of iron catalysts for use in addition, substitution, hydrogenation, rearrangement, and polymerization reactions.[2-5]

Among iron complexes, ferrocene is one of the most stable and well–known metal complexes.[6] The η^5–C_5H_5 cyclopentadienyl ligand is widely–regarded as versatile, imparting excellent stability on metal complexes bearing either one or two of these ligands.[7] The cyclopentadienyl (Cp) aromatic rings of ferrocene are susceptible to electrophilic substitution reactions, offering an avenue for creating substituted ferrocenes with a variety of qualities.[8,9] One such quality is the ability to synthesize chiral ferrocenes. Chiral ferrocenes are ferrocenes that have been substituted with chiral groups onto the Cp ring. An example of this chirality is in the stereochemistry of the amine in *N,N*–dimethyl–α–ferrocenylethylamine (**38**, Ugi's Amine), shown in Figure 5.1. One step further, a ferrocene can be 'planar chiral' when two different groups are substituted onto one of the Cp rings (Figure 5.1). Chiral ferrocenes have found great utility in catalytic applications with their use as chiral auxiliaries and also as chiral ligands. In addition to chiral ferrocenes offering necessary structural properties, their ability to be fine–tuned electronically, their thermal stability, and their tolerance to oxygen, moisture, and a variety of functional groups make them invaluable in catalytic applications.[10-12] While the

use of chiral ferrocenes has been fruitful in catalytic applications, these metal complexes are almost always used as chiral auxiliaries, not as the actual catalyst.[13]

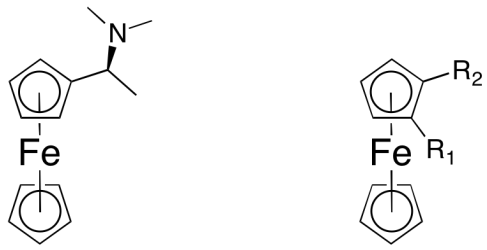

(*S*)–*N,N*–dimethyl–α–ferrocenylethylamine "Ugi's Amine" **38**

general structure planar chiral

Figure 5.1. Examples of chiral and planar chiral ferrocenes.

To that end, we chose to explore the use of chiral ferrocenes or ferrocenium salts as catalysts in propargylic etherification reactions. Previous work in our laboratory has demonstrated that ferrocenium hexafluorophosphate ($Fc^+PF_6^-$) could be used to synthesize propargylic ethers in yields up to 90%.[14] It is our hypothesis that when employing an oxidized chiral ferrocene to perform catalytic etherification reactions, transfer of chiral information from the complex to the propargylic ether product could be achieved. The mechanism of the interaction between ferrocenium and propargylic alcohols is not well understood. Iron chlorides have been established to act as a Lewis acid in a variety of reactions.[2,3] More so, $FeCl_3$ has been demonstrated to facilitate propargylic nucleophilic substitution reactions.[15] Half–sandwich iron complexes bearing only one Cp ring have been demonstrated to form stable complexes with alkynes and propargylic alcohols, in the form of iron vinylidenes or iron allenylidenes.[16-18] Ferrocenes have also been demonstrated to undergo acylation of a Cp ring by an alkyne in the

presence of a strong acid.[19,20] Based on these literature examples, we set out to first synthesize a chiral ferrocenium salt to be employed as catalyst in enantioselective etherification reactions.

5.3. Results and Discussion

5.3.1. Preparation of Ugi's Amine and Initial Exploration of Oxidation

At the outset, we intended to synthesize a planar chiral ferrocene, using methods developed by Ivar Ugi and coworkers for the *ortho*–lithiation of *N,N*–dimethyl–α–ferrocenylethylamine (Ugi's amine **38**).[21,22] Other methods for *ortho*–substitution exist, but derivatization from α–ferrocenylethylamine is one of the most well–established routes to synthesize planar chiral ferrocenes.[23-26] A general scheme showing this method is given in Scheme 5.1, where directed *ortho*-lithiation followed by quenching with an electrophile gives a planar-chiral ferrocene in optically pure form.

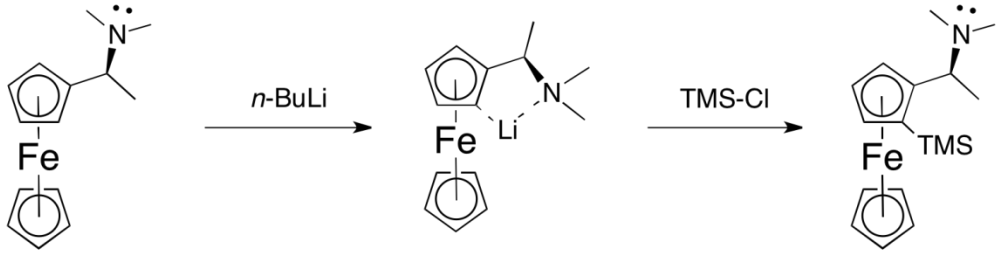

Scheme 5.1. Synthesis of 1,2–substituted ferrocene by *ortho*–lithiation of (*S)*–38 and addition of TMS.

The amine substituent on the ferrocene acts as an *ortho*–director for a lithium base to abstract a proton from the Cp ring. The lithiated ferrocene could then be employed as a nucleophile to create ferrocenes with 1,2–substituted Cp rings (*orthogonally–substituted on one ring*). We first employed racemic Ugi's amine to save time and costs, and it was

synthesized according to literature procedures from ferrocene.[22] The product was characterized and found to match literature ^{1}H NMR and IR values, but demonstrated a slightly depressed melting point. Chiral resolution using tartaric acid was attempted using literature described procedures, but a pure enantiomer was not able to be obtained. Even though we had not yet obtained a single enantiomer of the amine, we were curious as to whether or not the amine would survive chemical oxidation of the ferrocene.

The racemic Ugi's amine was oxidized using procedures well established for the synthesis of ferrocenium salts. $FeCl_3$, 1,4–benzoquinone, and silver salts were explored as oxidizing reagents using several procedures described by Connelly and Geiger.[27] For one method, the amine was dissolved into a solution of Et_2O. A separate solution of 1,4–benzoquinone and HBF_4•Et_2O was slowly added to the amine solution. When employing this procedure using ferrocene, the precipitation of a blue solid proceeded as described in literature. When the same procedure was attempted for Ugi's amine, the solution changed to a dark green color. Attempts to salt out the complex were ineffective, as multiple crystallization attempts resulted in a dark green or brown solution.

A second method of oxidation was attempted. The amine was dissolved into a 2:1 mixture of water and acetone. A sub–stoichiometric amount of $FeCl_3$ was added to this orange solution, which immediately turned dark blue green. Coordinating anions of BF_4^-, PF_6^-, $BAr^F{}_4^-$, and SbF_6^- were employed in the different experiments in their various salts as described, in an effort to gain better chances of recrystallization. Again, this procedure generates the corresponding ferrocenium salts from ferrocene as expected but was unsuccessful for the oxidation of Ugi's amine. A third procedure, of employing silver salts with the amine in an ether solution was also ineffective.

The oxidation of Ugi's amine was again attempted in deuterated solvents, using a mixture of acetone–d_6 and D_2O and treatment with $FeCl_3$. The crude solution of the emerald–green ionic liquid was filtered through cotton and examined by NMR. Due to ferrocenium's paramagnetic nature, the acquisition of ^1H NMR was obtained with an increase in the sweep width setting of the instrument. It was our assumption that although the peak for the Cp ring protons would shift dramatically downfield in the spectrum, we would still be able to differentiate the trivial proton assignments for the methyl groups attached to the amine. We were unable to assign methyl amines in the ^1H NMR spectrum. It appeared that chemical oxidation may result in a loss of the amine in the α–ethyl position of Ugi's amine. This is a reasonable explanation, as ferrocenyl–stabilized carbocations have been documented from the loss of functional groups at the α–position of alkyl substituents on ferrocene.[28-30] As well, the removal of the amine under strongly acidic or basic conditions is a strategy employed when changing functional groups on ferrocenes derived from Ugi's amine.[12,31-34] Overall, it turned out that Ugi's amine is not stable when being oxidized.

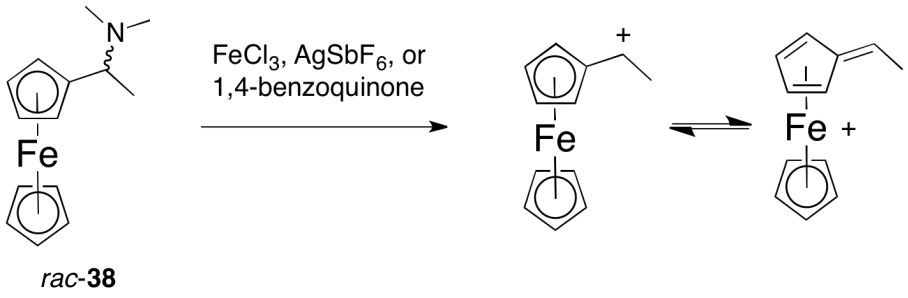

rac-**38**

Scheme 5.2. Possible loss of chirality after attempted oxidation of **38**.

Loss of chirality in the substituent on ferrocene does not fulfill our aim in this study, so we turned our attention towards the synthesis of a planar chiral ferrocene, staring with racemic Ugi's amine, again to save costs. Using the *ortho*–lithiation method shown in Scheme 5.1, we attempted to synthesize an orthogonally substituted $Si(CH_3)_3$ analog of Ugi's amine.[21] Efforts were unrewarded, as the TMS analog could not be separated from the starting material as these produced low yielding reactions. It appears that Ugi's amine does not withstand the oxidative conditions in Scheme 5.2. Future approaches to synthesize a planar chiral ferrocene should be directed toward two different alkyl substituents at the Cp ring that would be better at withstanding the oxidation conditions. We proceeded on with the synthesis of the next step, elimination of the amine **38** to yield 2-trimethylsilyl-1vinylferrocene (**39**), shown in Figure 5.2. It was our hypothesis that the diastereomers could be separated during flash chromatography, but I was unable to isolate a clean compound. However, we decided to further investigate the ferrocenes we had on hand for *in situ* oxidation and catalytic activity.

5.3.2. In Situ Oxidation of Ferrocenes and Catalytic Performance

Our curiosity grew about the potential for creating stable oxidized species of ferrocenes. A number of ferrocenes were purchased, obtained as gifts from our collaborator Dr. Michael Shaw (Southern Illinois University Edwardsville), or readily available because they are intermediates in the synthesis of Ugi's amine **38**. We chose to oxidize these complexes *in situ* and test them for catalytic activity in propargylic etherification reactions. The structures of some of these complexes are shown in Figure 5.2.

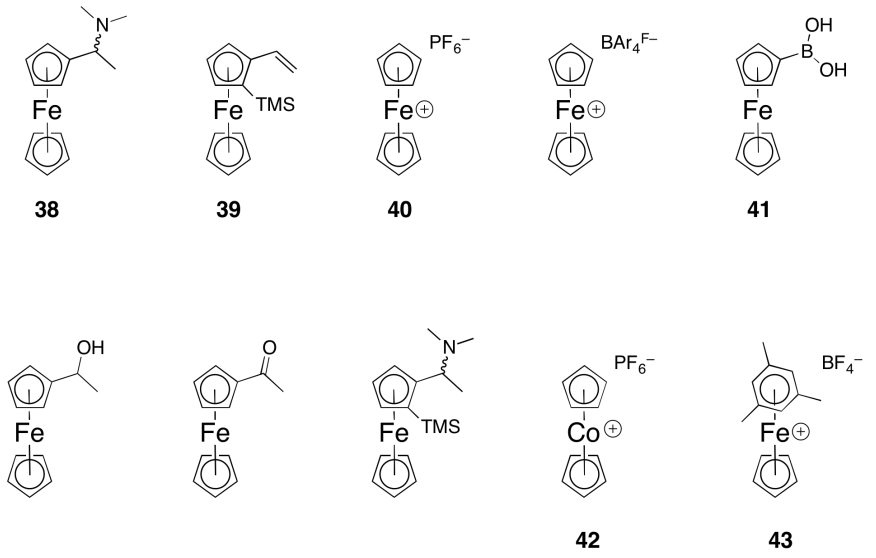

Figure 5.2. Ferrocenes and metal complexes screened for catalytic activity.

Previous work with $Fc^{+}PF_6^{-}$ has demonstrated the etherification of a limited range of propargylic alcohols.[14] We intended to explore as many facets of this reactivity as we could, employing many of the complexes shown in Figure 5.2. with varying degrees of purity and characterization. The neutral complexes were used with the addition of an oxidant. The complex salts **40**, **42**, and **43** were used as is. While the cobaltocenium **42** showed a small degree of reactivity, the gas chromatogram produced only a major peak that was associated with the elimination product. The mesitylene complex **43** offered no reactivity at all. Synthons from the synthesis of Ugi's amine **38** and from **38** to the complex 2-trimethylsilyl-1vinylferrocene **39**, are not numbered as they as well provided little to no reactivity, even in the presence of an additive.

A variety of oxidants were employed, such as $FeCl_3$, 1,4–benzoquinone, and $AgSbF_6$. While $FeCl_3$ did provide an observable colorimetric change during the oxidation of

ferrocene, it was avoided as an *in situ* oxidant due to published evidence of $FeCl_3$ being able to catalyze the title reaction.[15] The screening reaction of 2-phenyl-3-butyn-2-ol and *n*–butanol provided some insights as to which complexes provided significant catalytic activity. Reactions were performed in CH_2Cl_2 with approximately 5–10 mol % iron complex. A sub–stoichiometric amount of oxidant was added to the metal complex and allowed so sit for approximately 15 minutes. The substrates were then added and the reactions were allowed to progress overnight, heating at 45 °C for approximately 16 hours. The reaction mixtures were then filtered through a small amount of silica in a pipette and subjected to gas chromatography. The peaks were integrated and compared to amounts of the starting material to determine whether or not the catalytic activity was substantial enough to merit repeat experiments with the same conditions to provide isolated yields.

Under the conditions described above, most ferrocenes were not catalytically active until we began to use $AgSbF_6$ as the *in situ* oxidant. In a control reaction, it was observed that the silver salt itself does activate propargylic alcohols for catalytic transformation, but the reaction mixture exhibited a variety of products, each of them in small yields as judged by GC, after heating at 45 °C for 16 h. Investigation was continued with the most active ferrocene, ferrocenylboronic acid, and the *in situ* oxidant $AgSbF_6$. A summary of the findings are presented here in Table 5.1.

Table 5.1. Results of catalytic etherification of propargyl acetates.

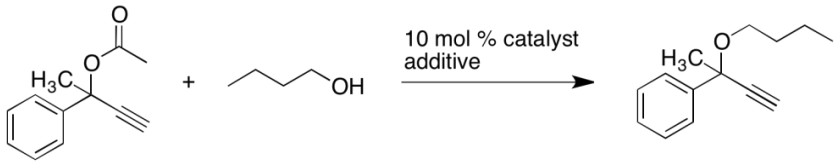

Entry	Catalyst	Additive	Conditions	Yield (%)
1	Fc-B(OH)$_2$ **41**	$AgSbF_6$	CH_2Cl_2, rt, 48 h	51
2	Fc^+ PF_6^- **40**	–	CH_2Cl_2, rt, 48 h	41
3	Fc	$PhB(OH)_2$, $AgSbF_6$	CH_2Cl_2, rt, 48 h	21
4	Fc-B(OH)$_2$ **41**	$AgSbF_6$	MeOH, rt, 48 h	< 10

General Conditions: 0.7 mmol propargyl acetate, 0.7 mmol alcohol, 5–7 mol % catalyst, 0.9 mol eq./catalyst for additive. Isolated yields via flash chromatography.

As can be seen from Table 5.1., a combination of Fc-B(OH)$_2$ (**41**) and $AgSbF_6$ is a promising catalytic system for the etherification of propargylic alcohols. It is more reactive than $Fc^+PF_6^-$ by itself, which our laboratory previously employed in propargylic etherification reactions. $AgSbF_6$ activates propargylic alcohols for the reaction in Table 5.1.; however, a mixture of several products was detected by GC, making it not a promising candidate for the reaction. Most significantly, the Fc-B(OH)$_2$ \ $AgSbF_6$ combination performs the reaction in Table 5.1. at room temperature. Neither the ruthenium catalyst systems presented in this thesis nor our previously performed iron-catalyzed etherification reactions worked at room temperature, even when propargylic acetates were employed.

For time constraints, it was not possible to investigate the reaction further within the scope of this thesis. However, the results in Table 5.1 are an excellent starting point for

further investigations in the iron-catalyzed etherification reactions of propargylic alcohols.

5.4. Summary and Perspective

The key finding of this chapter is that a combination of Fc-$B(OH)_2$ and $AgSbF_6$ is a promising catalytic system for the etherification of propargylic esters. Compared to previous work published from our laboratory, ferrocenylboronic acid with $AgSbF_6$ was able to catalyze etherification of 2-phenyl-3-butyn-2-acetate with *n*-butanol in a much shorter timeframe at room temperature. Further work is necessary to understand the mechanism of this reaction, as well as its scope and limitations.

The oxidation of chiral ferrocenes may be worth further investigation. If the substituents attached to a planar chiral ferrocene are durable enough to withstand the oxidation step, it may be possible to obtain a chiral, catalytically active ferrocene salt. Synthesis of these ferrocene derivatives will take careful design and precautions during work up, to avoid dearomatizaion of the Cp ring or loss of stereoinformation.

5.5. Experimental

General.

All chemicals were used as supplied from Sigma-Aldrich unless otherwise noted. Toluene, CH_2Cl_2, and Et_2O were freshly distilled. Starting carboxylic acid materials were used as received and acetylenes were distilled. $NaBAr^F_4$, 1-phenyl-2-propyn-1-ol, and all propargylic acetates were synthesized following literature procedures.[35-39] A portion of experiments used $NaPF_6$ recrystallized from dry, hot acetone. NMR spectra

for characterization were collected at room temperature on a Varian Unity 300 MHz or Bruker Avance 300 MHz instrument; all chemical shifts (δ) are reported in ppm and are referenced to a residual solvent signal. IR spectra were collected on a Thermo Nicolet 360 FT-IR spectrometer. FAB and exact mass data were collected on a JEOL MStation [JMS-700] Mass Spectrometer. Melting points were determined on a Thomas Hoover uni-melt capillary melting point apparatus and are uncorrected.

General Catalytic Experiments.

The propargyl alcohol or acetate (0.7 mmol) was placed into a screw-top scintillation vial along with 1 equivalent of the alcohol (0.7 mmol), the catalyst (0.05 mmol, 5–7 mol %), 0.9 molar equivalents (0.04 mmol) of additive, and 1 mL CH_2Cl_2 or other specified solvent. A cap was tightened on the vial and the mixture was heated in a heating block for the specified time frame. The mixture was then filtered through a pipette with a small amount of silica gel and the solvent was removed. Purification was achieved via column chromatography using 1.5 cm x 10 cm silica with 9:1 v/v hexanes/ethyl acetate as eluent, unless otherwise specified. Spectroscopic data for all products matched those available in literature.[14]

5.6. References

(1) Bolm, C.; Legros, J.; Le Paih, J.; Zani, L. *Chem. Rev.* **2004**, *104* (12), 6217–6254.
(2) Bauer, E. B. *Curr. Org. Chem.* **2008**, *12* (16), 1341–1369.
(3) Bauer, I.; Knölker, H.-J. *Chem. Rev.* **2015**, *115* (9), 3170–3387.
(4) Correa, A.; García Mancheño, O.; Bolm, C. *Chem. Soc. Rev.* **2008**, *37* (6), 1108–1117.
(5) Czaplik, W. M.; Mayer, M.; Cvengroš, J.; Wangelin, von, A. J. *ChemSusChem* **2009**, *2* (5), 396–417.
(6) Crabtree, R. H. *The Organometallic Chemistry of the Transition Metals*, 5 ed.; John Wiley & Sons, Inc.: Hoboken, 2014; pp 1–522.
(7) O'Connor, J. M.; Casey, C. P. *Chem. Rev.* **1987**, *87* (2), 307–318.
(8) Heinze, K.; Lang, H. *Organometallics* **2013**, *32* (20), 5623–5625.
(9) Astruc, D. *Eur. J. Inorg. Chem.* **2016**, No.1, 6–29.
(10) Dai, L.-X.; Tu, T.; You, S.-L.; Deng, W.-P.; Hou, X.-L. *Acc. Chem. Res.* **2003**, *36* (9), 659–667.

(11) Gómez Arrayás, R.; Adrio, J.; Carretero, J. C. *Angew. Chem. Int. Ed.* **2006**, *45* (46), 7674–7715.
(12) Togni, A. *Angew. Chem. Int. Ed.* **1996**, *35* (13-14), 1475–1477.
(13) Colacot, T. J. *Chem. Rev.* **2003**, *103* (8), 3101–3118.
(14) Queensen, M. J.; Rabus, J. M.; Bauer, E. B. *J Mol Catal A-Chem* **2015**, *407*, 221–229.
(15) Zhan, Z.-P.; Yu, J.-L.; Liu, H.-J.; Cui, Y.-Y.; Yang, R.-F.; Yang, W.-Z.; Li, J.-P. *J. Org. Chem.* **2006**, *71* (21), 8298–8301.
(16) Venâncio, A. I. F.; Guedes da Silva, M. F. C.; Martins, L. M. D. R. S.; Fraústo da Silva, J. J. R.; Pombeiro, A. J. L. *Organometallics* **2005**, *24* (19), 4654–4665.
(17) Byrne, L. T.; Koutsantonis, G. A.; Sanford, V.; Selegue, J. P.; Schauer, P. A.; Iyer, R. S. *Organometallics* **2010**, *29* (5), 1199–1209.
(18) Selegue, J. P. *Coord. Chem. Rev.* **2004**, *248* (15-16), 1543–1563.
(19) Plażuk, D.; Vessières, A.; Hillard, E. A.; Buriez, O.; Labbé, E.; Pigeon, P.; Plamont, M.-A.; Amatore, C.; Zakrzewski, J.; Jaouen, G. *J. Med. Chem.* **2009**, *52* (15), 4964–4967.
(20) Plażuk, D.; Zakrzewski, J. *J. Organomet. Chem.* **2009**, *694* (12), 1802–1806.
(21) Marquarding, D.; Klusacek, H.; Gokel, G.; Hoffman, P.; Ugi, I. K. *J. Am. Chem. Soc.* **1970**, *92* (18), 5389–5393.
(22) Gokel, G. W.; Ugi, I. K. *J. Chem. Educ.* **1972**, *49* (4), 294.
(23) Nishibayashi, Y.; Arikawa, Y.; Ohe, K.; Uemura, S. *J. Org. Chem.* **1996**, *61* (3), 1172–1174.
(24) Ueberbacher, B. J.; Griengl, H.; Weber, H. R. *Chem. Commun.* **2008**, *9* (28), 3287.
(25) Butler, I. R.; M ssig, S.; Plath, M. *Inorganic Chemistry Communications* **1999**, *2* (9), 424–427.
(26) Herbert, S. A.; Castell, D. C.; Clayden, J.; Arnott, G. E. *Org. Lett.* **2013**, *15* (13), 3334–3337.
(27) Connelly, N. G.; Geiger, W. E. *Chem. Rev.* **1996**, *96* (2), 877–910.
(28) Cully, N.; Watts, W. E. *J. Organomet. Chem.* **1979**, *182* (1), 99–103.
(29) Bunton, C. A.; Carrasco, N.; Davoudzadeh, F.; Watts, W. E. *J. Chem. Soc., Perkin Trans. 2* **1980**, No. 10, 1520–1529.
(30) Shevaldina, E. V.; Shagina, A. D.; Kalinin, V. N.; Ponomaryov, A. B.; Smol'yakov, A. F.; Moiseev, S. K. *J. Organomet. Chem.* **2017**, *836-837*, 1–7.
(31) Togni, A.; Breutel, C.; Schnyder, A.; Spindler, F.; Landert, H.; Tijani, A. *J. Am. Chem. Soc.* **1994**, *116* (9), 4062–4066.
(32) Jia, X.; Li, X.; Lam, W. S.; Kok, S. H. L.; Xu, L.; Lu, G.; Yeung, C.-H.; Chan, A. S. C. *Tetrahedron: Asymmetry* **2004**, *15* (14), 2273–2278.
(33) Pandey, S.; Sárosi, M. B.; Lönnecke, P.; Hey-Hawkins, E. *Eur. J. Inorg. Chem.* **2016**, *2017* (2), 256–262.
(34) Sammakia, T.; Latham, H. A.; Schaad, D. R. *J. Org. Chem.* **1995**, *60* (1), 10–11.
(35) Reger, D. L.; Little, C. A.; Lamba, J.; Brown, K. J. *Inorganic Syntheses* **2004**, *34*, 5–8.
(36) Brookhart, M.; Grant, B.; Volpe, A. F., Jr. *Organometallics* **1992**, *11* (11), 3920–3922.
(37) Pünner, F.; Hilt, G. *Chem. Commun.* **2012**, *48* (30), 3617–3619.
(38) Sathyamoorthy, B.; Axelrod, A.; Farwell, V. *Organometallics* **2010**, 3431–3441.
(39) Riveiros, R.; Rodríguez, D.; Pérez Sestelo, J.; Sarandeses, L. A. *Org. Lett.* **2006**, *8* (7), 1403–1406.

Conclusions

The ability to fine–tune transition metal complexes for catalytic applications remains an intriguing concept of high economic relevance. A significant amount of chemistry employs such catalysts to overcome synthetic challenges. Therefore, working towards a better understanding of what makes transition metal complexes more or less ideal for specific catalytic applications is worthwhile for a variety of academic and industrial pursuits. Almost all disciplines of synthetic chemistry rely on optimization of experimental conditions and fine–tuning of transition metal catalysts for increased activity is simply an extension of that philosophy.

The research in this thesis set out to test the hypothesis that systematically changing ligands on metal complexes can affect the catalytic activity of those complexes. We initially chose to work on propargylic nucleophilic substitution reactions for optimization efforts. The reaction is known from the literature, but frequently requires elevated reaction temperatures of 60 °C and above. In Chapters 2 and 3, several new ruthenium complexes with demonstrably different electronic properties were synthesized to test our hypothesis: Can electronic changes at the metal center of the complex affect the catalytic activity of the complex? While the observed electronic environment and structural parameters of the new ruthenium complexes were in accordance with our expectations, the catalytic application did not provide evidence for positive effects of electronic tuning on the yields of the reactions. All new complexes within Chapters 2 and 3 exhibited catalytic activity in propargylic substitution reactions, however, one of the major goals – a reduced reaction temperature – could not be achieved.

We chose to take a closer look at reaction mechanisms to uncover more information. This investigation utilized NMR spectroscopic investigations into the kinetics of the reaction by monitoring reactions over time to generate both a kinetics plot and a Hammett plot. The Hammett reactivity plot did not provide confident evidence of a positive charge accumulation at the reaction center due to substantial error in some of the reactions. However, a trend in the isolated yields could be observed; it appeared that the yields from the reaction are substrate–dependent. Tertiary propargylic alcohols seemed to give better yields in comparison to secondary propargylic alcohols, corroborating a positively charged intermediate supported by the reactivity study. As well, kinetic data seems to demonstrate that the catalyst showed high activity at the beginning of the reaction, which dwindles over time. NMR investigations later determined that for every reaction, the metal complex and coordinating anion were both decomposing over the course of the reaction to yield a variety of unknown Lewis and Brønsted acids in the catalytic mixture.

All of the propargylic etherification reactions presented required elevated temperatures and long reaction times to proceed to completion. Under these conditions, we observed both the metathesis and decomposition of the phosphine ligands. Without the firm establishment of catalytic species formed *in situ*, we could not confidently attribute changes in reactivity that affected reaction yields. Furthermore, the mechanistic details are quite inconclusive; the observations provide some amount of support for hypothetical carbocation intermediate, with replacement facilitated by a Lewis or Brønsted acid. From what we learned in Chapters 2 and 3, we can conclude that for the propargylic substitution reactions under investigation, the studies were unable to provide

direct evidence that the electronic fine–tuning of the metal complexes affected the catalytic efficiency.

Future Work

While the studies from Chapters 2 and 3 did not give results that increased the confidence in our main hypothesis, the studies did support the argument that reaction mechanisms should always be closely examined. From the knowledge we have gained, we know where to focus further efforts. Future work in the realm of catalytic activation of propargylic alcohols should focus on reactions that can proceed at lower temperatures. As demonstrated in Chapter 5 of the thesis, ferrocenium salts allow for propargylic substitution reactions to proceed at or close to room temperature. Thus, turning the attention from ruthenium to cationic iron complexes might constitute a new field of research in the area of transition metal catalyzed propargylic substitution reactions.

A study of propargylic substitution reactions catalyzed by Brønsted acids also seems relevant in order to determine the extent of the role, if any, that a strong acid plays in catalytic performance. If Brønsted acids catalyze propargylic substitution reactions, they may compromise transition-metal catalyzed substitution reactions. This point also deserves further attention because Brønsted acid–catalyzed side reactions can have negative impact on enantioselective propargylic substitution reactions.

Appendix A: Crystallography Data

RuCl(indenyl)(PPh_3){$P(pyrl)_3$}] (13)

Empirical formula	C_{47} H_{50} Cl N_3 O_2 P_2 Ru
Formula weight	887.36
Temperature	100(2) K
Wavelength	0.71073 Å
Crystal system	Monoclinic
Space group	P2**1**/c
Unit cell dimensions	a = 17.4752(11) Å α= 90°.
	b = 25.8809(16) Å β= 90.281(4)°.
	c = 17.6438(13) Å γ = 90°.
Volume	7979.7(9) $Å^3$
Z	8
Density (calculated)	1.477 Mg/m^3
Absorption coefficient	0.585 mm^{-1}
F(000)	3680
Crystal size	0.254 x 0.176 x 0.089 mm^3
Theta range for data collection	0.787 to 27.297°.
Index ranges	-21<=h<=22, -33<=k<=31, -22<=l<=22
Reflections collected	68253
Independent reflections	17724 [R(int) = 0.0740]
Completeness to theta = 26.000°	100.0 %
Absorption correction	Semi-empirical from equivalents
Max. and min. transmission	0.8620 and 0.7819
Refinement method	Full-matrix least-squares on F^2
Data / restraints / parameters	17724 / 250 / 989
Goodness-of-fit on F^2	1.050
Final R indices [I>2sigma(I)]	R1 = 0.0594, wR2 = 0.1372
R indices (all data)	R1 = 0.0948, wR2 = 0.1597
Extinction coefficient	n/a
Largest diff. peak and hole	1.356 and -1.912 $e.Å^{-3}$

RuCl(indenyl){P(pyrl)$_3$}$_2$] (14)

Empirical formula	C_{33} H_{31} Cl N_6 P_2 Ru	
Formula weight	710.10	
Temperature	100(2) K	
Wavelength	0.71073 Å	
Crystal system	Monoclinic	
Space group	P $2_1/c$	
Unit cell dimensions	a = 13.2598(6) Å	α= 90°.
	b = 9.5844(4) Å	β= 99.205(2)°.
	c = 24.8271(11) Å	γ = 90°.
Volume	3114.6(2) Å^3	
Z	4	
Density (calculated)	1.514 Mg/m^3	
Absorption coefficient	0.726 mm^{-1}	
F(000)	1448	
Crystal size	0.256 x 0.151 x 0.135 mm^3	
Theta range for data collection	1.556 to 36.325°.	
Index ranges	-22≤h≤22, -15≤k≤14, -41≤l≤41	
Reflections collected	69845	
Independent reflections	15058 [R(int) = 0.0603]	
Completeness to theta = 26.000°	100.0 %	
Absorption correction	Semi-empirical from equivalents	
Max. and min. transmission	0.8625 and 0.7561	
Refinement method	Full-matrix least-squares on F^2	
Data / restraints / parameters	15058 / 0 / 388	
Goodness-of-fit on F^2	1.019	
Final R indices [I>2sigma(I)]	R1 = 0.0361, wR2 = 0.0745	
R indices (all data)	R1 = 0.0559, wR2 = 0.0831	
Extinction coefficient	n/a	
Largest diff. peak and hole	0.759 and -0.683 e.Å^{-3}	

[RuCl(indenyl)(PPh_3){P(*p*–$C_6H_4CF_3$)$_3$}] (26)

Empirical formula	$C_{99}\ H_{71}\ Cl_{11}\ F_{18}\ P_4\ Ru_2$	
Formula weight	2318.52	
Temperature	100(2) K	
Wavelength	0.71073 Å	
Crystal system	Triclinic	
Space group	P1	
Unit cell dimensions	a = 9.5521(3) Å	α= 90.0613(19)°.
	b = 11.5438(4) Å	β= 90.123(2)°.
	c = 21.3297(8) Å	γ = 90.9485(18)°.
Volume	2351.64(14) $Å^3$	
Z	1	
Density (calculated)	1.637 Mg/m^3	
Absorption coefficient	0.786 mm^{-1}	
F(000)	1162	
Crystal size	0.499 x 0.348 x 0.337 mm^3	
Theta range for data collection	1.764 to 37.238°.	
Index ranges	-16≤h≤16, -17≤k≤19, -36≤l≤36	
Reflections collected	59057	
Independent reflections	59057 [R(int) = 0.018]	
Completeness to theta = 25.242°	100.0 %	
Absorption correction	Semi-empirical from equivalents	
Max. and min. transmission	0.791035 and 0.737117	
Refinement method	Full-matrix least-squares on F^2	
Data / restraints / parameters	59057 / 37 / 624	
Goodness-of-fit on F^2	1.058	
Final R indices [I>2sigma(I)]	R1 = 0.0497, wR2 = 0.1241	
R indices (all data)	R1 = 0.0646, wR2 = 0.1341	
Largest diff. peak and hole	2.245 and -1.603 $e.Å^{-3}$	

[RuCl(Ind)(PPh_3){P(3,5–$C_6H_3(CF_3)_2)_3$}] (27)

Empirical formula	$C_{106}\ H_{70}\ Cl_2\ F_{36}\ O_2\ P4\ Ru_2$	
Formula weight	2456.54	
Temperature	100(2) K	
Wavelength	0.71073 Å	
Crystal system	Triclinic	
Space group	P1	
Unit cell dimensions	a = 11.3198(4) Å	α= 101.841(2)°.
	b = 20.1160(10) Å	β= 93.1865(18)°.
	c = 22.2959(10) Å	γ = 94.4486(19)°.
Volume	4940.7(4) $Å^3$	
Z	2	
Density (calculated)	1.651 Mg/m^3	
Absorption coefficient	0.545 mm^{-1}	
F(000)	2456	
Crystal size	0.406 x 0.337 x 0.189 mm^3	
Theta range for data collection	0.936 to 27.799°.	
Index ranges	-14≤h≤14, -26≤k≤25, 0≤l≤29	
Reflections collected	22976	
Independent reflections	22976 [R(int) = 0.0415]	
Completeness to theta = 25.242°	99.9 %	
Absorption correction	Semi-empirical from equivalents	
Max. and min. transmission	0.862066 and 0.748420	
Refinement method	Full-matrix least-squares on F^2	
Data / restraints / parameters	22976 / 343 / 1392	
Goodness-of-fit on F^2	1.011	
Final R indices [I>2sigma(I)]	R1 = 0.0499, wR2 = 0.1144	
R indices (all data)	R1 = 0.0712, wR2 = 0.1289	
Largest diff. peak and hole	1.617 and -0.837 $e.Å^{-3}$	

[Ru(MeCN)(Ind)(PPh_3)$_2$]PF_6 (28)

Empirical formula	C_{47} H_{40} F_6 N P_3 Ru	
Formula weight	926.78	
Temperature	100(2) K	
Wavelength	0.71073 Å	
Crystal system	Monoclinic	
Space group	$P2_1$	
Unit cell dimensions	a = 10.5101(13) Å	α= 90°.
	b = 17.3270(19) Å	β= 96.677(7)°.
	c = 11.2487(13) Å	γ = 90°.
Volume	2034.6(4) $Å^3$	
Z	2	
Density (calculated)	1.513 Mg/m^3	
Absorption coefficient	0.567 mm^{-1}	
F(000)	944	
Crystal size	0.598 x 0.365 x 0.219 mm^3	
Theta range for data collection	1.823 to 40.516°.	
Index ranges	-18≤h≤19, -28≤k≤30, -20≤l≤19	
Reflections collected	92778	
Independent reflections	24235 [R(int) = 0.0282]	
Completeness to theta = 25.242°	100.0 %	
Absorption correction	Semi-empirical from equivalents	
Max. and min. transmission	0.7693 and 0.7103	
Refinement method	Full-matrix least-squares on F^2	
Data / restraints / parameters	24235 / 1 / 523	
Goodness-of-fit on F^2	1.053	
Final R indices [I>2sigma(I)]	R1 = 0.0236, wR2 = 0.0519	
R indices (all data)	R1 = 0.0264, wR2 = 0.0530	
Absolute structure parameter	-0.021(4)	
Largest diff. peak and hole	0.763 and -0.551 $e.Å^{-3}$	

$[Ru(\eta^2–O_2)(Ind)(PPh_3)_2]PF_6$ (30)

Empirical formula	$C_{45}\ H_{37}\ F_6\ O_2\ P_3\ Ru$	
Formula weight	917.72	
Temperature	100(2) K	
Wavelength	0.71073 Å	
Crystal system	Triclinic	
Space group	P1	
Unit cell dimensions	a = 9.8032(5) Å	α= 72.190(3)°.
	b = 14.8889(8) Å	β= 79.428(3)°.
	c = 19.5349(10) Å	γ = 71.868(3)°.
Volume	2567.5(2) $Å^3$	
Z	2	
Density (calculated)	1.187 Mg/m^3	
Absorption coefficient	0.451 mm^{-1}	
F(000)	932	
Crystal size	0.384 x 0.199 x 0.107 mm^3	
Theta range for data collection	1.100 to 26.492°.	
Index ranges	$-9\leq h\leq 12$, $-18\leq k\leq 18$, $-24\leq l\leq 24$	
Reflections collected	39837	
Independent reflections	10242 [R(int) = 0.0698]	
Completeness to theta = 25.242°	96.8 %	
Absorption correction	Semi-empirical from equivalents	
Max. and min. transmission	0.7672 and 0.6547	
Refinement method	Full-matrix least-squares on F^2	
Data / restraints / parameters	10242 / 73 / 545	
Goodness-of-fit on F^2	1.044	
Final R indices [I>2sigma(I)]	R1 = 0.0788, wR2 = 0.1679	
R indices (all data)	R1 = 0.1073, wR2 = 0.1803	
Largest diff. peak and hole	1.356 and -1.905 $e.Å^{-3}$	

[RuCl(dap)(PPh_3)$_2$]BAr^F_4 (35)

Empirical formula	C_{77} H_{51} B Cl F_{24} N O_2 P_2 Ru
Formula weight	1687.45
Temperature	100(2) K
Wavelength	0.71073 Å
Crystal system	Orthorhombic
Space group	Pbca
Unit cell dimensions	a = 28.958(4) Å α= 90°.
	b = 13.8777(17) Å β= 90°.
	c = 36.757(4) Å γ = 90°.
Volume	14772(3) $Å^3$
Z	8
Density (calculated)	1.518 Mg/m^3
Absorption coefficient	0.400 mm^{-1}
F(000)	6784
Crystal size	0.414 x 0.349 x 0.058 mm^3
Theta range for data collection	1.719 to 26.648°.
Index ranges	-27≤h≤36, -17≤k≤17, -46≤l≤46
Reflections collected	146876
Independent reflections	15248 [R(int) = 0.0866]
Completeness to theta = 25.242°	100.0 %
Absorption correction	Semi-empirical from equivalents
Max. and min. transmission	0.8620 and 0.7400
Refinement method	Full-matrix least-squares on F^2
Data / restraints / parameters	15248 / 954 / 994
Goodness-of-fit on F^2	1.030
Final R indices [I>2sigma(I)]	R1 = 0.0692, wR2 = 0.1636
R indices (all data)	R1 = 0.1050, wR2 = 0.1942
Largest diff. peak and hole	2.105 and -0.930 $e.Å^{-3}$

Appendix B: NMR Spectra

Chapter 2 Spectra

[RuCl(ind)(PPh_3){P(pyr)$_3$}] **(13)**

^{1}H

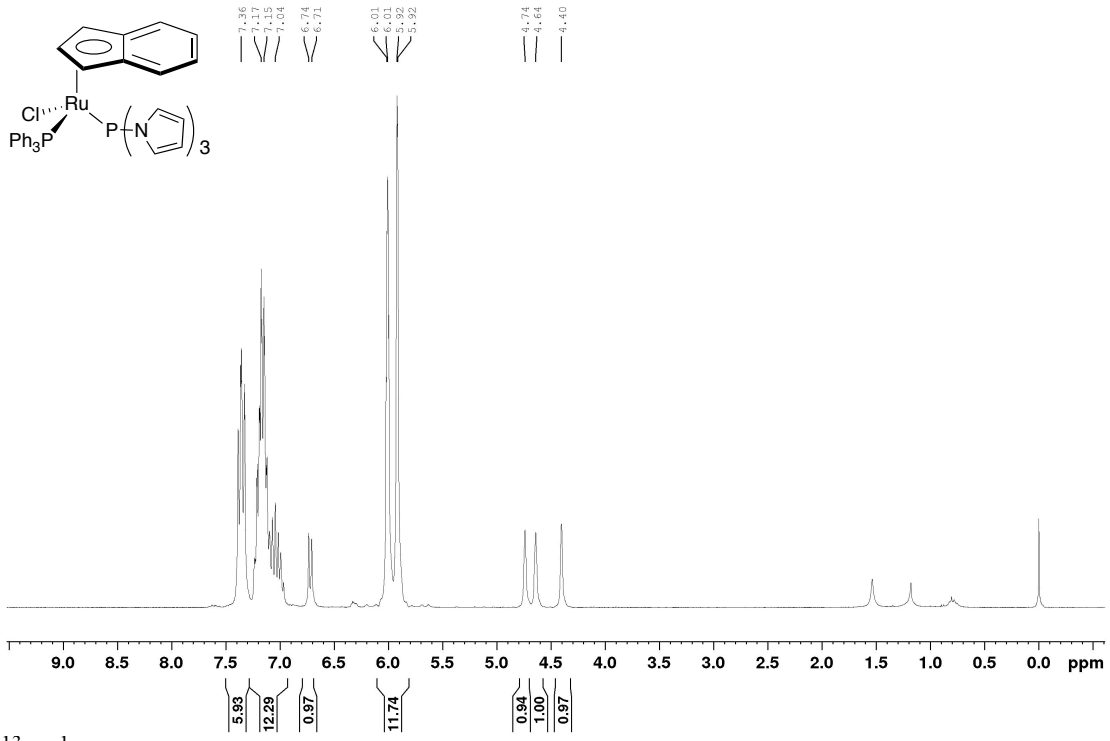

^{13}C{^{1}H}

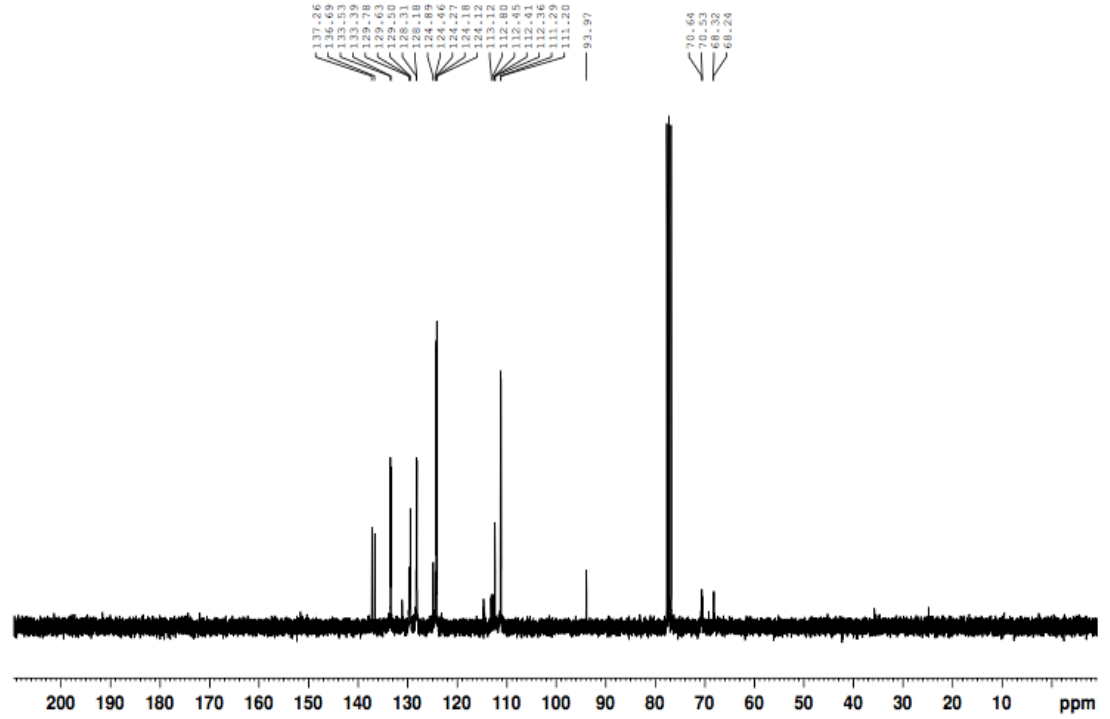

$^{31}P\{^{1}H\}$

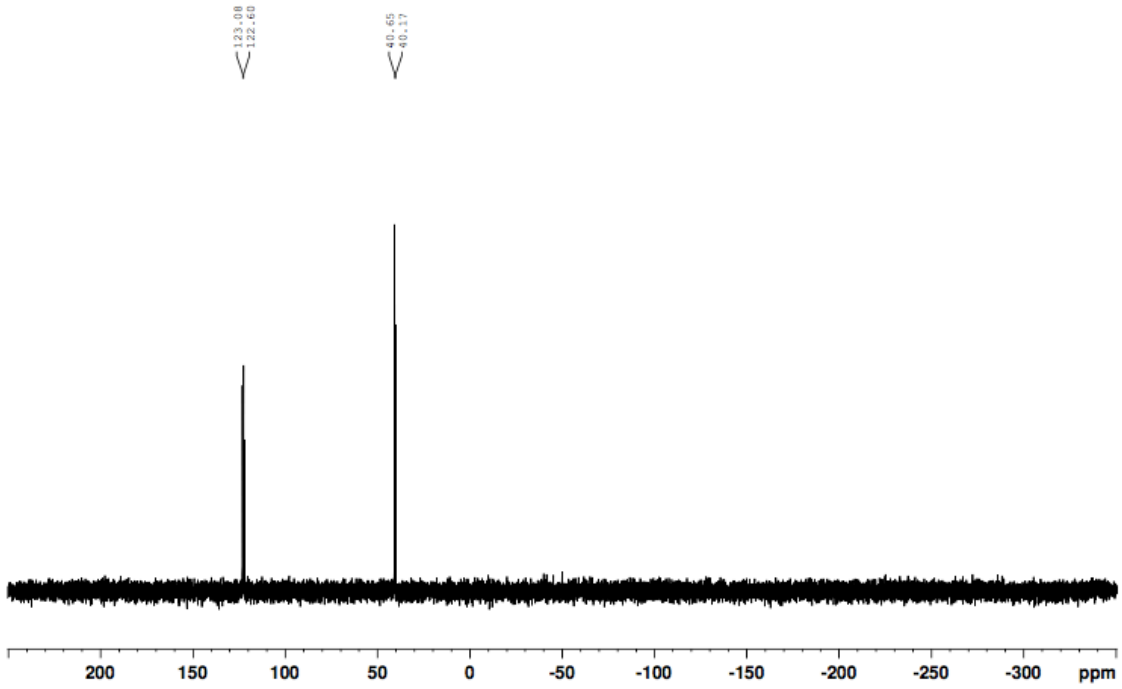
123.08
122.60
40.65
40.17
200
150
100
50
0
-50
-100
-150
-200
-250
-300
ppm

[RuCl(ind){P(pyr)$_3$}$_2$] (**14**)

^{1}H

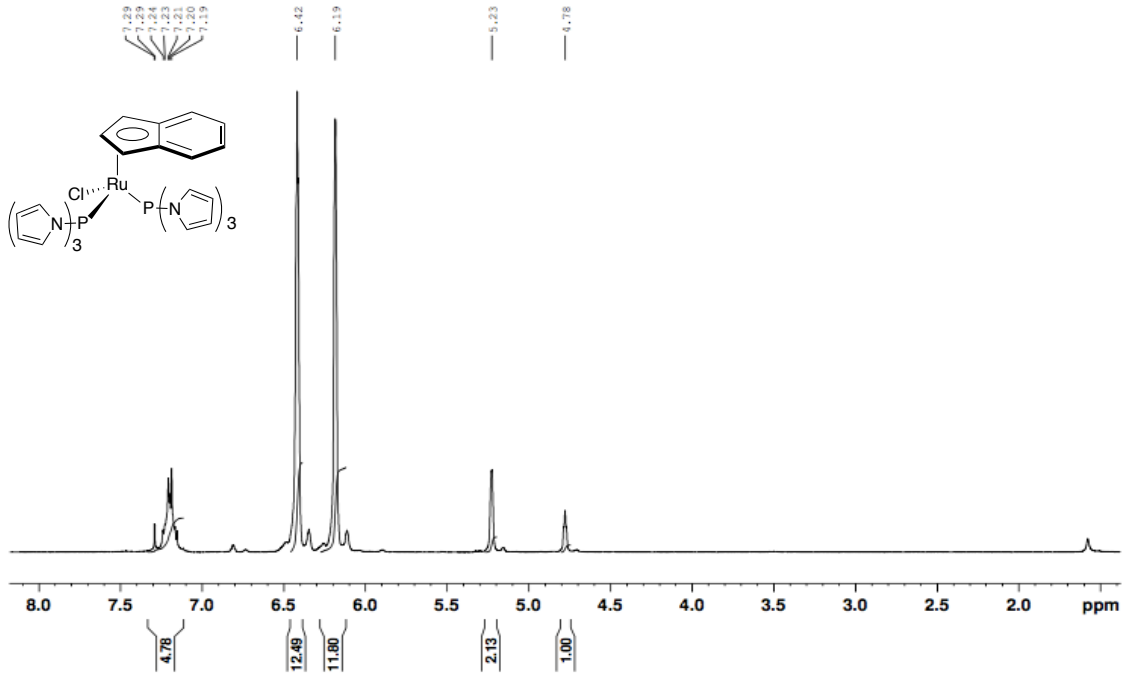

^{13}C{^{1}H}

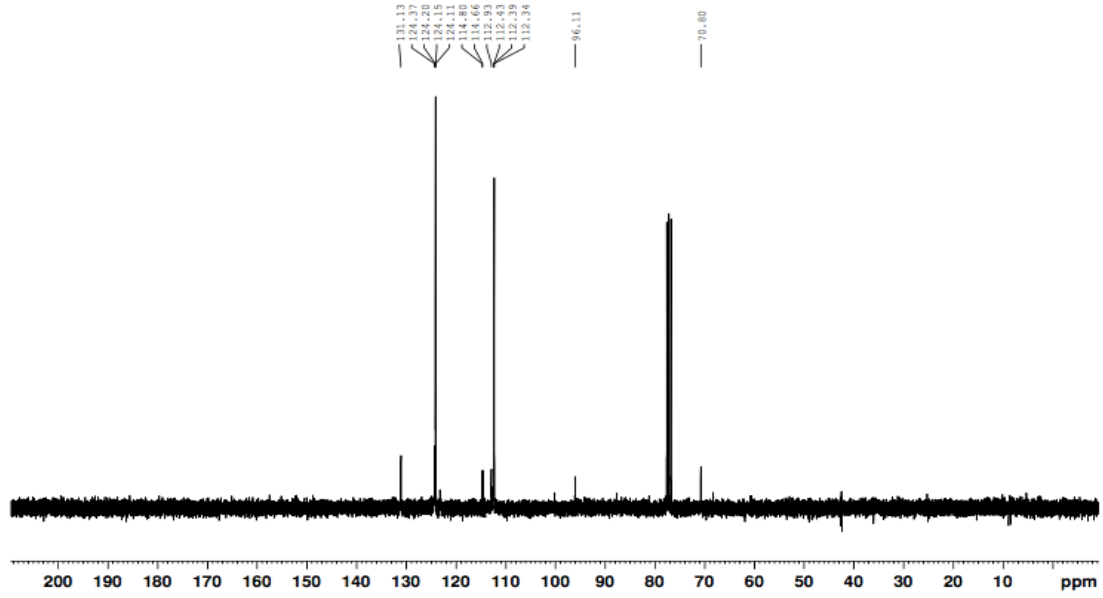

$^{31}P\{^{1}H\}$

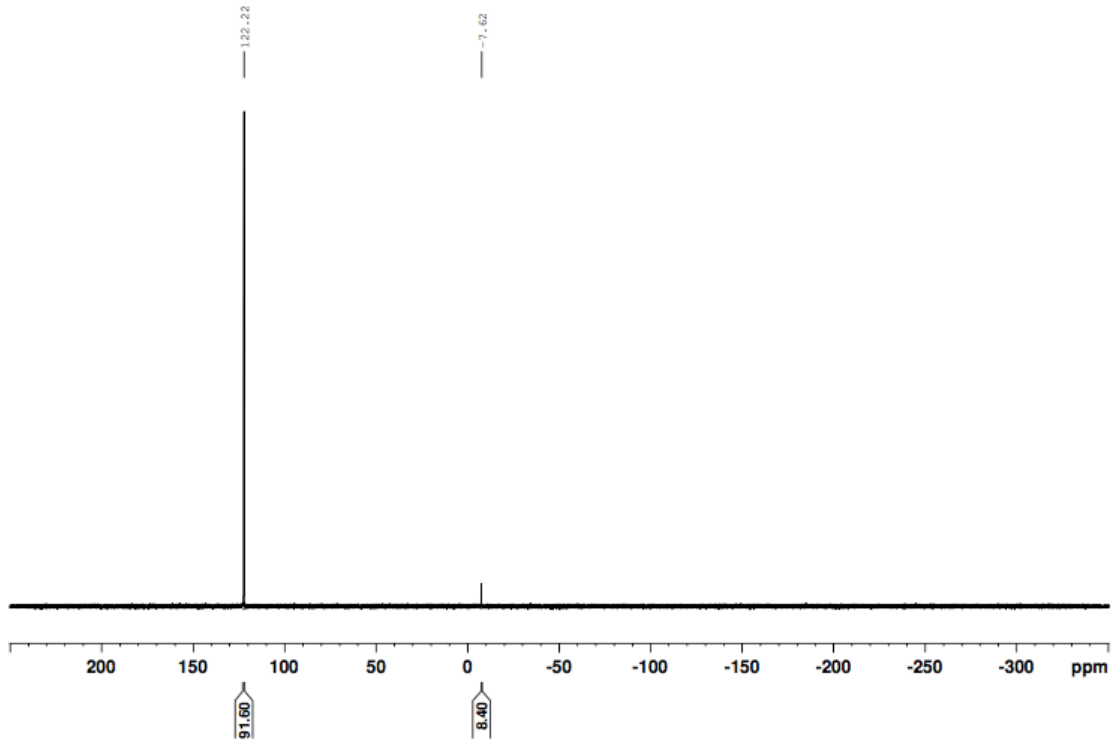

^{1}H

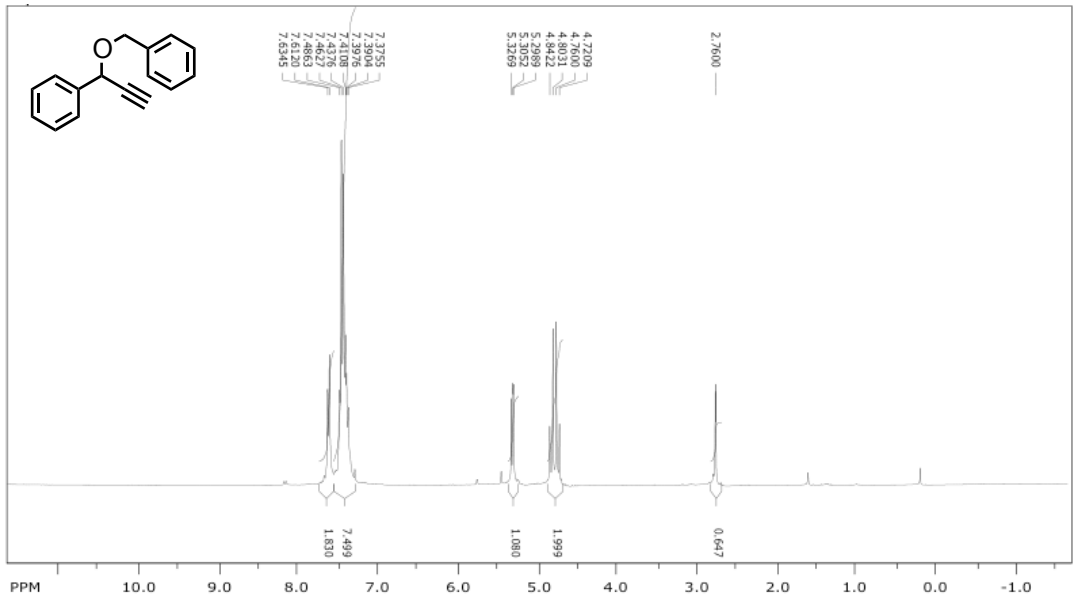
7.6345
7.6120
7.4863
7.4625
7.4108
7.3976
7.3904
7.3755
5.3269
5.3052
5.2989
4.8422
4.8031
4.7600
4.7209
2.7600
1.830
7.499
1.080
1.999
0.647
PPM
10.0
9.0
8.0
7.0
6.0
5.0
4.0
3.0
2.0
1.0
0.0
-1.0

$^{13}C\{^{1}H\}$

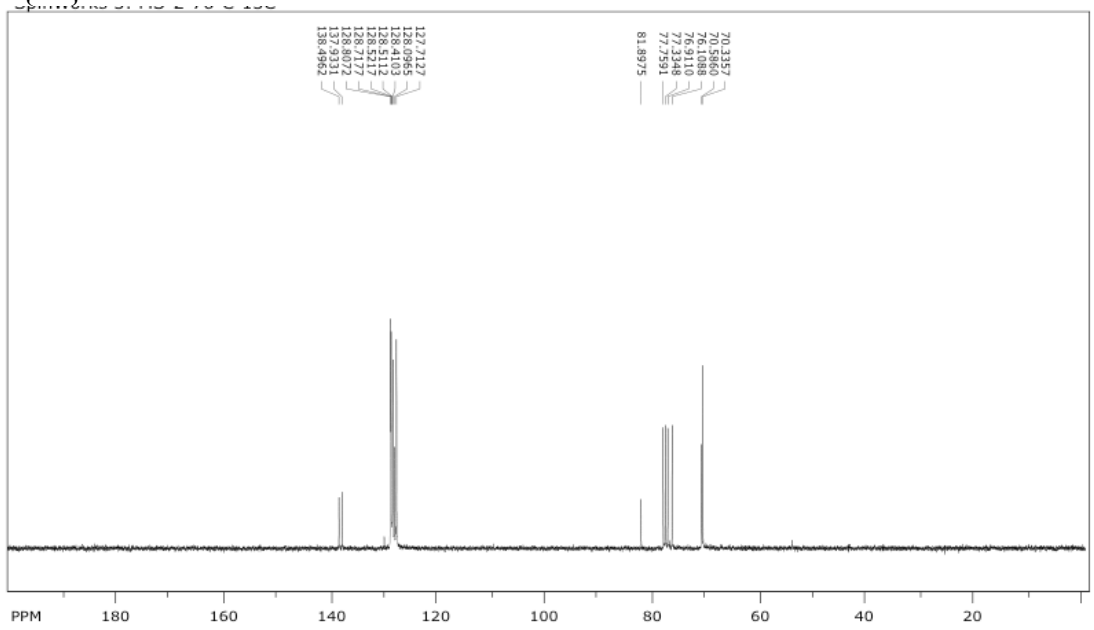
138.4962
137.9331
128.6077
128.5217
128.5112
128.4103
128.0965
127.7127
81.8975
77.7591
77.3348
76.9110
76.1088
70.5860
70.3357
PPM
180
160
140
120
100
80
60
40
20

^{1}H

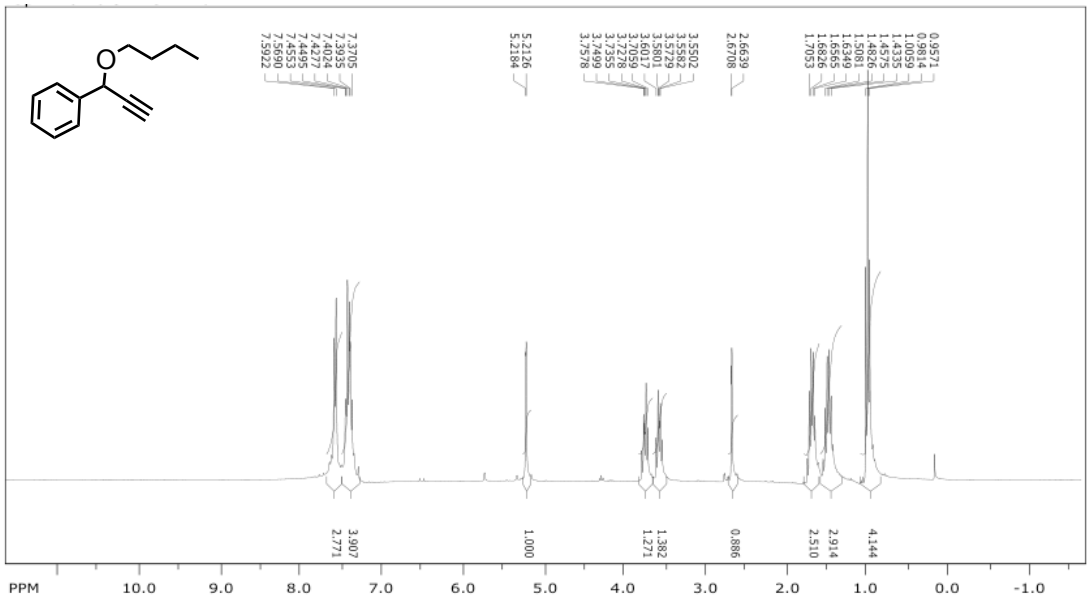
7.3705
7.3935
7.4024
7.4277
7.4553
7.5690
7.5922
5.2126
5.2184
3.5502
3.5582
3.5729
3.5801
3.6017
3.7059
3.7278
3.7499
3.7578
2.6639
2.6708
0.9571
0.9814
1.0059
1.4335
1.4575
1.4826
1.5081
1.6349
1.6826
1.7053
2.771
3.907
1.000
1.271
1.382
0.886
2.510
2.914
4.144
PPM
10.0
9.0
8.0
7.0
6.0
5.0
4.0
3.0
2.0
1.0
0.0
-1.0

$^{13}C\{^{1}H\}$

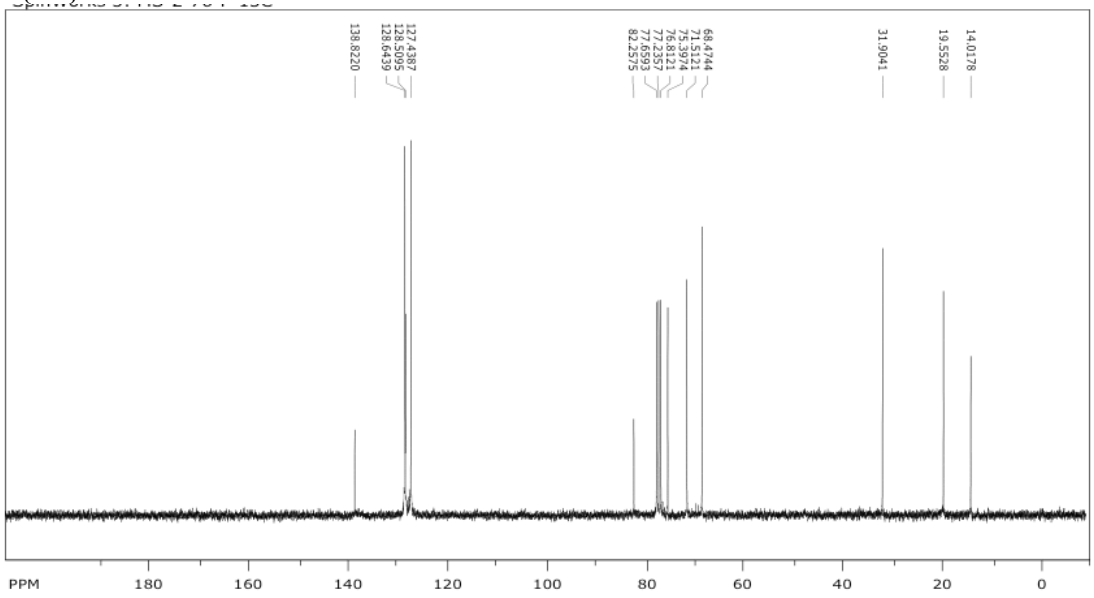
138.8220
128.6439
128.5095
127.4387
82.2575
77.6593
77.2357
76.8121
75.3974
71.5121
68.4744
31.9041
19.5528
14.0178
PPM
180
160
140
120
100
80
60
40
20
0

^{1}H

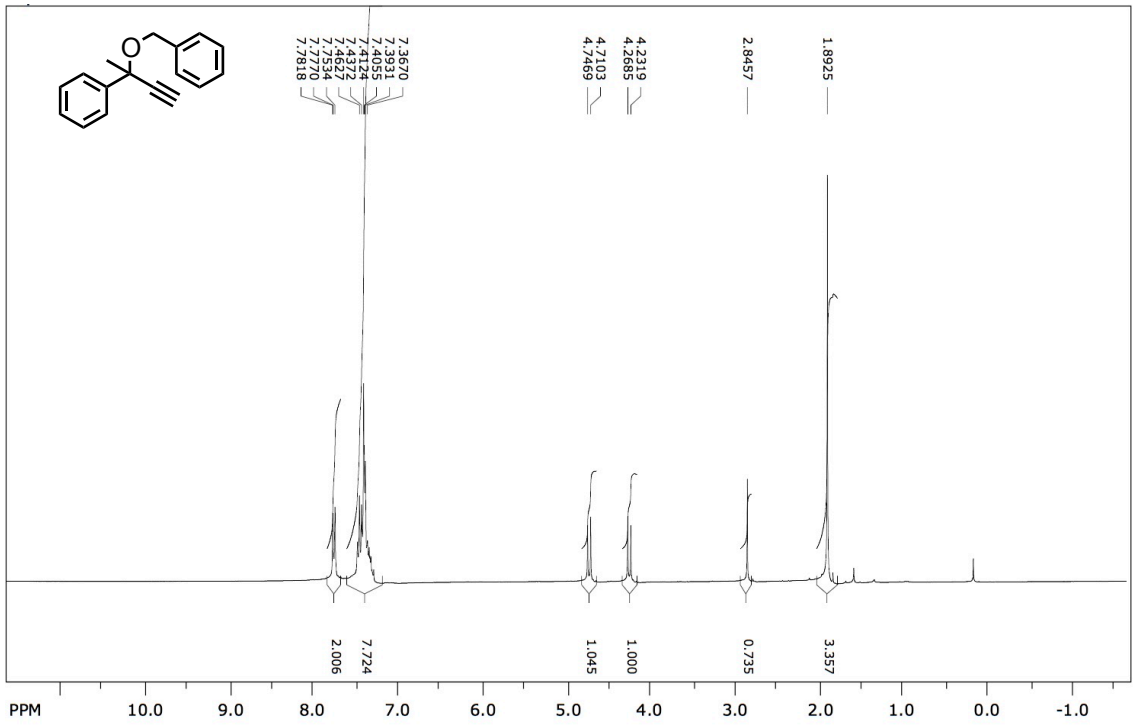
7.7818
7.7770
7.7534
7.4627
7.4372
7.4124
7.4055
7.3931
7.3670
4.7469
4.7103
4.2685
4.2319
2.8457
1.8925
2.006
7.724
1.045
1.000
0.735
3.357
PPM
10.0
9.0
8.0
7.0
6.0
5.0
4.0
3.0
2.0
1.0
0.0
-1.0

$^{13}C\{^{1}H\}$

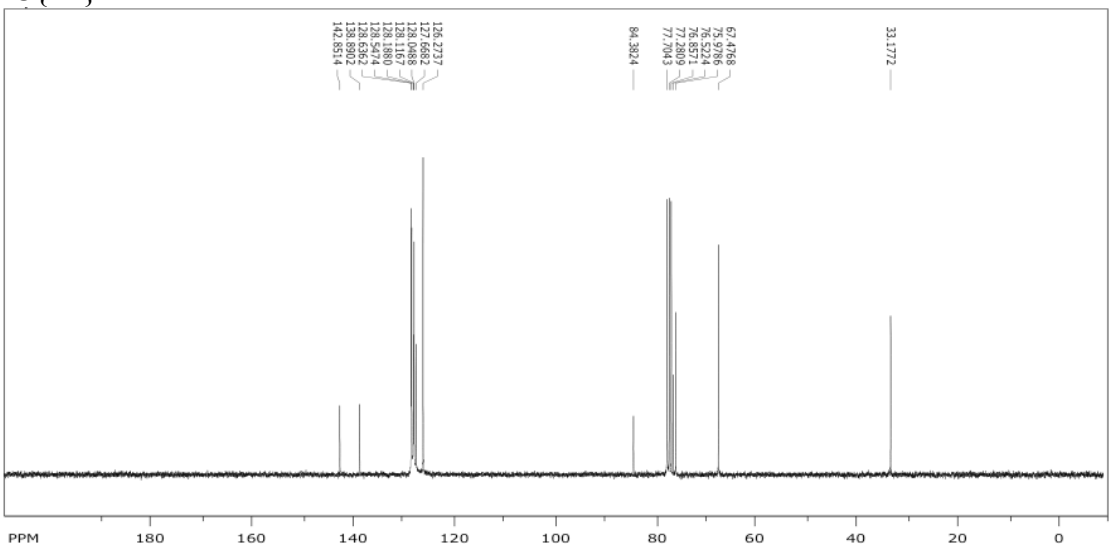
142.8514
138.8902
128.6362
128.5490
128.1680
128.1167
128.0488
127.6682
126.2737
84.3824
77.7043
77.2809
76.8571
76.5224
75.9786
67.4768
33.1772
PPM
180
160
140
120
100
80
60
40
20
0

^{1}H

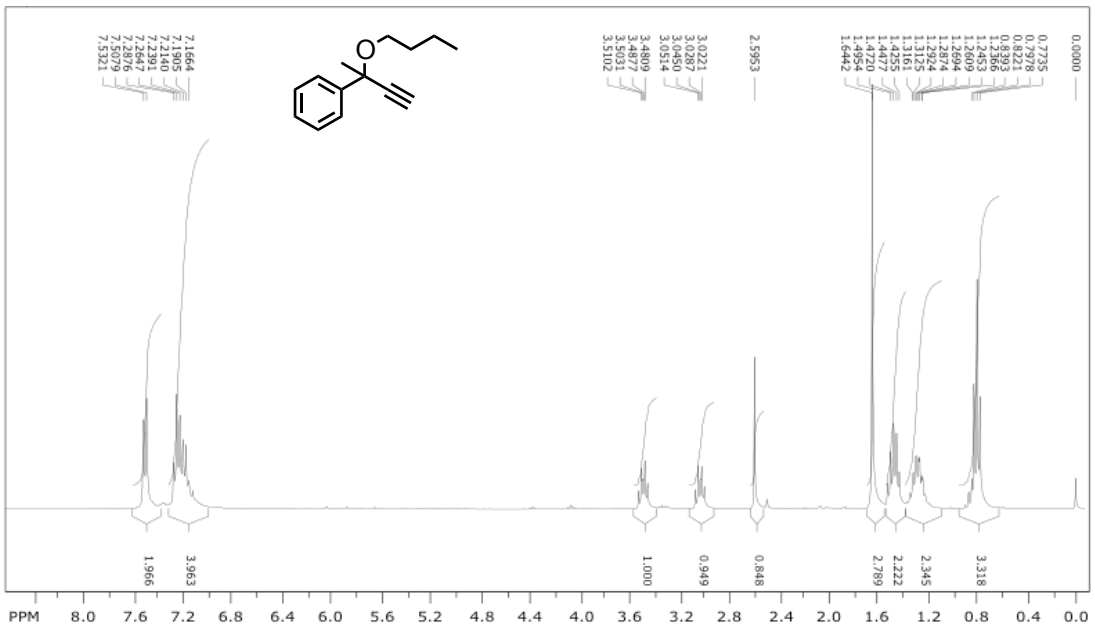
7.1664
7.1485
7.2140
7.2391
7.2647
7.2876
7.5079
7.5321
3.5102
3.5031
3.4877
3.4809
3.0514
3.0450
3.0287
3.0221
2.5953
1.6442
1.4954
1.4720
1.4477
1.4255
1.3161
1.2925
1.2874
1.2694
1.2609
1.2453
1.2366
0.8393
0.8328
0.7735
0.7578
0.0000
1.966
3.963
1.000
0.949
0.848
2.789
2.222
2.345
3.318
PPM 8.0 7.6 7.2 6.8 6.4 6.0 5.6 5.2 4.8 4.4 4.0 3.6 3.2 2.8 2.4 2.0 1.6 1.2 0.8 0.4 0.0

$^{13}C\{^{1}H\}$

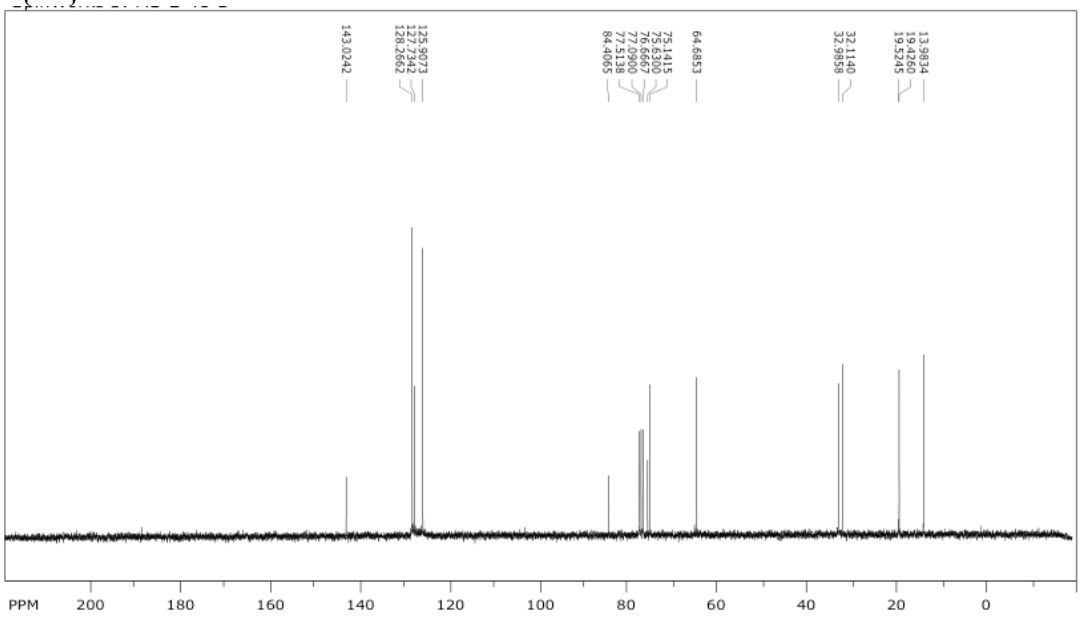
143.0242
128.2662
127.7242
125.9073
84.4065
77.5138
77.0900
76.6667
75.6300
75.1415
64.6853
32.9858
32.1140
19.5245
19.4260
13.9834
PPM 200 180 160 140 120 100 80 60 40 20 0

^{1}H

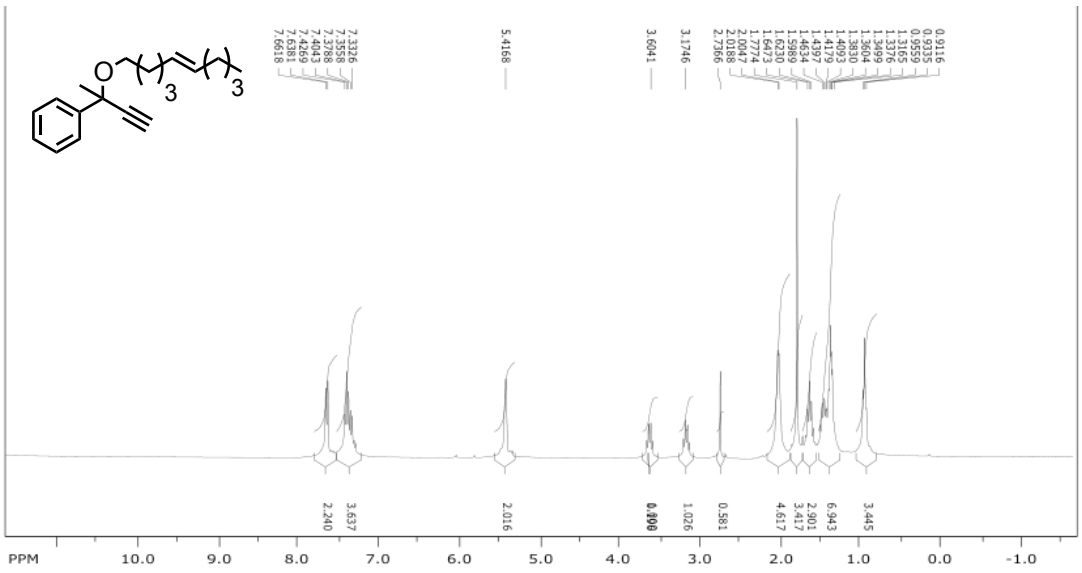
7.7618
7.6381
7.4243
7.3788
7.3558
7.3326
5.4168
3.6041
3.1746
2.7366
2.0188
2.0047
1.7774
1.6473
1.6290
1.5989
1.4634
1.4397
1.4179
1.4093
1.3830
1.3604
1.3489
1.3165
1.3037
0.9559
0.9335
0.9116
2.240
3.637
2.016
1.026
0.581
4.617
3.417
2.901
6.943
3.445
PPM
10.0
9.0
8.0
7.0
6.0
5.0
4.0
3.0
2.0
1.0
0.0
-1.0

$^{13}C\{^{1}H\}$

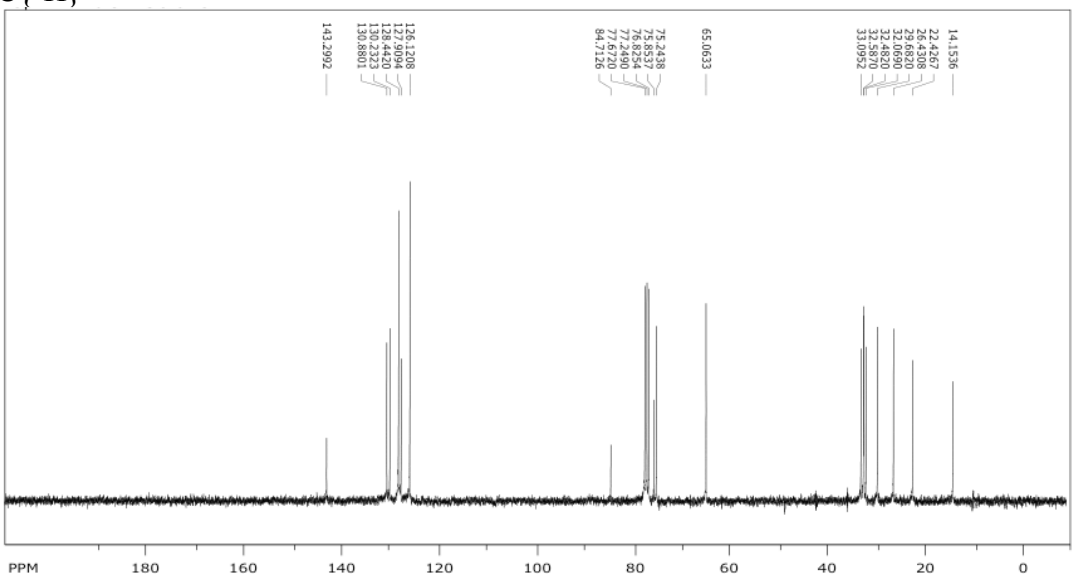
143.2992
130.8801
130.2323
128.4020
127.9094
126.1208
84.7126
77.6720
76.8254
75.8537
75.2438
65.0633
33.0952
32.5870
32.4820
32.0690
29.6820
26.4308
22.4267
14.1536
PPM
180
160
140
120
100
80
60
40
20
0

^{1}H

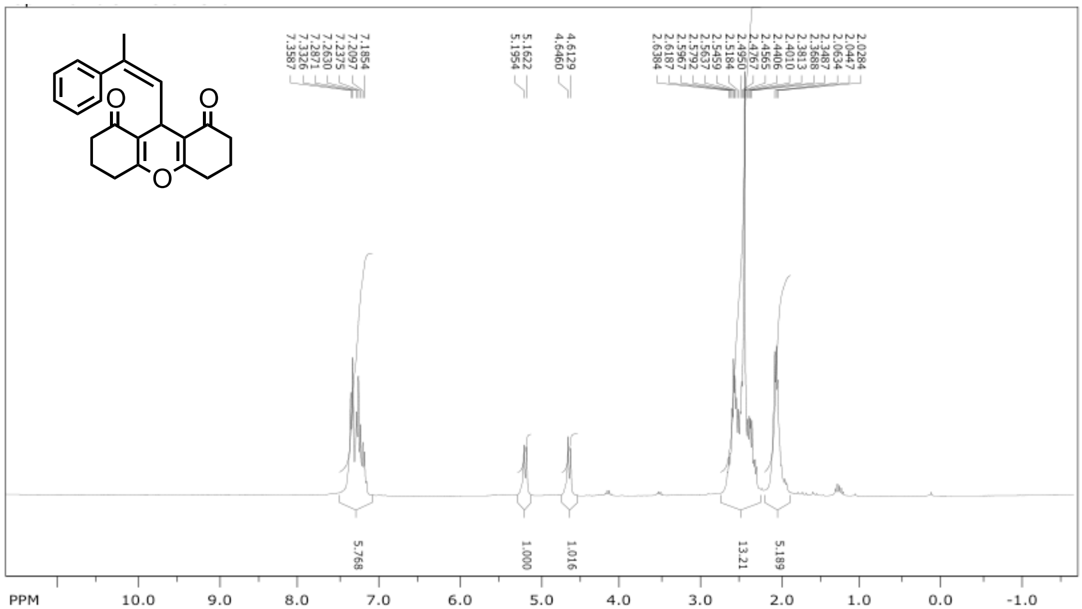

$^{13}C\{^{1}H\}$

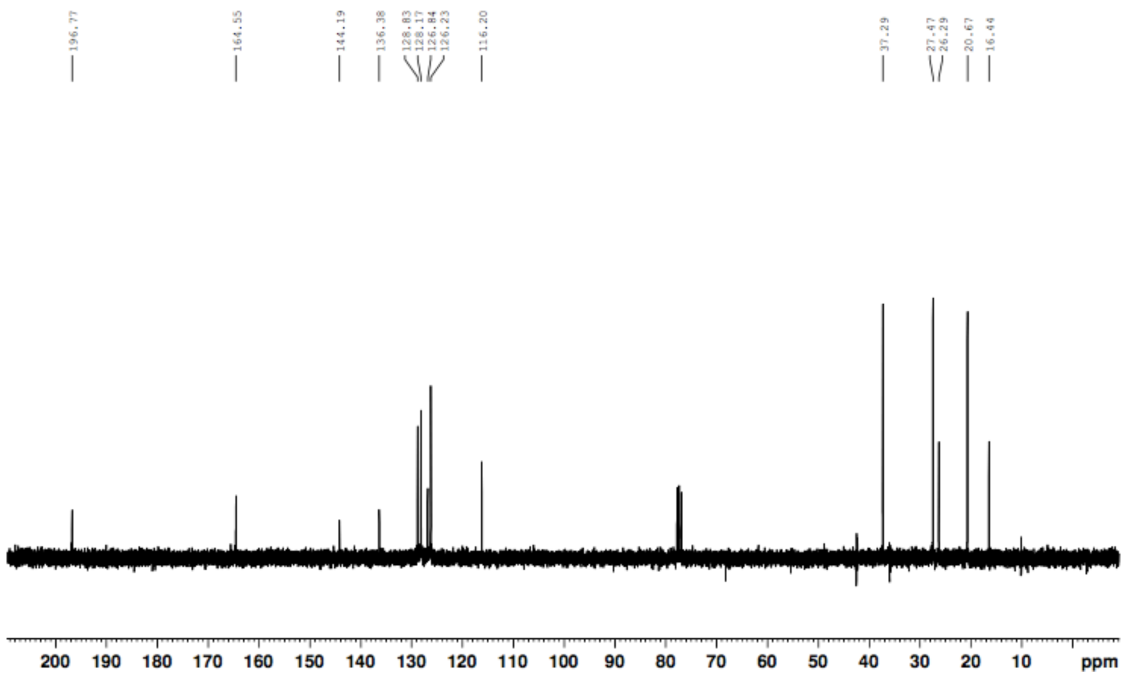
196.77
164.55
144.19
136.38
128.83
128.17
126.84
126.23
116.20
37.29
27.47
26.29
20.67
16.44
200 190 180 170 160 150 140 130 120 110 100 90 80 70 60 50 40 30 20 10 ppm

^{1}H

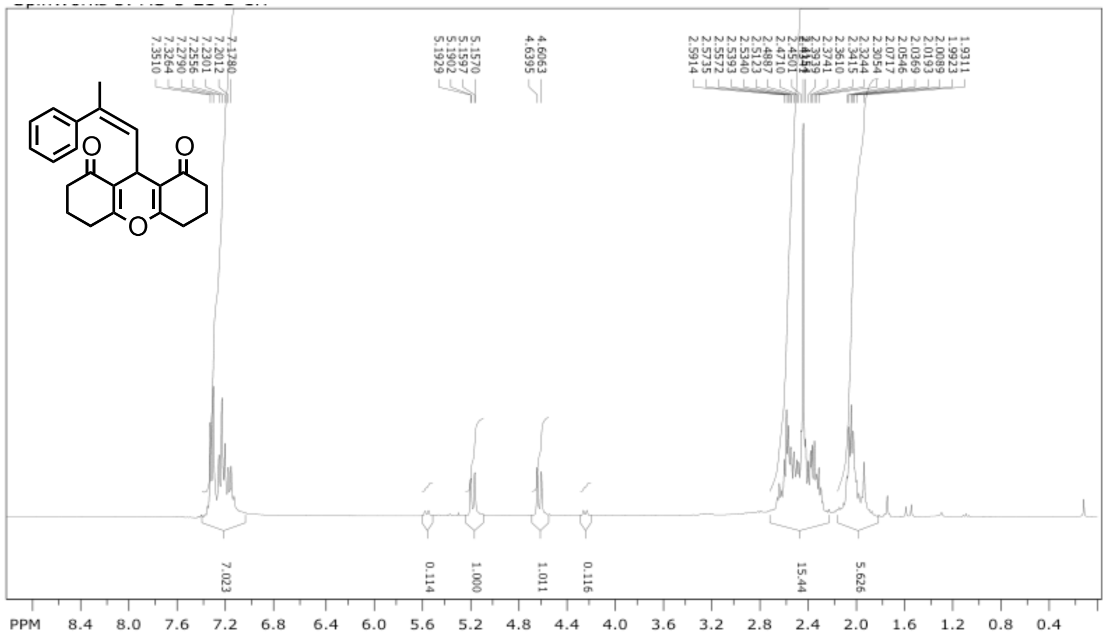

$^{13}C\{^{1}H\}$

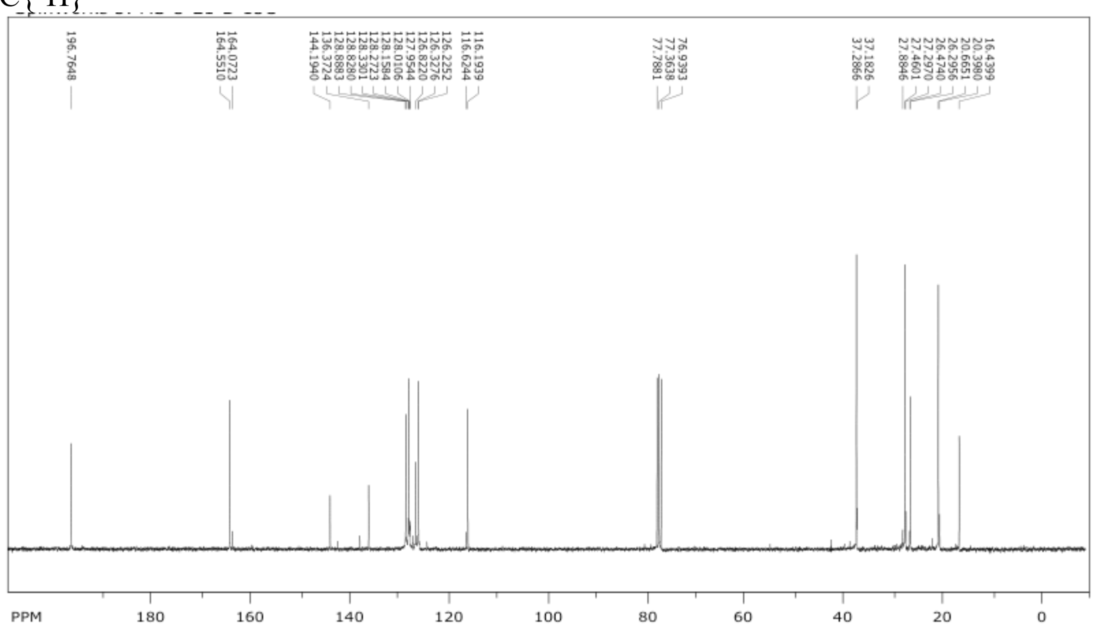

^{1}H

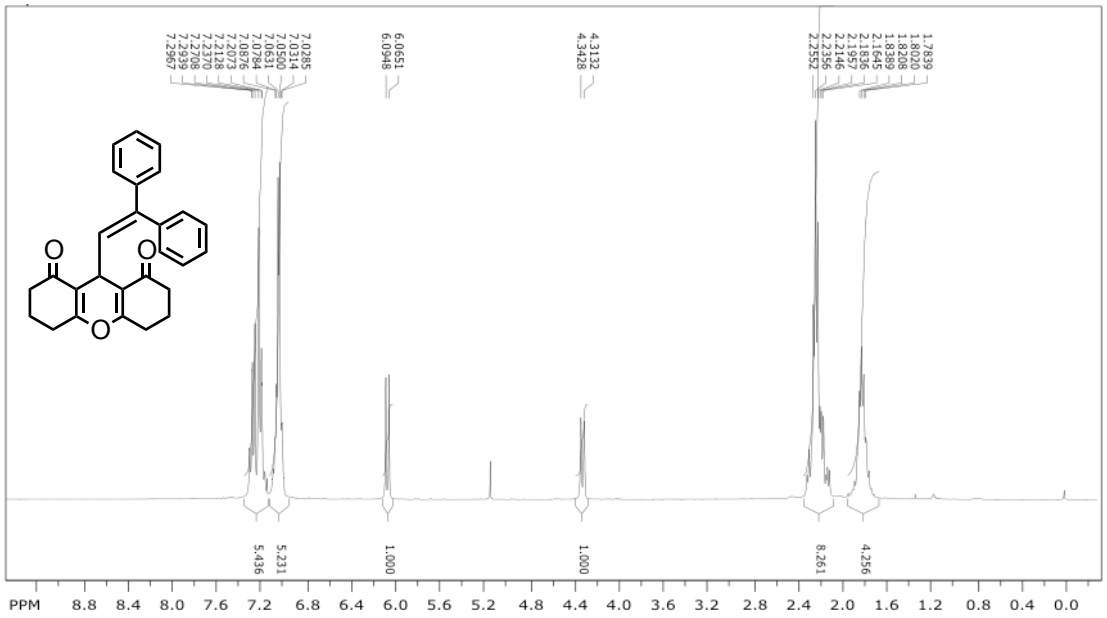
7.0285
7.0314
7.0500
7.0631
7.0784
7.0876
7.2028
7.2170
7.2708
7.2939
7.2967
6.0651
6.0948
4.3132
4.3428
2.2552
2.2356
2.2146
2.1957
2.1836
2.1649
1.8208
1.8020
1.7839
5.436
5.231
1.000
1.000
8.261
4.256
PPM
8.8 8.4 8.0 7.6 7.2 6.8 6.4 6.0 5.6 5.2 4.8 4.4 4.0 3.6 3.2 2.8 2.4 2.0 1.6 1.2 0.8 0.4 0.0

$^{13}C\{^{1}H\}$

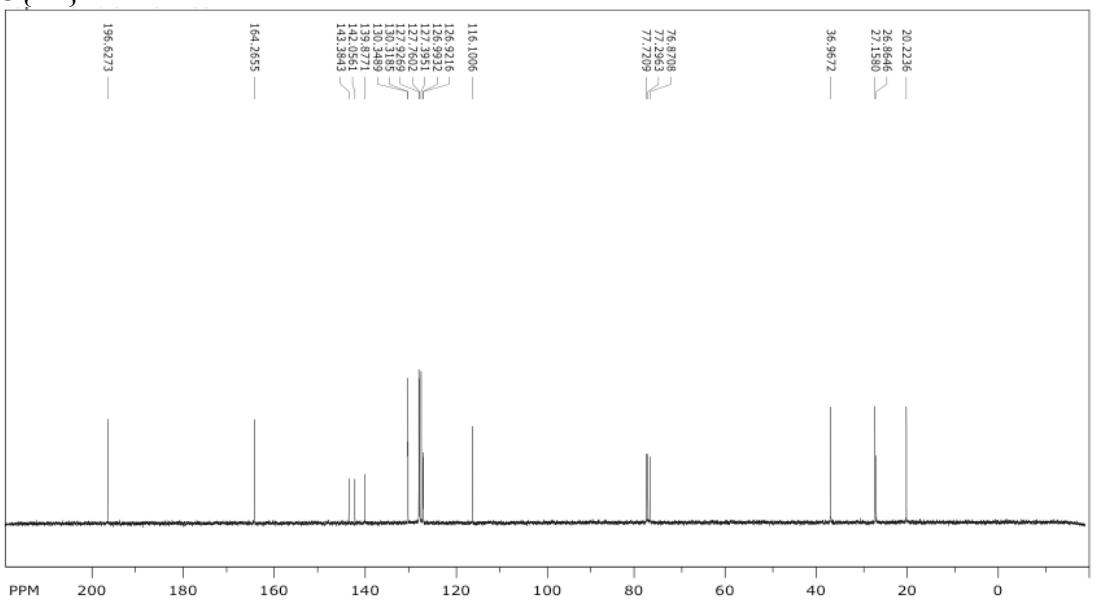
196.6273
164.2655
143.3843
142.0561
139.8771
130.3489
130.3185
127.7602
127.3951
126.9932
126.9216
116.1006
77.7209
76.8708
36.9672
27.1580
26.8646
20.2236
PPM
200 180 160 140 120 100 80 60 40 20 0

^{1}H

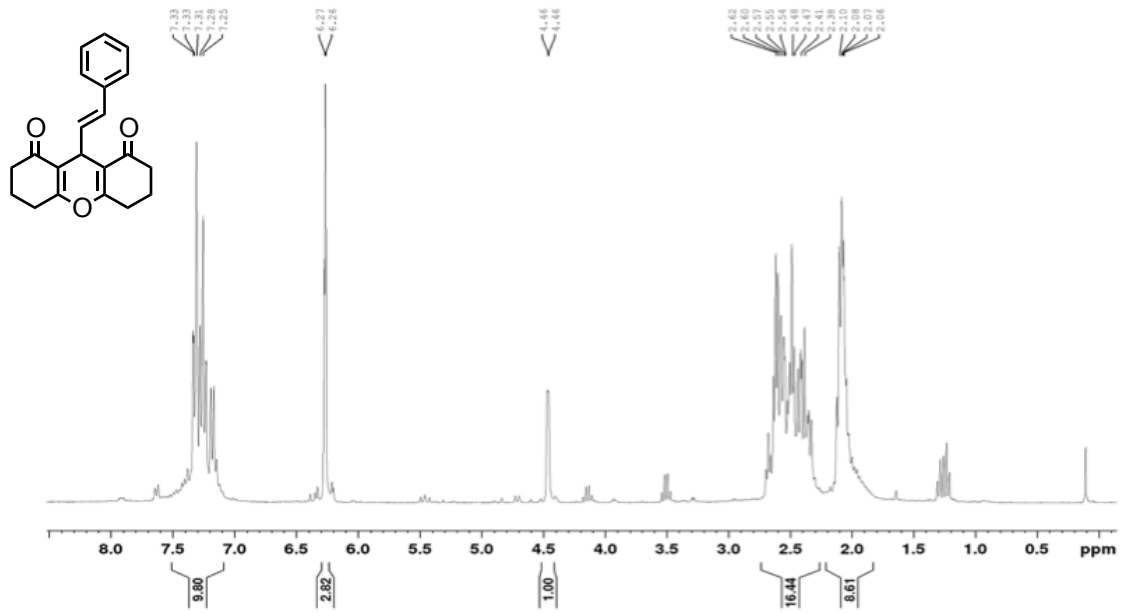
7.33
7.33
7.31
7.28
7.25
6.27
6.26
4.46
4.46
2.62
2.60
2.57
2.55
2.54
2.49
2.47
2.41
2.38
2.10
2.08
2.07
2.04
8.0
7.5
7.0
6.5
6.0
5.5
5.0
4.5
4.0
3.5
3.0
2.5
2.0
1.5
1.0
0.5
ppm
9.80
2.82
1.00
16.44
8.61

$^{13}C\{^{1}H\}$

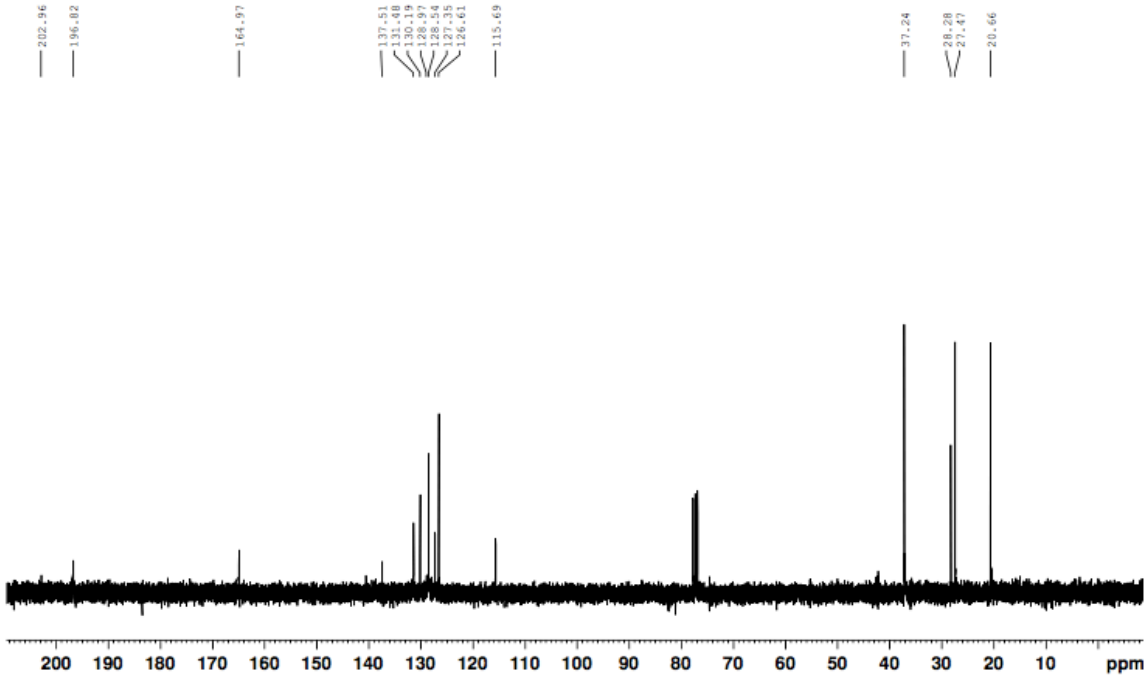
202.96
196.82
164.97
137.51
131.48
130.19
128.97
128.54
127.35
126.61
115.69
37.24
28.28
27.47
20.66
200
190
180
170
160
150
140
130
120
110
100
90
80
70
60
50
40
30
20
10
ppm

^{1}H

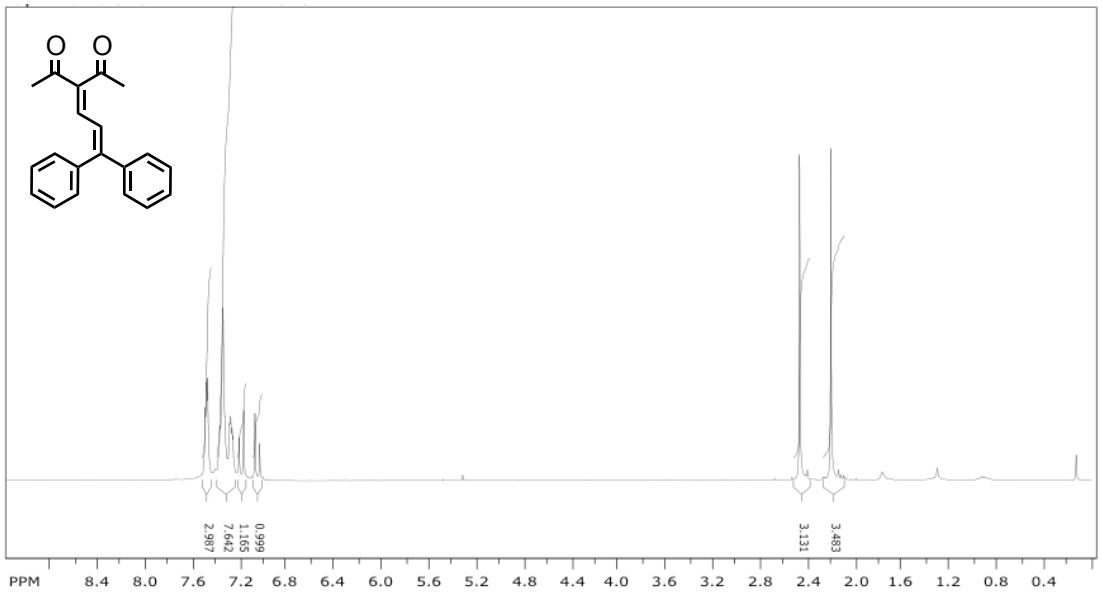
2.987
7.642
1.165
0.999
3.131
3.483
PPM
8.4 8.0 7.6 7.2 6.8 6.4 6.0 5.6 5.2 4.8 4.4 4.0 3.6 3.2 2.8 2.4 2.0 1.6 1.2 0.8 0.4

$^{13}C\{^{1}H\}$

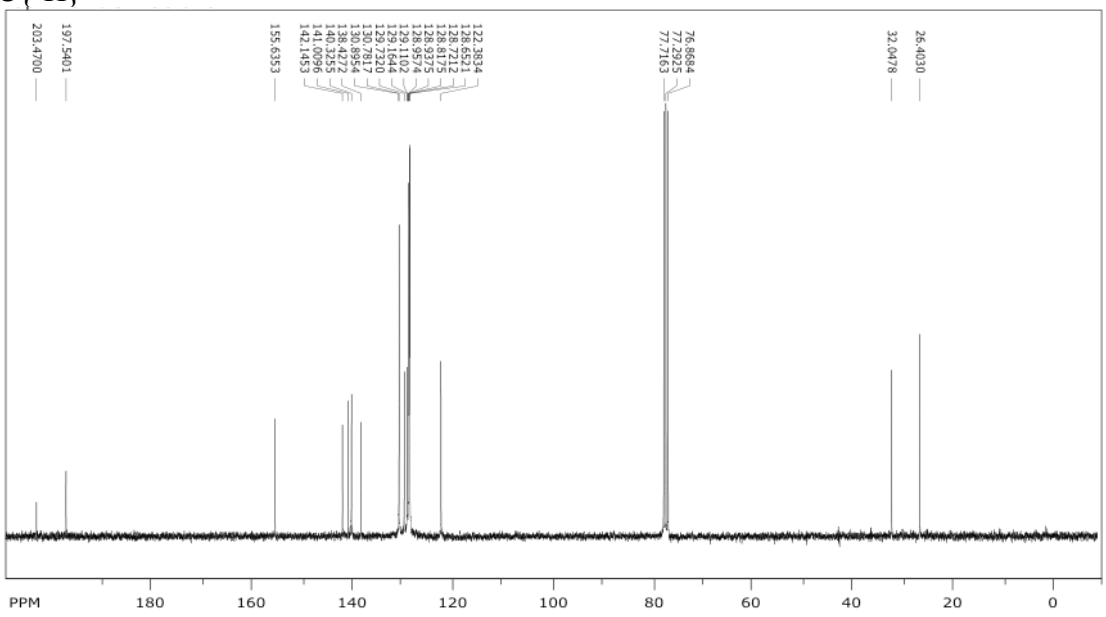
203.4700
197.5401
155.6353
142.1453
141.0096
138.4272
130.8954
130.7817
129.7320
129.1644
129.1102
128.9574
128.8377
128.7212
128.6521
122.3834
77.7163
77.2925
76.8684
32.0478
26.4030
PPM
180 160 140 120 100 80 60 40 20 0

^{1}H

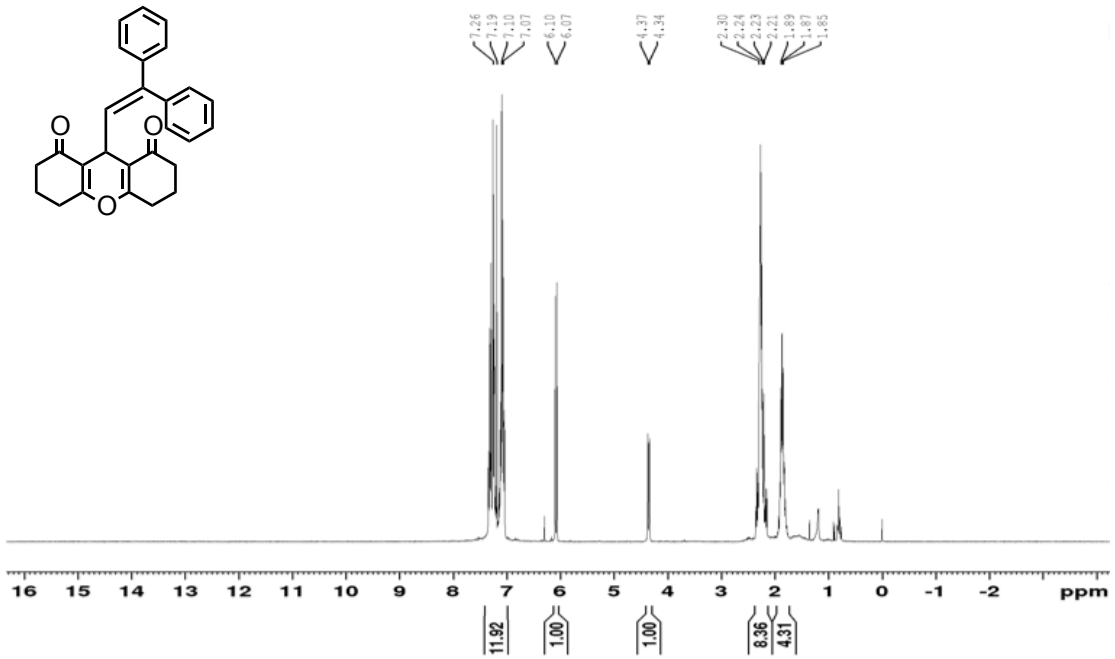
7.26
7.19
7.10
7.07
6.10
6.07
4.37
4.34
2.30
2.24
2.23
2.21
1.89
1.87
1.85
16 15 14 13 12 11 10 9 8 7 6 5 4 3 2 1 0 -1 -2 ppm
11.92
1.00
1.00
8.36
4.31

$^{13}C\{^{1}H\}$

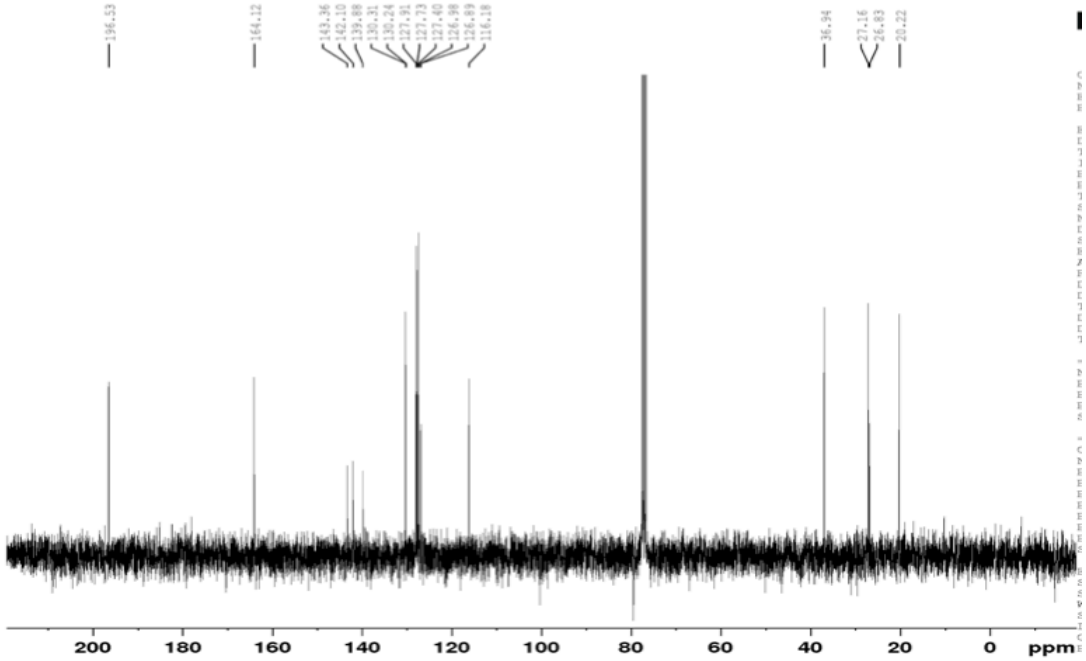
196.53
164.12
143.36
142.10
139.88
130.31
130.24
127.91
127.73
127.40
126.98
126.89
116.18
36.94
27.16
26.83
20.22
200 180 160 140 120 100 80 60 40 20 0 ppm

Chapter 3 Spectra

[RuCl(Ind)(PPh_3){P(*p*-$C_6H_4CF_3$)$_3$}] (**26**)

^1H

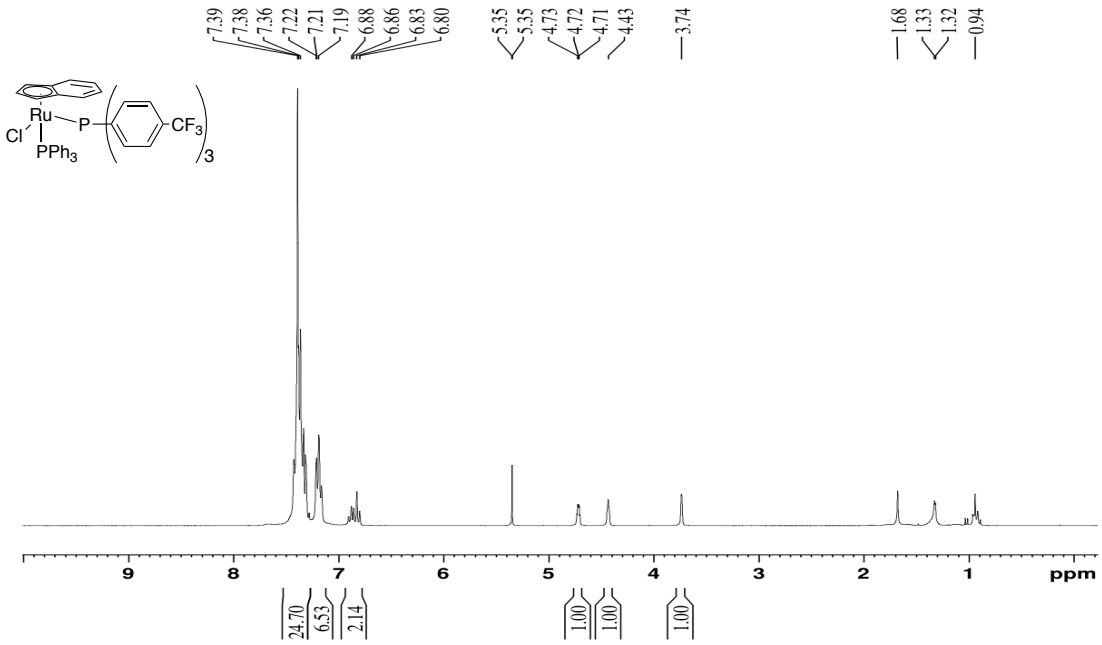

$^{13}C\{^1H\}$

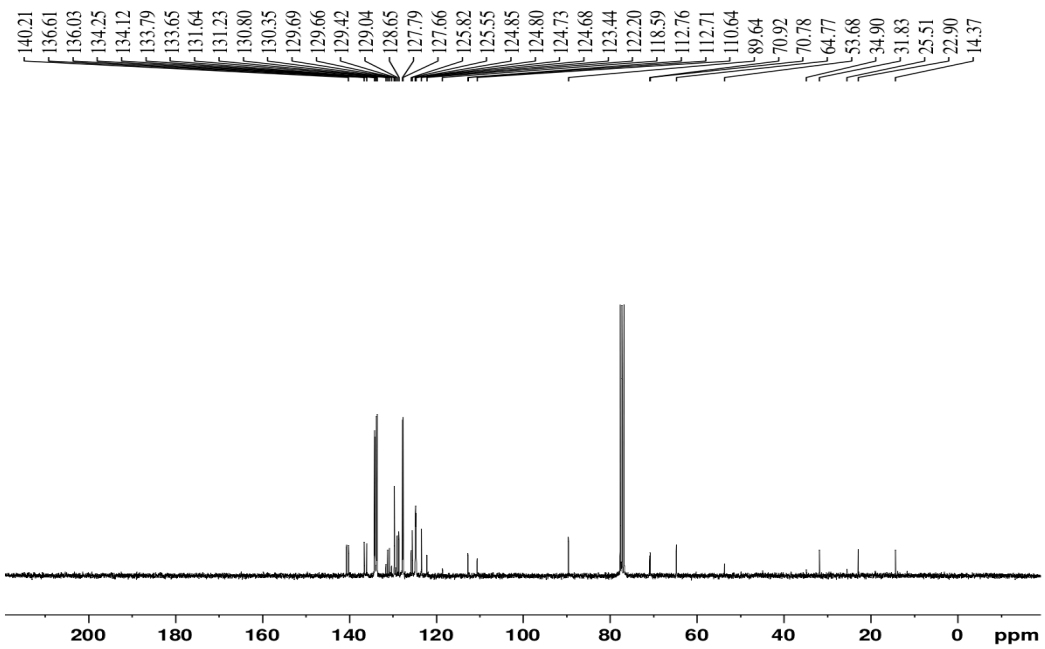

$^{31}P\{^{1}H\}$

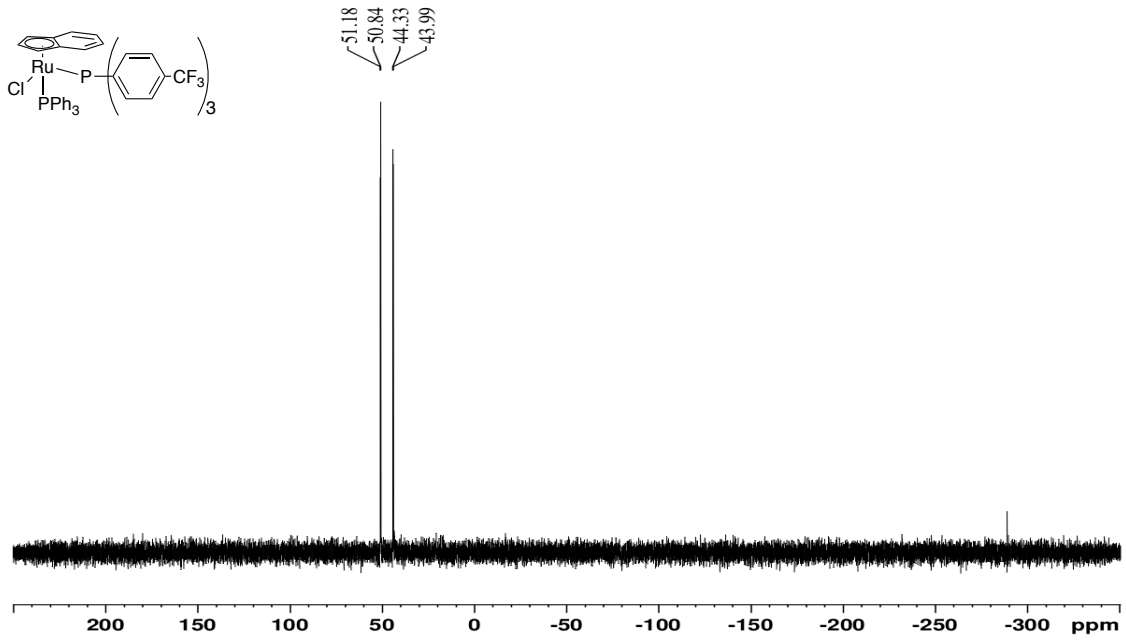
51.18
50.84
44.33
43.99
Ru
Cl
PPh3
P
CF3
3
200
150
100
50
0
-50
-100
-150
-200
-250
-300
ppm

[RuCl(Ind)(PPh_3){P(3,5-$C_6H_3(CF_3)_2)_3$}] (**27**)

^1H

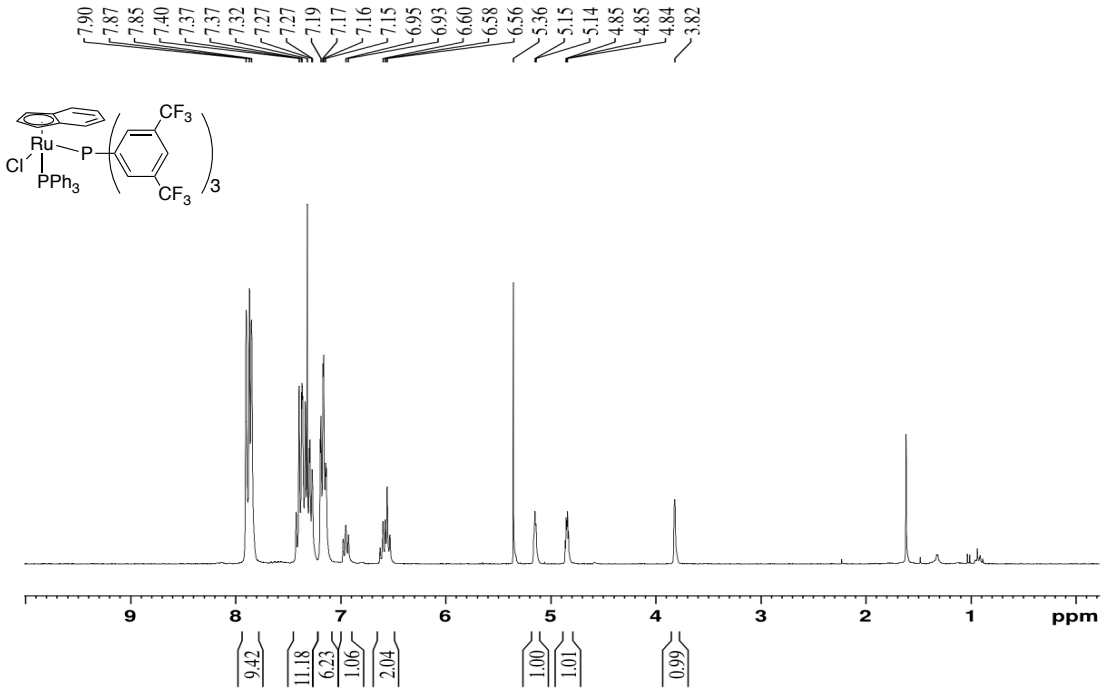

$^{13}C\{^1H\}$

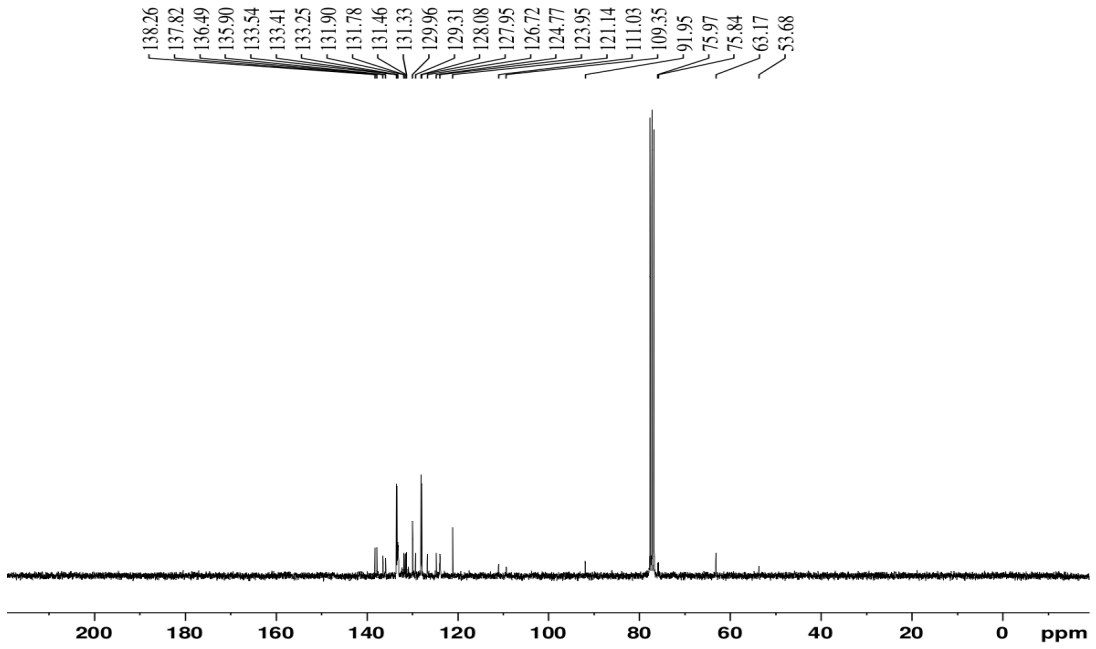

$^{31}P\{^{1}H\}$

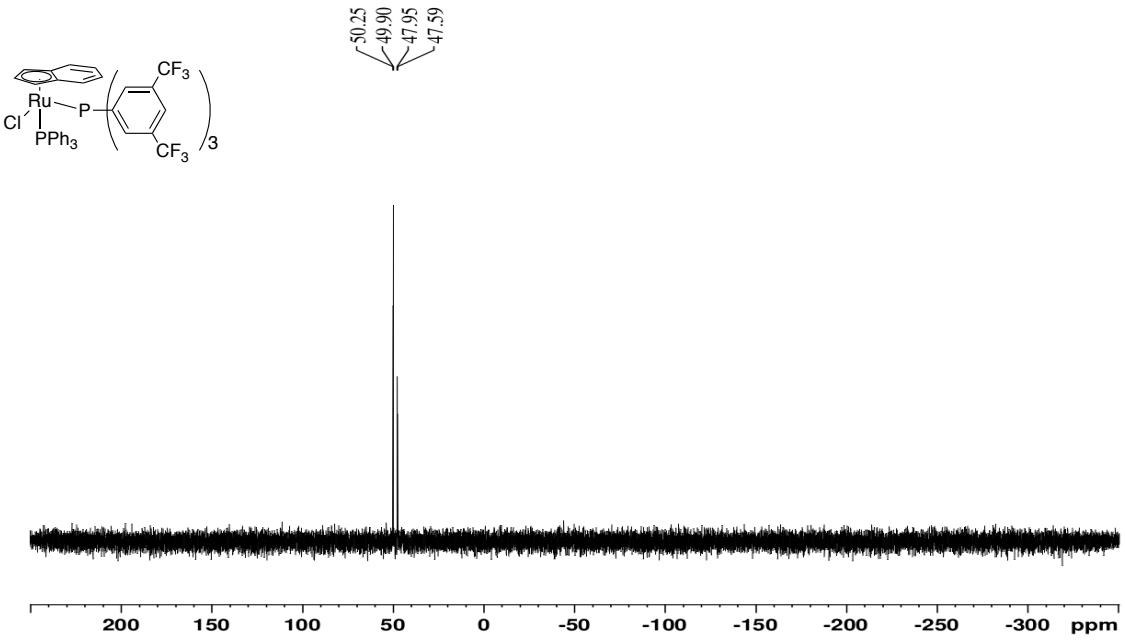
50.25
49.90
47.95
47.59
CF3
Ru
P
Cl
PPh3
CF3
3
200
150
100
50
0
-50
-100
-150
-200
-250
-300
ppm

[Ru(MeCN)(Ind)(PPh_3){P(*p*-$C_6H_4CF_3$)$_3$}] PF_6 (**29**)

^1H

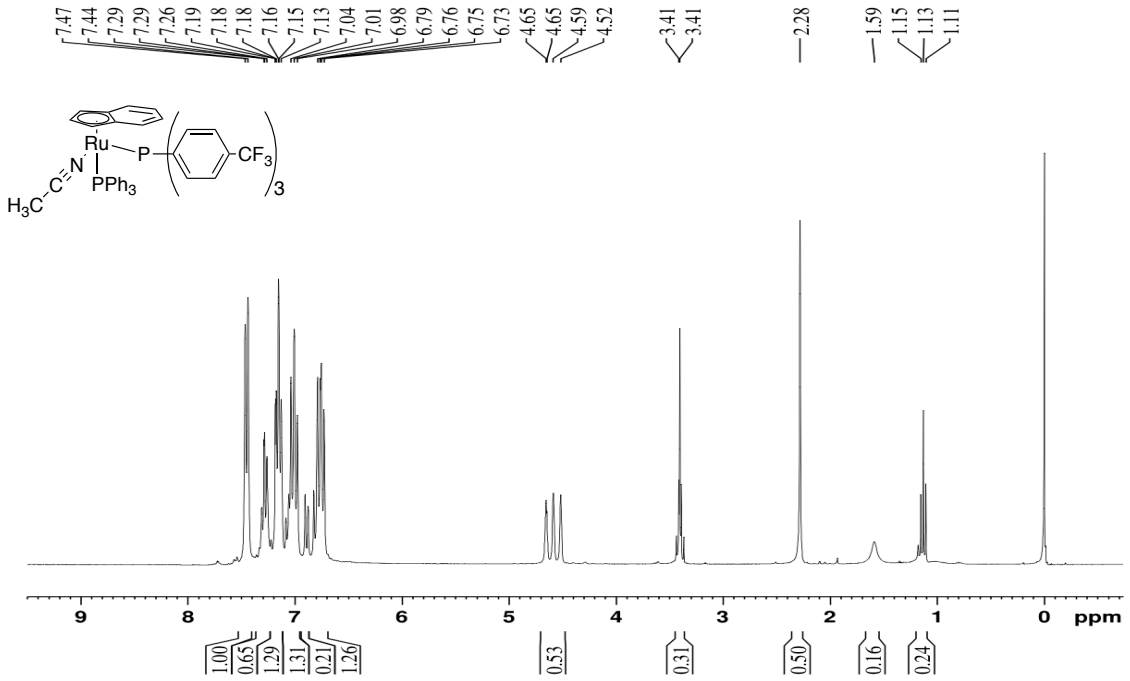

$^{31}P\{^1H\}$

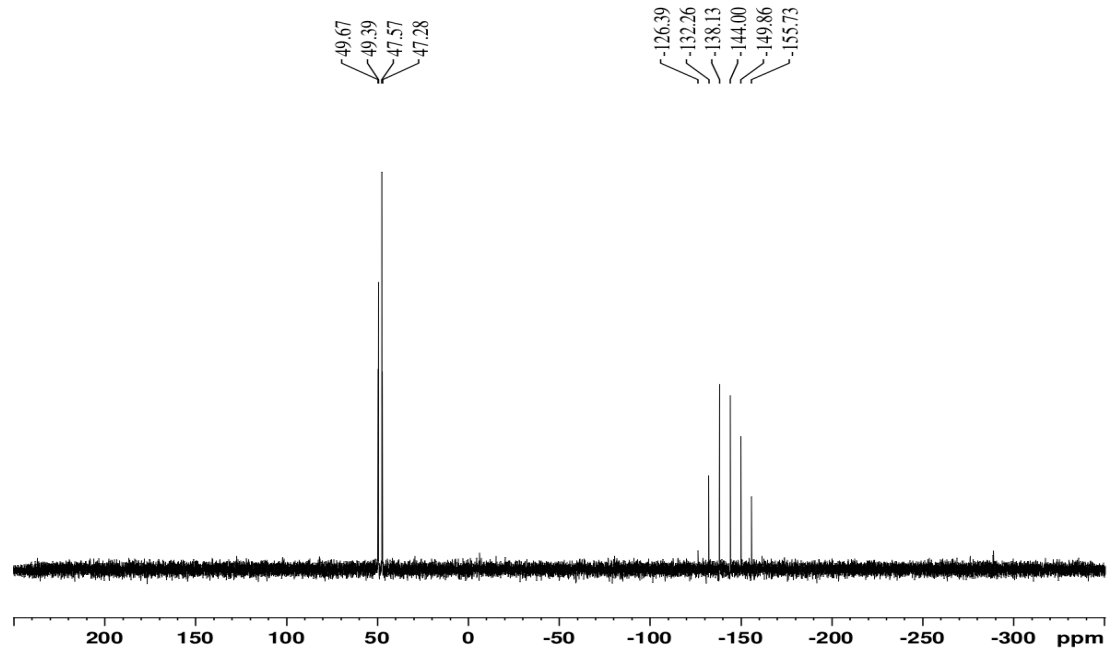

^{1}H

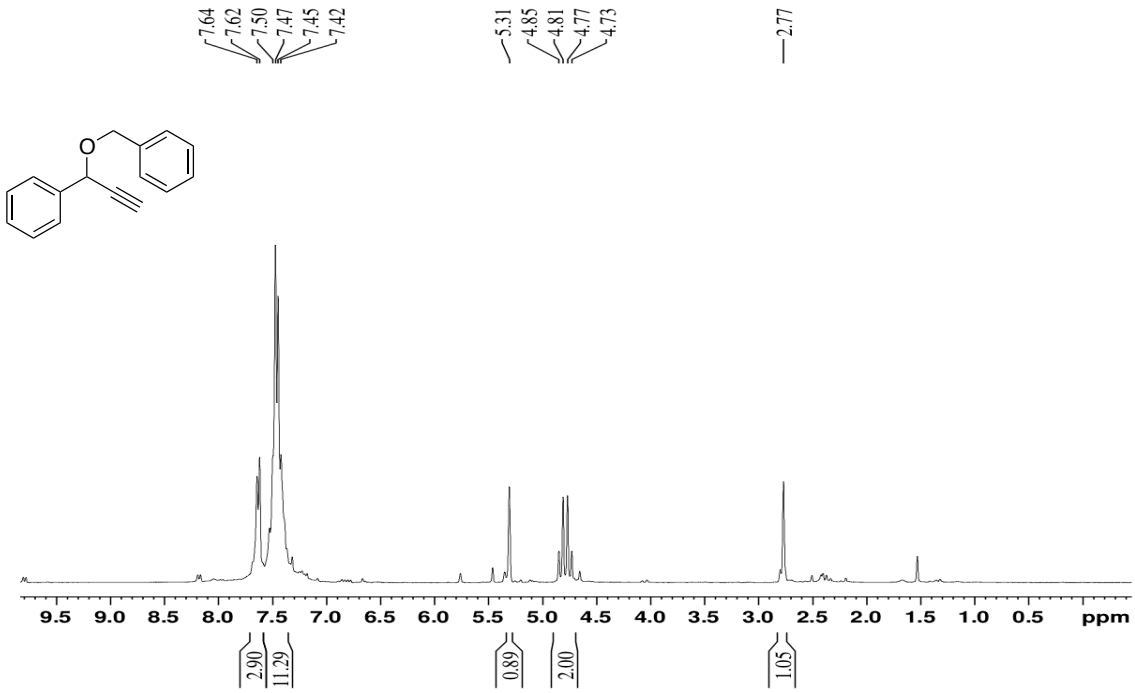
7.64
7.62
7.50
7.47
7.45
7.42
5.31
4.85
4.81
4.77
4.73
2.77
O
9.5 9.0 8.5 8.0 7.5 7.0 6.5 6.0 5.5 5.0 4.5 4.0 3.5 3.0 2.5 2.0 1.5 1.0 0.5 ppm
2.90
11.29
0.89
2.00
1.05

$^{13}C\{^{1}H\}$

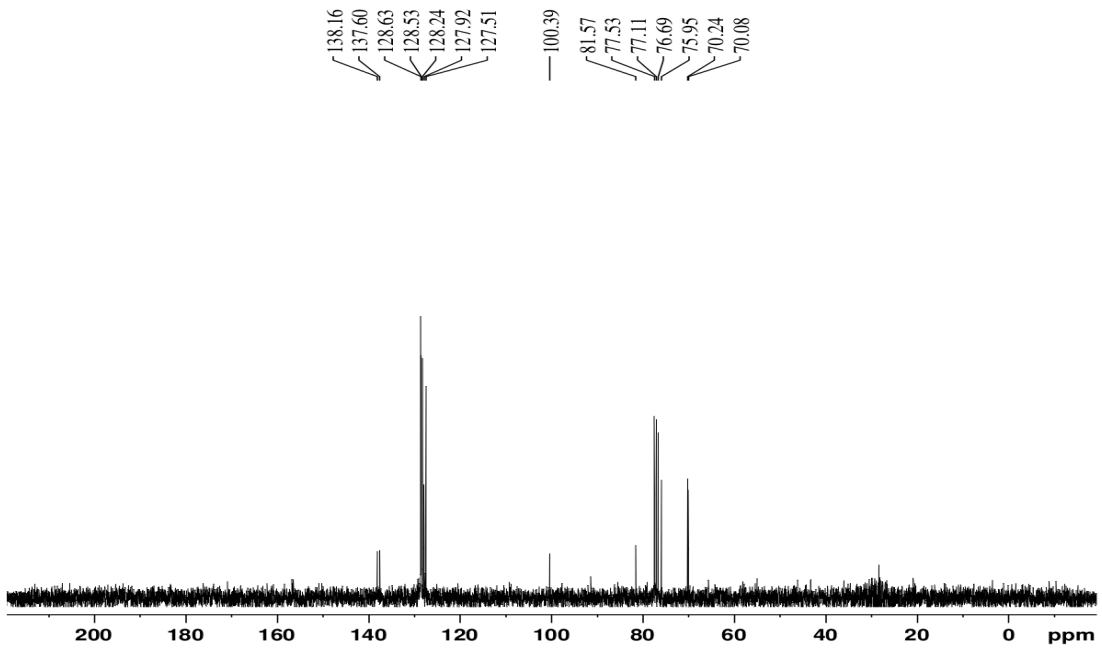
138.16
137.60
128.63
128.53
128.24
127.92
127.51
100.39
81.57
77.53
77.11
76.69
75.95
70.24
70.08
200 180 160 140 120 100 80 60 40 20 0 ppm

^{1}H

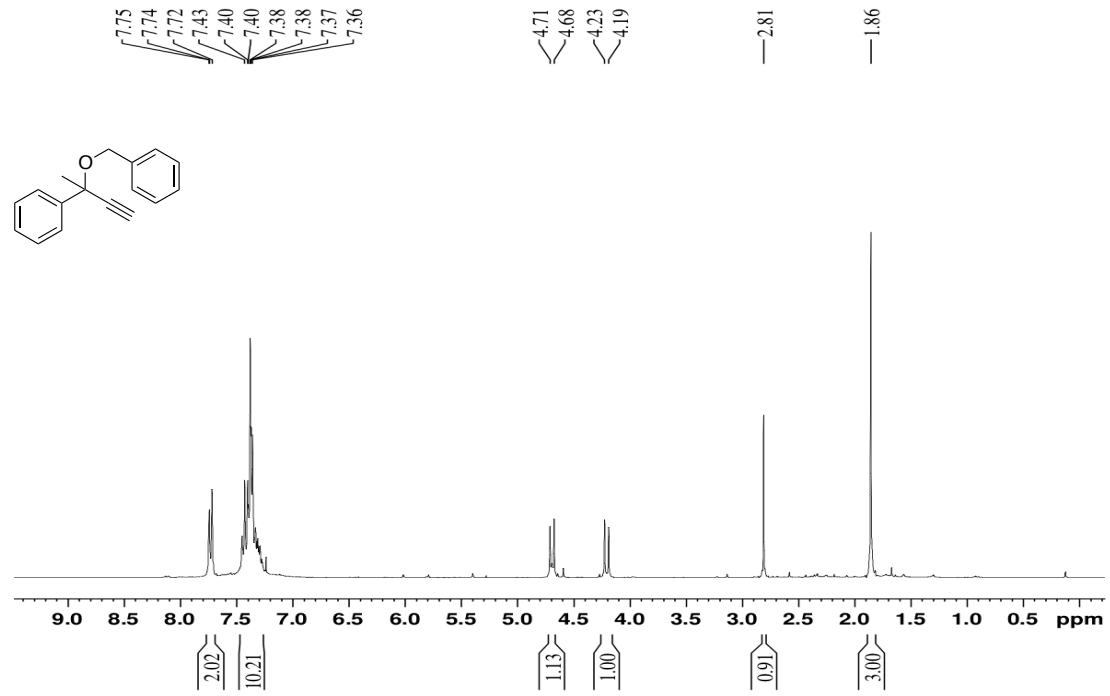
7.75
7.74
7.72
7.43
7.40
7.40
7.38
7.38
7.37
7.36
4.71
4.68
4.23
4.19
2.81
1.86
9.0 8.5 8.0 7.5 7.0 6.5 6.0 5.5 5.0 4.5 4.0 3.5 3.0 2.5 2.0 1.5 1.0 0.5 ppm
2.02
10.21
1.13
1.00
0.91
3.00

$^{13}C\{^{1}H\}$

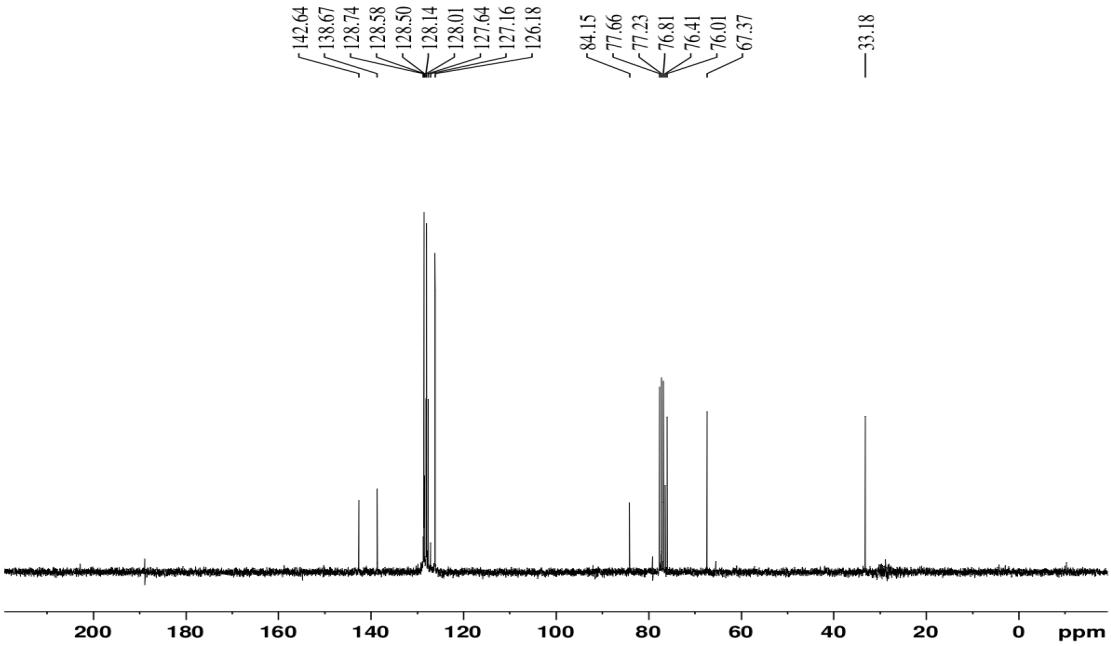
142.64
138.67
128.74
128.58
128.50
128.14
128.01
127.64
127.16
126.18
84.15
77.66
77.23
76.81
76.41
76.01
67.37
33.18
200 180 160 140 120 100 80 60 40 20 0 ppm

^{1}H

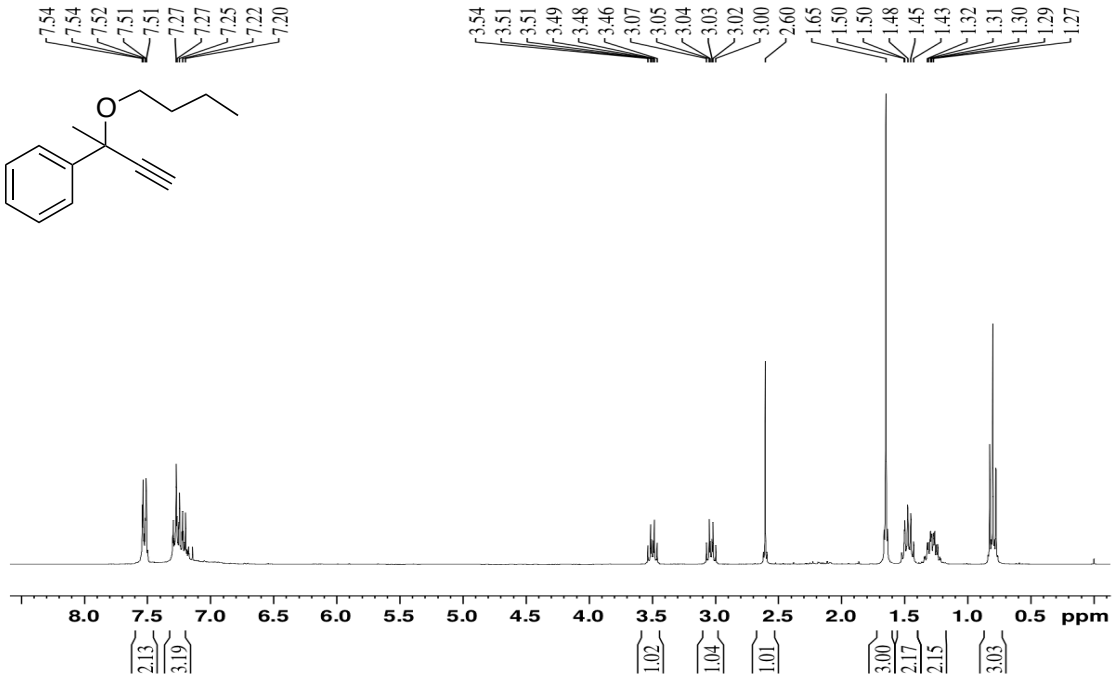
7.54
7.54
7.52
7.51
7.51
7.27
7.27
7.25
7.22
7.20
3.54
3.51
3.51
3.49
3.48
3.46
3.07
3.05
3.04
3.03
3.02
3.00
2.60
1.65
1.50
1.50
1.48
1.45
1.43
1.32
1.31
1.30
1.29
1.27
O
8.0 7.5 7.0 6.5 6.0 5.5 5.0 4.5 4.0 3.5 3.0 2.5 2.0 1.5 1.0 0.5 ppm
2.13
3.19
1.02
1.04
1.01
3.00
2.17
2.15
3.03

$^{13}C\{^{1}H\}$

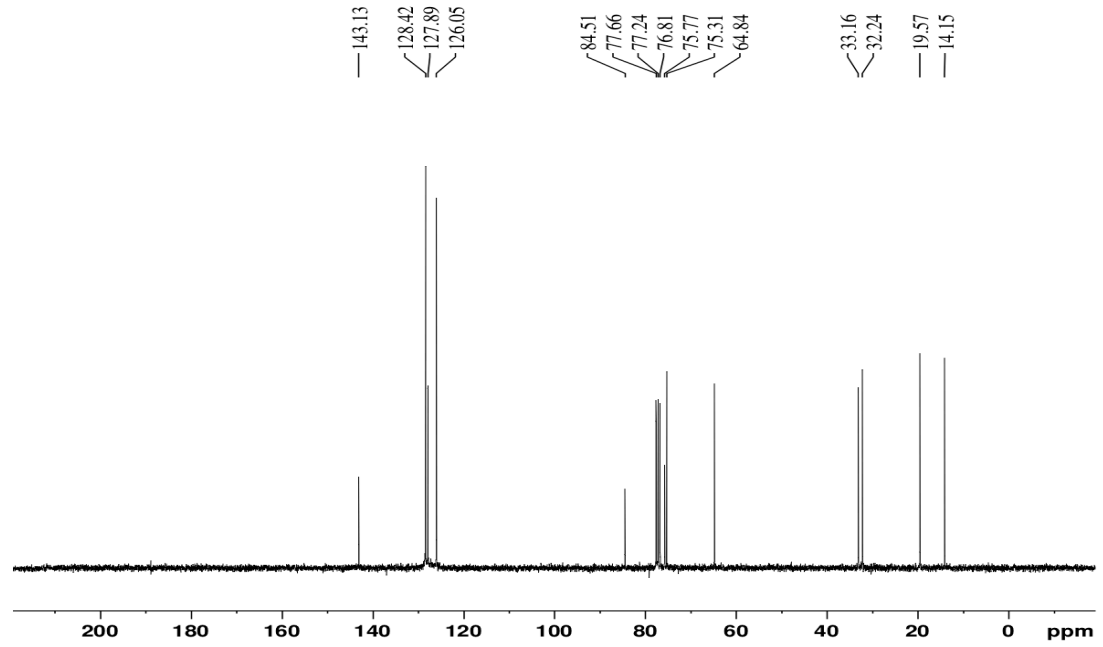
143.13
128.42
127.89
126.05
84.51
77.66
77.24
76.81
75.77
75.31
64.84
33.16
32.24
19.57
14.15
200 180 160 140 120 100 80 60 40 20 0 ppm

Chapter 4 Spectra

[RuCl(dap)(PPh_3)$_2$]BAr^F_4 (**35**)

^1H

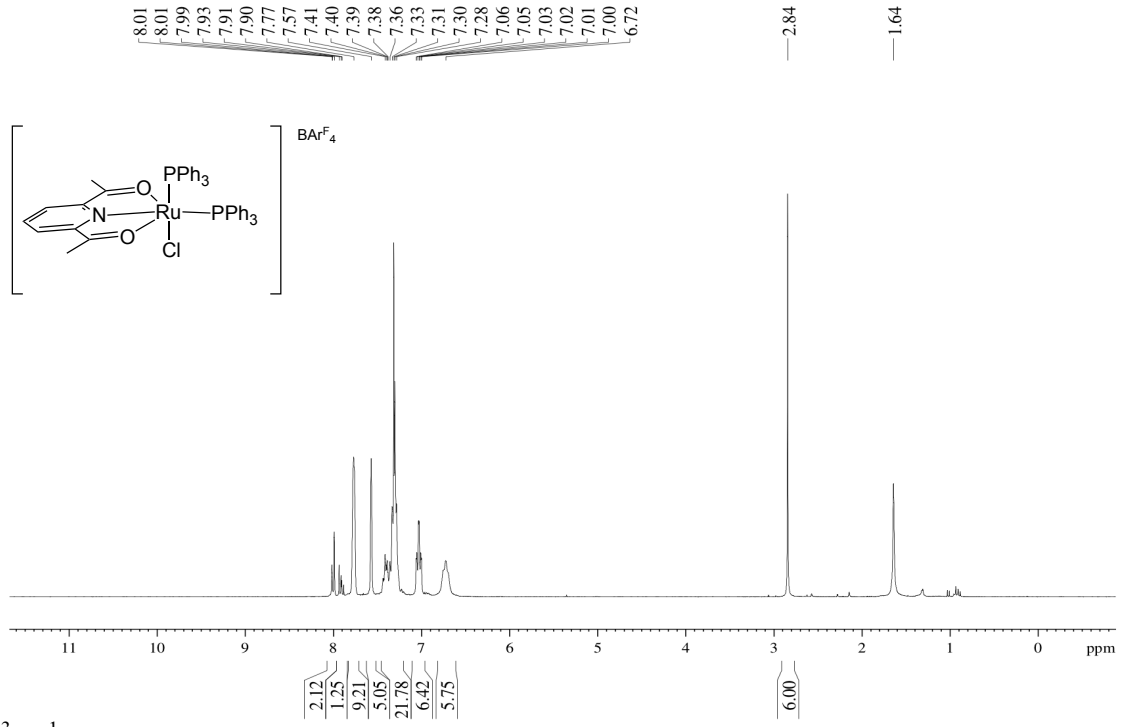

$^{13}C\{^1H\}$

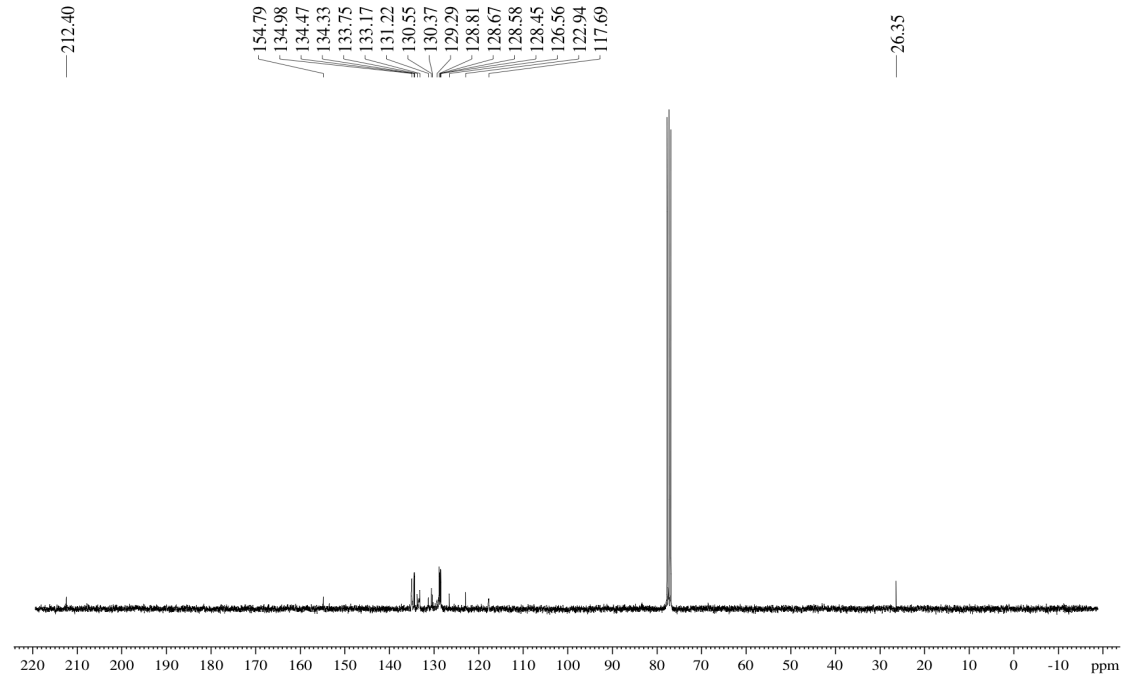

$^{19}F\{^{1}H\}$

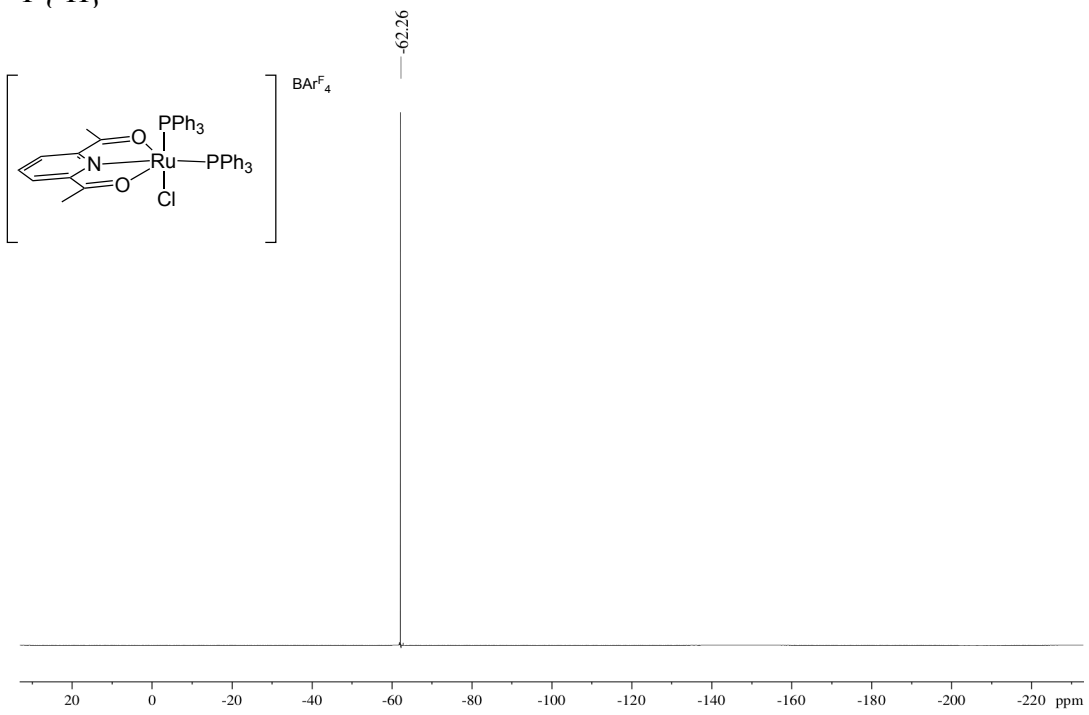
-62.26
BAr$^{F}_{4}$
PPh3
O
N
Ru
PPh3
O
Cl
20
0
-20
-40
-60
-80
-100
-120
-140
-160
-180
-200
-220
ppm

$^{31}P\{^{1}H\}$

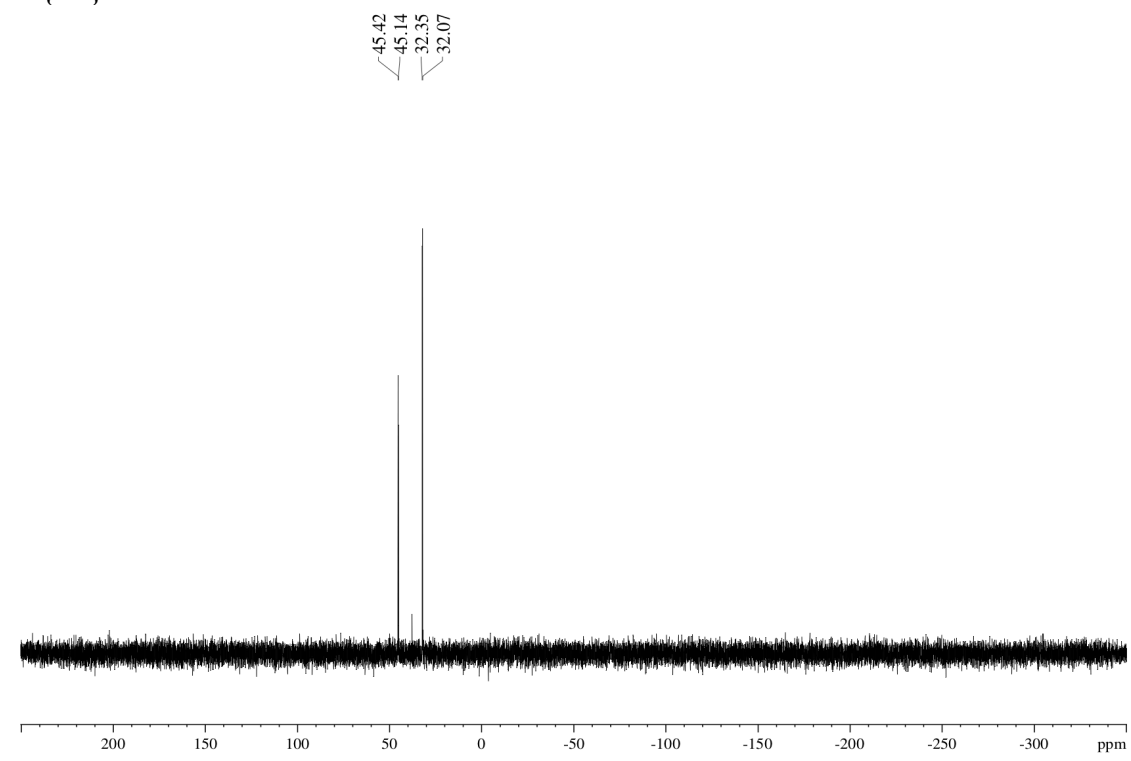
45.42
45.14
32.35
32.07
200
150
100
50
0
-50
-100
-150
-200
-250
-300
ppm

^{1}H

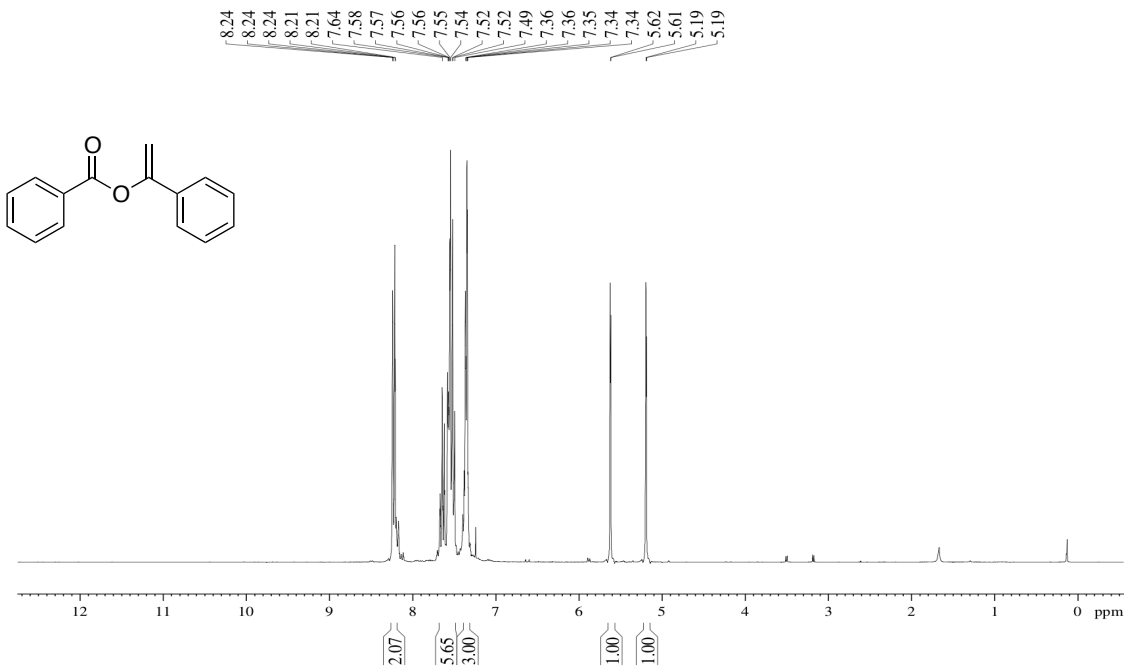
8.24
8.24
8.24
8.21
8.21
7.64
7.58
7.57
7.56
7.56
7.55
7.54
7.52
7.52
7.49
7.36
7.36
7.35
7.34
7.34
5.62
5.61
5.19
5.19
O
O
12
11
10
9
8
7
6
5
4
3
2
1
0
ppm
2.07
5.65
3.00
1.00
1.00

$^{13}C\{^{1}H\}$

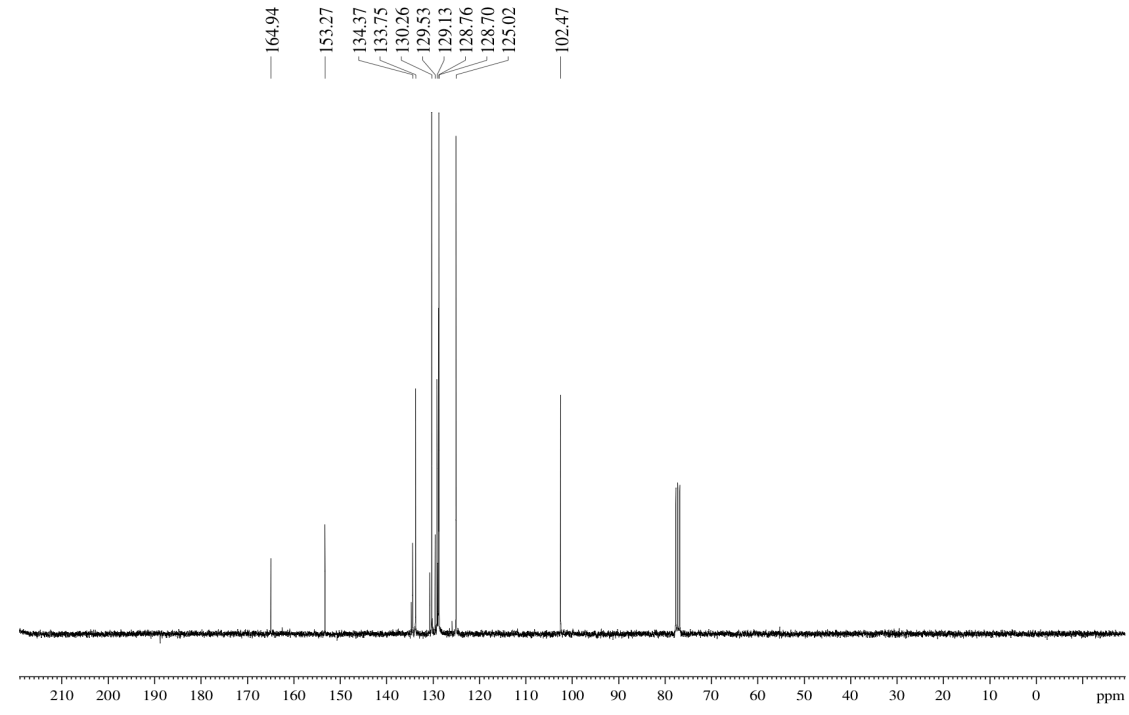
164.94
153.27
134.37
133.75
130.26
129.53
129.13
128.76
128.70
125.02
102.47
210
200
190
180
170
160
150
140
130
120
110
100
90
80
70
60
50
40
30
20
10
0
ppm

^{1}H

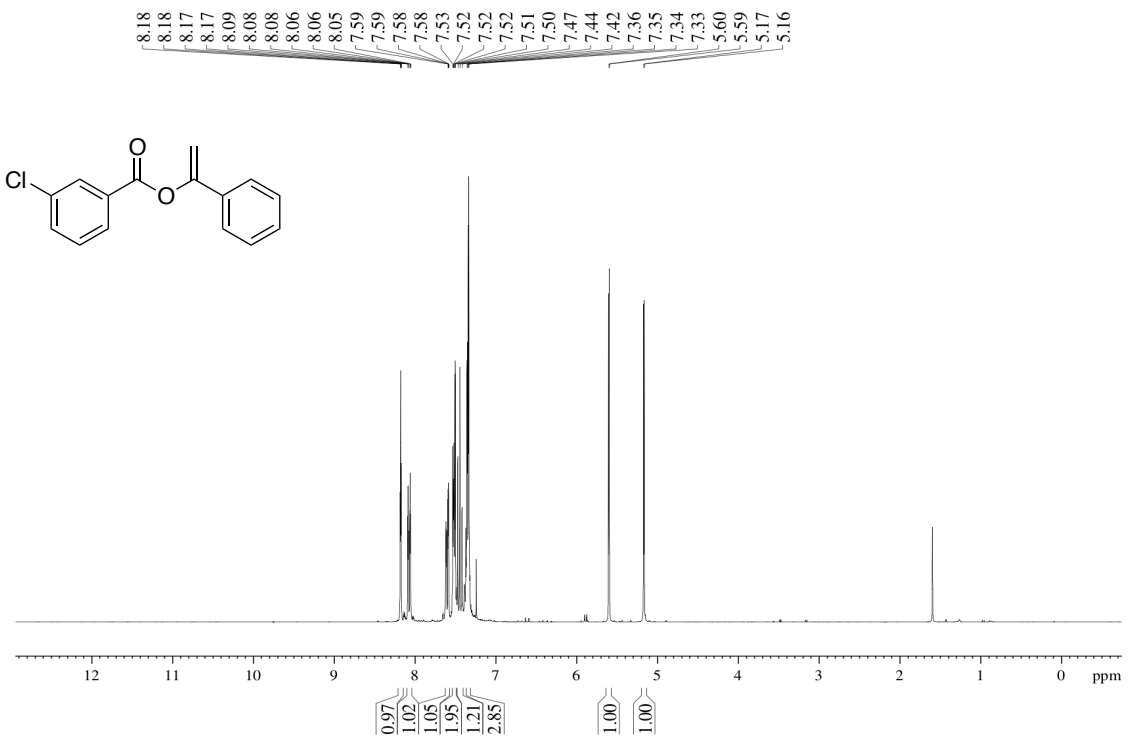
8.18
8.18
8.17
8.17
8.09
8.08
8.08
8.06
8.06
8.05
7.59
7.59
7.58
7.58
7.53
7.52
7.52
7.52
7.51
7.50
7.47
7.44
7.42
7.36
7.35
7.34
7.33
5.60
5.59
5.17
5.16
Cl
O
O
12
11
10
9
8
7
6
5
4
3
2
1
0
ppm
0.97
1.02
1.05
1.95
1.21
2.85
1.00
1.00

$^{13}C\{^{1}H\}$

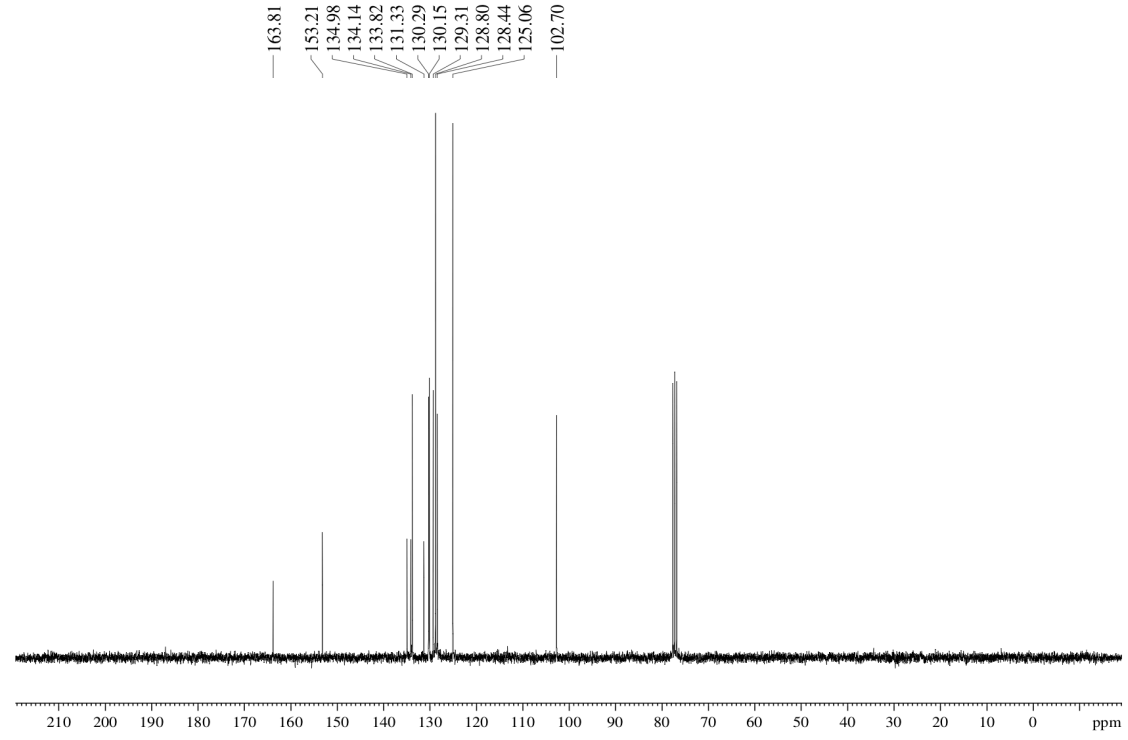
163.81
153.21
134.98
134.14
133.82
131.33
130.29
130.15
129.31
128.80
128.44
125.06
102.70
210
200
190
180
170
160
150
140
130
120
110
100
90
80
70
60
50
40
30
20
10
0
ppm

^{1}H


8.05
8.04
8.03
8.02
8.02
7.74
7.73
7.73
7.71
7.71
7.58
7.57
7.57
7.56
7.56
7.55
7.55
7.54
7.46
7.45
7.43
7.43
7.41
7.40
7.38
7.38
7.37
7.35
7.34
7.33
7.32
7.24
5.59
5.58
5.22
5.21

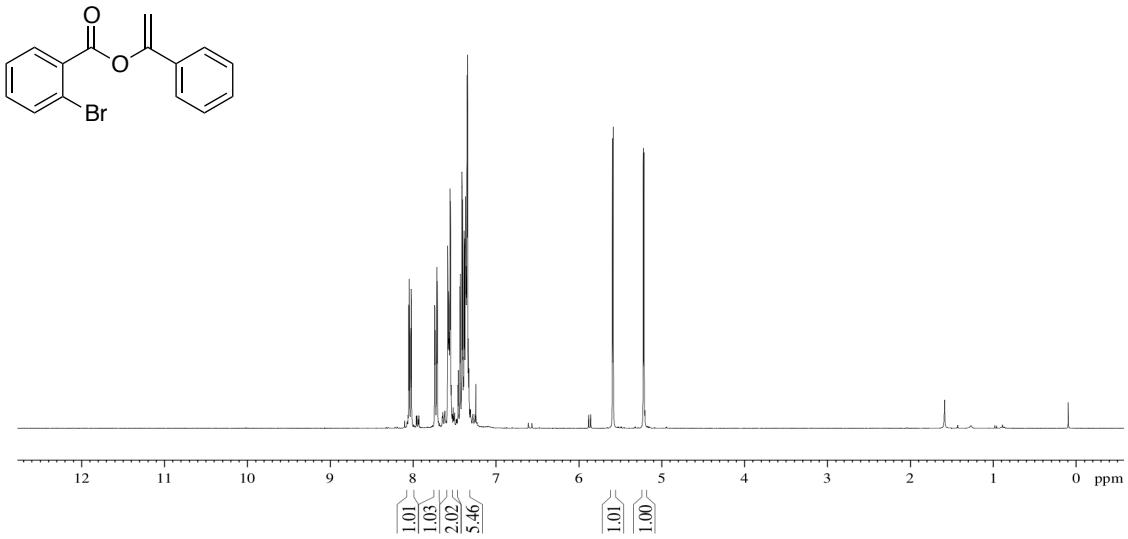
O
O
Br
12
11
10
9
8
7
6
5
4
3
2
1
0
ppm
1.01
1.03
2.02
5.46
1.01
1.00

$^{13}C\{^{1}H\}$

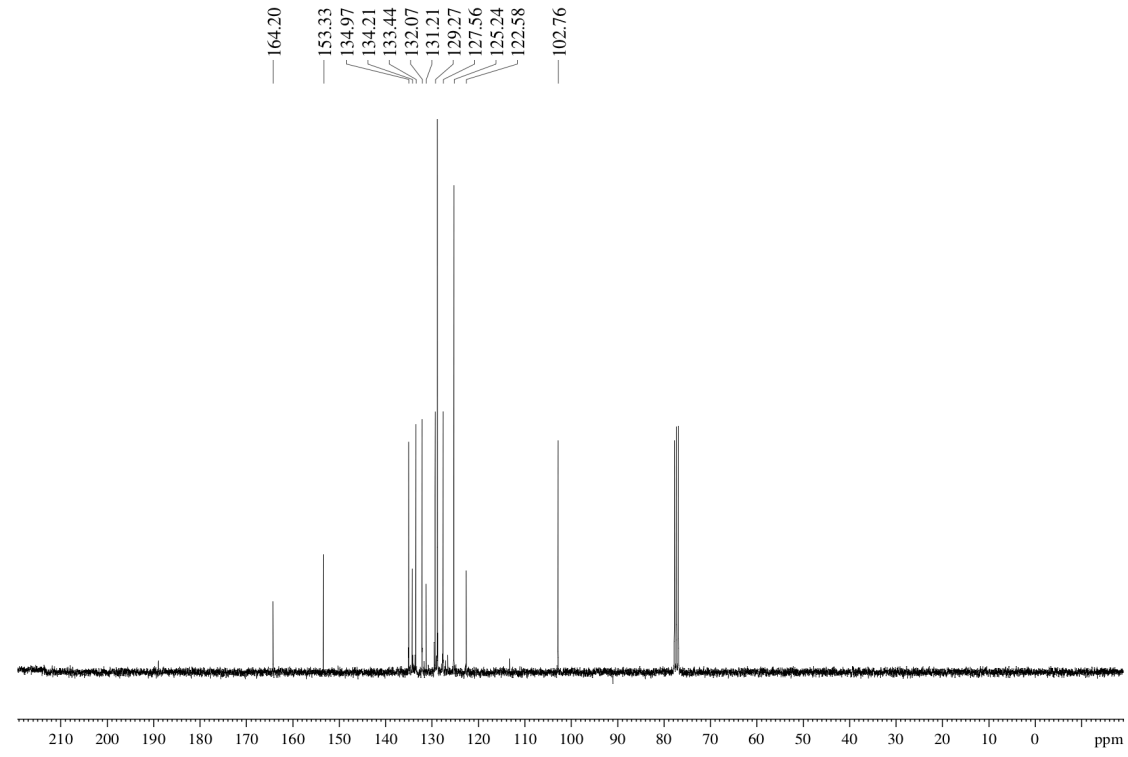
164.20
153.33
134.97
134.21
133.44
132.07
131.21
129.27
127.56
125.24
122.58
102.76
210
200
190
180
170
160
150
140
130
120
110
100
90
80
70
60
50
40
30
20
10
0
ppm

^{1}H

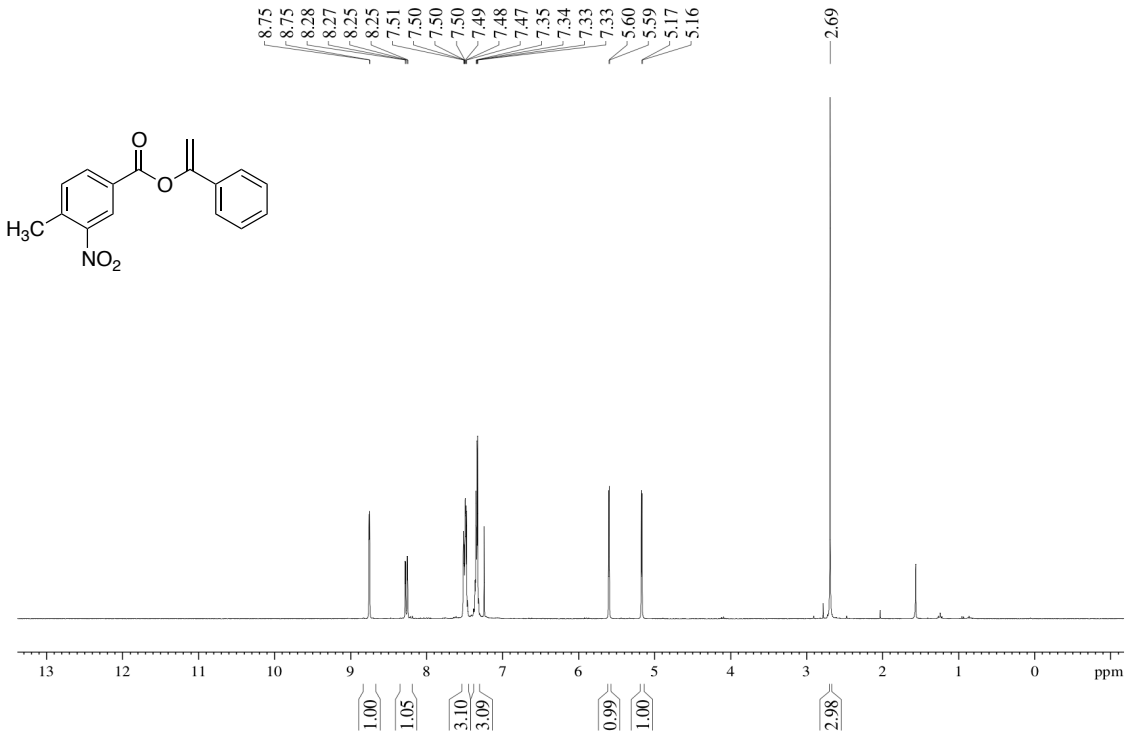
8.75
8.75
8.28
8.27
8.25
8.25
7.51
7.50
7.50
7.50
7.49
7.48
7.47
7.35
7.34
7.33
7.33
5.60
5.59
5.17
5.16
2.69
O
O
H3C
NO2
13
12
11
10
9
8
7
6
5
4
3
2
1
0
ppm
1.00
1.05
3.10
3.09
0.99
1.00
2.98

$^{13}C\{^{1}H\}$

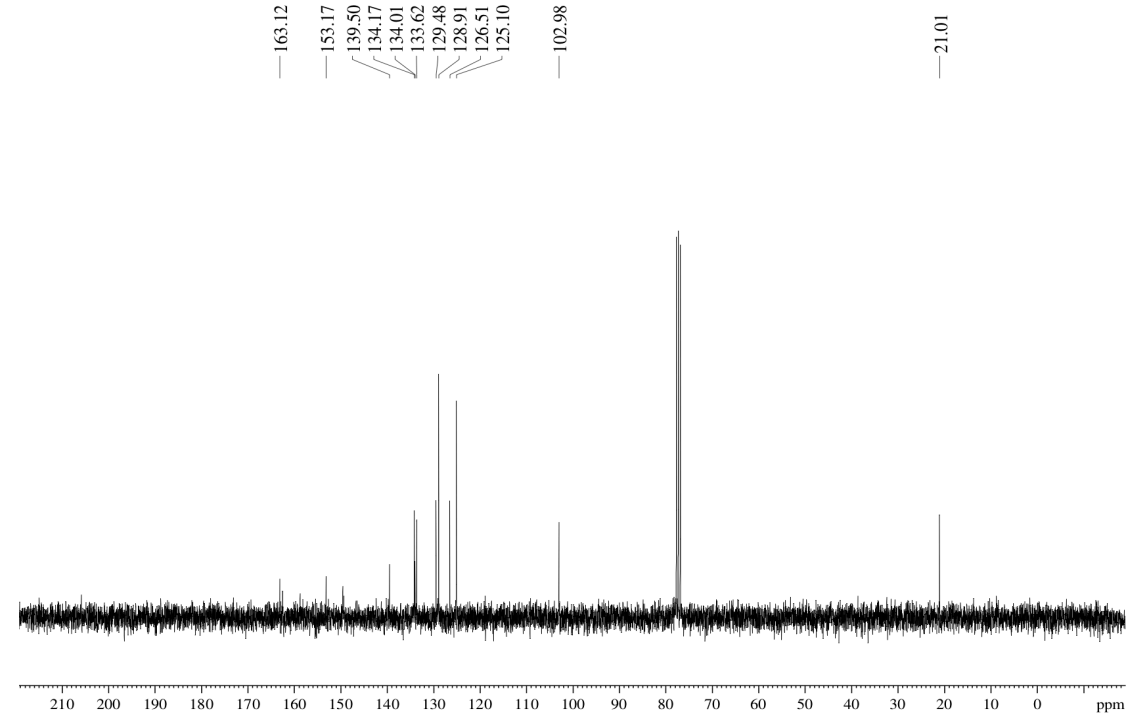
163.12
153.17
139.50
134.17
134.01
133.62
129.48
128.91
126.51
125.10
102.98
21.01
210
200
190
180
170
160
150
140
130
120
110
100
90
80
70
60
50
40
30
20
10
0
ppm

^{1}H

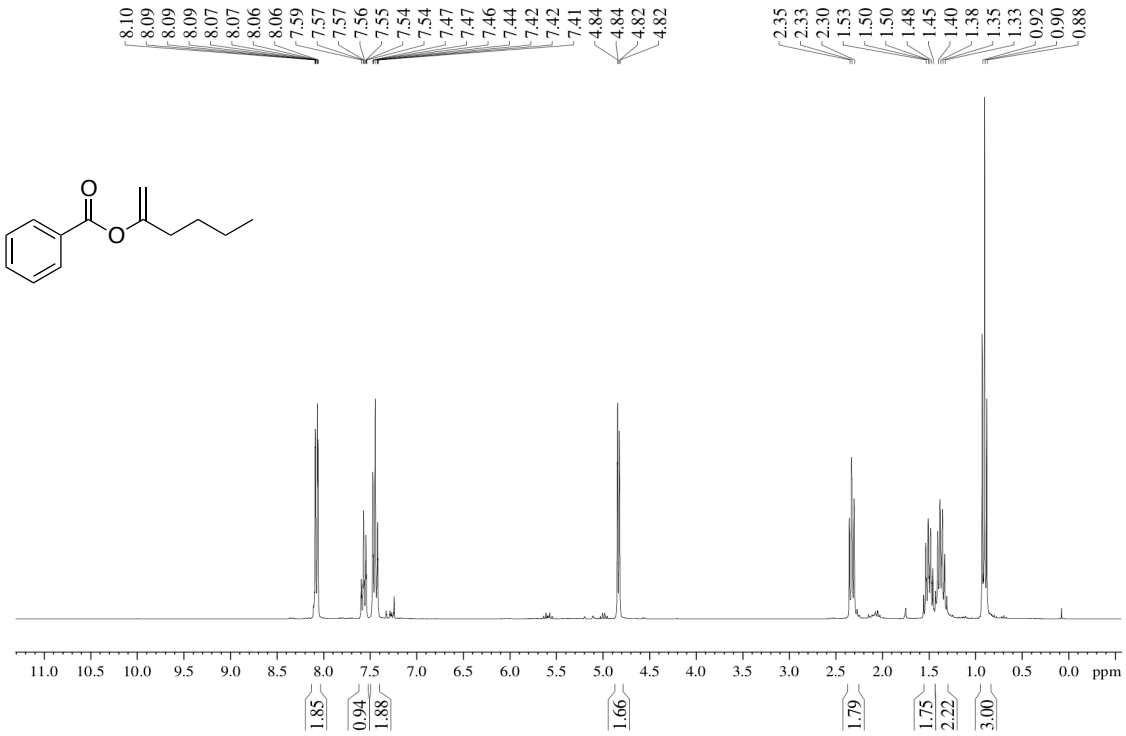
8.10
8.09
8.09
8.09
8.07
8.07
8.06
8.06
7.59
7.57
7.57
7.56
7.55
7.54
7.54
7.47
7.47
7.46
7.44
7.42
7.42
7.41
4.84
4.84
4.82
4.82
2.35
2.33
2.30
1.53
1.50
1.50
1.48
1.45
1.40
1.38
1.35
1.33
0.92
0.90
0.88
O
O
11.0 10.5 10.0 9.5 9.0 8.5 8.0 7.5 7.0 6.5 6.0 5.5 5.0 4.5 4.0 3.5 3.0 2.5 2.0 1.5 1.0 0.5 0.0 ppm
1.85
0.94
1.88
1.66
1.79
1.75
2.22
3.00

$^{13}C\{^{1}H\}$

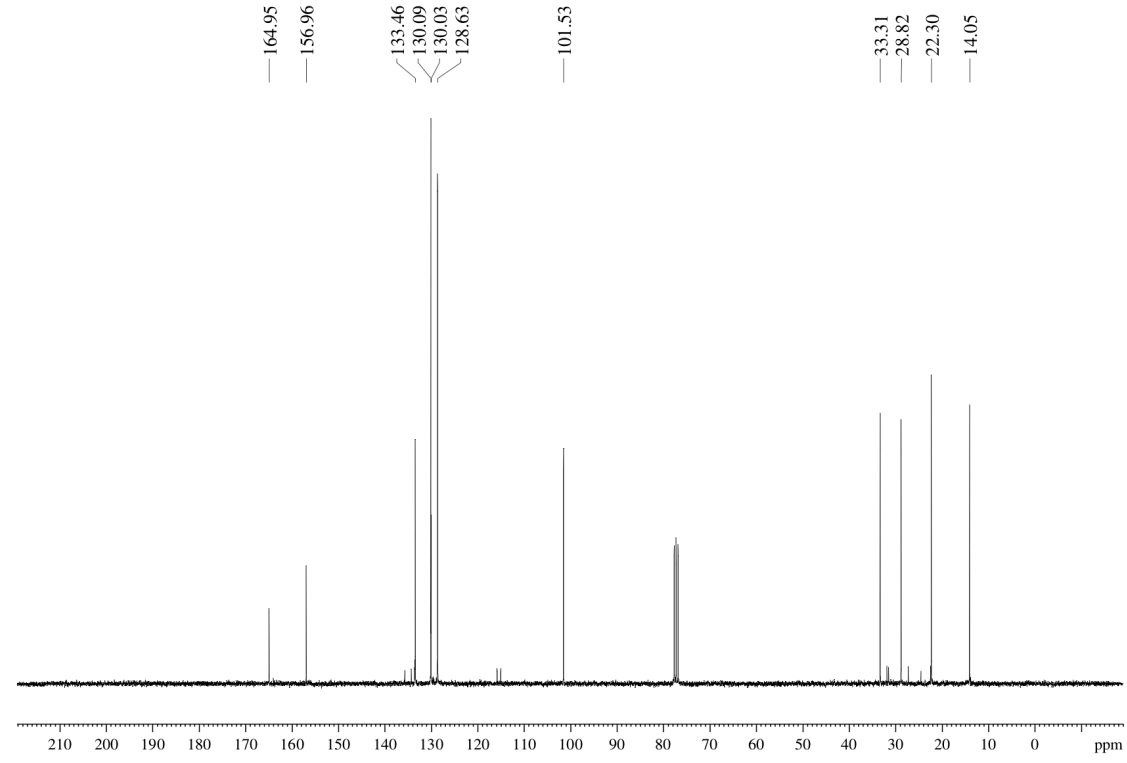
164.95
156.96
133.46
130.09
130.03
128.63
101.53
33.31
28.82
22.30
14.05
210 200 190 180 170 160 150 140 130 120 110 100 90 80 70 60 50 40 30 20 10 0 ppm

^{1}H

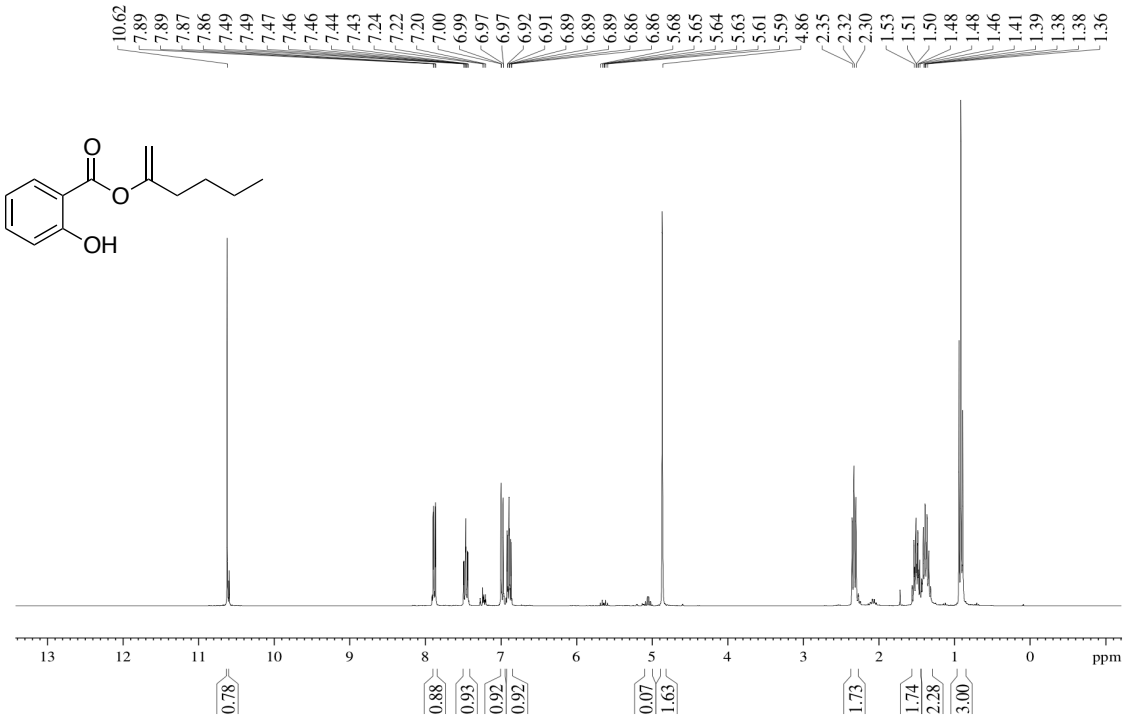
10.62
7.89
7.89
7.87
7.86
7.49
7.49
7.47
7.46
7.46
7.44
7.43
7.24
7.22
7.20
7.00
6.99
6.97
6.97
6.92
6.91
6.89
6.89
6.89
6.86
6.86
5.68
5.65
5.64
5.63
5.61
5.59
4.86
2.35
2.32
2.30
1.53
1.51
1.50
1.48
1.48
1.46
1.41
1.39
1.38
1.38
1.36
O
O
OH
13
12
11
10
9
8
7
6
5
4
3
2
1
0
ppm
0.78
0.88
0.93
0.92
0.92
0.07
1.63
1.73
1.74
2.28
3.00

$^{13}C\{^{1}H\}$

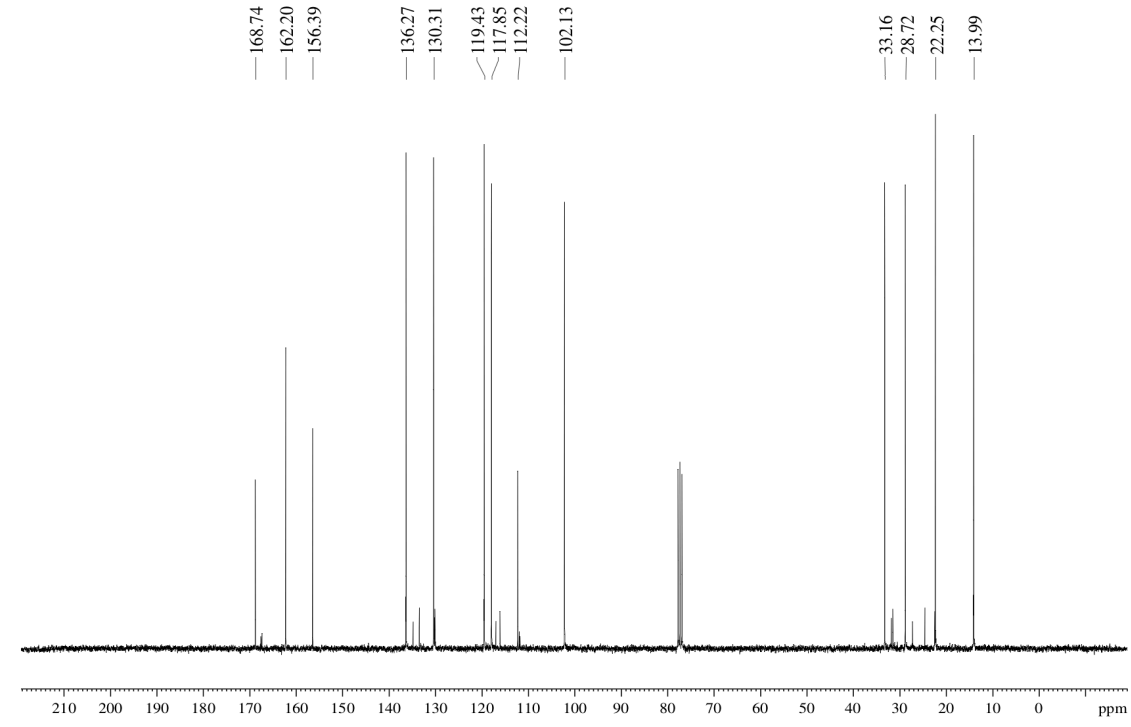
168.74
162.20
156.39
136.27
130.31
119.43
117.85
112.22
102.13
33.16
28.72
22.25
13.99
210
200
190
180
170
160
150
140
130
120
110
100
90
80
70
60
50
40
30
20
10
0
ppm

^{1}H

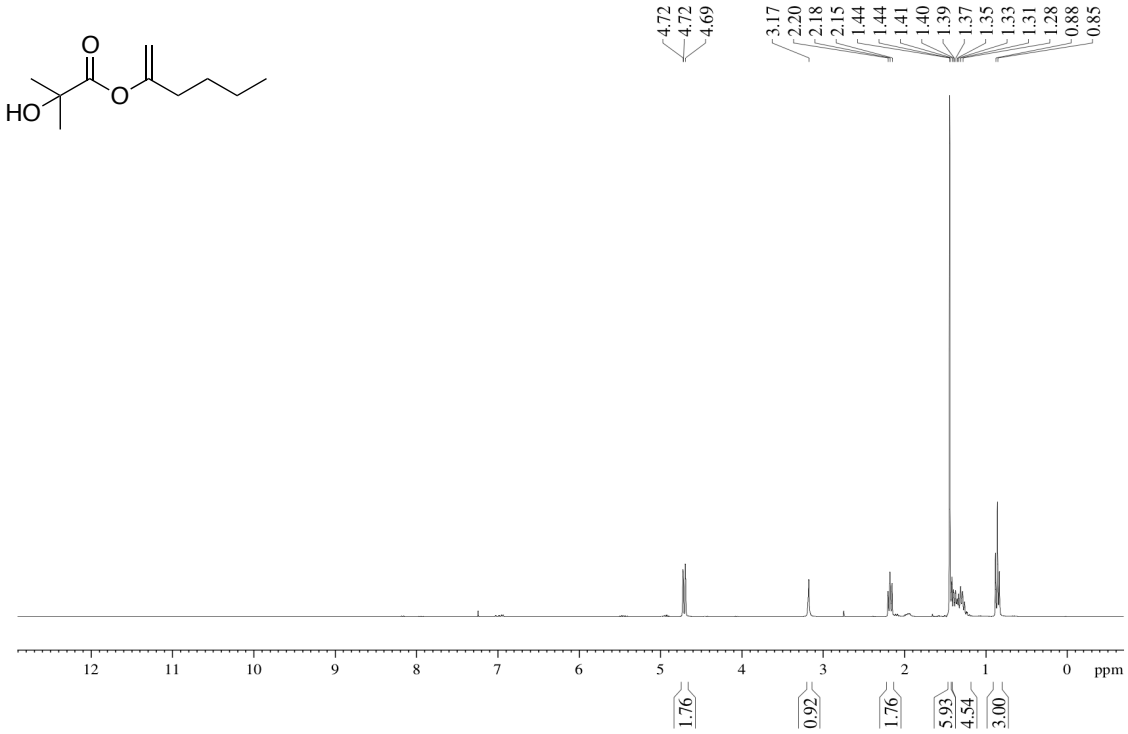
HO
O
O
4.72
4.72
4.69
3.17
2.20
2.18
2.15
1.44
1.44
1.41
1.40
1.39
1.37
1.35
1.33
1.31
1.28
0.88
0.85
12
11
10
9
8
7
6
5
4
3
2
1
0
ppm
1.76
0.92
1.76
5.93
4.54
3.00

$^{13}C\{^{1}H\}$

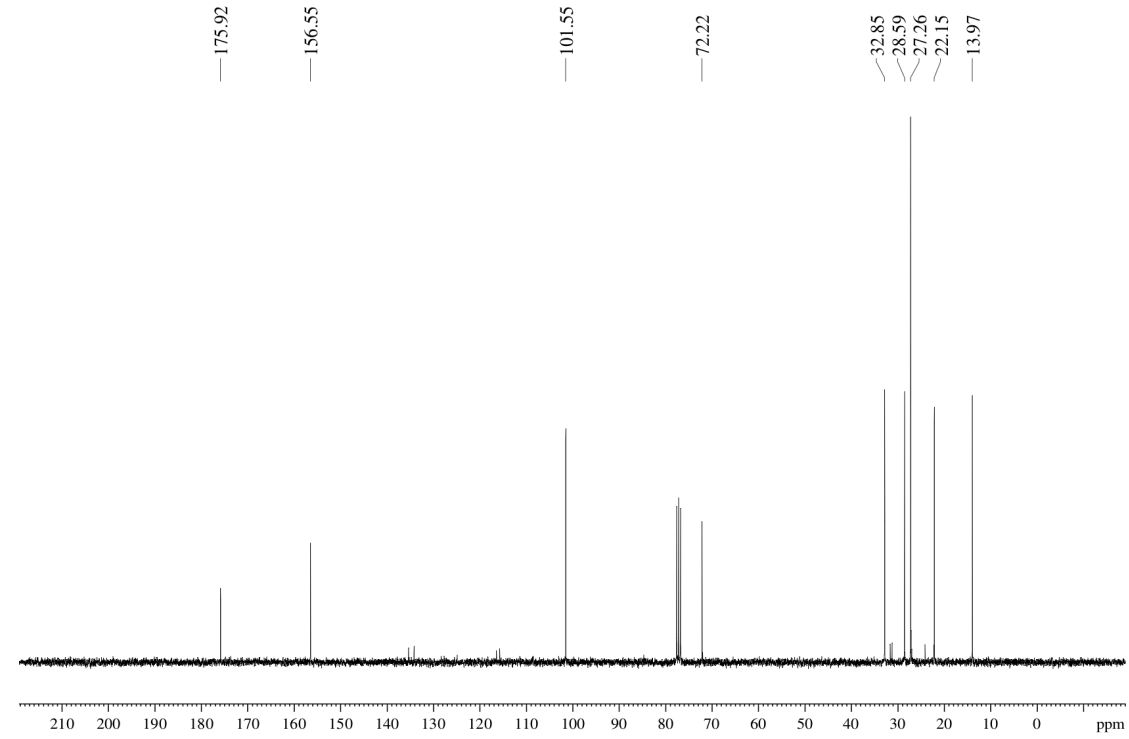
175.92
156.55
101.55
72.22
32.85
28.59
27.26
22.15
13.97
210
200
190
180
170
160
150
140
130
120
110
100
90
80
70
60
50
40
30
20
10
0
ppm

^{1}H

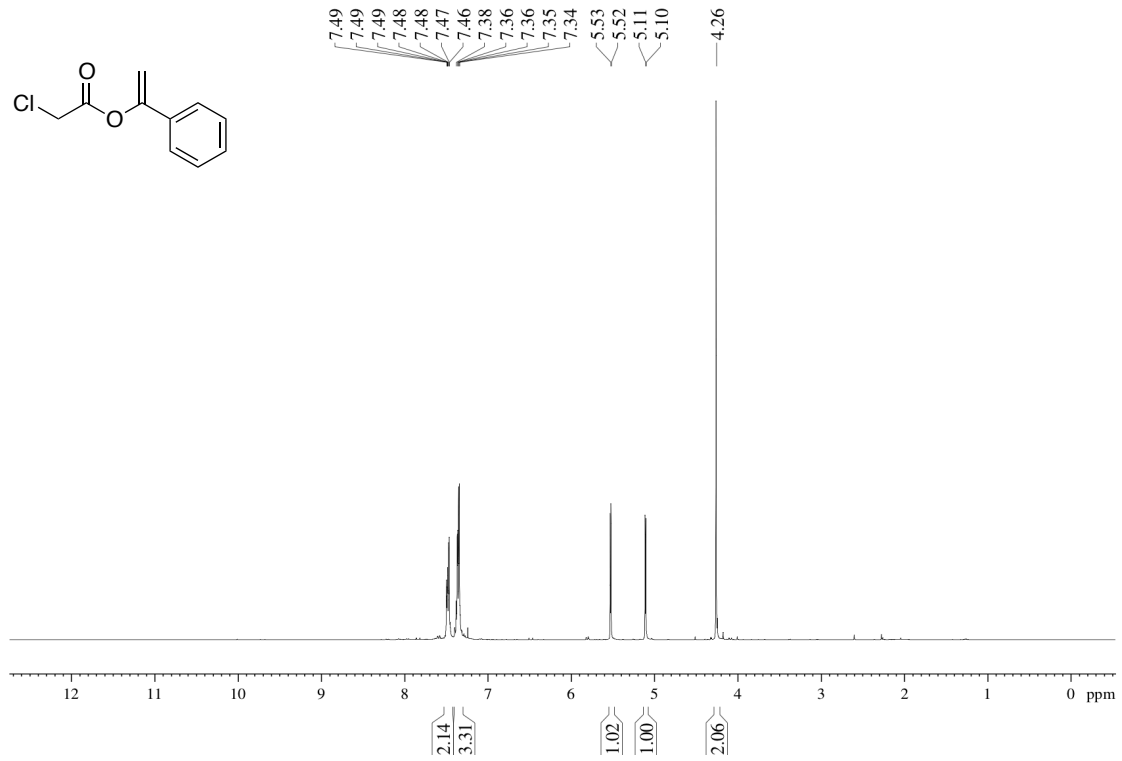
7.49
7.49
7.49
7.48
7.48
7.47
7.46
7.38
7.36
7.36
7.35
7.34
5.53
5.52
5.11
5.10
4.26
Cl
O
O
12 11 10 9 8 7 6 5 4 3 2 1 0 ppm
2.14
3.31
1.02
1.00
2.06

$^{13}C\{^{1}H\}$

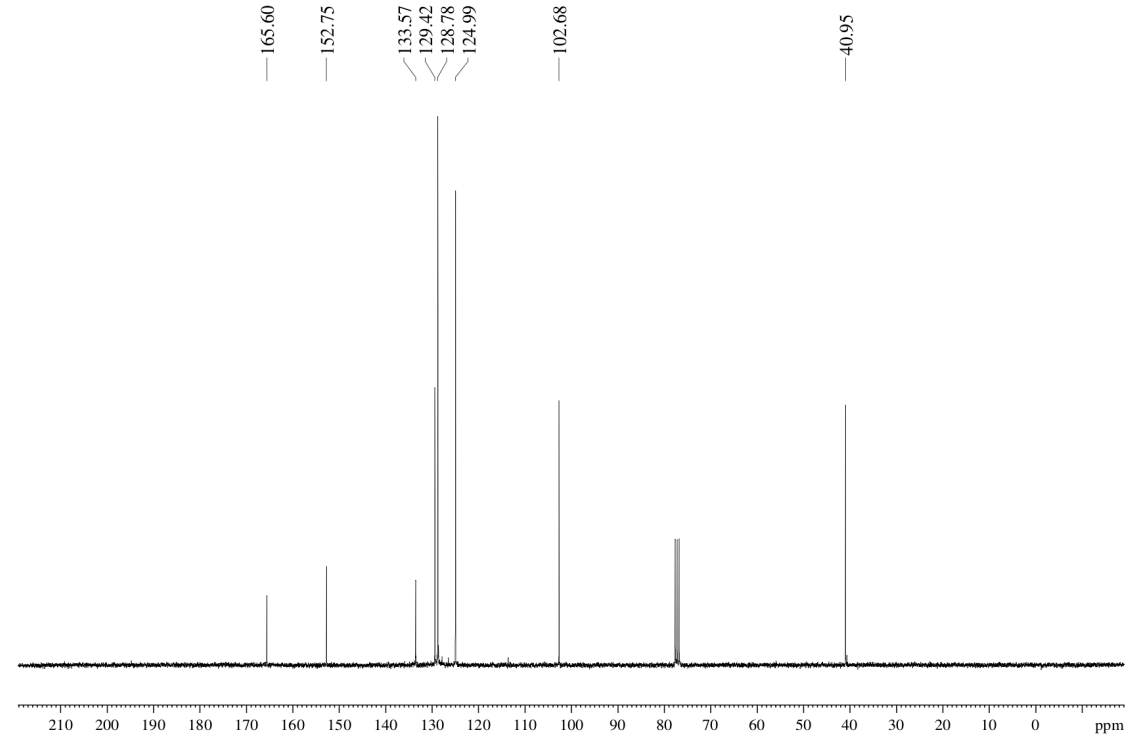
165.60
152.75
133.57
129.42
128.78
124.99
102.68
40.95
210 200 190 180 170 160 150 140 130 120 110 100 90 80 70 60 50 40 30 20 10 0 ppm

^{1}H

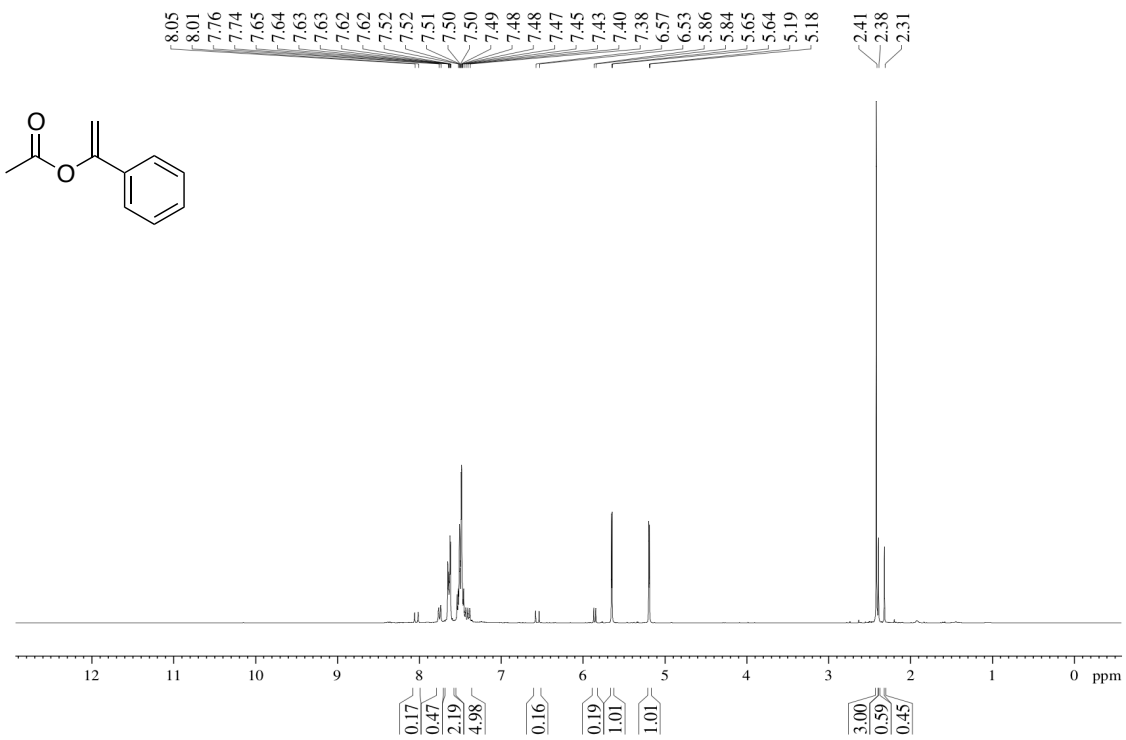
8.05
8.01
7.76
7.74
7.65
7.64
7.63
7.63
7.62
7.62
7.52
7.52
7.51
7.50
7.50
7.49
7.48
7.48
7.47
7.45
7.43
7.40
7.38
6.57
6.53
5.86
5.84
5.65
5.64
5.19
5.18
2.41
2.38
2.31
O
O
12
11
10
9
8
7
6
5
4
3
2
1
0
ppm
0.17
0.47
2.19
4.98
0.16
0.19
1.01
1.01
3.00
0.59
0.45

$^{13}C\{^{1}H\}$

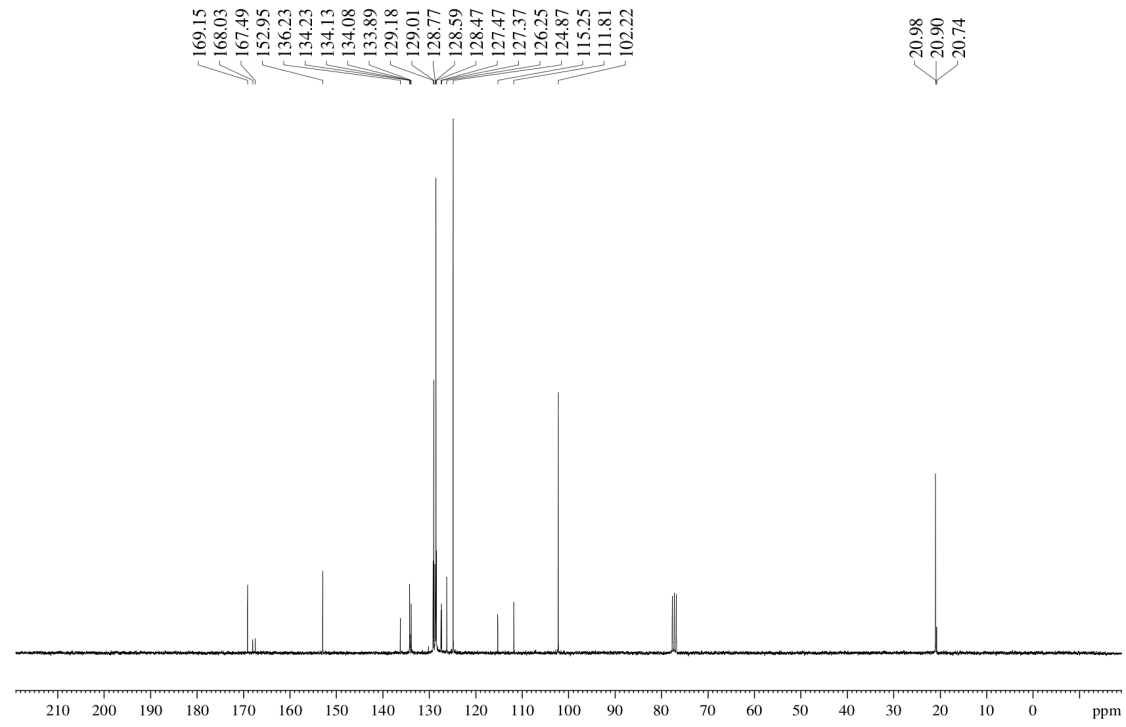
169.15
168.03
167.49
152.95
136.23
134.23
134.13
134.08
133.89
129.18
129.01
128.77
128.59
128.47
127.47
127.37
126.25
124.87
115.25
111.81
102.22
20.98
20.90
20.74
210
200
190
180
170
160
150
140
130
120
110
100
90
80
70
60
50
40
30
20
10
0
ppm

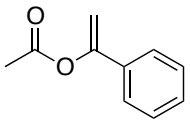

^{1}H – integrated to determine isomer ratio

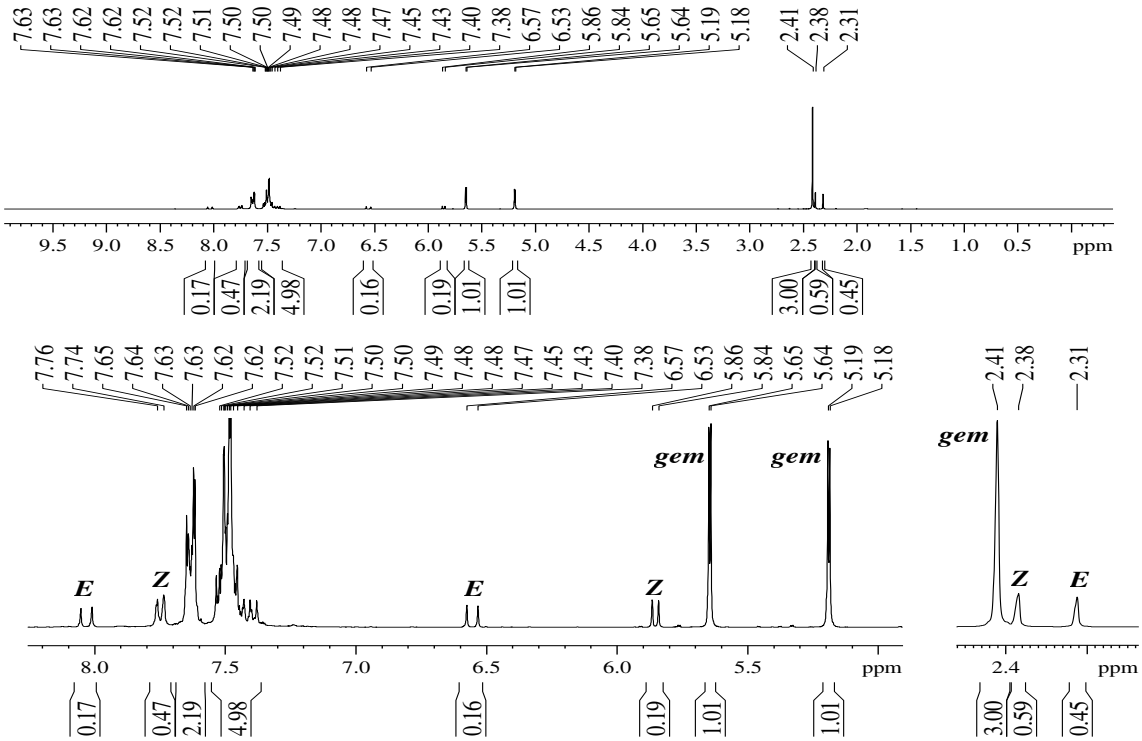

^{1}H

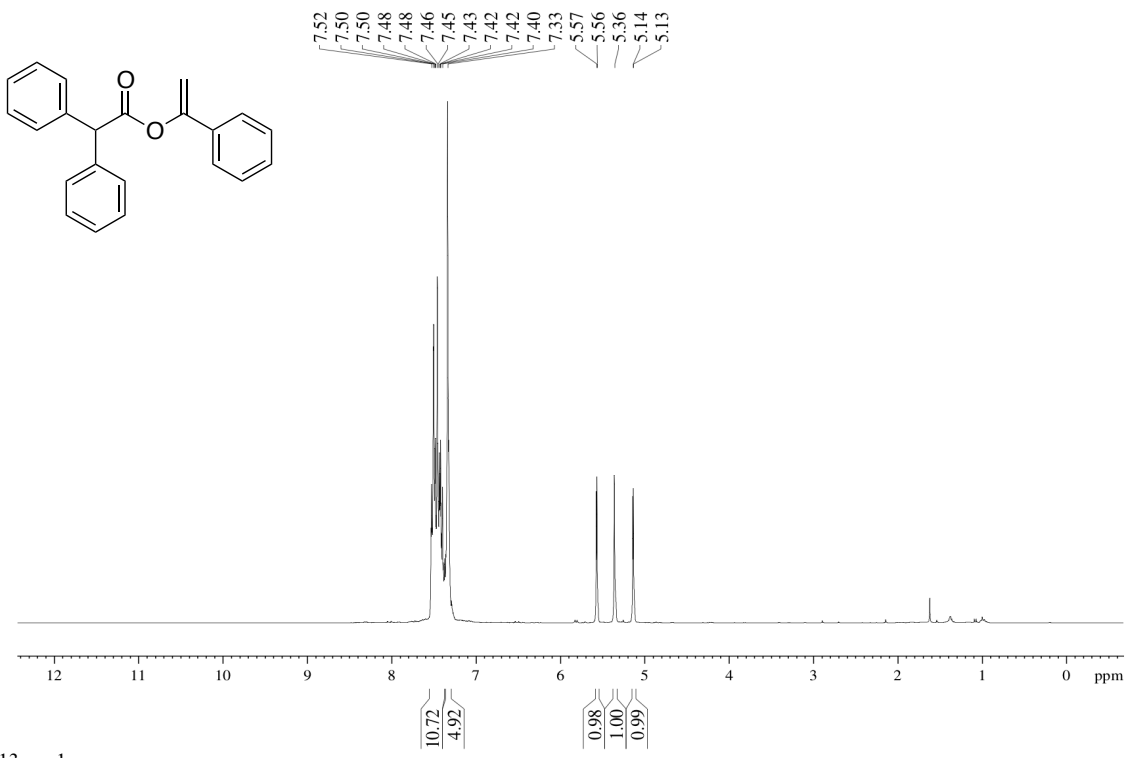
7.52
7.50
7.50
7.48
7.48
7.46
7.45
7.43
7.42
7.42
7.40
7.33
5.57
5.56
5.36
5.14
5.13
O
O
12
11
10
9
8
7
6
5
4
3
2
1
0
ppm
10.72
4.92
0.98
1.00
0.99

$^{13}C\{^{1}H\}$

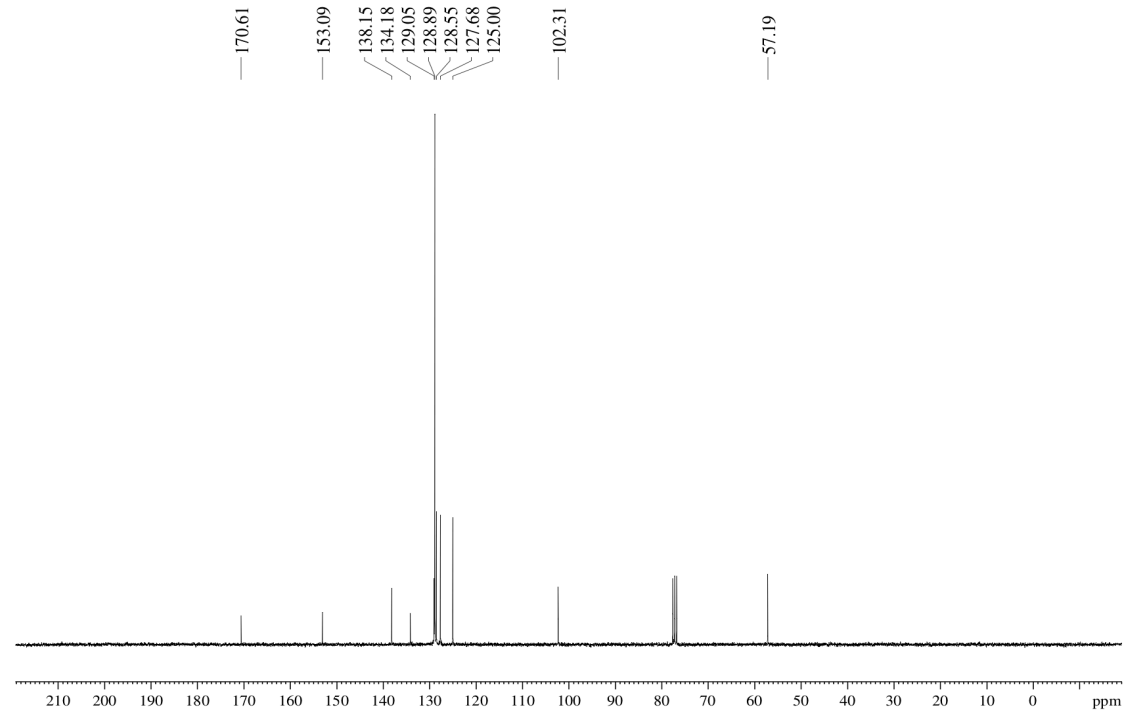
170.61
153.09
138.15
134.18
129.05
128.89
128.55
127.68
125.00
102.31
57.19
210
200
190
180
170
160
150
140
130
120
110
100
90
80
70
60
50
40
30
20
10
0
ppm

^{1}H

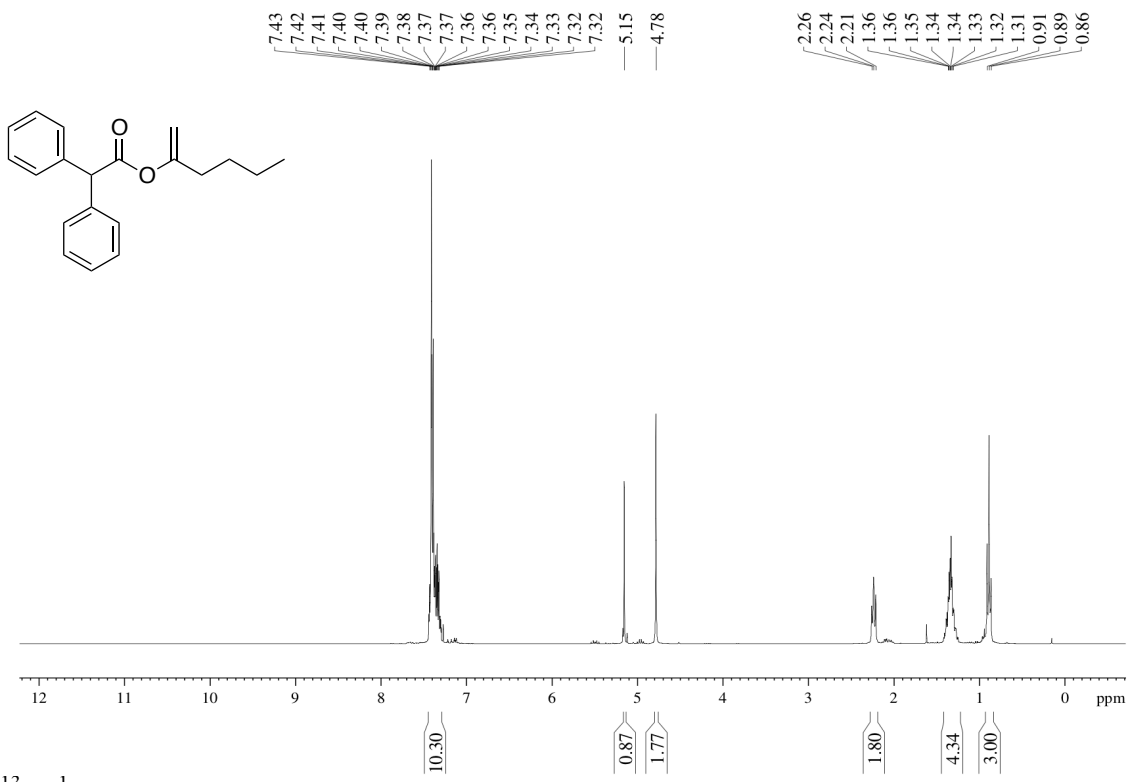
7.43
7.42
7.41
7.40
7.40
7.39
7.38
7.37
7.37
7.36
7.36
7.35
7.34
7.33
7.32
7.32
5.15
4.78
2.26
2.24
2.21
1.36
1.36
1.35
1.34
1.34
1.33
1.32
1.31
0.91
0.89
0.86
O
O
12
11
10
9
8
7
6
5
4
3
2
1
0
ppm
10.30
0.87
1.77
1.80
4.34
3.00

$^{13}C\{^{1}H\}$

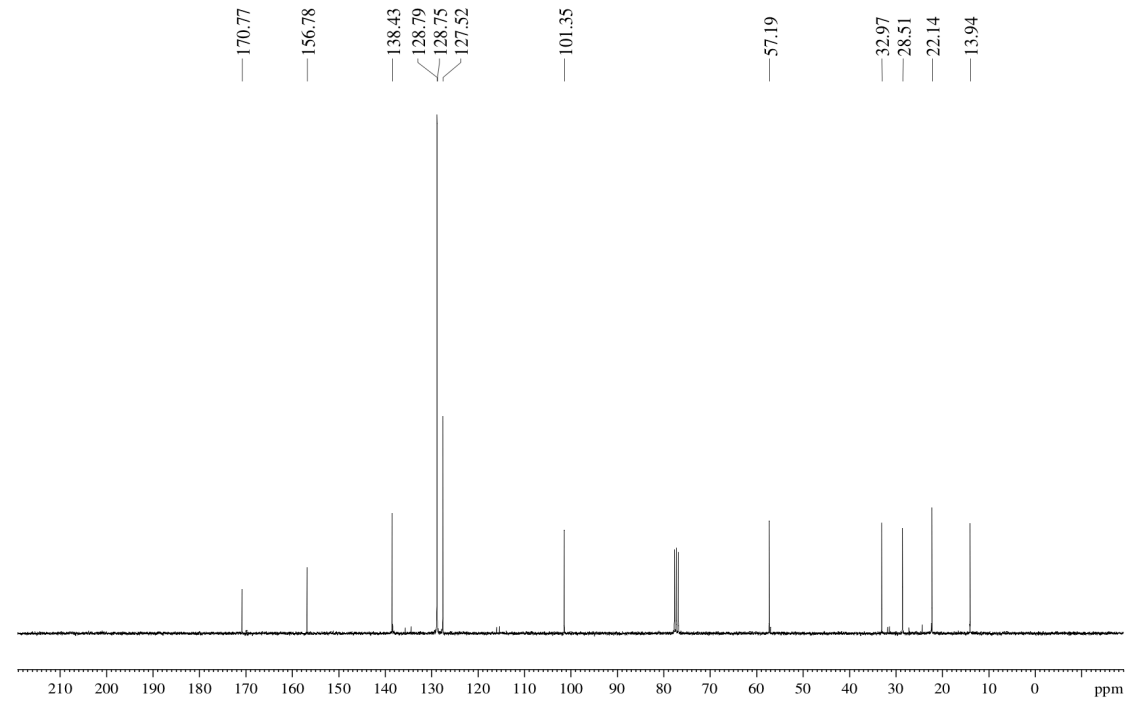
170.77
156.78
138.43
128.79
128.75
127.52
101.35
57.19
32.97
28.51
22.14
13.94
210
200
190
180
170
160
150
140
130
120
110
100
90
80
70
60
50
40
30
20
10
0
ppm

^{1}H

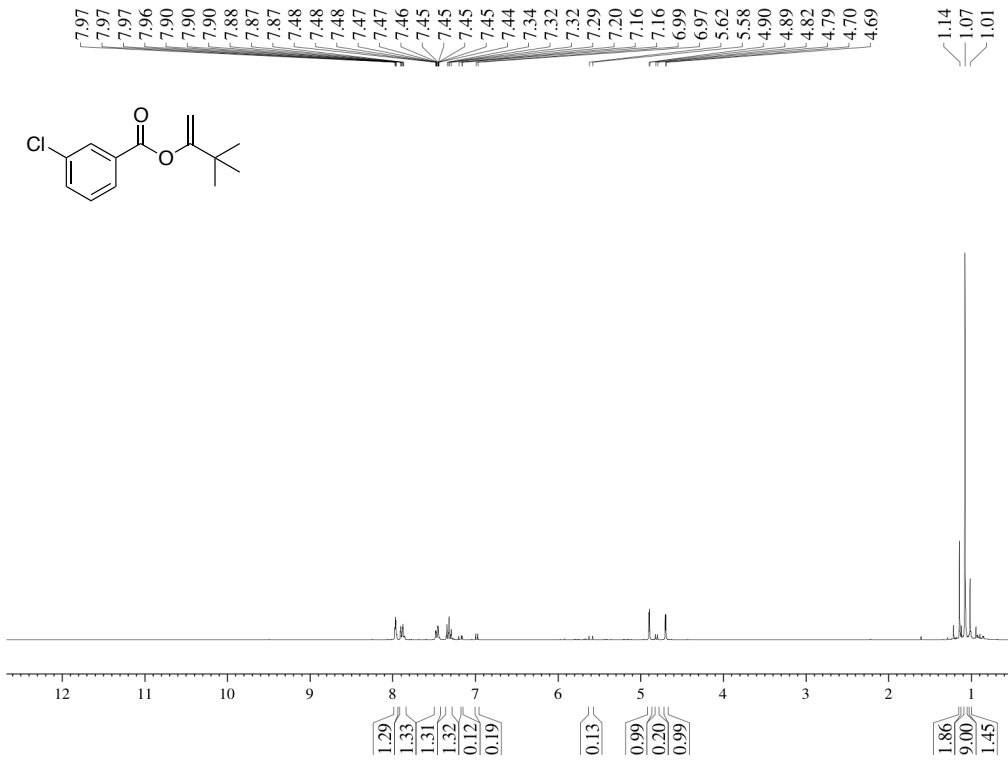

$^{13}C\{^{1}H\}$

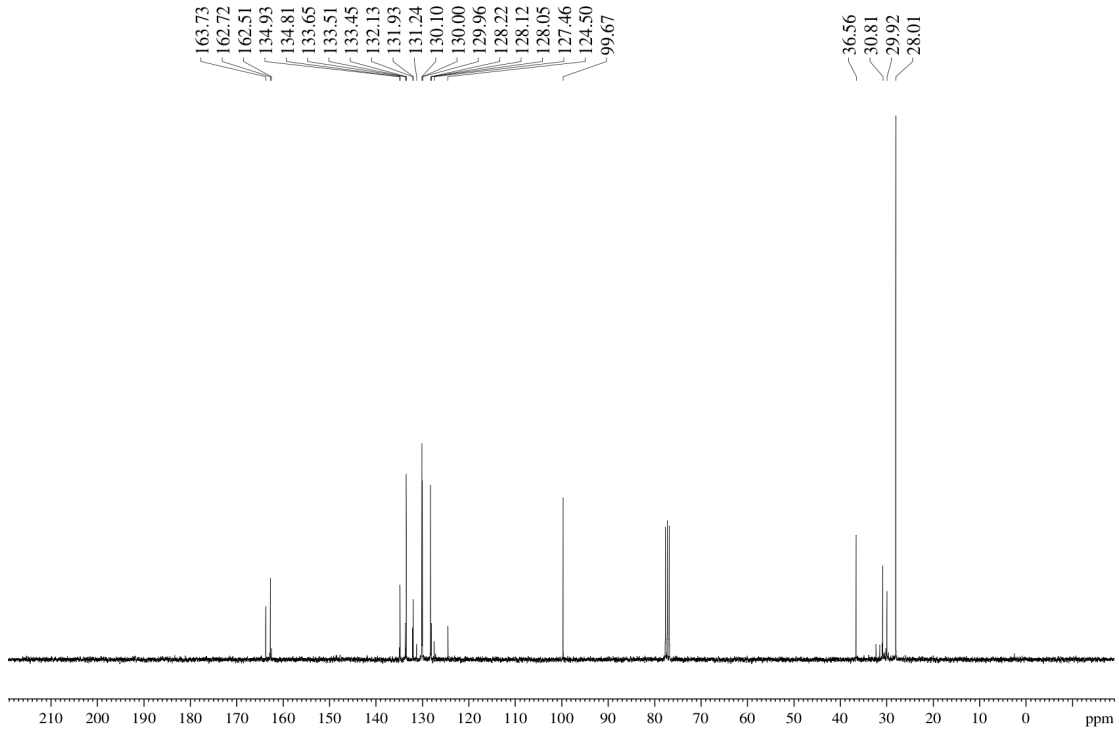

~ END OF DOCUMENT ~